ALE-FEM For Two-Phase Flows With Surfactants

Dissertation

zur Erlangung des akademischen Grades

doctor rerum naturalium
(Dr. rer. nat.)

von **Dipl.-Math. Andreas Hahn**

geb. am 09.06.1980 in Dresden, Deutschland

genehmigt durch die Fakultät für Mathematik
der Otto-von-Guericke-Universität Magdeburg

Gutachter: **Prof. Dr. rer. nat. habil. Lutz Tobiska**

Prof. Dr. rer. nat. habil. Gert Lube

eingereicht am: 05.09.2017

Verteidigung am: 30.11.2017

Zusammenfassung

Diese Arbeit behandelt die numerische Simulation von Mehrphasen-Strömungen mit Surfactants. Die Mehrphasen-Strömung ist eine Strömung von zwei nicht mischbaren Flüssigkeiten, dabei können diese Flüssigkeiten sogenannte oberflächenaktive Substanzen (Surfactants) mit sich führen. Der Surfactant ist in den Flüssigkeiten gelöst und kann sich an dem Interface anlagern. Auf dem Interface verändert der Surfactant die Oberflächenspannung, was zu einen nicht-homogenen Oberflächenspannungskoeffizienten führt, was wiederum viele verschiedene physikalische Effekte nach sich zieht. Z.B. kann die Marangoni-Konvektion einen erheblichen Einfluss auf die Strömungsstruktur solcher Zweiphasen-Strömungen haben.

Die mathematische Beschreibung solcher Strömungen führt auf ein System der Navier-Stokes Gleichungen und ein System für den Bulk- und Oberflächen Transport. Diese Systeme sind gekoppelt und nichtlinear. Diese Arbeit stellt eine Finite Element Methode vor, die solche gekoppelten Systeme von Strömungs und Transport Gleichungen behandelt. Die Finite Element Methode bedient sich dabei des ALE-Bezugsystem, d.h. es werden bewegte Gitter und ausgerichtete Oberflächengitter verwendet. Der Vorteil dieser Methode is eine sehr genaue Einbindung der von dem Surfactant abhängigen Oberflächenspannung, was zu einer Methode führt, die in vielen verschiedenen Anwendungsfällen gute Resulate erzielt.

Ein sehr wichtiger Aspekt, bei der numerischen Behandlung von Zweiphasen-Strömungen, ist die Handhabung der Unstetigkeiten am Interface. Daher wird der Standard stetige Taylor-Hood Finite Element Raum zu einem nur phasenweise stetigen Raum erweitert. Das ist ein Raum, welcher einen stetigen Druck in jeder Flüssigkeitsphase hat, aber eine Unstetigkeit im Druck über das Interface erlaubt. In Kapitel 4 wird dann gezeigt, dass dieser erweiterte Finite Element Raum dabei inf-sup stabil bleibt, was wesentlich ist, um ein stabile numerische Methode zu erhalten, und um sogenannte unphysikalischen Oszillationen zu vermeiden.

Ein anderer wichtiger Aspekt der ALE-Methoden ist die Behandlung des Gitters, insbesondere des Oberflächengitters. Gitter geringer Qualität benötigen eine Neuvernetzung des gesamten Gebietes, was teuer zu berechnen ist und was zusätzliche Fehler in der numerische Lösung mit sich bringt. Verschiedene Gitterglättungstechnicken werden betrachtet und verglichen, die zu einer erheblichen Verbesserung der Gitterqualität führen.

Desweiteren wird die Methode, die in dieser Arbeit vorgestellt wird, validiert und mit anderen numerischen Verfahren und mit analytischen Näherungen für Zweiphasen-Strömungen verglichen. Diese Ergebnisse werden in Kapitel 5 vorgestellt.

Abstract

This work treats the numerical simulation of two-phase flows with surfactants. A two-phase flow is the flow of two immiscible fluids, where the fluids can carry so called surface active agents (surfactant). The surfactant is dissolved in the fluids and can accumulate on the interface. On the interface, the surfactant alters the surface tension force, leading to a non-homogeneous surface tension coefficient, which induces many physical effects. E.g. Marangoni convection can have a significant influence on the flow pattern of such two-phase flows.

The mathematical description of such flows leads to a system of two-phase Navier-Stokes equations and a system of bulk- and surface transport equations. This system is coupled and nonlinear. This work presents a finite element method handling these coupled flow and transport equations. The finite element method employs the ALE-framework, i.e. uses moving meshes and fitted surface grids. The advantage of this method is a very accurate incorporation of the surfactant depending surface tension coefficient, which renders a method applicable in many different scenarios.

An important aspect is the handling of the discontinuities across the interface. A careful choice for the finite element space has to be taken. Therefore, the standard continuous Taylor-Hood finite element space is extended to a domain-wise continuous Taylor-Hood finite element space. That is a space in which the pressure is continuous in each fluid phase, but is allowed to exhibit a jump across the interface. It is shown in Chapter 4, that this extended Taylor-Hood finite element space is still inf-sup stable, which is crucial to prevent so called spurious oscillations and get a stable scheme.

Another important part of ALE techniques is the handling of the mesh, especially the surface mesh of the interface. Meshes of poor quality require a re-meshing of the whole domain. That is very costly in terms of computational work, and it introduces additional errors to the numerical solution. Different mesh smoothing techniques for the surface mesh are considered and compared, which result in a significant improvement of the mesh quality.

The method presented in this work is validated and compared with other numerical schemes and analytical approximation for two-phase flows with surfactants. These results are presented in Chapter 5.

Contents

List of Figures

List of Tables

Chapter 1

Introduction

Two-Phase flows are important in nature and in several applications in engineering, chemistry, biology, and science. A two-phase flow consists of two fluids, that do not mix completely, i.e. the fluids form an interface that separates both participating phases. At the interface an additional force occurs, due to the different properties of the fluids. This force is called *surface tension force*. The surface tension force is well known in every day life. It responsible for the shape of droplets of water in air or resting on a plate, it makes the surface of water in a bottle curved, or it allows a water strider to walk on a puddle. But, the surface tension is also important in engineering. It makes foams stable, it allows contact less sealing of shafts, or it creates bubbles in chemical reactors.

An important property of the surface tension force, is that it can be altered by so called *surface active agents (surfactants)*. Surfactants are impurities that are dissolved in the fluids and can be adsorbed by the interface. Many applications of two-phase flows wouldn't be possible without a surfactant. An important surfactant, known in every day life is soap, which allows hydrophobic substance to mix with water in form of small droplets.

In the mathematical and numerical treatment of two-phase flows with surfactants, one is concerned with several problems. A flow problem for the fluids and a transport problem for the surfactant. Since, the surfactant can be dissolved in the fluid or accumulated on the interface, it is distinguished between the *bulk transport*, which is the transport in the fluid phase, and the *surface transport*, which is the transport on the interface. The fluid phases are also called the bulk.

Usually, the flow problem is described by the *Navier-Stokes equations*. While the numerical treatment of the one-phase Navier-Stokes equations is well developed and has already a long history, the numerical treatment of two-phase flows is still in its infancy. Most results were developed only in the recent years, where several different approaches were followed.

The wide field of numerical treatment of two-phase flows based on continuum mechanics can be divided into two main branches. Methods using the diffuse interface models and methods using the sharp interface models. Diffuse interface models treat the two-phase flow as a flow of a mixture of fluids. The interface is not defined. Rather,

there is a region of transition from one fluid to the other. This region is a result of a demixing of the fluids and has a small thickness depending on the participating fluids. The demixing is driven by physical processes, following the energy minimisation of the free energy of the fluid system [1, 2, 9, 36, 54, 114]. Numerical methods were developed for those models and successfully applied [3, 7, 63, 109]. Methods based on the diffuse interface model handle topological changes in the fluid domains very well, since the interface is not pre-defined. Topological changes in the fluid domain are situation like droplet break up or droplet coalescence. Also, the dynamics of such topological changes are physically accurate, since it is based on physical modelling. A problem for numerical methods based on diffuse interface models is the resolution of the interface. In real world applications the interface is often very thin. Adaptive meshes near the interface can solve some of the related problems. But in some important cases, the interface is so thin, that it is impossible to resolve it with modern computers. Such systems are for example air-water systems. The high resolution of the interface usually leads to larger computation times, compared with sharp interface based methods.

Sharp interface models for two-phase flows assume an infinite thin interface between the fluids. The position of the interface is defined by additional equations for its evolution, or in some cases given a priori. Numerical methods employing the sharp interface model are distinguished into two classes. Methods that treat the position of the interface implicit are the so called interface capturing methods. And methods that have an explicit representation of the interface position are the interface tracking methods.

Capturing methods are methods that describe the motion of the interface by means of an secondary marker. Thus, the surface is given implicit and has to be reconstructed from this marker function. Examples for capturing methods are the volume of fluid (VOF) technique, and the level set method. The VOF methods are mostly used together with finite volume methods. In the VOF methods, each cell of a mesh holds the information about what fraction of the fluids occupies the cell, from which the interface and its properties can be reconstructed [10, 30, 76]. Level set methods describe the interface by a function indicating the fluid phase by a value. Then, the interface is an isoline or isosurface of this level set function. Mostly, this function is the signed distance function to the interface and the interface is represented by the zero level [68, 70, 107]. Level set and VOF methods can handle topological changes easily. Although, the break up or coalescence of the interface might not be physically accurate.

Tracking methods employ a distinct mesh for the interface. It is distinguished between Eulerian methods and Lagrangian or ALE methods. Eulerian methods use a fixed background mesh over which the mesh for the interface moves. This methods are also called front tracking methods or immersed boundary methods. This methods have been successfully applied to two-phase flows using finite volume methods [90, 111], in the finite difference context [112], and with finite element methods [18, 20, 21].

In the Lagrangian or ALE methods, the mesh for the interface consists of faces of the background mesh, and thus is part of the background mesh. Faces belonging to the interface are marked as such, and usually don't change this property (there are exceptions [22]). Thus, the background mesh must follow the movement of the interface and hence,

this methods employ a moving mesh, instead of a fixed background mesh. Moving mesh techniques have been used in the finite difference context [75], finite volume context [44, 45], and the finite element context [16, 58, 61, 92]

The capturing methods and the front tracking methods are so called unfitted methods, while the moving mesh techniques are used as fitted methods. In unfitted methods, the interface can cut mesh cells. In fitted methods the interface is always aligned and no cutting of mesh cells occurs.

In unfitted methods, discontinuities and kinks of functions, that can appear in the interior of a mesh cell, have to be handled carefully. In the finite element context, a whole class of new methods have been developed, the so called extended finite element (XFEM) or CutFEM methods. These methods are used to solve flow and bulk equations [34, 69, 73] and for partial differential equations on surfaces as well [35, 95, 96].

In the fitted methods, the discontinuities also have to be handled. But here, this is less of a problem, since jumps appear across mesh cell boundaries only and discontinuous finite element spaces are available.

A disadvantage of the tracking methods is the difficulty in handling of topological changes. In fact, this is nearly impossible. Although, there are successful attempts to handle the break up and coalescence of fluid phases [94], these schemes are essentially mesh handling algorithms, and do not guarantee a physical accurate coalescence or break up.

The finite element analysis for two-phase flows coupled with bulk-surface transport equations in the framework of ALE finite element methods is still in its infancy. In the following a short overview is given, without claim of completeness.

The ALE finite element method for coupled bulk-surface problems works well together with parametric finite element methods on surfaces. Since a surface mesh is given explicit, these methods can easily be applied for the surface transport of the surfactant. In recent years these methods have been developed a lot. Although, the first occurrence of such methods has been several decades back in [48]. For transport problems on evolving surfaces, using a finite element method with linear elements, an analysis was done for the semi-discrete problem in [46, 47] and later for the fully discrete problem in [49]. Surface finite element methods also using the ALE framework for the surface, instead of an Lagrangian description, were used in [53]. For fixed surfaces, higher order finite element methods for diffusion (Laplace-Beltrami operator) were considered in [43]. Methods for evolving surfaces using space-time finite elements methods were studied in [95] and [97]. An overview of different parametric surface finite element methods is given in [50].

Existing finite element analysis for the bulk equations in the ALE framework are restricted to the case that domain evolution is given a priori. Mostly transport equations are considered in a one-phase setting. A finite element analysis of a transport and a diffusion problem using different time discretization is found already in [93] and [92]. An important role plays the so called geometric conversation law (GCL), although it is not quite clear which role. The GCL is a condition on the time integration. In short, it states that the Reynolds transport theorem also has to hold for the time-discrete scheme [25,

56]. However, it is also shown that the GCL condition is neither sufficient nor necessary, for the stability of a scheme [25].

An analysis of a stabilised ALE finite element method for convection diffusion problems can be found in [13]. An analysis of time-discrete ALE methods for transport problems, using higher order discontinuous Galerkin methods in time are found in [27] and [28]. Further, an analysis of the unsteady Stokes problem in a time dependent domain using a ALE finite element method can be found in [104].

For the coupled bulk-surface transport problem are also some works available already, which are concerned with the analysis of finite element methods. Although, only the stationary case is treated yet. An analysis for coupled elliptic problems can be found in [52] and [99], and in the context of unfitted methods an analysis is found recently in [67]

This work is concerned with the two-phase flows with surfactants in the ALE finite element framework. It tries to contribute to the relative young field of finite element methods for coupled flow and transport problems. This work is structured as follows.

In the remaining first chapter, some mathematical notations and preliminaries are introduced.

In the second chapter, the governing equations are introduced. The one-phase Navier-Stokes is equation is derived, which is then extended to the two-phase Navier-Stokes system. After that, the bulk transport and surface transport equations, including the coupling conditions, are derived. These equations are augmented by equations of state for the adsorption and desorption processes, and the dependencies for surface tension force. Then, the equations are transferred to a dimensionless form. Finally, a weak formulation is obtained.

In Chapter 3, the ALE framework is introduced. The handling of the ALE mapping and the domain velocity is described. Different methods for constructing an ALE mapping for the bulk and for the surface are presented. After that, the stability of a reduced problem (flow problem only) is studied. Finally, some special formulation used in the numerical simulations are introduced.

The finite element discretization is introduced in Chapter 4. First, the space discretization is obtained. The influence of the chosen pair of finite element space for the flow problem is discussed. After that, the inf-sup stability of the domain-wise discontinuous Taylor-Hood finite element space used is shown. Then, the time discretization is introduced. The most common time-stepping scheme in the context of the Navier-Stokes equations, the θ-scheme, and the fractional Θ-scheme are applied in the ALE framework. Chapter 4 is closed with different finite element discretizations of the surface evolution equations.

Finally in Chapter 5, the numerical scheme is validated and several numerical results are presented. A Taylor flow is considered with and without surfactants and the results are compared to other schemes. An oscillating drop is compared with results obtained from analytic approximations. And closing Chapter 5, the behaviour of the different surface mesh evolution algorithm are shown.

1.1 Mathematical Preliminaries

The basic notation and standard mathematical preliminaries, which are important in this work, are introduced. No proofs are given, since these are standard results from mathematical literature like [50, 57].

1.1.1 Basic Notations

Throughout this work, the following notations and definitions are used.

For a scalar function $f : \Omega \subset \mathbb{R}^d \to \mathbb{R}$, $f = f(x_1, \dots, x_d)$, sufficiently smooth, the partial derivative with respect to the i-th component is denoted with

$$\partial_i f := \frac{\partial f}{\partial x_i} ,$$

analogue, if the components are named, e.g $f = f(x, \dots, z, t)$

$$\partial_x f := \frac{\partial f}{\partial x} , \quad \dots , \quad \partial_z f := \frac{\partial f}{\partial z} , \quad \partial_t f := \frac{\partial f}{\partial t} .$$

The material derivative of a function $f = f(\mathbf{x}, t)$, sufficiently smooth, respecting a velocity $\mathbf{u}$, is denoted with

$$\partial_t^{\mathbf{u}} f := \partial_t f + \mathbf{u} \cdot \nabla f .$$

For a scalar function $f : \Omega \to \mathbb{R}$ and a vector valued function $\mathbf{F} : \Omega \to \mathbb{R}^d$ for which the following quantities exist, the following notations for integral values are used. For the volume integral V and $\mathbf{V}$ of f and $\mathbf{F}$ respectively, the notation

$$V = \int_\Omega f \, \mathrm{d}V , \quad \text{and} \quad \mathbf{V} = \int_\Omega \mathbf{F} \, \mathrm{d}V .$$

is used.

Surface integrals of the first kind A_1 and of the second kind A_2 are denoted with

$$A_1 = \int_{\partial\Omega} f \, \mathrm{d}A , \quad \text{and} \quad A_2 = \int_{\partial\Omega} \mathbf{F} \cdot \mathrm{d}\mathbf{A} .$$

The vector valued versions are written analogue. When necessary, the notation of line integrals is also used, and similar to surface integrals. For line integrals L_1 of first kind and of second kind L_2, the notation

$$L_1 = \int_{\partial\Omega} f \, \mathrm{d}C , \quad \text{and} \quad L_2 = \int_{\partial\Omega} \mathbf{F} \cdot \mathrm{d}\mathbf{C} ,$$

is used.

Let V be a Banach space, the norm for $v \in V$ is denoted with $\|v\|_V$. The dual space of V is denoted with V'. If the space is a Sobolev space $W^{s,p}(\Omega)$, the notation $\|v\|_{s,p,\Omega}$

for the norm of $v \in W^{s,p}(\Omega)$ is used. For the Hilbert spaces $W^{s,2}(\Omega)$ the notation $H^s(\Omega) = W^{s,p}(\Omega)$ is used and the norm is denoted with $\|v\|_{s,\Omega}$. The $L^2(\Omega)^d$ inner product is written as

$$(f,g)_\Omega := \int_\Omega f \cdot g \ \mathrm{d}V \ .$$

and analogue, on a surface it is defined

$$\langle f,g\rangle_{\partial\Omega} := \int_{\partial\Omega} f \cdot g \ \mathrm{d}A \ .$$

For matrix valued functions, it is set for $A, B \in \mathbb{R}^{m\times n}$, with $A = (a_{ij})_{i,j}$ and $B = (b_{ij})_{i,j}$

$$(A,B)_\Omega := \int_\Omega A : B \ \mathrm{d}V \quad \text{and} \quad \langle A,B\rangle_{\partial\Omega} := \int_{\partial\Omega} A : B \ \mathrm{d}A \ ,$$

where $A : B$ is the matrix scalar product

$$A : B := \sum_{i,j} a_{ij} b_{ij} \ .$$

The following two theorems define traces of functions and partial integration.

Theorem 1.1.1 (Traces and Green's formula)**.** *Let $1 \le p < \infty$ and Ω be a Lipschitz domain. There exists a uniquely determined continuous linear mapping $\gamma_0^\Omega : W^{1,p}(\Omega) \to L^p(\partial\Omega)$ such that*

$$\gamma_0^\Omega(f) = f|_{\partial\Omega} \ , \quad \forall f \in C^\infty(\overline{\Omega}) \ .$$

If $1 < p < \infty$, then Green's formula

$$\int_\Omega (f\partial_i g + g\partial_i f) \ \mathrm{d}V = \int_{\partial\Omega} \gamma_0^\Omega(f)\gamma_0^\Omega(g) n_i \ \mathrm{d}A \ ,$$

holds for $f \in W^{1,p}(\Omega)$, $g \in W^{1,\frac{p}{p-1}}(\Omega)$.

From which the divergence theorem follows.

Lemma 1.1.1 (Divergence formula)**.** *Let $1 < p < \infty$ and Ω be a Lipschitz domain, then the divergence formula*

$$\int_\Omega \nabla \cdot \mathbf{F} \ \mathrm{d}V = \int_{\partial\Omega} \mathbf{F} \cdot \mathrm{d}\mathbf{A} \tag{1.1.1}$$

holds for $\mathbf{F} \in W^{1,p}(\Omega)^d$.

1.1.2 Surfaces

The following notations, definitions, and theorems for surfaces are taken from [50], but they can also be found in standard textbooks about differential geometry.

Parametric surface and smooth functions thereon, are defined as follows.

Definition 1.1.1 (Parametric surface)**.** *A set $\Gamma \subset \mathbb{R}^{n+1}$ is called a n-dimensional parametrized C^k surface, if there exists for every point $x_0 \in \Gamma$ an open set $U \subset \mathbb{R}^{n+1}$ with $x_0 \in U$, an open connected set $V \in \mathbb{R}^n$ and a mapping $\gamma : V \to U \cap \Gamma$ for which the following holds. $\gamma \in C^k(V, \mathbb{R}^{n+1})$, γ is bijective, and the rank of $\nabla\gamma$ is n on V. The mapping γ is called a local parametrization of Γ.*

Definition 1.1.2. *A function $f : \Gamma \to \mathbb{R}$ is called k-times differentiable, if all functions $f \circ \gamma_i$, $i = 1, \ldots, n+1$, are k-times differentiable.*

Let $\Gamma \subset \mathbb{R}^{n+1}$ be a n-dimensional parametrized C^1 surface and let $\gamma : V \to \Gamma$ be a local parametrization of Γ. The first fundamental form $G(\mathbf{y}) = [g_{ij}(\mathbf{y})]_{ij=1,\ldots,n}$, for $\mathbf{y} \in V$ is defined as follows

$$g_{ij}(\mathbf{y}) = \partial_i\gamma(\mathbf{y}) \cdot \partial_j\gamma(\mathbf{y}) \qquad i, j = 1, \ldots, n \ .$$

The determinant of G is denoted with $g = det(G)$, and the inverse of G is denoted with superscripts g^{ij}, such that

$$G^{-1} = \left[g^{ij}\right]_{i,j=1\ldots,n} \ .$$

Then the surface differential operators are defined as follows.

Definition 1.1.3 (Tangential surface gradient)**.** *Let $\Gamma \subset \mathbb{R}^{n+1}$ be a n-dimensional parametrized C^1 surface, with the local parametrization $\gamma : V \to \Gamma$. Further, let $f : \Gamma \to \mathbb{R}$ be a differentiable function and let $F = f(\gamma(\mathbf{y}))$ for $\mathbf{y} \in V$. Then the tangential surface gradient $\nabla_\Gamma f : \Gamma \to \mathbb{R}^{n+1}$ is defined as follows*

$$\left(\nabla_\Gamma f\right)(\gamma(\mathbf{y})) := \sum_{i,j=1}^{d} g^{ij}(\mathbf{y})\partial_i F(\mathbf{y})\partial_j F(\mathbf{y}) \ ,$$

for $\mathbf{y} \in V$.

Definition 1.1.4 (Laplace-Beltrami operator)**.** *Let $\Gamma \subset \mathbb{R}^{n+1}$ be a n-dimensional parametrized C^2 surface, with the local parametrization $\gamma : V \to \Gamma$. Further, let $f : \Gamma \to \mathbb{R}$ be a two times differentiable function and let $F = f(\gamma(\mathbf{y}))$ for $\mathbf{y} \in V$. Then the Laplace-Beltrami operator $\Delta_\Gamma f : \Gamma \to \mathbb{R}$ is defined as follows*

$$(\Delta_\Gamma f)(\gamma(\mathbf{y})) := \frac{1}{\sqrt{g(\mathbf{y})}} \sum_{i,j=1}^{n} \partial_j \left(g^{ij}(\mathbf{y})\sqrt{g(\mathbf{y})}\partial_i F(\mathbf{y}) \right) \ ,$$

for $\mathbf{y} \in V$.

An alternative, and useful definition of a surface and the surface operators, is the following.

Definition 1.1.5 (Hypersurface)**.** *The set $\Gamma \in \mathbb{R}^{n+1}$ is called a C^k hypersurface, if for every point $\mathbf{x}_0$, there exists a open set $U \subset \mathbb{R}^{n+1}$ with $\mathbf{x}_0 \in U$ and a function $\phi \in C^k(U)$, with $\nabla\phi \neq 0$ on $\Gamma \cap U$ and*

$$U \cap \Gamma = \{\mathbf{x} \in U : \phi(\mathbf{x}) = 0\} \ .$$

Definition 1.1.6. *Let $\Gamma \subset \mathbb{R}^{n+1}$ be a C^1 hypersurface, and let $f : \Gamma \to \mathbb{R}$ be a differentiable function. Further, let $\mathbf{n}$ be the normal of Γ, and let $\bar{f} : U \to \mathbb{R}$ be a smooth extension of f, such that $\bar{f}|_\Gamma = f$, where $U \subset \mathbb{R}^{n+1}$, with $\Gamma \subset U$, is a neighbourhood of Γ. Then the tangential surface gradient $\nabla_\Gamma f$ is defined as*

$$\nabla_\Gamma f(\mathbf{x}) := \nabla \bar{f}(\mathbf{x}) - (\mathbf{n}(\mathbf{x}) \cdot \nabla \bar{f}(\mathbf{x}))\mathbf{n}(\mathbf{x}) \ ,$$

for $\mathbf{x} \in \Gamma$.

Note, the surface gradient of f on Γ is independent of the extension $\bar{f}$. For the following definition of the Laplace-Beltrami operator, let the surface gradient be written as

$$\nabla_\Gamma f = (D_1 f, \ldots, D_{n+1} f)^T \ .$$

Definition 1.1.7. *Let $\Gamma \subset \mathbb{R}^{n+1}$ be a n-dimensional parametrized C^1 surface, and let $f : \Gamma \to \mathbb{R}$ be a two times differentiable function. The Laplace-Beltrami operator is defined as follows*

$$\Delta_\Gamma f := \nabla_\Gamma \cdot \nabla_\Gamma f = \sum_{i=1}^{n+1} D_i D_i f \ .$$

Both definitions of the surface gradient and Laplace-Beltrami operator are equivalent [50].

In the following, the mean curvature is introduced in the setting of hypersurfaces. Note, this could also be done in the setting of parametrized surface and the second fundamental form.

Definition 1.1.8 (Weingarten map)**.** *Let $\Gamma \subset \mathbb{R}^{n+1}$ be an oriented C^2 hypersurface, and let $\mathbf{n}(\mathbf{x}) = (n_1(\mathbf{x}), \ldots, n_{n+1}(\mathbf{x}))^T$ be the normal of Γ. The extended Weingarten map is defined as*

$$H_{ij}(\mathbf{x}) = D_i n_j(\mathbf{x}) \ , \quad i, j = 1, \ldots, n+1 \ ,$$

for $\mathbf{x} \in \Gamma$. The restriction of H_{ij} to the tangent space is called Weingarten map.

Definition 1.1.9 (Mean curvature)**.** *Let $\Gamma \subset \mathbb{R}^{n+1}$ be an oriented C^2 hypersurface, the mean curvature $\mathcal{H}$ is defined as*

$$\mathcal{H}(\mathbf{x}) = \sum_{i=1}^{n+1} H_{ij}(\mathbf{x}) \ ,$$

for $\mathbf{x} \in \Gamma$.

With this definitions the partial integration on surfaces can be defined.

Lemma 1.1.2 (Partial integration on surfaces)**.** *Let $\Gamma \subset \mathbb{R}^{n+1}$ be a hypersurface with a smooth boundary $\partial\Gamma$ and let f be a differentiable function, then it holds*

$$\int_\Gamma \nabla_\Gamma f \ \mathrm{d}A = \int_\Gamma f\mathcal{H}\mathbf{n} \ \mathrm{d}A + \int_{\partial\Gamma} f\mu \ \mathrm{d}C \ ,$$

where $\mathbf{n}$ is the normal to Γ and μ the co-normal to $\partial\Gamma$.

Lemma 1.1.3 (Green's formula on surfaces)**.** *Let $\Gamma \subset \mathbb{R}^{n+1}$ be a hypersurface with a smooth boundary $\partial\Gamma$ and let f be a differentiable function and g be a two times differentiable function, then it holds*

$$\int_\Gamma \nabla_\Gamma f \cdot \nabla_\Gamma g \ \mathrm{d}A = -\int_\Gamma f \ \Delta_\Gamma g \ \mathrm{d}A + \int_{\partial\Gamma} f\nabla_\Gamma g \cdot \mathrm{d}\mathbf{C} \ .$$

Lemma 1.1.4 (Divergence theorem on surfaces)**.** *Let $\Gamma \subset \mathbb{R}^{n+1}$ be a hypersurface with a smooth boundary $\partial\Gamma$ and let $\Phi : \Gamma \to \mathbb{R}^d$ be a differentiable function, then it holds*

$$\int_\Gamma \nabla_\Gamma \cdot \Phi \ \mathrm{d}A - \int_\Gamma \mathcal{H}\Phi \cdot \ \mathrm{d}\mathbf{A} = \int_{\partial\Gamma} \Phi \cdot \ \mathrm{d}\mathbf{C} \ . \tag{1.1.2}$$

Chapter 2

Governing Equations

In the following chapter, the governing equations for the *two-phase flow with soluble surfactants* are introduced. The equations are derived in the strong form. Then, a weak formulation is obtained from the strong form.

The equations are derived from fundamental physical principles in fluid dynamic and mass transfer and interfacial phenomena [57, 81, 83, 103, 106, 108]. The conservation laws for the fluid and the surfactant are considered, where several simplifications are assumed. Here, only incompressible, isothermal, and isotropic flows are allowed. Moreover, the surfactant transport is assumed to be isotropic and homogeneous, in the bulk and on the surface as well. The interface is massless and has no viscosity.

First, the conservation laws for the flow in the bulk are obtained and the one-phase Navier-Stokes equations are derived. Then, the coupling conditions for two-phase Navier-Stokes equations are obtained. The coupling condition results in a kinematic condition for the evolution of the interface, and a dynamic condition for the surface tension and the Marangoni force.

After establishing the Navier-Stokes equations for the two-phase flow, the conservation laws for the mass transport of the surfactant is considered. From these balances the transport equations for the bulk and the surface surfactant, as well as the coupling condition are obtained. These equations have to be completed with the adsorption dynamics, where the Langmuir and the Henry model is assumed [81, 103].

Finally, the model is transferred into a dimensionless form and a weak formulation is introduced.

2.1 The Navier-Stokes Equations

A fluid and its motion during the time interval $[t_0, t_b] \subset \mathbb{R}$ is considered. At time $t \in [t_0, t_b]$ the fluid occupies the domain $\Omega(t) \subset \mathbb{R}^d$. The space time domain $\mathcal{Q}(t_0, t_b)$ the fluid occupies is given as

$$\mathcal{Q}(t_0, t_b) := \{(\mathbf{x}, t) \in \mathbb{R}^{d+1} : t \in [t_0, t_b], \mathbf{x} \in \Omega(t)\} \ . \tag{2.1.1}$$

There are two possibilities the motion of a fluid can be described [39, 57, 83]. In the Lagrangian description each individual particle of the fluid is considered. A particle at position $\mathbf{x}_0 \in \mathbb{R}^d$ at time t_0 follows the trajectory

$$\mathbf{x}(t) = \mathbf{X}(\mathbf{x}_0, t) \ .$$

The function $\mathbf{X} : \Omega(t_0) \times (t_0, t_1) \to \mathbb{R}^d$ describes the motion of a fluid occupying $\Omega(t_0)$ at time t_0. The position $\mathbf{x}_0$ of a particle is called the *Lagrangian coordinate*.

In the Eulerian description the motion of the fluid is determined by a velocity field $\mathbf{u} : \mathcal{Q}(t_0, t_b) \to \mathbb{R}^d$. Here, $\mathbf{u}(\mathbf{x}, t)$ is the velocity of the particle passing position $\mathbf{x}$ at time t. Using (2.1.1) the velocity is given by

$$\mathbf{u}(\mathbf{x}, t) = \partial_t \mathbf{X}(\mathbf{x}_0, t) \ ,$$

with $\mathbf{x} = \mathbf{X}(\mathbf{x}_0, t)$ and $\mathbf{x}$ is called the *Eulerian coordinate*.

The derivation of the Navier-Stokes equations considers arbitrary volumes of fluid in Lagrangian coordinates, the so called *material volumes*. They are defined as follows:

Definition 2.1.1 (Material volume)**.** *Let $\mathcal{V}_0 \subset \Omega(t_0)$ be a bounded subset of the domain at time t_0. A material volume $\mathcal{V}(t)$ is defined by*

$$\mathcal{V}(t) := \{\mathbf{x} \in \Omega : \mathbf{x} = \mathbf{X}(\mathbf{x}_0, t), \mathbf{x}_0 \in \mathcal{V}_0\} \ ,$$

for $t \in (t_0, t_b)$.

Remark 2.1.1. *At every time $t \in (t_0, t_b)$ a material volume $\mathcal{V}(t)$ consists of no other particles found in $\mathcal{V}_0$. By definition no particle can enter or leave $\mathcal{V}(t)$, since the boundary moves with the particle velocity $\mathbf{u}$.*

The description of a fluid can include other properties, than the position and the velocity. For an arbitrary quantity $f : \mathcal{Q}(t_0, t_b) \to \mathbb{R}$ associated with the fluid and sufficiently smooth the following holds

Lemma 2.1.1 (Reynolds transport theorem)**.** *Let $\mathcal{V}(t)$ be a material volume and $f : \mathcal{Q}(t_0, t_b) \to \mathbb{R}$ be a $C^1(\mathcal{Q}(t_0, t_b))$ function, then the following holds:*

$$\frac{d}{dt} \int_{\mathcal{V}(t)} f \ \mathrm{d}V = \int_{\mathcal{V}(t)} \partial_t f + \nabla \cdot (f\mathbf{u}) \ \mathrm{d}V \tag{2.1.2}$$

and

$$\frac{d}{dt} \int_{\mathcal{V}(t)} f \ \mathrm{d}V = \int_{\mathcal{V}(t)} \partial_t f \ \mathrm{d}V + \int_{\partial\mathcal{V}(t)} f\mathbf{u} \cdot \mathrm{d}\mathbf{A} \ . \tag{2.1.3}$$

Proof. The proof of (2.1.2) can be found in [57]. The second form of the transport theorem (2.1.3) is a direct consequence of the Gauss theorem (1.1.1) applied to (2.1.2). □

The Reynolds transport theorem is fundamental for the derivation of partial differential equations describing physical phenomena based on conservation laws, like the Navier-Stokes equations. The quantity f considered can be physical properties like momentum, density, temperature, energy, or surfactant concentration. In order to derive the partial differential equations for an isothermal flow it is sufficient to consider the mass- and momentum density.

2.1.1 Mass Balance

Let $\rho : \mathcal{Q}(t_0, t_b) \to \mathbb{R}$ be the mass density field of the fluid. Then, the total mass $M(t)$ of fluid of a material volume $\mathcal{V}(t)$ at time t is given by

$$M(t) = \int_{\mathcal{V}(t)} \rho \, \mathrm{d}V \ .$$

Because of Remark 2.1.1, the mass of the material volume is constant for all $t \in (t_0, t_b)$. Thus the change of total mass is zero. Applying the Reynolds transport theorem (2.1.2), it follows

$$0 = \frac{d}{dt} \int_{\mathcal{V}(t)} \rho \, \mathrm{d}V = \int_{\mathcal{V}(t)} \partial_t \rho + \nabla \cdot (\rho \mathbf{u}) \, \mathrm{d}V \ .$$

Since the material volume $\mathcal{V}(t)$ is arbitrary, a localisation procedure can be applied [57], and a partial differential equation is derived. The *mass balance equation* describes the mass balance locally, and reads as follows

$$\partial_t \rho + \nabla \cdot (\rho \mathbf{u}) = 0 \qquad \text{in } \Omega(t) \ . \tag{2.1.4}$$

Since it is assumed that the fluid is incompressible, the mass balance equation can be simplified further. An incompressible fluid implies a constant density, such that it follows for all $t \in (t_0, t_b)$

$$\nabla \cdot \mathbf{u} = 0 \qquad \text{in } \Omega(t) \ . \tag{2.1.5}$$

2.1.2 Momentum Balance

Let $\mathbf{p} : \mathcal{Q}(t_0, t_b) \to \mathbb{R}^d$ be the momentum density field $\mathbf{p} = \rho \mathbf{u}$ of the fluid in $\Omega(t)$. The total momentum $\mathbf{P}(t)$ of a material volume is given as

$$\mathbf{P}(t) = \int_{\mathcal{V}(t)} \mathbf{p} \, \mathrm{d}V.$$

Following Newton's laws of motion [84], the rate of change in momentum is equal to the sum of all acting forces. It is distinguished between two types of forces, volume forces and surface forces. The volume forces represent external forces acting on the body of fluid, like gravitation, electric fields, magnetic fields, etc. Here, a general force field $\mathbf{g} : \mathcal{Q}(t_0, t_b) \to \mathbb{R}^d$ is considered, which is interpreted as the gravitational force.

The total gravitational force $\mathbf{F}_1(t)$ acting on a material volume $\mathcal{V}(t)$ is given as

$$\mathbf{F}_1(t) = \int_{\mathcal{V}(t)} \rho \mathbf{g} \, \mathrm{d}V \ .$$

The surface forces model internal forces, that are forces the fluid is acting on its self. The fluid surrounding a material volume $\mathcal{V}(t)$ is carrying over momentum to the surface of $\mathcal{V}(t)$. A general principle of continuum mechanics, the *Cauchy stress theorem* [40, 83], states that the force acting on a point of the surface is a linear function of the normal in this point. Thus, the internal forces are described by a tensor field $\mathbb{S} : \mathcal{Q}(t_0, t_b) \to \mathbb{R}^{d \times d}$ and the force $\mathbf{f}$, which is carried over to $\mathcal{V}(t)$ at a point $\mathbf{x} \in \partial\mathcal{V}(t)$ on the surface with normal $\mathbf{n}$ is determined by

$$\mathbf{f} = \mathbb{S}\mathbf{n} \ .$$

$\mathbb{S}$ is called *Cauchy stress tensor* or just *stress tensor*.

The total surface force $\mathbf{F}_2(t)$ acting on the boundary of $\mathcal{V}(t)$ is given by

$$\mathbf{F}_2 = \int_{\partial\mathcal{V}(t)} \mathbb{S} \cdot \, \mathrm{d}\mathbf{A} \ .$$

Applying Newton's laws of motion, the rate of change in moment is then given by

$$\frac{d}{dt}\mathbf{P}(t) = \mathbf{F}_1(t) + \mathbf{F}_2(t) = \int_{\mathcal{V}(t)} \rho \mathbf{g} \, \mathrm{d}V + \int_{\partial\mathcal{V}(t)} \mathbb{S} \cdot \, \mathrm{d}\mathbf{A} \ .$$

After applying the Gauss theorem on the surface integral, it follows

$$\frac{d}{dt} \int_{\mathcal{V}(t)} \mathbf{p} \, \mathrm{d}V = \int_{\mathcal{V}(t)} \rho \mathbf{g} + \nabla \cdot \mathbb{S} \, \mathrm{d}V \ .$$

Now, the Reynolds transport theorem (2.1.2) can be used component-wise. Introducing the notation $\mathbf{u} = (u_1, \ldots, u_d)$, $\mathbf{p} = (p_1, \ldots, p_d)$, $\mathbf{g} = (g_1, \ldots, g_d)$, etc., the following balance for the momentum holds

$$\int_{\mathcal{V}(t)} \partial_t p_i + \nabla \cdot (p_i \mathbf{u}) \, \mathrm{d}V = \int_{\mathcal{V}(t)} \rho g_i + (\nabla \cdot \mathbb{S})_i \, \mathrm{d}V,$$

for $i = 1, \ldots, d$. Using a localisation procedure the local *momentum balance equation* is derived

$$\partial_t \mathbf{p} + \nabla \cdot (\mathbf{p} \otimes \mathbf{u}) = \rho \mathbf{g} + \nabla \cdot \mathbb{S} \qquad \text{in } \Omega(t) \ ,$$

for all $t \in (t_0, t_b)$.

Using the mass balance (2.1.4), the momentum balance can be simplified further. Reminding that $\mathbf{p} = \rho\mathbf{u}$ the momentum balance equation reads for all $t \in (t_0, t_b)$

$$\rho \left(\partial_t \mathbf{u} + (\mathbf{u} \cdot \nabla) \, \mathbf{u}\right) = \rho \mathbf{g} + \nabla \cdot \mathbb{S} \qquad \text{in } \Omega(t) \ . \tag{2.1.6}$$

In a viscous Newtonian fluid, the stress tensor is assumed to be linearly dependent on the pressure p and on the *deformation tensor*

$$\mathbb{D}(\mathbf{u}) = \frac{1}{2}\left(\nabla\mathbf{u} + (\nabla\mathbf{u})^T\right) .$$

The general form of the stress tensor is [40, 57]

$$\mathbb{S}(\mathbf{u}, p) = \mathcal{L}(\mathbb{D}(\mathbf{u})) - p\mathbb{I} ,$$

where $\mathcal{L}(\mathbb{D}(\mathbf{u}))$ is a linear mapping of the tensor $\mathbb{D}(\mathbf{u})$.

It can be further shown that the stress tensor for an isotropic medium must have the form [40]

$$\mathbb{S}(\mathbf{u}, p) = 2\mu\mathbb{D}(\mathbf{u}) + \lambda\,(\nabla\cdot\mathbf{u})\,\mathbb{I} - p\mathbb{I} .$$

Using the mass balance (2.1.5), the stress tensor for an incompressible Newtonian fluid simplifies to

$$\mathbb{S}(\mathbf{u}, p) = 2\mu\mathbb{D}(\mathbf{u}) - p\mathbb{I} . \tag{2.1.7}$$

The parameter μ is the *dynamic viscosity* and given by the material properties of the fluids.

The momentum balance equations (2.1.6) together with the mass balance equation (2.1.5) using the stress tensor (2.1.7) are the well known Navier-Stokes equations for incompressible, viscous flows:

Find $\mathbf{u} : \mathcal{Q}(t_0, t_b) \to \mathbb{R}^d$ and $p : \mathcal{Q}(t_0, t_b) \to \mathbb{R}$ such that it holds

$$\begin{aligned} \rho\,(\partial_t\mathbf{u} + \mathbf{u}\cdot\nabla\mathbf{u}) - \nabla\cdot\mathbb{S}(\mathbf{u}, p) &= \rho\mathbf{g} && \text{in } \Omega(t) , \\ \nabla\cdot\mathbf{u} &= 0 && \text{in } \Omega(t) , \end{aligned}$$

for all $t \in (t_0, t_b)$.

Naturally, these equations have to be closed with initial- and boundary conditions in order to get a well-posed problem. The boundary conditions are left open at this point, since they vary from case to case.

2.2 Two-Phase Flows

A two-phase flow is the flow of two immiscible fluids. Each fluid is occupying a separate subdomain, partitioning $\Omega(t)$ into two open subdomains. Let $\Omega_1(t)$ be the time-dependent "inner" domain and let $\Omega_2(t)$ be the time-dependent "outer" domain, with $\overline{\Omega(t)} = \overline{\Omega_1(t)} \cup \overline{\Omega_2(t)}$ and $\Omega_1(t) \cap \Omega_2(t) = \emptyset$. Then, $\Gamma(t) = \overline{\Omega_1(t)} \cap \overline{\Omega_2(t)}$ denotes the interface between the two domains. The domains $\Omega_i(t)$ of the fluid phases are also called *bulk domains* or *bulk phases*.

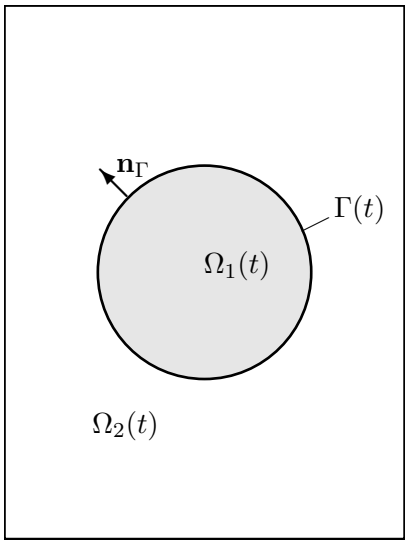

Figure 2.1: Schematic view of the two-phase domain

The space time domain, which the time-dependent interface forms, is

$$\mathcal{Q}_\Gamma(t_0, t_b) := \{(\mathbf{x}, t) \in \mathbb{R}^{d+1} : t \in [t_0, t_b], \mathbf{x} \in \Gamma(t)\} \ .$$

Each phase occupies the space time domain

$$\mathcal{Q}_i(t_0, t_b) := \{(\mathbf{x}, t) \in \mathbb{R}^{d+1} : t \in [t_0, t_b], \mathbf{x} \in \Omega_i(t)\} \ ,$$

for $i = 1, 2$.

The balance equations for the mass and the momentum in a material volume, that have been derived in the last section, are still valid for material volumes that are proper subsets of either the inner fluid or the outer fluid. But, for material volumes that contain a part of the interface, these balances are not valid any more. Also, the Reynolds transport Theorem 2.1.1 is not valid for discontinuous functions. This means that the Navier-Stokes equations are valid in each phase, but with different material properties ρ_i and μ_i, $i = 1, 2$, for each phase respectively.

In the case of the two-phase flow, the Navier-Stokes equations have to be completed by coupling conditions, that represent the balances of physical quantities across the interface, also called *jump conditions* or *interface conditions*. In order to derive these jump conditions a transport theorem is needed, that is valid for discontinuous, but domain-wise smooth functions. Those are functions that are smooth in each phase, but are allowed to exhibit a jump across the interface, are called *domain-wise continuous* or *domain-wise smooth* in the following.

Because the interface itself can have physical properties, which have to be considered in the balance equations, another transport theorem for control volumes on the interface is needed. These fundamental theorems are laid out in the following, starting with the definition of the jump of a function over the interface.

In the following $\mathbf{n}_\Gamma : \mathcal{Q}_\Gamma(t_0, t_b) \to \mathbb{R}^d$ denotes the normal to $\Gamma(t)$. The convention that the normal $\mathbf{n}_\Gamma$ is oriented such that it points outward $\Omega_1(t)$ into $\Omega_2(t)$ is used, as shown in Figure 2.1.

Definition 2.2.1. *Let $f : \mathcal{Q}(t_0, t_b) \to \mathbb{R}$ be a domain-wise continuous function with $f|_{\mathcal{Q}_i(t_0,t_b)} \in C^0(\mathcal{Q}_i(t_0, t_b))$, for $i = 1, 2$. The jump across $\Gamma(t)$ is defined as*

$$[\![f]\!]_\Gamma(\mathbf{x}, t) := \lim_{h \to +0} \left(f(\mathbf{x} - h\mathbf{n}_\Gamma(\mathbf{x}, t), t) - f(\mathbf{x} + h\mathbf{n}_\Gamma(\mathbf{x}, t), t) \right) ,$$

for $\mathbf{x} \in \Gamma(t)$.

In general, the interface can have a velocity different than the surrounding fluid. For example, if the interface itself has a mass, and can act as a source or sink of particles from the bulk domains. Even if the interface is assumed to be of zero mass, it can have a different velocity as the fluid, if a phase transition is allowed, or if there is no friction between the fluid and the tangential components of the velocity differ. Although, all these cases are neglected later on, for a general transport theorem these conditions have to be considered. Thus, a separate interface velocity $\mathbf{w}_\Gamma : \mathcal{Q}_\Gamma(t_0, t_b) \to \mathbb{R}^d$ is introduced. With this notation the following transport theorem holds:

Lemma 2.2.1 (Transport theorem)**.** *Let $\mathcal{V}(t)$ be a material volume with velocity $\mathbf{u}$, containing a part of the interface $\mathcal{W}(t) \subset \Gamma(t)$ with the velocity $\mathbf{w}_\Gamma$. Further, let $f : \mathcal{Q}(t_0, t_b) \to \mathbb{R}^d$ be a domain-wise continuous function with $f|_{\mathcal{Q}_i(t_0,t_b)} \in C^1(\mathcal{Q}_i(t_0, t_b))$, for $i = 1, 2$, then the following transport theorem holds*

$$\frac{d}{dt} \int_{\mathcal{V}(t)} f \, \mathrm{d}V = \int_{\mathcal{V}(t)} \partial_t f + \nabla \cdot (f\mathbf{u}) \, \mathrm{d}V + \int_{\mathcal{W}(t)} [\![f(\mathbf{w}_\Gamma - \mathbf{u})]\!]_\Gamma \cdot \mathrm{d}\mathbf{A} , \tag{2.2.1}$$

for $t \in (t_0, t_b)$.

Proof. The proof is based on applying the Reynolds transport theorem (2.1.3) in each bulk domain, where (2.1.3) is valid. At every time $t \in (t_0, t_b)$ the $\mathcal{V}(t)$ can be decomposed in $\mathcal{V}_1(t) \subset \Omega_1(t)$ and $\mathcal{V}_2(t) \subset \Omega_2(t)$ with $\overline{\mathcal{V}(t)} = \overline{\mathcal{V}_1(t)} \cup \overline{\mathcal{V}_2(t)}$ and $\mathcal{W}(t) = \overline{\mathcal{V}_1(t)} \cap \overline{\mathcal{V}_2(t)}$. In the domains $\mathcal{V}_i(t)$, $i = 1, 2$ the Reynolds transport theorem (2.1.3) is applied as follows

$$\begin{aligned}
\frac{d}{dt} \int_{\mathcal{V}(t)} f \, \mathrm{d}V &= \frac{d}{dt} \int_{\mathcal{V}_1(t)} f \, \mathrm{d}V + \frac{d}{dt} \int_{\mathcal{V}_2(t)} f \, \mathrm{d}V \\
&= \int_{\mathcal{V}_1(t)} \partial_t f \, \mathrm{d}V + \int_{\partial\mathcal{V}_1(t)} f|_{\mathcal{V}_1(t)} \mathbf{v}_1 \cdot \mathrm{d}\mathbf{A} \\
&\quad + \int_{\mathcal{V}_2(t)} \partial_t f \, \mathrm{d}V + \int_{\partial\mathcal{V}_2(t)} f|_{\mathcal{V}_2(t)} \mathbf{v}_2 \cdot \mathrm{d}\mathbf{A} ,
\end{aligned}$$

where $\mathbf{v}_i$, $i = 1, 2$ is the velocity on the boundary of $\mathcal{V}_i(t)$, $i = 1, 2$, respectively. Since

$\mathbf{v}_i = \mathbf{u}$ on $\partial\mathcal{V}(t)$ and $\mathbf{v}_i = \mathbf{w}_\Gamma$ on $\mathcal{W}(t)$ for $i = 1, 2$ it follows

$$\begin{aligned}\frac{d}{dt}\int_{\mathcal{V}(t)} f \,\mathrm{d}V &= \int_{\mathcal{V}(t)} \partial_t f \,\mathrm{d}V + \int_{\partial\mathcal{V}(t)} f\mathbf{u}\cdot\mathrm{d}\mathbf{A} \\ &\quad + \int_{\mathcal{W}(t)} f|_{\mathcal{V}_1(t)}\mathbf{w}_\Gamma\cdot\mathrm{d}\mathbf{A} - \int_{\mathcal{W}(t)} f|_{\mathcal{V}_2(t)}\mathbf{w}_\Gamma\cdot\mathrm{d}\mathbf{A} \\ &= \int_{\mathcal{V}(t)} \partial_t f \,\mathrm{d}V + \int_{\partial\mathcal{V}(t)} f\mathbf{u}\cdot\mathrm{d}\mathbf{A} + \int_{\mathcal{W}(t)} [\![f]\!]_\Gamma\mathbf{w}_\Gamma\cdot\mathrm{d}\mathbf{A}\ ,\end{aligned}$$

where the orientation of the normals was taken into account. Applying the Gauss theorem[1] on the boundary integral term over $\partial\mathcal{V}(t)$, it follows

$$\begin{aligned}\frac{d}{dt}\int_{\mathcal{V}(t)} f \,\mathrm{d}V &= \int_{\mathcal{V}(t)} \partial_t f + \nabla\cdot(f\mathbf{u}) \,\mathrm{d}V - \int_{\mathcal{W}(t)} [\![f\mathbf{u}]\!]_\Gamma\cdot\mathrm{d}\mathbf{A} + \int_{\mathcal{W}(t)} [\![f]\!]_\Gamma\mathbf{w}_\Gamma\cdot\mathrm{d}\mathbf{A} \\ &= \int_{\mathcal{V}(t)} \partial_t f + \nabla\cdot(f\mathbf{u}) \,\mathrm{d}V + \int_{\mathcal{W}(t)} [\![f(\mathbf{w}_\Gamma - \mathbf{u})]\!]_\Gamma\cdot\mathrm{d}\mathbf{A}\ ,\end{aligned}$$

which concludes the proof. □

A transport theorem on hypersurfaces holds as follows:

Lemma 2.2.2 (Transport theorem on surfaces)**.** *Let $\mathcal{W}(t) \subset \Gamma(t)$ be a control volume on the interface $\Gamma(t)$ moving with the velocity $\mathbf{v}$, and let $f : \mathcal{Q}_\Gamma(t_0, t_b) \to \mathbb{R}$ be a function defined on $\Gamma(t)$, and sufficiently smooth, then the following identity holds*

$$\frac{d}{dt}\int_{\mathcal{W}(t)} f_\Gamma \,\mathrm{d}A = \int_{\mathcal{W}(t)} \partial_t^{\mathbf{v}} f_\Gamma + f_\Gamma\nabla_\Gamma\cdot\mathbf{v} \,\mathrm{d}A\ , \tag{2.2.2}$$

for $t \in (t_0, t_b)$.

Proof. The proof can be found in [50, Lemma 5.1]. □

Remark 2.2.1. *The velocity $\mathbf{v}$ of the control volume $\mathcal{W}(t)$ can be decomposed into the velocity of the interface $\mathbf{w}_\Gamma$ plus a tangential velocity component $\mathbf{v}_t$, such that $\mathbf{v} = \mathbf{w}_\Gamma + \mathbf{v}_t$. The surface transport theorem can be written in the form*

$$\frac{d}{dt}\int_{\mathcal{W}(t)} f_\Gamma \,\mathrm{d}A = \int_{\mathcal{W}(t)} \partial_t^{\mathbf{w}_\Gamma} f_\Gamma + \nabla_\Gamma\cdot(f_\Gamma\mathbf{v}_t) + f_\Gamma\nabla_\Gamma\cdot\mathbf{w}_\Gamma \,\mathrm{d}A\ , \tag{2.2.3}$$

where the time derivative is with respect to $\mathbf{w}_\Gamma$.

In order to derive the coupling conditions, the limit $\delta \to 0$ for balances in a series of material volumes $\mathcal{V}_\delta(t)$ of special shape is considered. The material volumes are such that at time t, they have the shape of a thin layer around $\mathcal{W}(t)$ of thickness δ. A material volume $\mathcal{V}_\delta(t)$ is the result of the extrusion of $\mathcal{W}(t)$ by the amount $\pm\delta$ along the normal $\mathbf{n}_\Gamma$ into the adjacent bulk domain (Figure 2.2). Since the shape of $\mathcal{V}_\delta(t)$ is a curved box, it will also called *box material volume*, here. Further notations regarding the box material volume are introduced as follows. For a vivid representation see Figure 2.2.

[1] Gauss theorem for a domain-wise smooth flux Φ: $\int_{\mathcal{V}} \nabla\cdot\Phi \,\mathrm{d}V = \int_{\partial\mathcal{V}} \Phi\cdot\mathrm{d}\mathbf{A} + \int_{\mathcal{W}} [\![\Phi]\!]_\Gamma\cdot\mathrm{d}\mathbf{A}$.

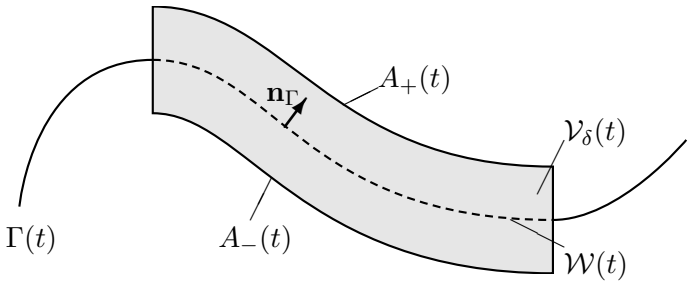

Figure 2.2: Box shaped material volume

Definition 2.2.2 (Box material volume)**.** *Let $\mathcal{W}(t)$ be an arbitrary subset of $\Gamma(t)$, with the normal $\mathbf{n}_\Gamma$. Further, let $\delta \in \mathbb{R}$, $\delta > 0$, the material volume $\mathcal{V}_\delta(t)$ is defined as*

$$\mathcal{V}_\delta(t) := \left\{ \mathbf{x} \in \mathbb{R}^d : \mathbf{x} = \mathbf{x}_0 + d\mathbf{n}_\Gamma,\ \mathbf{x}_0 \in \mathcal{W}(t),\ d \in \mathbb{R} : |d| < \delta \right\} .$$

The top surface of $\mathcal{V}_\delta(t)$ is $A_\pm(t) = A_+(t) \cup A_-(t)$, with

$$A_+(t) := \left\{ \mathbf{x} \in \mathbb{R}^d :\ \mathbf{x} = \mathbf{x}_0 + \delta\mathbf{n}_\Gamma,\ \mathbf{x}_0 \in \mathcal{W}(t) \right\} ,$$
$$A_-(t) := \left\{ \mathbf{x} \in \mathbb{R}^d :\ \mathbf{x} = \mathbf{x}_0 - \delta\mathbf{n}_\Gamma,\ \mathbf{x}_0 \in \mathcal{W}(t) \right\} ,$$

and the remaining, lateral surfaces of $\mathcal{V}_\delta(t)$ are $\mathcal{R}(t) = \partial\mathcal{V}_\delta(t) \setminus A_\pm(t)$.

A limit for $\delta \to 0$ is considered from which coupling conditions can be derived.

Lemma 2.2.3. *Let $\mathcal{V}_\delta(t)$ be boxed material volume, and let $\Phi : \mathcal{Q}(t_0, t_b) \to \mathbb{R}^d$ be a domain-wise smooth vector field, with $\Phi|_{\mathcal{Q}_i(t_0,t_b)} \in C^0(\mathcal{Q}_i(t_0, t_b))^d$, for $i = 1, 2$, and Φ is bounded in a neighbourhood of $\mathcal{W}(t)$. Further, let $\phi : \mathcal{Q}(t_0, t_b) \to \mathbb{R}$ be a function with $\phi \in C^0(\mathcal{Q}(t_0, t_b))$. Then, the following holds*

$$\lim_{\delta\to 0} \int_{\partial\mathcal{V}_\delta(t)} \Phi \cdot \mathrm{d}\mathbf{A} = -\int_{\mathcal{W}(t)} [\![\Phi]\!]_\Gamma \cdot \mathrm{d}\mathbf{A} , \tag{2.2.4}$$

and

$$\lim_{\delta\to 0} \int_{\mathcal{V}_\delta(t)} \phi \ \mathrm{d}V = 0 , \tag{2.2.5}$$

for $t \in (t_0, t_b)$.

Proof. For fixed $t \in (t_0, t_b)$ and $\delta > 0$, let $\eta_t : \mathcal{W}_0 \to \mathcal{W}(t)$ be a parametrization $\mathcal{W}(t)$, with $(u, v) \in \mathcal{W}_0 \mapsto \mathbf{x} \in \mathcal{W}(t)$. Then, a parametrization $\gamma_t : \mathcal{W}_0 \to A_+$ of A_+ is given as

$$\gamma_t = \eta_t + \delta\mathbf{n}_\Gamma .$$

The following holds

$$\begin{aligned}\lim_{\delta\to 0}\int_{A_+}\Phi\ \mathrm{d}A &= \lim_{\delta\to 0}\iint_{\mathcal{W}_0}\Phi\cdot(\partial_u\gamma_t\times\partial_v\gamma_t)\,\mathrm{d}u\,\mathrm{d}v\\ &= \lim_{\delta\to 0}\iint_{\mathcal{W}_0}\Phi\cdot(\partial_u\eta_t\times\partial_v\eta_t+\mathcal{O}(\delta))\,\mathrm{d}u\,\mathrm{d}v\\ &= \iint_{\mathcal{W}_0}\Phi\cdot(\partial_u\eta_t\times\partial_v\eta_t)\,\mathrm{d}u\,\mathrm{d}v\\ &= \int_{\mathcal{W}(t)}\Phi|_{\Omega_2(t)}\cdot\mathrm{d}\mathbf{A}\ .\end{aligned}$$

An analogue identity is derived in the same way for A_-, but with an opposite sign, because of the orientation of the normals

$$\lim_{\delta\to 0}\int_{A_-}\Phi\ \mathrm{d}A = -\int_{\mathcal{W}(t)}\Phi|_{\Omega_1(t)}\cdot\mathrm{d}\mathbf{A}\ .$$

The integral over the remaining surface $\mathcal{R}(t)$ vanishes, since $\mathcal{R}(t)$ vanishes for $\delta\to 0$ and Φ is bounded, thus

$$\begin{aligned}\lim_{\delta\to 0}\int_{\partial\mathcal{V}_\delta(t)}\Phi\cdot\mathrm{d}\mathbf{A} &= \lim_{\delta\to 0}\int_{A_+}\Phi\cdot\mathrm{d}\mathbf{A}+\lim_{\delta\to 0}\int_{A_-}\Phi\cdot\mathrm{d}\mathbf{A}+\lim_{\delta\to 0}\int_{\mathcal{R}(t)}\Phi\cdot\mathrm{d}\mathbf{A}\\ &= \int_{\mathcal{W}(t)}\Phi|_{\Omega_2(t)}\cdot\mathrm{d}\mathbf{A}-\int_{\mathcal{W}(t)}\Phi|_{\Omega_1(t)}\cdot\mathrm{d}\mathbf{A}\\ &= -\int_{\mathcal{W}(t)}[\![\Phi]\!]_\Gamma\ \mathrm{d}A\ .\end{aligned}$$

The second statement follows directly from the continuity of ϕ, which concludes the proof. □

All tools needed to derive the coupling conditions are available now. Next, the balances for mass and momentum in material volumes with an interface will be derived.

2.2.1 Mass Balance

The mass balance for a material volume $\mathcal{V}(t)$ containing a part $\mathcal{W}(t)\subset\Gamma(t)$ of the interface is derived. For the moment, the interface is allowed to have a mass itself, and there can be a mass exchange between the interface and the bulk domain. In the following. let $\rho_\Gamma:\mathcal{Q}_\Gamma(t_0,t_b)\to\mathbb{R}$ be the mass density of the interface.

Since, $\mathcal{V}(t)$ is a material volume, a particle can only enter or leave $\mathcal{V}(t)$ through the interface $\partial\mathcal{W}(t)$. Thus, it must hold

$$\frac{d}{dt}\int_{\mathcal{V}(t)}\rho\ \mathrm{d}V+\frac{d}{dt}\int_{\mathcal{W}(t)}\rho_\Gamma\ \mathrm{d}A=\int_{\partial\mathcal{W}(t)}\Pi_{\rho_\Gamma}\cdot\mathrm{d}\mathbf{C}\ ,$$

where $\Pi_{\rho_\Gamma} : \mathcal{Q}_\Gamma(t_0, t_b) \to \mathbb{R}^d$ models mass of the interface entering the volume through $\partial\mathcal{W}(t)$, that will not specified further. Note, that Π_{ρ_Γ} is needed, since $\mathcal{W}(t)$ is not necessary a material volume regarding the interface. Neglecting the contribution of mass through $\partial\mathcal{W}(t)$ would result in the wrong balance.

Applying the transport theorems for the bulk domain (2.2.1) and the surface (2.2.3) on material volumes, that are box material volumes, gives

$$\int_{\mathcal{V}_\delta(t)} \partial_t \rho + \nabla \cdot (\rho \mathbf{u}) \, \mathrm{d}V + \int_{\mathcal{W}(t)} [\![\rho(\mathbf{w}_\Gamma - \mathbf{u})]\!]_\Gamma \cdot \mathrm{d}\mathbf{A} \\ + \int_{\mathcal{W}(t)} \partial_t^{\mathbf{w}_\Gamma} \rho_\Gamma + \nabla_\Gamma \cdot (\rho_\Gamma \mathbf{v}_t) + \rho_\Gamma \nabla_\Gamma \cdot \mathbf{w}_\Gamma \, \mathrm{d}A = \int_{\partial\mathcal{W}(t)} \Pi_{\rho_\Gamma} \cdot \mathrm{d}\mathbf{C} \; .$$

Taking the limit $\delta \to 0$ by using (2.2.5) and applying the surface divergence theorem (1.1.2) on the right hand side, delivers

$$\int_{\mathcal{W}(t)} \{ [\![\rho \, (\mathbf{w}_\Gamma - \mathbf{u})]\!]_\Gamma \cdot \mathbf{n}_\Gamma + \partial_t^{\mathbf{w}_\Gamma} \rho_\Gamma + \nabla_\Gamma \cdot (\rho_\Gamma \mathbf{v}_t) + \rho_\Gamma \nabla_\Gamma \cdot \mathbf{w}_\Gamma \} \, \mathrm{d}A \\ = \int_{\mathcal{W}(t)} \nabla_\Gamma \cdot \Pi_{\rho_\Gamma} \, \mathrm{d}A - \int_{\mathcal{W}(t)} \mathcal{H} \Pi_{\rho_\Gamma} \cdot \mathrm{d}\mathbf{A} \; ,$$

for an arbitrary material volume $\mathcal{W}(t) \subset \Gamma(t)$ on the interface. The localisation procedure results in the *mass balance coupling condition.*

$$[\![\rho \, (\mathbf{w}_\Gamma - \mathbf{u})]\!]_\Gamma \cdot \mathbf{n}_\Gamma + \partial_t^{\mathbf{w}_\Gamma} \rho_\Gamma + \nabla_\Gamma \cdot (\rho_\Gamma \mathbf{v}_t) + \rho_\Gamma \nabla_\Gamma \cdot \mathbf{w}_\Gamma = \nabla_\Gamma \cdot \Pi_{\rho_\Gamma} - \mathcal{H} \Pi_{\rho_\Gamma} \mathbf{n}_\Gamma, \text{ on } \Gamma(t) \; .$$

Assuming the interface can not have a mass itself, the surface density is zero $\rho_\Gamma = 0$ and with it $\Pi_{\rho_\Gamma} = 0$, too. The coupling condition is reduced to

$$[\![\rho(\mathbf{w}_\Gamma - \mathbf{u})]\!]_\Gamma \cdot \mathbf{n}_\Gamma = 0 \quad \text{on } \Gamma(t) \; . \tag{2.2.6}$$

If the velocity $\mathbf{u}$ of the fluid is assumed to be continuous, it holds $[\![\mathbf{u}]\!]_\Gamma = 0$ and (2.2.6) can be written as $[\![\rho]\!]_\Gamma (\mathbf{w}_\Gamma - \mathbf{u}) \cdot \mathbf{n}_\Gamma = 0$. Thus, the coupling condition (2.2.6) is fulfilled if

$$[\![\mathbf{u}]\!]_\Gamma = 0, \quad \text{and} \quad \mathbf{w}_\Gamma \cdot \mathbf{n}_\Gamma = \mathbf{u} \cdot \mathbf{n}_\Gamma \quad \text{on } \Gamma(t) \; . \tag{2.2.7}$$

The equations (2.2.7) are the final coupling condition for the mass balance.

2.2.2 Momentum Balance

The same approach is used for the momentum balance. A surface momentum density $\mathbf{p}_\Gamma : \mathcal{Q}_\Gamma(t_0, t_b) \to \mathbb{R}^d$, with $\mathbf{p}_\Gamma = \rho_\Gamma \mathbf{w}_\Gamma$ is introduced. A change in momentum of the bulk and the interface can happen through different ways:

(i) External forces,

(ii) surface forces acting $\partial\mathcal{V}(t)$ induced by the surrounding bulk fluid,

(iii) and line forces acting on $\partial\mathcal{W}(t)$ induced by the surrounding interface.

All other internal forces must cancel each other, due to Newtons actio-reactio principle [83, 84]. Thus, the following abstract momentum balance for a material volume $\mathcal{V}(t)$, that contains a part $\mathcal{W}(t)$ of the interface, can be established

$$\begin{aligned}\frac{d}{dt}\int_{\mathcal{V}(t)} \mathbf{p}\ \mathrm{d}V + \frac{d}{dt}\int_{\mathcal{W}(t)} \mathbf{p}_\Gamma\ \mathrm{d}A \\ = \int_{\mathcal{V}(t)} \rho\mathbf{g}\ \mathrm{d}V + \int_{\mathcal{W}(t)} \rho_\Gamma\mathbf{g}\ \mathrm{d}A + \int_{\partial\mathcal{V}(t)} \mathbb{S}(\mathbf{u},p)\cdot\ \mathrm{d}\mathbf{A} + \int_{\partial\mathcal{W}(t)} \mathbb{S}_\Gamma\cdot\ \mathrm{d}\mathbf{C}\ .\end{aligned}$$

The stress tensor $\mathbb{S}(\mathbf{u},p)$ for the bulk phases was already specified in the last section. Now, a surface stress tensor $\mathbb{S}_\Gamma : \mathcal{Q}_\Gamma(t_0,t_b) \to \mathbb{R}^{d\times d}$ needs to be introduced. The surface stress tensor models the forces coming from the interface, such as the surface tension force. The tensor $\mathbb{S}_\Gamma$ will be specified later.

Applying the transport theorems (2.2.1) and (2.2.3) component-wise for box material volumes $\mathcal{V}_\delta(t)$, and using the Gauss theorem on surfaces, gives the following momentum balance

$$\begin{aligned}&\int_{\mathcal{V}_\delta(t)} \partial_t\mathbf{p} + \nabla\cdot(\mathbf{p}\otimes\mathbf{u})\ \mathrm{d}V + \int_{\mathcal{W}(t)} [\![\mathbf{p}\otimes(\mathbf{w}_\Gamma-\mathbf{u})]\!]_\Gamma\cdot\ \mathrm{d}\mathbf{A} \\ &\qquad + \int_{\mathcal{W}(t)} \partial_t^{\mathbf{w}_\Gamma}\mathbf{p}_\Gamma + \nabla_\Gamma\cdot(\mathbf{p}_\Gamma\otimes\mathbf{v}_t) + \mathbf{p}_\Gamma\nabla_\Gamma\cdot\mathbf{w}_\Gamma\ \mathrm{d}A \\ &= \int_{\mathcal{V}_\delta(t)} \rho\mathbf{g}\ \mathrm{d}V + \int_{\partial\mathcal{V}_\delta(t)} \mathbb{S}(\mathbf{u},p)\cdot\ \mathrm{d}\mathbf{A} + \int_{\mathcal{W}(t)} \rho_\Gamma\mathbf{g}\ \mathrm{d}A \\ &\qquad + \int_{\mathcal{W}(t)} \nabla_\Gamma\cdot\mathbb{S}_\Gamma\ \mathrm{d}A - \int_{\mathcal{W}(t)} \mathcal{H}\mathbb{S}_\Gamma\cdot\ \mathrm{d}\mathbf{A}\ .\end{aligned}$$

Proceeding to the limit $\delta\to 0$ by using (2.2.4) and (2.2.5), and applying the localisation procedure, the momentum balance becomes the following coupling condition

$$\begin{aligned}&[\![\mathbf{p}\otimes(\mathbf{w}_\Gamma-\mathbf{u})]\!]_\Gamma\mathbf{n}_\Gamma + \partial_t^{\mathbf{w}_\Gamma}\mathbf{p}_\Gamma + \nabla_\Gamma\cdot(\mathbf{p}_\Gamma\otimes\mathbf{v}_t) + \mathbf{p}_\Gamma\nabla_\Gamma\cdot\mathbf{w}_\Gamma \\ &\qquad = -[\![\mathbb{S}(\mathbf{u},p)]\!]_\Gamma\mathbf{n}_\Gamma + \rho_\Gamma\mathbf{g} + \nabla_\Gamma\cdot\mathbb{S}_\Gamma - \mathcal{H}\mathbb{S}_\Gamma\mathbf{n}_\Gamma \qquad \text{on } \Gamma(t)\ .\end{aligned}$$

Since, it is assumed that the interface has no mass, the coupling condition simplifies further. With $\mathbf{p}_\Gamma = \rho_\Gamma\mathbf{w}_\Gamma = 0$ the momentum coupling condition gets

$$[\![\mathbf{p}\otimes(\mathbf{w}_\Gamma-\mathbf{u})]\!]_\Gamma\mathbf{n}_\Gamma + [\![\mathbb{S}(\mathbf{u},p)]\!]_\Gamma\mathbf{n}_\Gamma = \nabla_\Gamma\cdot\mathbb{S}_\Gamma - \mathcal{H}\mathbb{S}_\Gamma\mathbf{n}_\Gamma \qquad \text{on } \Gamma(t)\ .$$

Using the mass jump condition (2.2.7) the momentum coupling condition finally reads

$$[\![\mathbb{S}(\mathbf{u},p)]\!]_\Gamma\mathbf{n}_\Gamma = \nabla_\Gamma\cdot\mathbb{S}_\Gamma - \mathcal{H}\mathbb{S}_\Gamma\mathbf{n}_\Gamma \qquad \text{on } \Gamma(t)\ . \tag{2.2.8}$$

All together, the full *Navier-Stokes equations for a two-phase flow* read:

Find $\mathbf{u} : \mathcal{Q}(t_0, t_b) \to \mathbb{R}^d$, $\mathbf{w}_\Gamma : \mathcal{Q}_\Gamma(t_0, t_b) \to \mathbb{R}^d$, and $p : \mathcal{Q}(t_0, t_b) \to \mathbb{R}$ such that for all $t \in (t_0, t_b)$

$$\begin{aligned}
\rho\left(\partial_t \mathbf{u} + \mathbf{u} \cdot \nabla \mathbf{u}\right) - \nabla \cdot \mathbb{S}(\mathbf{u}, p) &= \rho \mathbf{g} && \text{in } \Omega_i(t),\ i = 1, 2\ , \\
\nabla \cdot \mathbf{u} &= 0 && \text{in } \Omega_i(t),\ i = 1, 2\ , \\
[\![\mathbf{u}]\!]_\Gamma &= 0 && \text{on } \Gamma(t)\ , \\
(\mathbf{w}_\Gamma - \mathbf{u}) \cdot \mathbf{n}_\Gamma &= 0 && \text{on } \Gamma(t)\ , \\
[\![\mathbb{S}(\mathbf{u}, p)]\!]_\Gamma \mathbf{n}_\Gamma &= \nabla_\Gamma \cdot \mathbb{S}_\Gamma - \mathcal{H}\mathbb{S}_\Gamma \mathbf{n}_\Gamma && \text{on } \Gamma(t)\ .
\end{aligned}$$

As in the case for the standard Navier-Stokes equations, the equations have to be augmented with initial- and boundary conditions in order to get a well-posed problem.

2.3 Capillary Forces

In this subsection, a closer look to the surface stress tensor $\mathbb{S}_\Gamma$ is taken.

It is assumed, that for the surface stress tensor similar principles hold, as for the stress tensor $\mathbb{S}(\mathbf{u}, p)$ in the bulk phases. The surface stress tensor is linearly dependent on the *surface pressure* $\sigma : \mathcal{Q}_\Gamma(t_0, t_b) \to \mathbb{R}$ and the *surface deformation tensor* $\mathbb{D}_\Gamma(\mathbf{u}) : \mathcal{Q}_\Gamma(t_0, t_b) \to \mathbb{R}^{d \times d}$, with

$$\mathbb{D}_\Gamma(\mathbf{u}) = \frac{1}{2}\left(\nabla_\Gamma \mathbf{u} + (\nabla_\Gamma \mathbf{u})^T\right)\ ,$$

and has the form

$$\mathbb{S}_\Gamma(\mathbf{u}, \sigma) = \mathcal{L}(\mathbb{D}_\Gamma(\mathbf{u})) + \sigma \mathbb{P}_\Gamma\ ,$$

where $\mathcal{L} : \mathbb{R}^{d \times d} \to \mathbb{R}^{d \times d}$ is a linear mapping and $\mathbb{P}_\Gamma : \mathbb{R}^d \to \mathbb{R}^d$ is the surface projection $\mathbb{P}_\Gamma = \mathbb{I} - \mathbf{n}_\Gamma^T \mathbf{n}_\Gamma$.

The dynamic part $\mathcal{L}(\mathbb{D}_\Gamma(\mathbf{u}))$ will be neglected. Only a surface pressure is considered, the *surface tension*. Noting that $\mathbb{P}_\Gamma \mathbf{n}_\Gamma = 0$, the momentum coupling condition (2.2.8) becomes

$$[\![\mathbb{S}(\mathbf{u}, p)]\!]_\Gamma \mathbf{n}_\Gamma = \nabla_\Gamma \cdot (\sigma \mathbb{P}_\Gamma)\ .$$

Remark 2.3.1. *Note, that the projection operator $\mathbb{P}_\Gamma$ can be written as*

$$\mathbb{P}_\Gamma = \nabla_\Gamma id_\Gamma\ ,$$

where id_Γ is the identity function on $\Gamma(t)$. If the surface pressure σ is assumed to be constant σ_0, it holds

$$\nabla_\Gamma \cdot (\sigma_0 \mathbb{P}_\Gamma) = \sigma_0\, \Delta_\Gamma\, id_\Gamma\ .$$

Employing the Laplace-Beltrami identity $\Delta_\Gamma\, id_\Gamma = -\mathcal{H}\mathbf{n}_\Gamma$ the standard form of the momentum coupling condition for capillary flows appears:

$$[\![\mathbb{S}(\mathbf{u}, p)]\!]_\Gamma \mathbf{n}_\Gamma = -\sigma_0 \mathcal{H} \mathbf{n}_\Gamma\ ,$$

where σ_0 identifies as the surface tension coefficient, given by the material properties of the fluids forming the interface.

Further, if the fluids are at rest, i.e. $\mathbf{u} = 0$, the Young-Laplace equation is recovered:

$$[\![p]\!]_\Gamma = \sigma_0 \mathcal{H} \ .$$

Contrary to Remark 2.3.1, in this work the surface tension coefficient σ is allowed to vary over the interface. The surface tension coefficient is assumed to be a function of the surfactant concentrations at the interface. The dependencies are introduced later, after the surfactant transport equations are introduced in the next sections.

Remark 2.3.2. *The surface stress tensor used here, is a specialisation of the Boussinesq-Scriven model for the surface stress* [102, 106, 29]

$$\mathbb{S}_\Gamma(\mathbf{u}, \sigma) = (\sigma + (\lambda_\Gamma - \mu_\Gamma)(\nabla_\Gamma \cdot \mathbf{u}))\, \mathbb{P}_\Gamma + \mu_\Gamma \mathbb{D}_\Gamma(\mathbf{u}) \ .$$

If the shear and area viscous effects μ_Γ and λ_Γ are neglected the surface stress tensor used above is obtained.

The Navier-Stokes equations for the two-phase flow now read:

Find $\mathbf{u} : \mathcal{Q}(t_0, t_b) \to \mathbb{R}^d$, $\mathbf{w}_\Gamma : \mathcal{Q}_\Gamma(t_0, t_b) \to \mathbb{R}^d$, and $p : \mathcal{Q}(t_0, t_b) \to \mathbb{R}$ such that for all $t \in (t_0, t_b)$

$$\begin{aligned}
\rho\left(\partial_t \mathbf{u} + \mathbf{u} \cdot \nabla \mathbf{u}\right) - \nabla \cdot \mathbb{S}(\mathbf{u}, p) &= \rho \mathbf{g} && \text{in } \Omega_i(t),\ i = 1, 2 \ , \\
\nabla \cdot \mathbf{u} &= 0 && \text{in } \Omega_i(t),\ i = 1, 2 \ , \\
[\![\mathbf{u}]\!]_\Gamma &= 0 && \text{on } \Gamma(t) \ , \\
(\mathbf{w}_\Gamma - \mathbf{u}) \cdot \mathbf{n}_\Gamma &= 0 && \text{on } \Gamma(t) \ , \\
[\![\mathbb{S}(\mathbf{u}, p)]\!]_\Gamma \mathbf{n}_\Gamma - \nabla_\Gamma \cdot (\sigma \mathbb{P}_\Gamma) &= 0 && \text{on } \Gamma(t) \ ,
\end{aligned}$$

where these equations have to be completed with initial- and boundary conditions.

2.4 Surfactant Transport

In the following two subsections, the balances for the surfactant in bulk phases and on the interface are derived. This results in a system of transport equations for the surfactant. Note, that the surfactant will not be considered to be a separate fluid. Otherwise, the flow of a mixture of fluids would have to be considered. The mixture would then consist of the solvent and the solute. Instead, the surfactant concentrations are considered as an additional property of the fluid. Note, one consequence is that the assumption, that the interface has no mass, is admissible.

The surfactant concentration is a quantity attached to the particles of the fluids. As showed in the last section, a quantity f can undergo a change through external sources and fluxes. External forces act on the body of a material volume and fluxes act through the surface of a material volume. The fluxes model the exchange of f with the

surrounding fluid. In the last sections, for the Navier-Stokes equations, these quantities were the mass density and the momentum of the fluid. Now, these quantities will be the surfactant concentrations.

This means, in general a balance must have the following abstract form. For a material volume $\mathcal{V}(t)$ in the bulk, it must hold

$$\frac{d}{dt}\int_{\mathcal{V}(t)} f \, \mathrm{d}V = \int_{\mathcal{V}(t)} \mathcal{Q} \, \mathrm{d}V - \int_{\partial\mathcal{V}(t)} \mathbf{j} \cdot \mathrm{d}\mathbf{A} \, ,$$

where $\mathcal{Q}$ represents an external source and $\mathbf{j}$ a surface flux. The sign of the surface integral is a consequence of the normal pointing outward.

Analogue, for a material volume $\mathcal{W}(t)$ on the interface the abstract balance reads

$$\frac{d}{dt}\int_{\mathcal{W}(t)} f_\Gamma \, \mathrm{d}A = \int_{\mathcal{W}(t)} \mathcal{Q}_\Gamma \, \mathrm{d}A - \int_{\partial\mathcal{W}(t)} \mathbf{j}_\Gamma \cdot \mathrm{d}\mathbf{C} \, ,$$

where $\mathcal{Q}_\Gamma$ is the corresponding external source and $\mathbf{j}_\Gamma$ the corresponding surface flux.

The derivation of the transport equation follows the same approach as for the Navier-Stokes equations. Identifying the sources and fluxes by physical means, applying the appropriate transport theorem, and using the localisation procedure, that results in a partial differential equation. Considering a material volume containing a part of the interface will result in coupling conditions.

2.4.1 Bulk Surfactant Transport

Let $c_i : \mathcal{Q}_i(t_0, t_b) \to \mathbb{R}$ be surfactant concentrations of the bulk surfactant in the fluid domains $\Omega_i(t)$, for $i = 1, 2$.

It is assumed, that the bulk surfactant can not be created inside the bulk. Chemical reaction which could create surfactant molecules are neglected. This implies, that the external source vanishes, i.e. $\mathcal{Q} = 0$. Further, diffusion of surfactant can take place. The diffusion is modelled by *Fick's law* [108] in each phase. The diffusion flux reads

$$\mathbf{j}_i = -D_i \nabla c_i \, , \tag{2.4.1}$$

for $i = 1, 2$. The diffusion coefficient matrix D_i for the bulk phase $\Omega_i(t)$, is given by the material properties of the surfactant and the bulk fluids. For isotropic media, i.e. all directions are equal, D_i is a number. It is also assumed, that the fluid is homogeneous regarding the diffusion, such that D_i is a constant, for $i = 1, 2$.

In the following, let $\mathcal{V}_i(t) \subset \Omega_i(t)$ denote a material volume, that is a proper subset of $\Omega_i(t)$. Using the diffusion flux (2.4.1), the balance for the bulk surfactant is obtained

$$\frac{d}{dt}\int_{\mathcal{V}_i(t)} c_i \, \mathrm{d}V = \int_{\partial\mathcal{V}_i(t)} D_i \nabla c_i \cdot \mathrm{d}\mathbf{A} \, ,$$

for $i = 1, 2$.

Using the transport theorem (2.1.2) on the left side, and the Gauss theorem on the right side, the balance becomes

$$\int_{\mathcal{V}_i(t)} \partial_t c_i + \nabla \cdot (c_i \mathbf{u}) \, \mathrm{d}V = \int_{\mathcal{V}_i(t)} D_i \, \Delta \, c_i \, \mathrm{d}V \ .$$

The localisation procedure applied, a differential equation is obtained

$$\partial_t c_i + \nabla \cdot (c_i \mathbf{u}) = D_i \, \Delta \, c \ .$$

Using the mass balance equation (2.1.5) for $\mathbf{u}$, the final form of the transport equation of the bulk surfactant is derived.

$$\partial_t c_i + \mathbf{u} \cdot \nabla c_i = D_i \, \Delta \, c_i \qquad \text{in } \Omega_i(t) \ ,$$

for $i = 1, 2$ and $t \in (t_0, t_b)$.

2.4.2 Surface Surfactant Transport

Let $\gamma : \mathcal{Q}_\Gamma(t_0, t_b) \to \mathbb{R}$ be the surface surfactant.

The surface surfactant on the interface is surfactant that is adsorbed from the bulk phases. The bulk surfactant acts as an external source for the interface. Therefore, the source $\mathcal{Q}_\Gamma$ on the interface is not zero. It is assumed that $\mathcal{Q}_\Gamma$ is a function of the surfactant concentration

$$\mathcal{Q}_\Gamma = \mathcal{Q}_\Gamma(c_1, c_2, \gamma) \ .$$

The particular dependencies will be introduced later.

For the diffusion of the surface surfactant a Fick's law on the interface is assumed. The surface diffusion flux reads

$$\mathbf{j}_\Gamma = -D_\Gamma \nabla_\Gamma \gamma \ , \tag{2.4.2}$$

where D_Γ is the surface diffusion coefficient. Like in the bulk, the surface diffusion is assumed to be isotropic and homogeneous. Thus, D_Γ is a constant as well. The surface diffusion coefficient is given by the material properties.

For a material volume $\mathcal{W}(t)$ on the interface, the surface surfactant balance reads

$$\frac{d}{dt} \int_{\mathcal{W}(t)} \gamma \, \mathrm{d}A = \int_{\mathcal{W}(t)} \mathcal{Q}_\Gamma(c_1, c_2, \gamma) \, \mathrm{d}A + \int_{\partial \mathcal{W}(t)} D_\Gamma \nabla_\Gamma \gamma \cdot \, \mathrm{d}\mathbf{C} \ . \tag{2.4.3}$$

Applying the surface transport theorem (2.2.2) to the left hand side and using a surface divergence theorem on the line integral, the balance becomes

$$\int_{\mathcal{W}(t)} \partial_t^{\mathbf{u}} \gamma + \gamma \nabla_\Gamma \cdot \mathbf{u} \, \mathrm{d}A = \int_{\mathcal{W}(t)} \mathcal{Q}_\Gamma(c_1, c_2, \gamma) \, \mathrm{d}A + \int_{\mathcal{W}(t)} D_\Gamma \, \Delta_\Gamma \, \gamma \, \mathrm{d}A \ .$$

The localisation procedure generates a partial differential equation on the surface for the surfactant transport

$$\partial_t^{\mathbf{u}} \gamma + \gamma \nabla_\Gamma \cdot \mathbf{u} = \mathcal{Q}_\Gamma(c_1, c_2, \gamma) + D_\Gamma \, \Delta_\Gamma \, \gamma \quad \text{on } \Gamma(t) \ , \tag{2.4.4}$$

for $t \in (t_0, t_b)$.

2.5 Coupled Problem

A coupling condition is needed for the surfactant transport equation. In order to derive the coupling condition, a material volume $\mathcal{V}(t)$ that contains a part of the interface is considered.

Since internal surfactant transport must cancel each other, the balance for the material volume $\mathcal{V}(t)$ reads

$$\frac{d}{dt}\int_{\mathcal{V}(t)} c \,\mathrm{d}V + \frac{d}{dt}\int_{\mathcal{W}(t)} \gamma \,\mathrm{d}A = -\int_{\partial\mathcal{V}(t)} \mathbf{j}\cdot \,\mathrm{d}\mathbf{A} - \int_{\partial\mathcal{W}(t)} \mathbf{j}_\Gamma \cdot \,\mathrm{d}\mathbf{C} \,.$$

The balances on a series of box material volumes $\mathcal{V}_\delta(t)$ are considered. Using the transport theorems (2.1.2) and (2.2.2) on the left hand side and applying the appropriate divergence theorems on the surface and line integrals on the right hand side, the balance becomes

$$\int_{\mathcal{V}_\delta(t)} \partial_t c + \nabla\cdot(c\mathbf{u}) \,\mathrm{d}V + \int_{\mathcal{W}(t)} \partial_t^{\mathbf{u}}\gamma + \gamma\nabla_\Gamma\cdot\mathbf{u} \,\mathrm{d}A = -\int_{\partial\mathcal{V}_\delta(t)} \mathbf{j}\cdot\,\mathrm{d}\mathbf{A} - \int_{\mathcal{W}(t)} \nabla_\Gamma\cdot\mathbf{j}_\Gamma \,\mathrm{d}A \,.$$

Taking the limit $\delta\to 0$ and using (2.2.4) and (2.2.5), it follows

$$\int_{\mathcal{W}(t)} [\![\mathbf{j}]\!]_\Gamma\cdot\,\mathrm{d}\mathbf{A} = \int_{\mathcal{W}(t)} \partial_t^{\mathbf{u}}\gamma + \gamma\nabla_\Gamma\cdot\mathbf{u} + \nabla_\Gamma\cdot\mathbf{j}_\Gamma \,\mathrm{d}A \,.$$

Using the localisation procedure and substituting the fluxes (2.4.1) and (2.4.2), the coupling condition for the surfactant is obtained

$$-[\![D\nabla c]\!]_\Gamma\cdot\mathbf{n}_\Gamma = \partial_t^{\mathbf{u}}\gamma + \gamma\nabla_\Gamma\cdot\mathbf{u} - D_\Gamma\,\Delta_\Gamma\,\gamma \qquad \text{on } \Gamma(t)\,.$$

Substituting the equation for the surface surfactant transport (2.4.4), the coupling condition takes its final form

$$-[\![D\nabla c]\!]_\Gamma\cdot\mathbf{n}_\Gamma = \mathcal{Q}_\Gamma(c_1,c_2,\gamma) \qquad \text{on } \Gamma(t)\,,$$

for $t\in(t_0,t_b)$.

The model equations for the *two-phase flow with soluble surfactant* read:

Find $\mathbf{u}$, $\mathbf{w}_\Gamma$, p, c and γ such that for all $t\in(t_0,t_b)$

$$\rho\left(\partial_t\mathbf{u} + (\mathbf{u}\cdot\nabla)\,\mathbf{u}\right) - \nabla\cdot\mathbb{S}(\mathbf{u},p) = \rho\mathbf{g} \qquad \text{in } \Omega_i(t),\ i=1,2\,, \tag{2.5.1a}$$

$$\nabla\cdot\mathbf{u} = 0 \qquad \text{in } \Omega_i(t),\ i=1,2\,, \tag{2.5.1b}$$

$$\partial_t c_i - D\,\Delta\,c_i + \mathbf{u}\cdot\nabla c_i = 0 \qquad \text{in } \Omega_i(t),\ i=1,2\,, \tag{2.5.1c}$$

$$\partial_t^{\mathbf{u}}\gamma - D_\Gamma\,\Delta_\Gamma\,\gamma + \gamma\nabla_\Gamma\cdot\mathbf{u} = \mathcal{Q}_\Gamma(c_1,c_2,\gamma) \qquad \text{on } \Gamma(t)\,, \tag{2.5.1d}$$

$$[\![\mathbf{u}]\!]_\Gamma = 0 \qquad \text{on } \Gamma(t)\,, \tag{2.5.1e}$$

$$(\mathbf{w}_\Gamma - \mathbf{u})\cdot\mathbf{n}_\Gamma = 0 \qquad \text{on } \Gamma(t)\,, \tag{2.5.1f}$$

$$[\![\mathbb{S}(\mathbf{u},p)]\!]_\Gamma\mathbf{n}_\Gamma + \nabla_\Gamma\cdot(\sigma\mathbb{P}_\Gamma) = 0 \qquad \text{on } \Gamma(t)\,, \tag{2.5.1g}$$

$$-[\![D\nabla c]\!]_\Gamma\cdot\mathbf{n}_\Gamma = \mathcal{Q}_\Gamma(c_1,c_2,\gamma) \qquad \text{on } \Gamma(t)\,. \tag{2.5.1h}$$

The equations have to be augmented with initial- and boundary conditions.

2.5.1 Soluble Surfactant

The surfactant that is dissolved in the bulk phases, can be adsorbed by the interface. Surfactant that is adsorbed on the interface can dissolve into each of the phases by a desorption process. The surfactant at the interface also has an influence on the surface pressure. The surfactant changes the surface tension coefficient $\sigma = \sigma(\gamma)$. The adsorption and desorption process, and the dependencies of the surface pressure are introduced in this section.

In general there is a correlation between surface pressure and surfactant concentrations in thin films, the *Gibb's equation of state* [81, 103]

$$\gamma = -\frac{1}{RT}\frac{d\sigma}{d\ln c} , \tag{2.5.2}$$

where R is the universal gas constant, and T is the temperature. Having a correlation between the bulk surfactant concentration and the surface surfactant concentration, a equation for the behaviour of the surface pressure can be derived. Considering equilibrium of the ad- and desorption dynamics, an equation of state for the surfactants is derived, also called the *adsorption isotherm*. With this adsorption isotherm the Gibbs equation (2.5.2) can be integrated and the surface tension is derived.

For the adsorption and desorption dynamics, it is assumed that the interface is a thin mono-layer, i.e. there is exactly one layer of surfactant molecules. There exist several models for such mono-layer films. Here, the *Langmuir model* is chosen. The Langmuir model results into multi-linear equations. From the Langmuir model a linearisation can be derived, resulting in the linear Henry model. The Henry model is valid for small changes in surface surfactant and is also considered here.

In the Langmuir model several assumptions are made. The places where the surfactant molecules can occupy the interface are called sites. For the sites the following three basic assumptions are:

(i) The interface consists of a finite number of sites per surface area, and every site is equivalent for every surfactant molecule.

(ii) The probability to occupy an empty site is independent from the sites in the neighbourhood.

(iii) There are no interaction between sites.

From this assumptions the ad- and desorption fluxes are derived.

The surface source $\mathcal{Q}_\Gamma$ is decomposed into two parts, $\mathcal{Q}_\Gamma = q_a + q_d$. Where, q_a represents the mass flux of surfactant adsorbing at the interface, and q_d the mass flux of surfactant desorbing from the interface. The rate of surfactant adsorption q_a from each phase $\Omega_i(t)$ depends linear on the surfactant concentration on the interface and the concentration in the bulk

$$q_a = k_a^i c_i \left(\gamma^\infty - \gamma\right) \quad \text{on } \Gamma(t) ,$$

since there is a finite number of sites on the interface. The maximum surfactant concentration possible, i.e. all sites are occupied, is denoted with γ^∞, and k_a^i is the rate of adsorption into the respective phase i. k_a^i is also called *adsorption coefficient* and is given as a material parameter. γ^∞ is also denoted as the *maximum packing concentration.*

The rate of surfactant desorption depends only linear on the amount of surfactant on the surface

$$q_d = -k_d^i \gamma \quad \text{on } \Gamma(t) \ ,$$

since there is no limit in sites for the surfactant in the bulk phases. k_d^i is the desorption coefficient into the respective phase i and given as a material parameter.

Together, the following source terms $\mathcal{Q}_\Gamma(c_i, \gamma)$ for each phase are obtained

$$\mathcal{Q}_\Gamma(c_i, \gamma) = k_a^i c_i \left(\gamma^\infty - \gamma\right) - k_d^i \gamma \ .$$

The total source $\mathcal{Q}_\Gamma(c_1, c_2, \gamma)$ is then

$$\mathcal{Q}_\Gamma(c_1, c_2, \gamma) = \sum_{i=1}^{2} \mathcal{Q}_\Gamma(c_i, \gamma) \quad \text{on } \Gamma(t) \ .$$

Both phases are in equilibrium to the interface, if the adsorption rates equal the desorption rates

$$\mathcal{Q}_\Gamma(c_i, \gamma) = 0 \ .$$

for $i = 1, 2$. Let $K_L^i = k_a^i / k_d^i$ be the Langmuir coefficient for phase $i = 1, 2$, the equilibrium condition results in

$$\gamma(c_i) = \gamma^\infty \frac{K_L^i c_i}{1 + K_L^i c_i} \quad \text{or} \quad c_i(\gamma) = \frac{\gamma}{K_L^i \left(\gamma^\infty - \gamma\right)} \ ,$$

as the Langmuir isotherms.

Using these isotherms to integrate the Gibb's equation results in different forms, depending whether the first or second form is used. With $c_i(\gamma)$ the *Szyszkowski equation of state* [103] is obtained

$$\sigma - \sigma_0 = -RT\gamma^\infty \ln(1 + K_L c_i) \ ,$$

where σ_0 is a reference surface tension, usually that of a clean interface.

Unfortunately, the Szyszkowski equation is not useful here, since it gives not a unique surface tension coefficient if the surfactant is soluble in both phases. Using the second form $\gamma(c_i)$ leads to the *Frumkin equation of state* [103]

$$\sigma - \sigma_0 = RT\gamma^\infty \ln\left(1 - \frac{\gamma}{\gamma^\infty}\right) \ .$$

Note, that the Frumkin equation is independent from the bulk phases. It delivers a unique surface tension coefficient, depending only on the surface surfactant concentration.

A linearisation of the Langmuir model results in the Henry model. An approximation for a low surfactant concentration on the interface compared to the maximum packing concentration, i.e. $\gamma/\gamma^\infty \to 0$ is

$$\mathcal{Q}_\Gamma(c_i, \gamma) = k_a^i \gamma^\infty c_i - k_d^i \gamma \ ,$$

which is the Henry model.

The corresponding isotherm is

$$\gamma/\gamma^\infty = K_H^i c_i \ ,$$

with the Henry coefficients $K_H^i = k_a^i/k_d^i$. This isotherm results in the following surface equation of state

$$\sigma - \sigma_0 = -RT\gamma \ .$$

In summary, the following jump conditions are obtained. For the Langmuir model it holds:

$$\begin{aligned}
&[\![\mathbb{S}(\mathbf{u}, p)]\!]_\Gamma \cdot \mathbf{n}_\Gamma = -\nabla_\Gamma \cdot (\sigma(\gamma)\mathbb{P}_\Gamma) \quad \text{with} \quad \sigma(\gamma) = \sigma_0 + RT\gamma^\infty \ln\left(1 - \frac{\gamma}{\gamma^\infty}\right) \ , \\
&-[\![D\nabla c]\!]_\Gamma \cdot \mathbf{n}_\Gamma = \sum_{i=1}^{2} k_a^i c_i \left(\gamma^\infty - \gamma\right) - k_d^i \gamma \ .
\end{aligned}$$

While for the Henry model the jump conditions read:

$$\begin{aligned}
&[\![\mathbb{S}(\mathbf{u}, p)]\!]_\Gamma \cdot \mathbf{n}_\Gamma = -\nabla_\Gamma \cdot (\sigma(\gamma)\mathbb{P}_\Gamma) \quad \text{with} \quad \sigma(\gamma) = \sigma_0 - RT\gamma \ , \\
&-[\![D\nabla c]\!]_\Gamma \cdot \mathbf{n}_\Gamma = \sum_{i=1}^{2} k_a^i \gamma^\infty c_i - k_d^i \gamma \ .
\end{aligned}$$

2.5.2 Insoluble Surfactant

In the case of an insoluble surfactant, the surfactant is restricted to the interface and can not dissolve into the bulk. The equations for the two-phase flow with an insoluble surfactant result from the equations for soluble surfactants. Setting the adsorption and desorption rates to zero, i.e. $\mathcal{Q}_\Gamma(c_1, c_2, \gamma) = 0$ and neglecting the bulk surfactant transport, the following system of equation is obtained:

Find $\mathbf{u}$, $\mathbf{w}_\Gamma$, p, and γ such that for all $t \in (t_0, t_b)$

$$\begin{aligned}
\rho\left(\partial_t \mathbf{u} + (\mathbf{u}\cdot\nabla)\,\mathbf{u}\right) - \nabla\cdot\mathbb{S}(\mathbf{u},p) &= \rho\mathbf{g} && \text{in } \Omega_i(t),\ i=1,2\ ,\\
\nabla\cdot\mathbf{u} &= 0 && \text{in } \Omega_i(t),\ i=1,2\ ,\\
\partial_t^{\mathbf{u}}\gamma - D_\Gamma\,\Delta_\Gamma\,\gamma + \gamma\nabla_\Gamma\cdot\mathbf{u} &= 0 && \text{on } \Gamma(t)\ ,\\
[\![\mathbf{u}]\!]_\Gamma &= 0 && \text{on } \Gamma(t)\ ,\\
(\mathbf{w}_\Gamma - \mathbf{u})\cdot\mathbf{n}_\Gamma &= 0 && \text{on } \Gamma(t)\ ,\\
[\![\mathbb{S}(\mathbf{u},p)]\!]_\Gamma\mathbf{n}_\Gamma - \nabla_\Gamma\cdot(\sigma\mathbb{P}_\Gamma) &= 0 && \text{on } \Gamma(t)\ ,
\end{aligned}$$

which have to be augmented with initial- and boundary conditions.

2.5.3 Free Surface Flow

In case of free surface flows the outer phase is neglected. All values in the phase $\Omega_2(t)$ are assumed to be zero. Therefore, the jump conditions become a boundary condition

$$[\![f]\!]_\Gamma(\mathbf{x},t) = \lim_{h\to+0} f(\mathbf{x} - h\mathbf{n}_\Gamma(\mathbf{x},t),t) - 0 = f|_{\partial\Omega_1(t)}(\mathbf{x},t)\ .$$

Substituting this into the equations for the two-phase flow with surfactant, results in:

Find $\mathbf{u}$, $\mathbf{w}_\Gamma$, p, c_1 and γ such that for all $t \in (t_0, t_b)$

$$\begin{aligned}
\rho\left(\partial_t \mathbf{u} + (\mathbf{u}\cdot\nabla)\,\mathbf{u}\right) - \nabla\cdot\mathbb{S}(\mathbf{u},p) &= \rho\mathbf{g} && \text{in } \Omega_1(t)\ ,\\
\nabla\cdot\mathbf{u} &= 0 && \text{in } \Omega_1(t)\ ,\\
\partial_t c_1 - D\,\Delta\,c_1 + \mathbf{u}\cdot\nabla c_1 &= 0 && \text{in } \Omega_1(t)\ ,\\
\partial_t^{\mathbf{u}}\gamma - D_\Gamma\,\Delta_\Gamma\,\gamma + \gamma\nabla_\Gamma\cdot\mathbf{u} &= \mathcal{Q}_\Gamma(c_1,\gamma) && \text{on } \partial\Omega_1(t)\ ,\\
(\mathbf{w}_\Gamma - \mathbf{u})\cdot\mathbf{n}_\Gamma &= 0 && \text{on } \partial\Omega_1(t)\ ,\\
\mathbb{S}(\mathbf{u},p)\mathbf{n}_\Gamma - \nabla_\Gamma\cdot(\sigma\mathbb{P}_\Gamma) &= 0 && \text{on } \partial\Omega_1(t)\ ,\\
-D\nabla c\cdot\mathbf{n}_\Gamma &= \mathcal{Q}_\Gamma(c_1,\gamma) && \text{on } \partial\Omega_1(t)\ ,
\end{aligned}$$

which have to be augmented with initial- and boundary conditions.

2.6 Dimensionless Formulation

The aim of this subsection is to introduce a dimensionless formulation of the equations (2.5.1a)–(2.5.1h). For a dimensionless formulation, all variables are transformed by scaling factors. The characteristics of the flow is then determined by these numbers.

First the Navier-Stokes equations are rescaled. Let the new dimensionless variables for time, position and the velocity and pressure be $\hat{t}$, $\hat{\mathbf{x}}$, $\hat{\mathbf{u}}$, and $\hat{p}$, respectively. Further, let L be a characteristics length scale, U be a characteristics velocity, and P be a characteristics pressure, the dimensionless variables are as follows

$$\hat{\mathbf{x}} = \frac{\mathbf{x}}{L}\ ,\quad \hat{\mathbf{u}} = \frac{\mathbf{u}}{U}\ ,\quad \hat{t} = \frac{U}{L}t\ ,\quad \hat{p} = \frac{p}{P}\ .$$

Substituting the variables into the Navier-Stokes equations, for each phase the following rescaling is obtained

$$\partial_{\hat{t}}\hat{\mathbf{u}} + (\hat{\mathbf{u}}\cdot\nabla_{\hat{\mathbf{x}}})\,\hat{\mathbf{u}} - \nabla_{\hat{\mathbf{x}}}\cdot\left[\frac{2\mu_i}{\rho_i UL}\hat{\mathbb{D}}(\hat{\mathbf{u}}) - \frac{P}{\rho_i U^2}\hat{p}\mathbb{I}\right] = \frac{gL}{U}\mathbf{e}_g \quad \text{in } \Omega_i(t)\ .$$

By choosing $P = \rho_1 U^2$ the dimensionless Navier-Stokes equations become in the inner domain $\Omega_1(t)$

$$\partial_{\hat{t}}\hat{\mathbf{u}} + (\hat{\mathbf{u}}\cdot\nabla_{\hat{\mathbf{x}}})\,\hat{\mathbf{u}} - \nabla_{\hat{\mathbf{x}}}\cdot\left[2\,\mathrm{Re}_1^{-1}\,\hat{\mathbb{D}}(\hat{\mathbf{u}}) - \hat{p}\mathbb{I}\right] = \mathrm{Fr}^{-1}\,\mathbf{e}_g \quad \text{in } \Omega_1(t)\ ,$$

and in the outer domain

$$\partial_{\hat{t}}\hat{\mathbf{u}} + (\hat{\mathbf{u}}\cdot\nabla_{\hat{\mathbf{x}}})\,\hat{\mathbf{u}} - \nabla_{\hat{\mathbf{x}}}\cdot\left[2\,\mathrm{Re}_2^{-1}\,\hat{\mathbb{D}}(\hat{\mathbf{u}}) - \frac{\rho_1}{\rho_2}\hat{p}\mathbb{I}\right] = \mathrm{Fr}^{-1}\,\mathbf{e}_g \quad \text{in } \Omega_2(t)\ .$$

Here, the Reynolds numbers Re_i and Froude number Fr

$$\mathrm{Re}_i = \frac{\rho_i UL}{\mu_i}\ ,\ i = 1,2\ ,\ \text{and} \quad \mathrm{Fr} = \frac{U^2}{gL}\ ,$$

are the first three characteristic dimensionless numbers.

Scaling with ρ_2/ρ_1 in the bulk phase $\Omega_2(t)$ leads to

$$\frac{\rho_2}{\rho_1}\left(\partial_{\hat{t}}\hat{\mathbf{u}} + (\hat{\mathbf{u}}\cdot\nabla_{\hat{\mathbf{x}}})\,\hat{\mathbf{u}}\right) - \nabla_{\hat{\mathbf{x}}}\cdot\left[2\frac{\rho_2}{\rho_1}\,\mathrm{Re}_2^{-1}\,\hat{\mathbb{D}}(\hat{\mathbf{u}}) - \hat{p}\mathbb{I}\right] = \frac{\rho_2}{\rho_1}\,\mathrm{Fr}^{-1}\,\mathbf{e}_g \quad \text{in } \Omega_2(t)\ ,$$

for the Navier-Stokes equation in $\Omega_2(t)$.

Introducing the fourth characteristic number ρ_1/ρ_2 as the density ratio, and setting

$$\varrho = \begin{cases} 1 & \text{in } \Omega_1(t) \\ \dfrac{\rho_2}{\rho_1} & \text{in } \Omega_2(t) \end{cases}\ , \quad \mathrm{Re} = \begin{cases} \mathrm{Re}_1 & \text{in } \Omega_1(t) \\ \mathrm{Re}_2 & \text{in } \Omega_2(t) \end{cases}\ ,$$

the Navier-Stokes equations are written as

$$\begin{aligned} \varrho\left(\partial_{\hat{t}}\hat{\mathbf{u}} + (\hat{\mathbf{u}}\cdot\nabla_{\hat{\mathbf{x}}})\,\hat{\mathbf{u}}\right) - \nabla_{\hat{\mathbf{x}}}\cdot\left[2\varrho\,\mathrm{Re}^{-1}\,\hat{\mathbb{D}}(\hat{\mathbf{u}}) - \hat{p}\mathbb{I}\right] &= \varrho\,\mathrm{Fr}^{-1}\,\mathbf{e}_g \qquad \text{in } \Omega_i(t), i = 1,2\ , \\ \nabla_{\hat{\mathbf{x}}}\cdot\mathbf{u} &= 0 \qquad \text{in } \Omega_i(t), i = 1,2\ . \end{aligned}$$

With the dimensionless stress tensor introduced as

$$\hat{\mathbb{S}}(\hat{\mathbf{u}},\hat{p}) = 2\varrho\,\mathrm{Re}^{-1}\,\hat{\mathbb{D}}(\hat{\mathbf{u}}) - \hat{p}\mathbb{I}\ ,$$

the jump of the stress tensor scales as follows

$$[\![\mathbb{S}(\mathbf{u},p)]\!]_\Gamma = \rho_1 U^2 [\![\hat{\mathbb{S}}(\hat{\mathbf{u}},\hat{p})]\!]_\Gamma = P[\![\hat{\mathbb{S}}(\hat{\mathbf{u}},\hat{p})]\!]_\Gamma\ .$$

Then, the momentum coupling condition becomes after scaling with L/σ_0

$$[\![\hat{\mathbb{S}}(\hat{\mathbf{u}},\hat{p})]\!]_\Gamma = \frac{\sigma_0}{\rho_1 U^2 L}\nabla_{\hat{\Gamma}}\cdot(\hat{\sigma}\mathbb{P}_\Gamma) = \mathrm{We}^{-1}\,\nabla_{\hat{\Gamma}}\cdot(\hat{\sigma}\mathbb{P}_\Gamma)\ ,$$

where the fifth characteristic number We and the sixth characteristic number E occur,

$$\mathrm{We} = \frac{\rho_1 U^2 L}{\sigma_0}\ ,\quad \hat{\sigma} = \begin{cases} 1+\mathrm{E}\ln\left(1+\dfrac{\gamma}{\gamma^\infty}\right) & \text{Langmuir} \\ 1-\mathrm{E}\,\dfrac{\gamma}{\gamma^\infty} & \text{Henry} \end{cases}\ ,\quad \mathrm{E} = \frac{RT\gamma^\infty}{\sigma_0}\ .$$

The number We is the Weber number and the number E is the surface elasticity.

The surfactant concentration are scaled by introducing a characteristic concentration C in the bulk phase, and using the maximum packing concentration as a characteristic concentration on the surface. The dimensionless surfactant concentration are given as follows

$$\hat{c}_i = \frac{c_i}{C}\ ,\ i=1,2\ ,\quad \hat{\gamma} = \frac{\gamma}{\gamma^\infty}\ .$$

The bulk concentration equation becomes

$$\partial_{\hat{t}}\hat{c}_i - \mathrm{Pe}_i^{-1}\,\Delta\,\hat{c}_i + \hat{\mathbf{u}}\cdot\nabla\hat{c}_i = 0 \quad \text{in } \Omega_i(t),\ i=1,2\ ,$$

with the two Peclet numbers

$$\mathrm{Pe}_i = \frac{UL}{D_i}\ ,\ i=1,2\ ,$$

which are the seventh and eighth characteristic numbers. The surface surfactant concentration equation scales as follows

$$\partial_{\hat{t}}^{\mathbf{u}}\hat{\gamma} - \mathrm{Pe}_\Gamma^{-1}\,\Delta_\Gamma\,\hat{\gamma} + \hat{\gamma}\nabla_\Gamma\cdot\hat{\mathbf{u}} = \hat{\mathcal{Q}}_\Gamma(\hat{c}_1,\hat{c}_2,\hat{\gamma})\ ,$$

with the surface Peclet number

$$\mathrm{Pe}_\Gamma = \frac{UL}{D_\Gamma}\ ,$$

which is the ninth characteristic number. The bulk surfactant jump condition gets

$$\begin{aligned} -[\![\mathrm{Pe}^{-1}\,\nabla\hat{c}]\!]_\Gamma\cdot\hat{\mathbf{n}}_\Gamma &= \frac{1}{UC}[\![D\nabla c]\!]_\Gamma\cdot\hat{\mathbf{n}}_\Gamma = \frac{1}{UC}\mathcal{Q}_\Gamma(c_1,c_2,\gamma) \\ &= \beta\,\hat{\mathcal{Q}}_\Gamma(\hat{c}_1,\hat{c}_2,\hat{\gamma})\ , \end{aligned}$$

with the characteristic numbers

$$\beta = \frac{\gamma^\infty}{LC}\ ,\quad \mathrm{Da} = \frac{k_a\gamma^\infty}{U}\ ,\quad \mathrm{Bi} = \frac{k_d L}{U}\ ,$$

and the dimensionless adsorption and desorption laws for $i = 1, 2$

$$\hat{\mathcal{Q}}_\Gamma(\hat{c}_i, \hat{\gamma}) = \begin{cases} \beta^{-1}\,\mathrm{Da}\,\hat{c}_i(1-\hat{\gamma}) - \mathrm{Bi}\,\hat{\gamma} & \text{Langmuir} \\ \beta^{-1}\,\mathrm{Da}\,\hat{c}_i - \mathrm{Bi}\,\hat{\gamma} & \text{Henry} \end{cases} .$$

This makes twelve characteristic numbers that have to be determined. In summary they are

$$\varrho = \begin{cases} 1 & \text{in } \Omega_1(t) \\ \dfrac{\rho_2}{\rho_1} & \text{in } \Omega_2(t) \end{cases} , \ \mathrm{Re} = \begin{cases} \dfrac{\rho_1 U L}{\mu_1} & \text{in } \Omega_1(t) \\ \dfrac{\rho_2 U L}{\mu_2} & \text{in } \Omega_2(t) \end{cases} , \ \mathrm{Fr} = \frac{U}{gL} , \ \mathrm{We} = \frac{\rho_1 U^2 L}{\sigma_0} ,$$

$$\mathrm{E} = \frac{RT\gamma^\infty}{\sigma_0} , \ \mathrm{Pe} = \begin{cases} \dfrac{UL}{D_1} & \text{in } \Omega_1(t) \\ \dfrac{UL}{D_2} & \text{in } \Omega_2(t) \end{cases} , \ \mathrm{Pe}_\Gamma = \frac{UL}{D_\Gamma} , \ \beta = \frac{\gamma^\infty}{LC} ,$$

$$\mathrm{Da} = \frac{k_a \gamma^\infty}{U} , \quad \mathrm{Bi} = \frac{k_d L}{U} .$$

The dimensionless model then reads

Find $\hat{\mathbf{u}}$, $\hat{\mathbf{w}}_\Gamma$, $\hat{p}$, $\hat{c}_i$, and $\hat{\gamma}$ such that for all $\hat{t} \in (\hat{t}_0, \hat{t}_b)$

$$\varrho\left(\partial_{\hat{t}}\hat{\mathbf{u}} + \hat{\mathbf{u}}\cdot\nabla_{\hat{\mathbf{x}}}\hat{\mathbf{u}}\right) - \nabla_{\hat{\mathbf{x}}}\cdot\hat{\mathbb{S}}(\hat{\mathbf{u}},\hat{p}) = \varrho\,\mathrm{Fr}^{-1}\,\mathbf{e}_g \qquad \text{in } \hat{\Omega}_i(\hat{t}),\ i=1,2\ , \qquad (2.6.1a)$$

$$\nabla_{\hat{\mathbf{x}}}\cdot\hat{\mathbf{u}} = 0 \qquad \text{in } \hat{\Omega}_i(\hat{t}),\ i=1,2\ , \qquad (2.6.1b)$$

$$\partial_{\hat{t}}\hat{c}_i - \mathrm{Pe}^{-1}\,\Delta_{\hat{\mathbf{x}}}\,\hat{c}_i + \hat{\mathbf{u}}\cdot\nabla_{\hat{\mathbf{x}}}\cdot\hat{c}_i = 0 \qquad \text{in } \hat{\Omega}_i(\hat{t}),\ i=1,2\ , \qquad (2.6.1c)$$

$$\partial_{\hat{t}}^{\mathbf{u}}\hat{\gamma} - \mathrm{Pe}_\Gamma^{-1}\,\Delta_{\hat{\Gamma}}\,\gamma + \hat{\gamma}\nabla_{\hat{\Gamma}}\cdot\hat{\mathbf{u}} = \hat{\mathcal{Q}}_\Gamma(\hat{c}_1,\hat{c}_2,\hat{\gamma}) \qquad \text{on } \hat{\Gamma}(\hat{t})\ , \qquad (2.6.1d)$$

$$[\![\hat{\mathbf{u}}]\!]_\Gamma = 0 \qquad \text{on } \hat{\Gamma}(\hat{t})\ , \qquad (2.6.1e)$$

$$(\hat{\mathbf{w}} - \hat{\mathbf{u}})\cdot\hat{\mathbf{n}_\Gamma} = 0 \qquad \text{on } \hat{\Gamma}(\hat{t})\ , \qquad (2.6.1f)$$

$$[\![\hat{\mathbb{S}}(\hat{\mathbf{u}},\hat{p})]\!]_\Gamma\hat{\mathbf{n}_\Gamma} - \mathrm{We}^{-1}\,\nabla_{\hat{\Gamma}}\cdot(\hat{\sigma}\mathbb{P}_\Gamma) = 0 \qquad \text{on } \hat{\Gamma}(\hat{t})\ , \qquad (2.6.1g)$$

$$-[\![\mathrm{Pe}^{-1}\,\nabla\hat{c}]\!]_\Gamma\cdot\hat{\mathbf{n}_\Gamma} = \beta\,\hat{\mathcal{Q}}_\Gamma(\hat{c}_1,\hat{c}_2,\hat{\gamma}) \qquad \text{on } \hat{\Gamma}(\hat{t})\ , \qquad (2.6.1h)$$

with appropriate initial- and boundary conditions.

The dimensionless model will be used in the remaining work, but the "hat" in the notation will be dropped.

2.7 Weak Formulation

Finally, the weak formulation of the model for the two-phase flow with soluble surfactants will be derived. What closes chapter two.

The momentum balance equation (2.6.1a) is multiplied with a test function $\mathbf{v}$ and integrated over each domain $\Omega_i(t)$, $i = 1, 2$, separately

$$\left(\varrho\left(\partial_t\mathbf{u} + \mathbf{u}\cdot\nabla\mathbf{u}\right),\mathbf{v}\right)_{\Omega_i(t)} - \left(\nabla\cdot\mathbb{S}(\mathbf{u},p),\mathbf{v}\right)_{\Omega_i(t)} = \left(\varrho\,\mathrm{Fr}^{-1}\,\mathbf{e}_g,\mathbf{v}\right)_{\Omega_i(t)} , \quad \text{for } i = 1,2\ .$$

The divergence of the stress tensor is integrated by parts for each domain

$$(\nabla \cdot \mathbb{S}(\mathbf{u},p),\mathbf{v})_{\Omega_i(t)} = -(\mathbb{S}(\mathbf{u},p),\nabla\mathbf{v})_{\Omega_i(t)} + \langle \mathbb{S}(\mathbf{u},p)\mathbf{n},\mathbf{v}\rangle_{\partial\Omega_i(t)} \ , \quad \text{for } i=1,2 \ .$$

A homogeneous Dirichlet boundary condition on $\partial\Omega(t)$ is assumed, and therefore $\mathbf{v} \in H_0^1(\Omega(t))^d$. Summing up the equations for $i=1,2$ and considering the vanishing test functions on $\partial\Omega(t)$, it holds

$$(\nabla \cdot \mathbb{S}(\mathbf{u},p),\mathbf{v})_{\Omega(t)} = \langle [\![\mathbb{S}(\mathbf{u},p)]\!]_\Gamma \mathbf{n}_\Gamma,\mathbf{v}\rangle_{\Gamma(t)} - (\mathbb{S}(\mathbf{u},p),\nabla\mathbf{v})_{\Omega(t)} \ .$$

After substituting the stress jump condition (2.6.1g) and applying integration by parts, it is obtained

$$\begin{aligned}(\nabla \cdot \mathbb{S}(\mathbf{u},p),\mathbf{v})_{\Omega(t)} &= \left\langle \mathrm{We}^{-1}\,\nabla_\Gamma\cdot(\sigma\mathbb{P}_\Gamma),\mathbf{v}\right\rangle_{\Gamma(t)} - (\mathbb{S}(\mathbf{u},p),\nabla\mathbf{v})_{\Omega(t)} \\ &= -\left\langle \mathrm{We}^{-1}\,\sigma\mathbb{P}_\Gamma,\nabla_\Gamma\mathbf{v}\right\rangle_{\Gamma(t)} - (\mathbb{S}(\mathbf{u},p),\nabla\mathbf{v})_{\Omega(t)} \, .\end{aligned}$$

Thus, the weak form of (2.6.1a) becomes

$$\left(\varrho\left(\partial_t\mathbf{u}+\mathbf{u}\cdot\nabla\mathbf{u}\right),\mathbf{v}\right)_{\Omega(t)} + (\mathbb{S}(\mathbf{u},p),\nabla\mathbf{v})_{\Omega(t)} = \left(\varrho\,\mathrm{Fr}^{-1}\,\mathbf{e}_g,\mathbf{v}\right)_{\Omega(t)} - \left\langle \mathrm{We}^{-1}\,\sigma\mathbb{P}_\Gamma,\nabla_\Gamma\mathbf{v}\right\rangle_{\Gamma(t)} \ .$$

The term $(\mathbb{S}(\mathbf{u},p),\nabla\mathbf{v})_\Omega$ can be written as

$$(\mathbb{S}(\mathbf{u},p),\nabla\mathbf{v})_{\Omega(t)} = \left(2\varrho\,\mathrm{Re}^{-1}\,\mathbb{D}(\mathbf{u}),\mathbb{D}(\mathbf{v})\right)_{\Omega(t)} - (p,\nabla\cdot\mathbf{v})_{\Omega(t)} \ ,$$

where the symmetry of $\mathbb{D}(\mathbf{u})$ is exploited.

The weak form of the momentum balance reads

$$\begin{aligned}(\varrho\partial_t\mathbf{u},\mathbf{v})_{\Omega(t)} + (\varrho\mathbf{u}\cdot\nabla\mathbf{u},\mathbf{v})_{\Omega(t)} + \left(2\varrho\,\mathrm{Re}^{-1}\,\mathbb{D}(\mathbf{u}),\mathbb{D}(\mathbf{v})\right)_{\Omega(t)} - (p,\nabla\cdot\mathbf{v})_{\Omega(t)} \\ = \left(\varrho\,\mathrm{Fr}^{-1}\,\mathbf{e}_g,\mathbf{v}\right)_{\Omega(t)} - \left\langle \mathrm{We}^{-1}\,\sigma\mathbb{P}_\Gamma,\nabla_\Gamma\mathbf{v}\right\rangle_{\Gamma(t)} \ ,\end{aligned}$$

for all $\mathbf{v} \in H_0^1(\Omega(t))^d$.

The weak mass balance (2.6.1b) is derived similar, multiplying with $q \in L_0^2(\Omega)$ and integration over the domain Ω results in

$$(\nabla\cdot\mathbf{u},q)_{\Omega(t)} = 0 \ ,$$

for all $q \in L_0^2(\Omega)$

Next, the bulk surfactant transport equation is considered. To simplify the notation the following abbreviation is introduced: $v \in H^1(\Omega_1\cup\Omega_2) \Leftrightarrow (v_1,v_2) \in H^1(\Omega_1)\times H^1(\Omega_2)$ with the scalar product

$$(u,v)_\Omega = (u_1,v_1)_{\Omega_1} + (u_2,v_2)_{\Omega_2} \quad \forall u,v \in H^1(\Omega_1\cup\Omega_2) \ .$$

Multiplying equation (2.6.1c) with a test function $\phi_i \in H^1(\Omega_i)$ for each domain, and integrating by parts and using (2.6.1h) leads to

$$(\partial_t c,\phi)_{\Omega(t)} + \left(\mathrm{Pe}^{-1}\,\nabla c,\nabla\phi\right)_{\Omega(t)} + (\mathbf{u}\cdot\nabla c,\phi)_{\Omega(t)} = \langle \beta\,\mathcal{Q}_\Gamma(c_1,c_2,\gamma),\phi\rangle_{\Gamma(t)} \ ,$$

for all $\phi \in H^1(\Omega_1(t) \cup \Omega_2(t))$.

Multiplying equation (2.4.3) with a test function $\xi \in H^1(\Gamma(t))$, and integrating by parts, the weak form of the surface balance becomes

$$\langle \partial_t^{\mathbf{u}} \gamma, \xi \rangle_{\Gamma(t)} + \left\langle \mathrm{Pe}_\Gamma^{-1} \nabla_\Gamma \gamma, \nabla_\Gamma \xi \right\rangle_{\Gamma(t)} + \langle \gamma \nabla_\Gamma \cdot \mathbf{u}, \xi \rangle_{\Gamma(t)} = \langle \mathcal{Q}_\Gamma(c_1, c_2, \gamma), \xi \rangle_{\Gamma(t)} \ ,$$

for all $\xi \in H^1(\Gamma(t))$.

All together the following weak problem is formulated:

Problem 2.7.1. *For almost all $t \in (t_0, t_b)$, find $\mathbf{u} \in H^1(\Omega)^d$, $p \in L_0^2(\Omega)$, $c \in H^1(\Omega_1(t) \cup \Omega_2(t))$, $\gamma \in H^1(\Gamma(t))$, such that*

$$\begin{aligned} (\varrho \partial_t \mathbf{u}, \mathbf{v})_{\Omega(t)} + (\varrho \mathbf{u} \cdot \nabla \mathbf{u}, \mathbf{v})_{\Omega(t)} + \left(2\varrho \,\mathrm{Re}^{-1} \,\mathbb{D}(\mathbf{u}), \mathbb{D}(\mathbf{v})\right)_{\Omega(t)} - (p, \nabla \cdot \mathbf{v})_{\Omega(t)} \\ = \left(\varrho \,\mathrm{Fr}^{-1} \,\mathbf{e}_g, \mathbf{v}\right)_{\Omega(t)} - \left\langle \mathrm{We}^{-1} \,\sigma \mathbb{P}_\Gamma, \nabla_\Gamma \mathbf{v} \right\rangle_{\Gamma(t)} \ , \end{aligned}$$

$$\begin{aligned} (\nabla \cdot \mathbf{u}, q) &= 0 \ , \\ (\partial_t c, \phi) + \left(\mathrm{Pe}^{-1} \nabla c, \nabla \phi\right) + (\mathbf{u} \cdot \nabla c, \phi) &= \langle \beta \, \mathcal{Q}_\Gamma(c_1, c_2, \gamma), \phi \rangle \ , \\ \langle \partial_t^{\mathbf{u}} \gamma, \xi \rangle + \left\langle \mathrm{Pe}_\Gamma^{-1} \nabla_\Gamma \gamma, \nabla_\Gamma \xi \right\rangle + \langle \gamma \nabla_\Gamma \cdot \mathbf{u}, \xi \rangle &= \langle \mathcal{Q}_\Gamma(c_1, c_2, \gamma), \xi \rangle \ , \end{aligned}$$

for all $\mathbf{v} \in H^1(\Omega)^d$, $q \in L_0^2(\Omega)$, $\phi \in H^1(\Omega_1(t) \cup \Omega_2(t))$, $\xi \in H^1(\Gamma(t))$.

Chapter 3

Moving Domains

In Chapter 3, the *Arbitrary Lagrangian Eulerian* (ALE) frame is introduced. The ALE frame is used to track the moving domains. It is based on introducing a fixed reference domain, similar to the full Lagrangian approach. An appropriate mapping is used to describe the evolution of the fluid domain.

First, the mathematical foundation is laid out to reformulate the Navier-Stokes equations and the transport equations in the ALE frame. Then, the construction of the ALE mapping is considered. The ALE mapping is found by solving an additional problem, since it is not given by the flow problem. Here, different methods are considered. Finally, a stable formulation of the Navier-Stokes equations for capillary flows, i.e. the two-phase Navier-Stokes equation without the surfactant transport and hence a constant surface tension coefficient, is considered.

3.1 Arbitrary Lagrangian Eulerian (ALE) Formulation

In the *Arbitrary Lagrangian Eulerian* (ALE) description of the motion of a fluid a reference domain is used, that is fixed in time. This is similar to the Lagrangian description, where the Lagrangian coordinates of a particle are fixed, too. However, in the ALE description a domain point does not necessarily follow a fluid particle path. The fluid and the domain are allowed to move differently, with different velocities. Even so, the ALE domain can occupy the same space time domain $\mathcal{Q}(t_0, t_b)$ as the fluid, which makes it suitable to describe the shape of a fluid volume.

Let $\tilde{\Omega} \subset \mathbb{R}^d$ be a reference domain. A mapping $\mathcal{A}_t : \tilde{\Omega} \to \Omega(t)$ is introduced, which maps for every time $t \in (t_0, t_b)$ the reference domain $\tilde{\Omega}$ onto the fluid domain $\Omega(t)$. A point $\mathbf{y} \in \tilde{\Omega}$ in the reference domain is mapped to a point $\mathbf{x} \in \Omega(t)$ via

$$\mathbf{x} = \mathbf{x}(\mathbf{y}, t) = \mathcal{A}_t(\mathbf{y}) \ .$$

It is assumed that $\mathcal{A}_t$ is a homeomorphism from $\tilde{\Omega}$ onto $\Omega(t)$, for almost every $t \in (t_0, t_b)$, i.e. $\mathcal{A}_t$ is bijective and continuous and its inverse is continuous, as well. It is further assumed, that the partial derivative with respect to t exists for almost every t.

Similar to the Lagrangian description, the reference domain $\tilde{\Omega}$ is referred to as the *ALE frame*, and $\mathbf{y} \in \tilde{\Omega}$ is referred to as the *ALE coordinate* of a point $\mathbf{x} \in \Omega(t)$. The current domain $\Omega(t)$ is referred to as the Eulerian frame and $\mathbf{x} \in \Omega(t)$ as the Eulerian coordinate.

A function $f : \mathcal{Q}(t_0, t_b) \to \mathbb{R}$ given in the Eulerian frame has a representation $\tilde{f} : \tilde{\Omega} \times \mathbb{R} \to \mathbb{R}$ in the ALE frame as follows

$$\tilde{f}(\mathbf{y}, t) := f(\mathcal{A}_t(\mathbf{y}), t) \ .$$

Let $\mathbf{w} : \mathcal{Q}(t_0, t_b) \to \mathbb{R}^d$ denote the velocity of the domain, given by the ALE mapping. The domain velocity $\mathbf{w}$, in the ALE frame, is given as

$$\tilde{\mathbf{w}} = \partial_t \mathcal{A}_t \ .$$

This translates to the Eulerian frame as follows

$$\mathbf{w}(\mathbf{x}, t) = \tilde{\mathbf{w}}(\mathcal{A}_t^{-1}(\mathbf{x}), t) = (\partial_t \mathcal{A}_t)\left(\mathcal{A}_t^{-1}(\mathbf{x})\right) \ . \tag{3.1.1}$$

Remark 3.1.1. *Note, that for a function f, $\left(\partial_t \tilde{f}\right)\left(\mathcal{A}_t^{-1}(\mathbf{x}), t\right)$ is the material derivative of f with respect to the velocity field* $\mathbf{w}$

$$\left(\partial_t^{\mathbf{w}} f\right)(\mathbf{x}, t) = \left(\partial_t \tilde{f}\right)\left(\mathcal{A}_t^{-1}(\mathbf{x}), t\right) \ .$$

Thus, the velocity of the domain is given in the Eulerian frame as the material derivative

$$\mathbf{w} = \partial_t^{\mathbf{w}} \mathbf{x} \ . \tag{3.1.2}$$

In the following $\partial_t^{\mathbf{w}}$ will be called ALE time derivative *or just* ALE derivative.

For a function $f : \mathcal{Q}(t_0, t_b) \to \mathbb{R}$ the time derivative transforms between the Lagrangian- and the Eulerian frame, as follows. By applying the chain rule it is obtained

$$\partial_t \tilde{f}(\mathbf{y}, t) = \partial_t f(\mathcal{A}_t(\mathbf{y}), t) = (\partial_t f)(\mathcal{A}_t(\mathbf{y}), t) + \partial_t \mathcal{A}_t(\mathbf{y}) \cdot (\nabla f)(\mathcal{A}_t(\mathbf{y}), t) \ .$$

Substituting $\mathbf{y} = \mathcal{A}_t^{-1}(\mathbf{x})$ and using (3.1.1) it becomes

$$\partial_t^{\mathbf{w}} f = \partial_t f + \mathbf{w} \cdot \nabla f \ . \tag{3.1.3}$$

The ALE time derivative becomes the material derivative with respect to the domain velocity $\mathbf{w}$.

The material derivative (3.1.3) is used to transform a partial differential equation into its ALE form. Let $u : \mathcal{Q}(t_0, t_b) \to \mathbb{R}$ be a solution and $f : \mathcal{Q}(t_0, t_b) \to \mathbb{R}$ be the right hand side of a partial differential equation

$$\partial_t u + \mathcal{L}(u) = f \qquad \text{in } \Omega(t) \ , \tag{3.1.4}$$

where $\mathcal{L}$ is a differential operator in space. After substituting the partial time derivative with the ALE time derivative using (3.1.3), the generic partial differential equation (3.1.4) becomes

$$\partial_t^{\mathbf{w}} u - \mathbf{w} \cdot \nabla u + \mathcal{L}(u) = f \ , \tag{3.1.5}$$

which is the *ALE form* of (3.1.4).

Remark 3.1.2. *The ALE form* (3.1.5) *is the* non-conservative ALE form. *There are other possibilities to derive an ALE formulation [92, 93]. A* conservative ALE formulation *of the generic partial differential equation* (3.1.4) *would be*

$$\partial_t^{\mathbf{w}} u + u\nabla \cdot \mathbf{w} + \mathcal{L}(u) - \nabla \cdot (u\mathbf{w}) = f \ .$$

For a generic conservation law, the partial differential operator $\mathcal{L}(u)$ *has the form*

$$\mathcal{L}(u) = \nabla \cdot (\mathcal{F}(u)) \tag{3.1.6}$$

with generic flux $\mathcal{F}$. *Thus, the partial differential equation takes the form*

$$\partial_t^{\mathbf{w}} u + u\nabla \cdot \mathbf{w} + \nabla \cdot (\mathcal{F}(u) - u\mathbf{w}) = f \ ,$$

which results in the generic conservation law for u *using a transport theorem*

$$\frac{d}{dt}\int_{\Omega(t)} u \ \mathrm{d}V = \int_{\Omega(t)} f \ \mathrm{d}V - \int_{\partial\Omega(t)} (\mathcal{F}(u) - u\mathbf{w}) \cdot \ \mathrm{d}\mathbf{A} \ .$$

Hence, the name conservative ALE formulation.

In this work, for the bulk equations the non-conservative formulation is used, since the bulk differential operators are not used in the form (3.1.6). *That is because, it is assumed that* $\nabla \cdot \mathbf{u} = 0$, *a priori. For the surface equation it holds* $\nabla_\Gamma \cdot u \neq 0$. *The surface differential operator is used in the conservative form* (3.1.6), *in terms of the surface derivatives. For the surface equations a conservative ALE form will be derived, as shown later.*

Substituting the partial time derivative (3.1.3) in the Navier-Stokes equations, the momentum balance equations become

$$\varrho\,(\partial_t^{\mathbf{w}}\mathbf{u} + (\mathbf{u} - \mathbf{w}) \cdot \nabla\mathbf{u}) - \nabla \cdot \mathbb{S}(\mathbf{u}, p) = \varrho\,\mathrm{Fr}^{-1}\,\mathbf{e}_g \ , \tag{3.1.7}$$

the non-conservative ALE formulation of the Navier-Stokes equations. Using the substitution (3.1.3) for the time derivatives in the bulk surfactant transport equations, results in

$$\partial_t^{\mathbf{w}} c_i - \mathrm{Pe}^{-1}\,\Delta\, c_i + (\mathbf{u} - \mathbf{w}) \cdot \nabla c_i = 0 \ , \tag{3.1.8}$$

the non-conservative ALE formulation of the bulk transport for $i = 1, 2$.

An analogue approach is used for the interface and the equations on the interface. Let $\tilde{\Gamma} \subset \mathbb{R}^d$ be a reference interface for $\Gamma(t)$. An homeomorphism $\mathcal{A}_{t,\Gamma} : \tilde{\Gamma} \to \Gamma(t)$ is assumed between a reference interface $\tilde{\Gamma}$ and the interface $\Gamma(t)$, with

$$\mathbf{x} = \mathcal{A}_{t,\Gamma}(\mathbf{y}) \ ,$$

for $\mathbf{y} \in \tilde{\Gamma}$ and $\mathbf{x} \in \Gamma(t)$.

Analogue, the interface velocity $\mathbf{w}_\Gamma$ is then given as

$$\tilde{\mathbf{w}}_\Gamma = \partial_t \mathcal{A}_{t,\Gamma} \ ,$$

and for a function $f_\Gamma : \mathcal{Q}_\Gamma(t_0, t_b) \to \mathbb{R}$, defined in the Eulerian frame, an ALE representation is given as

$$\tilde{f_\Gamma}(\mathbf{y}, t) = f_\Gamma(\mathcal{A}_{t,\Gamma}(\mathbf{y}), t) \ .$$

For the material derivatives on the interface, respecting different velocities, it holds

$$\partial_t^{\mathbf{w}_\Gamma} f_\Gamma = \partial_t^{\mathbf{u}} f_\Gamma + (\mathbf{w}_\Gamma - \mathbf{u}) \cdot \nabla_\Gamma f_\Gamma \ .$$

Substituting the material derivatives, the surface transport equation is transformed into the a non-conservative ALE form, as follows

$$\partial_t^{\mathbf{w}_\Gamma} \gamma + (\mathbf{u} - \mathbf{w}_\Gamma) \cdot \nabla_\Gamma \gamma + \gamma \nabla_\Gamma \cdot \mathbf{u} = D_\Gamma \, \Delta_\Gamma \, \gamma + \mathcal{Q}_\Gamma(c_1, c_2, \gamma) \ .$$

Rearranging the terms, the conservative ALE formulation is obtained

$$\partial_t^{\mathbf{w}_\Gamma} \gamma + \gamma \nabla_\Gamma \cdot \mathbf{w}_\Gamma + \nabla_\Gamma \cdot [\gamma \, (\mathbf{u} - \mathbf{w}_\Gamma)] = D_\Gamma \, \Delta_\Gamma \, \gamma + \mathcal{Q}_\Gamma(c_1, c_2, \gamma) \ , \tag{3.1.9}$$

which will serve as a starting point for the weak formulation.

Using equations (3.1.7), (3.1.8) and (3.1.9) in the derivation of the weak formulation of the last chapter results in the following *weak ALE formulation*

Problem 3.1.1. *For almost all $t \in (t_0, t_b)$, find $\mathbf{u} \in H_0^1(\Omega(t))^d$, $\mathbf{w} \in H_0^1(\Omega(t))^d$, $\mathbf{w}_\Gamma \in H^1(\Gamma(t))^d$, $p \in L_0^2(\Omega(t))$, $c \in H^1(\Omega_1(t) \cup \Omega_2(t))$, $\gamma \in H^1(\Gamma(t))$, such that*

$$\begin{aligned}
&(\varrho \partial_t^{\mathbf{w}} \mathbf{u}, \mathbf{v}) + (\varrho(\mathbf{u} - \mathbf{w}) \cdot \nabla \mathbf{u}, \mathbf{v}) \\
&+ \left(2\varrho \, \mathrm{Re}^{-1} \, \mathbb{D}(\mathbf{u}), \mathbb{D}(\mathbf{v})\right) - (p, \nabla \cdot \mathbf{v}) = \left(\varrho \, \mathrm{Fr}^{-1} \, \mathbf{e}_g, \mathbf{v}\right) - \left\langle \mathrm{We}^{-1} \, \sigma(c) \mathbb{P}_\Gamma, \nabla \mathbf{v} \right\rangle \ , \\
&(\nabla \cdot \mathbf{u}, q) = 0 \ , \\
&(\partial_t^{\mathbf{w}} c, \phi) + ((\mathbf{u} - \mathbf{w}) \nabla c, \phi) + \left(\mathrm{Pe}^{-1} \, \nabla c, \nabla \phi\right) = \langle \beta \, \mathcal{Q}_\Gamma(c_1, c_2, \gamma), \phi \rangle \ , \\
&(\partial_t^{\mathbf{w}_\Gamma} \gamma, \xi) + (\gamma \nabla_\Gamma \cdot \mathbf{w}_\Gamma, \xi) \\
&\qquad + \langle \nabla_\Gamma \cdot [\gamma \, (\mathbf{u} - \mathbf{w}_\Gamma)], \xi \rangle + D_\Gamma \, \langle \nabla_\Gamma \gamma, \nabla_\Gamma \xi \rangle = \langle \mathcal{Q}_\Gamma(c_1, c_2, \gamma), \xi \rangle \ ,
\end{aligned}$$

for all $\mathbf{v} \in H_0^1(\Omega(t))^d$, $q \in L_0^2(\Omega(t))^d$, $\phi \in H^1(\Omega_1(t) \cup \Omega_2(t))$, $\xi \in H^1(\Gamma(t))$).

Note, this problem has to be augmented with equations for $\mathbf{w}$ and $\mathbf{w}_\Gamma$. These additional problems will be given in the next two sections.

3.2 The ALE Mapping

The ALE mappings $\mathcal{A}_t$ and $\mathcal{A}_{t,\Gamma}$ for the bulk domain and the surface, respectively, that were introduced in the last section are not determined. Like the name *Arbitrary Lagrangian Eulerian method* suggest, the mappings are arbitrary to a certain extend. As a first restriction, it is assumed that

$$\mathcal{A}_t|_{\Gamma(t)} = \mathcal{A}_{t,\Gamma} \ ,$$

for $t \in (t_0, t_b)$. In this way, one has to deal with only one mapping for the whole domain. This restriction also implies that

$$\mathbf{w}|_{\Gamma(t)} = \mathbf{w}_\Gamma \tag{3.2.1}$$

for $t \in (t_0, t_b)$.

One obvious choice for $\mathbf{w}$ could be

$$\mathbf{w} = \mathbf{u} \quad \text{in } \Omega(t) \ ,$$

for $t \in (t_0, t_b)$. The ALE formulation would recover the Lagrangian formulation for this choice of the domain velocity. The kinematic boundary condition (2.2.8) would be fulfilled trivially. However, a Lagrangian approach is not desired here. In terms of a discrete triangular domain, it is not preferable to deform the computational domain like a fluid.

Another choice could be setting the domain velocity to zero. This would result in a fully Eulerian method. However, the tracking property of the fluid domain would be lost, which is the purpose of the ALE method.

Instead, it is assumed that the image of the reference domain $\tilde{\Omega}$ under the mapping $\mathcal{A}_t$ is the fluid domain $\Omega(t)$, for all $t \in (t_0, t_b)$, i.e.

$$\mathbf{w} \cdot \mathbf{n} = \mathbf{u} \cdot \mathbf{n} \quad \text{on } \partial\Omega(t) \ . \tag{3.2.2}$$

Different methods to construct an ALE mapping from boundary data are considered in the following. There are more methods proposed in [92]. In order to construct the ALE mapping it is assumed that the velocity or the position of the boundary and the interface are given. Then, the task is to find an extension into the interior of the bulk domains.

The first method considered, is to find the domain velocity as a solution from the following Laplace problem.

Problem 3.2.1. *Given the evolution* $\mathbf{g}_i$ *of the boundaries* $\partial\Omega_i(t)$*, for every time* $t \in (t_0, t_b)$*, the evolution* $\mathbf{w}$ *is then obtained by solving*

$$-\Delta \mathbf{w} = 0 \qquad \text{in } \Omega_i(t) \ , \tag{3.2.3a}$$

$$\mathbf{w} = \mathbf{g}_i \qquad \text{on } \partial\Omega_i(t) \ , \tag{3.2.3b}$$

for $i = 1, 2$.

This method is also called *harmonic extension*. Using (3.1.2) the ALE mapping $\mathcal{A}_t$ is obtained. The harmonic extension is simple and easy to solve in terms of numerical methods. Further, it has the property to minimise the variation of $\mathbf{w}$ in a L^2-sense [94]. The Laplace problem is equivalent to the minimisation problem

$$\min_{\mathbf{w}\in H^1(\Omega_i(t))} \int_{\Omega_i(t)} (\nabla \mathbf{w})^2 \, \mathrm{d}V \ , \quad \mathbf{w}|_{\partial\Omega_i(t)} = \mathbf{g}_i \ .$$

Thus, it follows $\|\nabla \mathbf{w}\|_{L^2(\Omega(t))} \to \min$. This property helps to reduce mesh distortion in the discrete setting, which is a desired trait.

Remark 3.2.1. *The harmonic extension can also be formulated in terms of the absolute position $\mathcal{A}_t$ of the domain:*

Given the position of $\mathbf{x}$ of the boundaries $\partial\Omega_i(t)$ for every time $t \in (t_0, t_1)$, the evolution $\mathbf{w}$ is obtained by solving

$$\begin{aligned} -\Delta \mathcal{A}_t &= 0 && \text{in } \Omega_i(t) \ , \\ \mathcal{A}_t &= \mathbf{x} && \text{on } \partial\Omega_i(t) \ , \end{aligned}$$

for $i = 1, 2$.

Another approach to extend the ALE mapping, is to consider the domain as a linear elastic solid. The domain $\Omega(t)$ is considered to be the result of pushing a reference configuration $\tilde{\Omega}$ into its current configuration $\Omega(t)$. Let $\mathbf{d} = \mathbf{x} - \mathbf{y} = \mathcal{A}_t(\mathbf{y}) - \mathbf{y}$ be the displacement of the domain, an elasticity problem can be formulated as follows.

Problem 3.2.2. *Given the displacement $\mathbf{g}_i$ of the boundary of the domain $\Omega_i(t)$ for every time t, the displacement $\mathbf{d}$ is obtained b solvingy*

$$\begin{aligned} \nabla \cdot [\lambda_1(\nabla \cdot \mathbf{d})\mathbb{I} + 2\lambda_2 \mathbb{D}(\mathbf{d})] &= \mathbf{0} && \text{on } \Omega_i(t) \ , \\ \mathbf{y} &= \mathbf{g}_i && \text{on } \partial\Omega_i(t) \ , \end{aligned}$$

for $i = 1, 2$.

The linear elastic solid extension minimises the internal stresses defined by the stress tensor $[\lambda_1(\nabla \cdot \mathbf{y})\mathbb{I} + 2\lambda_2 \mathbb{D}(\mathbf{y})]$. Through Lame constants λ_i, $i = 1, 2$ the degree of the internal deformation can be controlled. In terms of a triangular mesh, the deformation of a mesh cell can be controlled, and is minimised. Provided the mesh of the reference domain is of good quality, the resulting mesh is expected of good quality, too.

This subsection is closed by an important result, regarding the regularity of the ALE mapping $\mathcal{A}_t$. In the finite element context Sobolev spaces are used, like $H^1(\Omega(t))$. The following theorem gives a cue about the regularity of $\mathcal{A}_t$ needed to have a suitable transformation of such Sobolev spaces from the ALE frame to the Eulerian frame. Although, $\mathcal{A}_t, \mathcal{A}_t^{-1} \in C^1$ would be sufficient to have $v = \tilde{v} \circ \mathcal{A}_t \in H^1(\Omega(t))$ if and only if $\tilde{v} \in H^1(\tilde{\Omega})$. Unfortunately, this requirement is to strong, since $\mathcal{A}_t$ or $\mathbf{w}$ are given in terms of finite element functions, which are in $H^1(\Omega(t))$. The following theorem relaxes the conditions on the regularity of $\mathcal{A}_t$.

Theorem 3.2.1. *Let $\tilde{\Omega}$ be bounded with a Lipschitz continuous boundary, and let $\mathcal{A}_t$ be a homeomorphism. For each $t \in (t_0, t_b)$, let $\Omega(t) = \mathcal{A}_t(\tilde{\Omega})$ be bounded and $\partial\Omega(t)$ be Lipschitz. Further, let $\mathcal{A}_t \in W^{1,\infty}(\tilde{\Omega})$ and $\mathcal{A}_t^{-1} \in W^{1,\infty}(\Omega(t))$, then, $v \in H^1(\Omega(t))$ if and only if $\tilde{v} \in H^1(\tilde{\Omega})$, and $\|v\|_{H^1(\Omega(t))}$ is equivalent to $\|\tilde{v}\|_{H^1(\tilde{\Omega})}$ for all $\tilde{v} \in H^1(\tilde{\Omega})$.*

Proof. The proof can be found in [92, Proposition, 1.3.1]. □

3.3 Surface Evolution

From the requirement (3.2.2) and from the kinematic interface condition (2.2.8) the boundary evolution of the bulk domains $\Omega_i(t)$, $i = 1, 2$ is not uniquely determined. The tangential component can be chosen freely. In order to construct the ALE mapping, both components of boundary evolution are needed, as shown in the last subsection. The freedom in the tangential component can be used to obtain different methods, that result in different discrete schemes. Different methods to construct an interface evolution are considered in the following.

Assuming the fluid velocity is given, the bulk domain velocities for the boundaries $\partial\Omega_i(t)$ could be taken in a full Lagrangian fashion, by setting

$$\mathbf{w} = \mathbf{u} \quad \text{on } \partial\Omega_i(t) \ ,$$

for $i = 1, 2$. Alternatively, the kinematic boundary condition could be used

$$\mathbf{w} = (\mathbf{u} \cdot \mathbf{n}_\Gamma)\mathbf{n}_\Gamma \quad \text{on } \partial\Omega_i(t) \ ,$$

for $i = 1, 2$ (Note that, $\partial\Omega_1(t) = \Gamma(t)$). Throughout this work, these methods will be referred to as the *classical methods*. In terms of numerical discretization, the classical methods provide a lightweight scheme. For each mesh node on the boundary, an ordinary differential equation has to be solved, that can be done explicitly.

Another approach is to use a weak formulation of kinematic condition (3.2.2):

For almost all $t \in (t_0, t_b)$, find $\mathbf{w} \in L^2(\partial\Omega_i(t))^d$, such that for all $\psi \in L^2(\partial\Omega_i(t))$ it holds

$$\langle \mathbf{u} - \mathbf{w}, \mathbf{n}_\Gamma \psi \rangle_{\partial\Omega_i(t)} = 0 \ , \tag{3.3.1}$$

for $i = 1, 2$.

The problem (3.3.1) is not well-posed, since it has no unique solution. Equation (3.3.1) considers the normal component of $\mathbf{w}$ only. It has to be augmented by a second equation for the tangential component of $\mathbf{w}$. The following method was proposed in [17]. Using the Laplace-Beltrami identity on $\Gamma(t)$

$$\Delta_\Gamma \, \mathrm{id}_\Gamma = -\mathcal{H}\mathbf{n}_\Gamma \ ,$$

leads to the following weak formulation of the boundary evolution.

Problem 3.3.1. *Given* $\mathbf{u}$*, for almost all* $t \in (t_0, t_b)$*, find* $\mathbf{w} \in L^2(\partial\Omega_i(t)))^d$ *and* $\mathcal{H} \in L^2(\partial\Omega_i(t)))$*, such that for all* $(\psi, \eta) \in L^2(\partial\Omega_i(t)) \times L^2(\partial\Omega_i(t))^d$ *it holds*

$$\langle \mathbf{u} - \mathbf{w}, \mathbf{n}_\Gamma \psi \rangle_{\partial\Omega_i(t)} = 0 \ , \tag{3.3.2a}$$

$$\langle \mathcal{H}\mathbf{n}_\Gamma, \eta \rangle_{\partial\Omega_i(t)} - \langle \nabla_\Gamma id_\Gamma, \nabla_\Gamma \eta \rangle_{\partial\Omega_i(t)} = 0 \ . \tag{3.3.2b}$$

The discrete solution of Problem 3.3.1 has some remarkable properties regarding the node distribution on the interface. This will be discussed in Chapter 4 and Chapter 5.

3.4 A Stable ALE Formulation

Combining Problem 3.3.1 with the Navier-Stokes equations for the two-phase capillary flow, has the advantage of resulting in a stable formulation, contrary to using the classical methods. This has been shown for non-ALE formulations in [18] and it holds true for the ALE formulation as well. That will be shown in the following.

In order to simplify the notation, the domain velocity $\mathbf{w}$ and the interface velocity $\mathbf{w}_\Gamma$ will be considered as independent throughout this subsection. Additionally, the domain velocity $\mathbf{w}$ will be considered as given throughout this subsection, since it turns out that the result will be independent of $\mathbf{w}$, anyway.

The capillary two-phase flow problem with a fixed surface tension coefficient is considered. Thus, the bulk and surface surfactant is neglected.

Problem 3.4.1. *Given* $\mathbf{w}$*, for almost all* $t \in (t_0, t_b)$ *find* $(\mathbf{u}, p, \mathbf{w}_\Gamma, \mathcal{H}) \in H_0^1(\Omega(t))^d \times L_0^2(\Omega(t)) \times H^1(\Gamma(t))^d \times L^2(\Gamma(t))$ *such that for all* $(\mathbf{v}, q, \eta, \psi) \in H_0^1(\Omega(t))^d \times L_0^2(\Omega(t)) \times H^1(\Gamma(t))^d \times L^2(\Gamma(t))$ *it holds*

$$(\varrho \partial_t^{\mathbf{w}} \mathbf{u}, \mathbf{v}) + (\varrho(\mathbf{u} - \mathbf{w}) \cdot \nabla \mathbf{u}, \mathbf{v}) + \left(2\varrho \operatorname{Re}^{-1} \mathbb{D}(\mathbf{u}), \mathbb{D}(\mathbf{v})\right) - (p, \nabla \cdot \mathbf{v}) = f(\mathbf{v}) \ , \tag{3.4.1a}$$

$$(\nabla \cdot \mathbf{u}, q) = 0 \ , \tag{3.4.1b}$$

$$\langle \mathbf{u} - \mathbf{w}_\Gamma, \mathbf{n}_\Gamma \psi \rangle_\Gamma = 0 \ , \tag{3.4.1c}$$

$$\langle \mathcal{H}\mathbf{n}_\Gamma, \eta \rangle_\Gamma - \langle \nabla_\Gamma id_\Gamma, \nabla_\Gamma \eta \rangle_\Gamma = 0 \ , \tag{3.4.1d}$$

where

$$f(\mathbf{v}) := \left(\varrho \operatorname{Fr}^{-1} \mathbf{e}_g, \mathbf{v}\right) - \left\langle \operatorname{We}^{-1} \sigma_0 \mathbb{P}_\Gamma, \nabla_\Gamma \mathbf{v} \right\rangle_\Gamma \ .$$

In the following, some preliminary results are obtained. First, the formula for partial integration is extended to domain-wise smooth functions, as follows.

Lemma 3.4.1. *For* $\varphi \in H_0^1(\Omega)$ *and* $\mathbf{v} \in H_0^1(\Omega)^d$ *it holds*

$$(\varrho \mathbf{v}, \nabla \varphi) = -(\varrho \varphi, \nabla \cdot \mathbf{v}) + \langle [\![\varrho \varphi \mathbf{v}]\!]_\Gamma, \mathbf{n}_\Gamma \rangle_\Gamma \ . \tag{3.4.2}$$

Proof. The result is obtained by using $\nabla \cdot (\varphi \mathbf{v}) = \mathbf{v} \cdot \nabla \varphi + \varphi \nabla \cdot \mathbf{v}$ a.e., and applying the divergence theorem (1.1.1) domain-wise. □

Further, the following useful identity holds.

Lemma 3.4.2. *Let $\Gamma(t)$ be a smooth, evolving hypersurface, then the following holds*

$$\frac{d}{dt}\int_{\Gamma(t)} \mathrm{d}A = \langle \nabla_\Gamma id_\Gamma, \nabla_\Gamma \mathbf{w}_\Gamma \rangle_{\Gamma(t)} \ . \tag{3.4.3}$$

Proof. Using the Reynolds transport theorem for the function $f = 1$, yields

$$\frac{d}{dt}\int_{\Gamma(t)} \mathrm{d}A = \int_{\Gamma(t)} \nabla_\Gamma \cdot \mathbf{w}_\Gamma \ \mathrm{d}A \ .$$

Applying the divergence theorem on surface (1.1.2), leads to

$$\int_{\Gamma(t)} \nabla_\Gamma \cdot \mathbf{w}_\Gamma \ \mathrm{d}A = \int_{\Gamma(t)} \mathcal{H}\mathbf{w}_\Gamma \cdot \mathrm{d}\mathbf{A} \ ,$$

where it was used that $\Gamma(t)$ has no boundary. Finally, using the Laplace-Beltrami identity $\Delta_\Gamma \mathrm{id}_\Gamma = -\mathcal{H}\mathbf{n}_\Gamma$ and applying integration by parts, the result (3.4.3) is obtained

$$\frac{d}{dt}\int_{\Gamma(t)} \mathrm{d}A = \int_{\Gamma(t)} \mathcal{H}\mathbf{w}_\Gamma \cdot \mathrm{d}\mathbf{A} = \langle \nabla_\Gamma \mathrm{id}_\Gamma, \nabla_\Gamma \mathbf{w}_\Gamma(t) \rangle_{\Gamma(t)} \ .$$

□

With the lemmata above, the following theorem regarding the stability of Problem 3.4.1 can be proven.

Theorem 3.4.1. *For Problem 3.4.1 the following holds*

$$\frac{d}{dt}\left(\frac{1}{2}\left\|\varrho^{\frac{1}{2}}\mathbf{u}\right\|^2_{L^2(\Omega(t))} + \sigma_0 \,\mathrm{We}^{-1}\,|\Gamma(t)|\right) + 2\,\|\epsilon\mathbb{D}(\mathbf{u})\|^2_{L^2(\Omega(t))} = \mathrm{Fr}^{-1}\,(\varrho\mathbf{e}_g, \mathbf{u}) \ ,$$

where $\epsilon = \left(\varrho\,\mathrm{Re}^{-1}\right)^{\frac{1}{2}}$.

Proof. Setting $\mathbf{v} = \mathbf{u}$ and considering the convective term

$$(\varrho\partial_t^{\mathbf{w}}\mathbf{u}, \mathbf{u}) + (\varrho(\mathbf{u}-\mathbf{w})\cdot\nabla\mathbf{u}, \mathbf{u}) = \frac{1}{2}\left(\varrho, \partial_t^{\mathbf{w}}\mathbf{u}^2\right) + \frac{1}{2}\left(\varrho(\mathbf{u}-\mathbf{w}), \nabla\mathbf{u}^2\right) \ .$$

Applying (3.4.2) on the convective term, yields

$$\begin{aligned}&\left(\varrho, \partial_t^{\mathbf{w}}\mathbf{u}^2\right) + \left(\varrho(\mathbf{u}-\mathbf{w}), \nabla\mathbf{u}^2\right)\\ &\quad= \left(\varrho, \partial_t^{\mathbf{w}}\mathbf{u}^2\right) - \left(\varrho\mathbf{u}^2, \nabla\cdot(\mathbf{u}-\mathbf{w})\right) + \left\langle [\![\varrho\mathbf{u}^2(\mathbf{u}-\mathbf{w})]\!]_\Gamma, \mathbf{n}_\Gamma\right\rangle_\Gamma \ .\end{aligned}$$

Using (3.4.1b) with $q = \varrho\mathbf{u}^2$ and Theorem 2.2.1, yields

$$\begin{aligned}&\left(\varrho, \partial_t^{\mathbf{w}}\mathbf{u}^2\right) + \left(\varrho(\mathbf{u}-\mathbf{w}), \nabla\mathbf{u}^2\right)\\ &\quad= \frac{d}{dt}\left(\varrho, \mathbf{u}^2\right) - \left\langle [\![\varrho\mathbf{u}^2(\mathbf{w}_\Gamma-\mathbf{w})]\!]_\Gamma, \mathbf{n}_\Gamma\right\rangle_\Gamma + \left\langle [\![\varrho\mathbf{u}^2(\mathbf{u}-\mathbf{w})]\!]_\Gamma, \mathbf{n}_\Gamma\right\rangle_\Gamma\\ &\quad= \frac{d}{dt}\left(\varrho, \mathbf{u}^2\right) + \left\langle \mathbf{u}-\mathbf{w}_\Gamma, \mathbf{n}_\Gamma [\![\varrho]\!]_\Gamma \mathbf{u}^2\right\rangle_\Gamma \ .\end{aligned}$$

Using (3.4.1c) with $\psi = [\![\varrho]\!]_\Gamma \mathbf{u}^2|_\Gamma$ yields

$$(\varrho \partial_t^{\mathbf{w}} \mathbf{u}, \mathbf{u}) + (\varrho(\mathbf{u}-\mathbf{w})\cdot\nabla\mathbf{u}, \mathbf{u}) = \frac{1}{2}\frac{d}{dt}\left(\varrho, \mathbf{u}^2\right) = \frac{1}{2}\frac{d}{dt}\left\|\varrho^{\frac{1}{2}}\mathbf{u}\right\|^2_{L^2(\Omega(t))} \ .$$

Considering the right hand side of (3.4.1a) with $\mathbf{v} = \mathbf{u}$ and using partial integration on the surface term, it is obtained

$$\begin{aligned} f(\mathbf{u}) &= \left(\varrho\,\mathrm{Fr}^{-1}\,\mathbf{e}_g, \mathbf{u}\right) - \left\langle \mathrm{We}^{-1}\,\sigma_0 \mathbb{P}_\Gamma, \nabla_\Gamma \mathbf{u}\right\rangle_\Gamma \\ &= \left(\varrho\,\mathrm{Fr}^{-1}\,\mathbf{e}_g, \mathbf{u}\right) + \mathrm{We}^{-1}\,\sigma_0 \left\langle \nabla_\Gamma \cdot \mathbb{P}_\Gamma, \mathbf{u}\right\rangle_\Gamma \\ &= \left(\varrho\,\mathrm{Fr}^{-1}\,\mathbf{e}_g, \mathbf{u}\right) - \mathrm{We}^{-1}\,\sigma_0 \left\langle \mathcal{H}\mathbf{n}_\Gamma, \mathbf{u}\right\rangle_\Gamma \ . \end{aligned}$$

Using (3.4.1c) with $\psi = \mathrm{We}^{-1}\,\sigma_0 \mathcal{H}$ the right hand side becomes

$$f(\mathbf{u}) = \left(\varrho\,\mathrm{Fr}^{-1}\,\mathbf{e}_g, \mathbf{u}\right) - \mathrm{We}^{-1}\,\sigma_0 \left\langle \mathcal{H}\mathbf{n}_\Gamma, \mathbf{w}_\Gamma\right\rangle_\Gamma \ ,$$

and after applying (3.4.1d) with $\eta = \mathbf{w}_\Gamma$

$$f(\mathbf{u}) = \left(\varrho\,\mathrm{Fr}^{-1}\,\mathbf{e}_g, \mathbf{u}\right) - \mathrm{We}^{-1}\,\sigma_0 \left\langle \nabla_\Gamma \mathrm{id}_\Gamma, \nabla_\Gamma \mathbf{w}_\Gamma\right\rangle_\Gamma \ .$$

Using Lemma 3.4.2 the right hand side becomes

$$f(\mathbf{u}) = \left(\varrho\,\mathrm{Fr}^{-1}\,\mathbf{e}_g, \mathbf{u}\right) - \mathrm{We}^{-1}\,\sigma_0 \frac{d}{dt}\left|\Gamma(t)\right| \ .$$

Setting $\epsilon = \left(\varrho\,\mathrm{Re}^{-1}\right)^{\frac{1}{2}}$, altogether it is obtained

$$\begin{aligned} \frac{1}{2}\frac{d}{dt}\left\|\varrho^{\frac{1}{2}}\mathbf{u}\right\|^2_{L^2\Omega} + 2\left\|\epsilon\mathbb{D}(\mathbf{u})\right\|^2_\Omega &= \mathrm{Fr}^{-1}\left(\varrho\mathbf{e}_g, \mathbf{u}\right) - \sigma_0\,\mathrm{We}^{-1}\,\frac{d}{dt}\left|\Gamma(t)\right| \ , \\ \frac{d}{dt}\left(\frac{1}{2}\left\|\varrho^{\frac{1}{2}}\mathbf{u}\right\|^2 + \sigma_0\,\mathrm{We}^{-1}\left|\Gamma(t)\right|\right) + 2\left\|\epsilon\mathbb{D}(\mathbf{u})\right\|^2 &= \mathrm{Fr}^{-1}\left(\varrho\mathbf{e}_g, \mathbf{u}\right) \ , \end{aligned}$$

which concludes the proof. □

3.5 Some Special Models

In the following subsections some specialisations of the model for two-phase flow with surfactant, derived above, are given.

3.5.1 Pressure Driven Periodic Channel Flow

A two-phase flow in a channel is considered. The surfactant is neglected, only surface tension is considered. The model is used to simulate a Taylor flow, in Chapter 5. A Taylor flow consists of several bubbles following each other in a channel. Each Taylor bubble moves through the wake of a Taylor bubble in front. Therefore, it is assumed

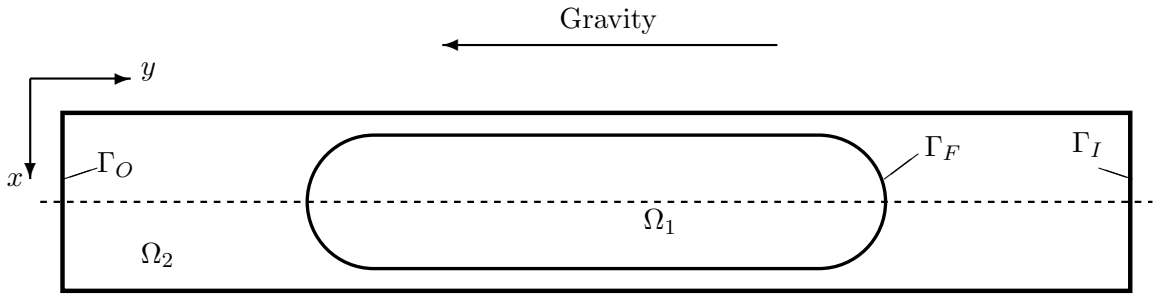

Figure 3.1: Schematic view of a domain for a two-phase channel flow.

that the flow pattern is periodic. The purpose of the following model is to incorporate periodic boundary conditions.

It is assumed, that one bubble is located in a specific channel segment, see Figure 3.1. The inflow boundary of the channel segment is denoted with Γ_I, the outflow boundary is denoted with Γ_O, and the remaining channel wall is denoted with Γ_W. The bubble interface is denoted with Γ_F. The channel is assumed to be of length L, and it holds

$$\Gamma_I = \left\{ \mathbf{x} \in \mathbb{R}^d : \mathbf{x} = \mathbf{y} + (0, L)^T \ , \mathbf{y} \in \Gamma_O \right\} \ . \tag{3.5.1}$$

The periodicity is assumed to be in y-direction. In the following let $\mathbf{y} = (0, L)^T$. It is required that

$$\mathbf{u}(\mathbf{x}, t) = \mathbf{u}(\mathbf{x} + \mathbf{y}, t) \ .$$

It is further assumed that the flow is smooth in the complete channel, which implies the velocity is smooth for any choice of segment from the channel. Hence, the following additional condition is enforced

$$(\mathbf{n} \cdot \nabla)\mathbf{u}(\mathbf{x}, t) = (\mathbf{n} \cdot \nabla)\mathbf{u}(\mathbf{x} + \mathbf{y}, t) \ , \quad \text{on } \Gamma_O \ .$$

Including these conditions, the equations of the strong form for this problem read:

$$\begin{aligned}
\partial_t^{\mathbf{w}} \mathbf{u} + ((\mathbf{u} - \mathbf{w}) \cdot \nabla)\mathbf{u} - \nabla \cdot \mathbb{S}(\mathbf{u}, p) &= 0 && \text{in } \Omega(t) \ , && \text{(3.5.2a)} \\
\nabla \cdot \mathbf{u} &= 0 && \text{in } \Omega(t) \ , && \text{(3.5.2b)} \\
[\![\mathbf{u}]\!]_\Gamma &= 0 && \text{in } \Omega(t) \ , && \text{(3.5.2c)} \\
\mathbf{w} \cdot \mathbf{n}_\Gamma &= \mathbf{u} \cdot \mathbf{n}_\Gamma && \text{on } \Gamma_F(t) \ , && \text{(3.5.2d)} \\
[\![\mathbb{S}(\mathbf{u}, p)]\!]_\Gamma \cdot \mathbf{n}_\Gamma &= \mathrm{We}^{-1} \sigma_0 \nabla_\Gamma \cdot \mathbb{P}_\Gamma && \text{on } \Gamma_F(t) \ , && \text{(3.5.2e)} \\
\mathbf{u}(\mathbf{x}, t) &= \mathbf{u}(\mathbf{x} + \mathbf{y}, t) && \text{on } \Gamma_O \ , && \text{(3.5.2f)} \\
(\mathbf{n} \cdot \nabla)\mathbf{u}(\mathbf{x}, t) &= (\mathbf{n} \cdot \nabla)\mathbf{u}(\mathbf{x} + \mathbf{y}, t) && \text{on } \Gamma_O \ , && \text{(3.5.2g)} \\
\mathbf{u} &= 0 && \text{on } \Gamma_W \ . && \text{(3.5.2h)}
\end{aligned}$$

In order to derive the weak form of the equations above, a periodic functions space is introduced

$$V(t) := \{\mathbf{v} \in H^1(\Omega(t))^d : \mathbf{v}(\mathbf{x}) = \mathbf{v}(\mathbf{x} + (0, L)) \text{ on } \Gamma_O, \mathbf{v} = 0 \text{ on } \Gamma_W\} \ .$$

Equation (3.5.2a) is multiplied with a test function $\mathbf{v} \in V(t)$. The term with the stress tensor is integrated by parts on each domain separately, which leads to

$$\begin{aligned}(\nabla \cdot \mathbb{S}(\mathbf{u}, p), \mathbf{v})_{\Omega(t)} = &- (\mathbb{S}(\mathbf{u}, p), \nabla \mathbf{v})_{\Omega(t)} - \mathrm{We}^{-1}\, \sigma_0 \, \langle \mathbb{P}_\Gamma, \nabla_\Gamma \mathbf{v} \rangle_{\Gamma(t)} \\ &+ \langle \mathbb{S}(\mathbf{u}, p)\mathbf{n}, \mathbf{v} \rangle_{\Gamma_I(t)} + (\mathbb{S}(\mathbf{u}, p)\mathbf{n}, \mathbf{v})_{\Gamma_O(t)} \ .\end{aligned}$$

In the interface integrals the momentum balance condition (3.5.2e) was substituted, analogue to the weak formulations before. The integral terms over the inflow boundary and the outflow boundary do not vanish this time, since the periodic boundary conditions are used.

Using (3.5.2g) the normal stress $\mathbb{S}(\mathbf{u}, p)\mathbf{n}$ on the outflow boundary Γ_O can be written as

$$\begin{aligned}\mathbb{S}(\mathbf{u}(\mathbf{x}, t), p(\mathbf{x}, t))\mathbf{n}(\mathbf{x}) &= \varrho \, \mathrm{Re}^{-1} \left(\nabla \mathbf{u}(\mathbf{x}, t) + (\nabla \mathbf{u}(\mathbf{x}, t))^T \right) \mathbf{n}(\mathbf{x}) - p(\mathbf{x}, t)\mathbf{n}(\mathbf{x}) \\ &= \varrho \, \mathrm{Re}^{-1} \left(\nabla \mathbf{u}(\mathbf{x} + \mathbf{y}, t) + (\nabla \mathbf{u}(\mathbf{x} + \mathbf{y}, t)^T \right) \mathbf{n}(\mathbf{x}) \\ &\quad - p(\mathbf{x}, t)\mathbf{n}(\mathbf{x}) \\ &= \mathbb{S}(\mathbf{u}(\mathbf{x} + \mathbf{y}), p(\mathbf{x}, t))\mathbf{n}(\mathbf{x})\end{aligned}$$

and after using (3.5.1) and considering the orientation of the normals it is obtained

$$\mathbb{S}(\mathbf{u}(\mathbf{x}, t), p(\mathbf{x}, t))\mathbf{n}_{\Gamma_O}(\mathbf{x}) = -\mathbb{S}(\mathbf{u}(\mathbf{x} + \mathbf{y}, t), p(\mathbf{x}, t))\mathbf{n}_{\Gamma_I}(\mathbf{x} + \mathbf{y}) \ .$$

Let $p_O(\mathbf{x}, t) = p(\mathbf{x} - \mathbf{y}, t)$ for $\mathbf{x} \in \Gamma_I$ be the pressure on outflow boundary transferred to the inflow boundary. Exploiting the periodicity of the test function $\mathbf{v}$, the integral term of the normal stress over the outflow boundary can be written as

$$\langle \mathbb{S}(\mathbf{u}, p)\mathbf{n}, \mathbf{v} \rangle_{\Gamma_O(t)} = - \langle \mathbb{S}(\mathbf{u}, p_O)\mathbf{n}, \mathbf{v} \rangle_{\Gamma_I(t)} \ ,$$

such that

$$\begin{aligned}\langle \mathbb{S}(\mathbf{u}, p)\mathbf{n}, \mathbf{v} \rangle_{\Gamma_I(t)} + \langle \mathbb{S}(\mathbf{u}, p)\mathbf{n}, \mathbf{v} \rangle_{\Gamma_O(t)} &= \langle [\mathbb{S}(\mathbf{u}, p) - \mathbb{S}(\mathbf{u}, p_O)] \, \mathbf{n}, \mathbf{v} \rangle_{\Gamma_I(t)} \\ &= \langle (p - p_O) \, \mathbf{n}, \mathbf{v} \rangle_{\Gamma_I(t)} \ .\end{aligned}$$

The pressure difference $\delta p := p - p_O$ is the pressure drop in the channel, and has to be given. For the stress term it is obtained

$$\begin{aligned}(\nabla \cdot \mathbb{S}(\mathbf{u}, p), \mathbf{v})_{\Omega(t)} = &- \left(2\varrho \, \mathrm{Re}^{-1} \, \mathbb{D}(\mathbf{u}), \mathbb{D}(\mathbf{u})\right)_{\Omega(t)} + (p, \nabla \cdot \mathbf{v})_{\Omega(t)} \\ &- \mathrm{We}^{-1} \, \sigma_0 \, \langle \mathbb{P}_\Gamma, \nabla_\Gamma \mathbf{v} \rangle_{\Gamma(t)} + \langle \delta p \mathbf{n}, \mathbf{v} \rangle_{\Gamma_I(t)} \ .\end{aligned}$$

The following abbreviations are introduced

$$\begin{aligned} a_t(\mathbf{b};\mathbf{u},\mathbf{v}) &:= (\varrho\,(\mathbf{b}\cdot\nabla)\,\mathbf{u},\mathbf{v})_{\Omega(t)} + \left(2\varrho\,\mathrm{Re}^{-1}\,\mathbb{D}(\mathbf{u}),\mathbb{D}(\mathbf{u})\right)_{\Omega(t)} \ , \\ b_t(\mathbf{v},q) &:= (\nabla\cdot\mathbf{v},q)_{\Omega(t)} \ , \\ f_t(\delta p;\mathbf{v}) &:= \langle \delta p\mathbf{n},\mathbf{v}\rangle_{\Gamma_I(t)} - \mathrm{We}^{-1}\,\sigma_0\,\langle \mathbb{P}_\Gamma,\nabla_\Gamma\mathbf{v}\rangle_{\Gamma(t)} \ . \end{aligned}$$

With these forms the weak formulation reads:

Problem 3.5.1 (Pressure driven periodic channel flow)**.** *For almost all $t\in(t_0,t_b)$, given $\delta p(t)$, find $(\mathbf{u},\mathbf{w},p)\in V(t)\times H_0^1(\Omega(t))\times L_0^2(\Omega(t))$ such that*

$$(\varrho\partial_t^{\mathbf{w}}\mathbf{u},\mathbf{v})_{\Omega(t)} + a_t((\mathbf{u}-\mathbf{w});\mathbf{u},\mathbf{v}) - b_t(\mathbf{v},p) = f_t(\delta p(t);\mathbf{v}) \ , \tag{3.5.3a}$$

$$b_t(\mathbf{u},q) = 0 \ , \tag{3.5.3b}$$

for all $(\mathbf{v},q)\in V(t)\times L_0^2(\Omega(t))$.

3.5.2 Three Dimensional Rotational Symmetric Flow

In many applications, the flow structure has a symmetry. This can be exploited in order to reduce the complexity of the problem. In the following a three dimensional rotational symmetric flow is considered. Such that, the three dimensional problem is transferred into a two dimensional problem.

The coordinates suited to describe a rotational symmetric problem are the cylindrical coordinates. Hence, the flow problem given in Cartesian coordinates, has to be transferred in cylindrical coordinates. Let a point $\mathbf{x}$ given in Cartesian coordinates be described by the tuple $\mathbf{x}=(x,y,z)^T$ and given in cylindrical coordinates by the tuple $\mathbf{x}=(r,\phi,z)^T$. In cylindrical coordinates r is the radial distance from the symmetry axis, ϕ is the azimuth angle, and z is the height.

Both coordinate systems can be transferred into each other, by

$$\begin{pmatrix}x\\y\\z\end{pmatrix} = \begin{pmatrix}r\cos\phi\\ r\sin\phi\\ z\end{pmatrix} \ , \quad \begin{pmatrix}r\\\phi\\z\end{pmatrix} = \begin{pmatrix}\sqrt{x^2+y^2}\\ \arctan(y/x)\\ z\end{pmatrix} \ , \quad 0\le\phi\le 2\pi \ .$$

For a scalar function f given in Cartesian coordinates $f=f(x,y,z)$, the corresponding counterpart, given in cylindrical coordinates will be denoted with $\tilde{f}=\tilde{f}(r,\phi,z)$. It holds

$$\tilde{f}(r,\phi,z) = f(x(r,\phi),y(r,\phi),z) \ .$$

With this definition, the differential operator transform as follows. The nabla operator in cylindrical coordinates is given as follows

$$\nabla\tilde{f} = \left(\partial_r\tilde{f}, r^{-1}\partial_\phi\tilde{f}, \partial_z\tilde{f}\right)^T \ . \tag{3.5.4}$$

The Laplace operator in cylindrical coordinates reads

$$\Delta\, \tilde{f} = r^{-1}\partial_r \left(r\partial_r \tilde{f} \right) + r^{-2}\partial^2_{\phi\phi}\tilde{f} + \partial^2_{zz}\tilde{f} \ .$$

A vector valued function $\mathbf{v} = (v_x, v_y, v_z)^T$ in Cartesian coordinates, will be denoted $\tilde{\mathbf{v}} = (v_r, v_\phi, v_z)^T$ in cylindrical coordinates. It holds

$$\begin{pmatrix} v_x \\ v_y \\ v_z \end{pmatrix} = \begin{pmatrix} v_r \cos\phi - v_\phi \sin\phi \\ v_r \sin\phi + v_\phi \cos\phi \\ u_z \end{pmatrix} \ .$$

The divergence operator is written in cylindrical coordinates as follows

$$\nabla \cdot \tilde{\mathbf{v}} = r^{-1}\partial_r(r v_r) + r^{-1}\partial_\phi v_\phi + \partial_z v_z \ .$$

Rotational symmetry implies, that a function is independent of the azimuth angle ϕ, i.e. $\partial_\phi \tilde{f} = 0$, $\partial_\phi v_r = 0$, and $\partial_\phi v_z = 0$. Further, it is assumed that the ϕ-component of a vector field vanishes, i.e. $v_\phi = 0$ and

$$\tilde{\mathbf{v}} = \left(v_r, 0, v_z\right)^T \ . \tag{3.5.5}$$

With this assumptions the Nabla operator gets

$$\nabla \tilde{f} = \left(\partial_r \tilde{f}, 0, \partial_z \tilde{f} \right)^T \ ,$$

and the divergence operator reads

$$\nabla \cdot \tilde{\mathbf{v}} = r^{-1}\partial_r v_r + v_r + \partial_z v_z \ .$$

Further, the convectional derivative $(\tilde{\mathbf{b}} \cdot \nabla)\tilde{\mathbf{u}}$ is as follows

$$\left(\tilde{\mathbf{b}} \cdot \nabla \right) \tilde{\mathbf{u}} = \begin{pmatrix} b_r\partial_r u_r + b_z \partial_z u_r \\ 0 \\ b_r \partial_r u_z + b_z \partial_z u_z \end{pmatrix} \ . \tag{3.5.6}$$

Using (3.5.4) component-wise, the Jacobian $\nabla \mathbf{v}$ written in cylindrical coordinates reads for a rotational symmetric function $\mathbf{v}$

$$\nabla \tilde{\mathbf{v}} = \begin{pmatrix} \cos\phi\partial_r v_r & -r^{-1}\sin\phi v_r & \cos\phi\partial_z v_r \\ \sin\phi\partial_r v_r & r^{-1}\cos\phi v_r & \cos\phi\partial_z v_r \\ \partial_r v_z & 0 & \partial_z v_z \end{pmatrix} \ .$$

It follows for the matrix scalar product $\nabla\tilde{\mathbf{u}} : \nabla\tilde{\mathbf{v}}$ that

$$\nabla\tilde{\mathbf{u}} : \nabla\tilde{\mathbf{v}} = \partial_r u_r \partial_r v_r + r^{-2} u_r v_r + \partial_z u_r \partial_z v_r + \partial_r u_z \partial_r v_z + \partial_z u_z \partial_z v_z \ .$$

From this, the matrix scalar product $\mathbb{D}(\tilde{\mathbf{u}}) : \mathbb{D}(\tilde{\mathbf{v}})$ of the deformation tensors can be deduced

$$\mathbb{D}(\tilde{\mathbf{u}}) : \mathbb{D}(\tilde{\mathbf{v}}) = \partial_r u_r \partial_r v_r + r^{-2} u_r v_r + \frac{1}{2} \left(\partial_z u_r + \partial_r u_z\right) \left(\partial_z v_r + \partial_r v_z\right) + \partial_z u_z \partial_z v_z \ . \tag{3.5.7}$$

In the following, let $\Omega(t)$ be a rotational symmetric domain, and let $\tilde{\Omega}(t)$ be the two dimensional domain, that generates $\Omega(t)$, i.e.

$$\tilde{\Omega}(t) := \left\{(r,z) \in \mathbb{R}^2 : (r,\phi,z) \in \Omega(t), 0 \le \phi \le 2\pi\right\} \ .$$

And let $\tilde{\Gamma}(t)$ be the curve generating $\Gamma(t)$, i.e.

$$\tilde{\Gamma}(t) = \left((r,z) \in \mathbb{R}^2 : (r,\phi,z) \in \Gamma(t)\right) \ .$$

With this notations the integral forms can be transferred to cylindrical coordinates. For a volume integral over and rotational symmetric function $\tilde{f} = \tilde{f}(r,z)$ it holds

$$\begin{aligned} \int_{\Omega(t)} f \ \mathrm{d}V &= \iiint_{\Omega(t)} f(x,y,z) \,\mathrm{d}x \,\mathrm{d}y \,\mathrm{d}z = \iiint_{\Omega(t)} \tilde{f}(r,z) r \,\mathrm{d}r \,\mathrm{d}\phi \,\mathrm{d}z \\ &= 2\pi \iint_{\tilde{\Omega}(t)} \tilde{f}(r,z) r \,\mathrm{d}r \,\mathrm{d}z \ . \end{aligned}$$

From this it follows, with using (3.5.5)

$$(\varrho \partial_t^{\mathbf{w}} \mathbf{u}, \mathbf{v})_{\Omega(t)} = 2\pi \iint_{\tilde{\Omega}(t)} \tilde{\varrho} \partial_t^{\mathbf{w}} \tilde{\mathbf{u}} \cdot \tilde{\mathbf{v}} r \,\mathrm{d}r \,\mathrm{d}z \ ,$$

and using (3.5.6)

$$(\varrho \left(\mathbf{b} \cdot \nabla\right) \mathbf{u}, \mathbf{v})_{\Omega(t)} = 2\pi \iint_{\tilde{\Omega}(t)} \tilde{\varrho} (\tilde{\mathbf{b}} \cdot \nabla) \tilde{\mathbf{u}} \cdot \tilde{\mathbf{v}} r \,\mathrm{d}r \,\mathrm{d}z \ ,$$

and using (3.5.7)

$$\begin{aligned} \left(\varrho \,\mathrm{Re}^{-1} \,\mathbb{D}(\mathbf{u}), \mathbb{D}(\mathbf{v})\right)_{\Omega(t)} &= 2\pi \iint_{\tilde{\Omega}(t)} \tilde{\varrho} \,\mathrm{Re}^{-1} \,\mathbb{D}(\tilde{\mathbf{u}}) : \mathbb{D}(\tilde{\mathbf{v}}) r \,\mathrm{d}r \,\mathrm{d}z \ , \\ (\nabla \cdot \mathbf{v}, q)_{\Omega(t)} &= 2\pi \iint_{\tilde{\Omega}(t)} \tilde{q} \left(\partial_r v_r + r^{-1} v_r + \partial_z v_z\right) r \,\mathrm{d}r \,\mathrm{d}z \ , \\ \langle \mathbf{u}, \mathbf{v} \rangle_{\Gamma(t)} &= 2\pi \int_{\tilde{\Gamma}(t)} \tilde{\mathbf{u}} \cdot \tilde{\mathbf{v}} r \ \mathrm{d}C \ , \\ \mathrm{We}^{-1} \left\langle \sigma \mathbb{P}_\Gamma, \nabla_\Gamma \mathbf{v} \right\rangle_{\Gamma(t)} &= 2\pi \,\mathrm{We}^{-1} \int_{\tilde{\Gamma}(t)} \tilde{\sigma} \left[\nabla_{\tilde{\Gamma}} r \cdot \nabla_{\tilde{\Gamma}} v_r + \nabla_{\tilde{\Gamma}} z \cdot \nabla_{\tilde{\Gamma}} v_z + r^{-1} v_r\right] r \ \mathrm{d}C \ . \end{aligned}$$

Substituting the above integral forms leads to the rotational symmetric formulation, for the components $(u_r, u_z) \in \mathbb{R}^2$. The symmetry axis $r = 0$ is an artificial boundary and needs additional boundary conditions. The boundary conditions are

$$\begin{aligned} u_r(r, z) &= 0 \ , \quad \text{for } r = 0 \ , \\ \partial_r u_z &= 0 \ , \quad \text{for } r = 0 \ . \end{aligned}$$

Chapter 4

Finite Element Method

In Chapter 4, the ALE finite element discretizations in space and time are introduced. First, the ALE finite element space is defined. In order to do so, some basic finite element concepts are recalled, and ALE meshes are introduced. Then, a space-discrete weak form is obtained.

The choice for the finite element space in the context of a discontinuous pressure, which is important for two-phase flows, is discussed. The finite elements used for the Navier-Stokes part have a discontinuous, domain-wise continuous pressure. This finite element space is an extended Taylor-Hood finite element space, that is a domain-wise Taylor-Hood finite element space. The velocity space is a space of piecewise polynomials of order s, which is continuous in the whole domain, while the pressure space consist of polynomials of order $s-1$, that are allowed to be discontinuous across the interface. It is shown that this domain-wise Taylor-Hood space is inf-sup stable.

After that, several time discretizations are introduced. A first order semi-implicit Euler method, a θ-scheme, from which the second order accurate Crank-Nicolson scheme follows, and the second order accurate and A-stable fractional step Θ-scheme. Further, decoupling strategies are presented, which decouple the Navier-Stokes equations from the transport equations.

Finally, different discretization of the surface evolution are discussed.

4.1 Spatial Discretization

In order to lay down the notation, a few basic finite element concepts are recalled. Most notations and definitions are taken from standard finite element textbooks, like [41, 55].

Let $\mathbb{P}_s$ be the polynomial space of order s. Thus, for $M \subset \mathbb{R}^d$

$$\mathbb{P}_s(M) := \left\{ p \in C^0(M) : p(\mathbf{x}) = \sum_{|\alpha| \leq s} \lambda_\alpha \mathbf{x}^\alpha \ , \ \lambda_\alpha \in \mathbb{R} \right\} \ ,$$

where the multi-index notation is used, i.e. $\alpha = (\alpha_1, \ldots, \alpha_d)$ and $\mathbf{x}^\alpha = x_1^{\alpha_1} \cdots x_d^{\alpha_d}$.

The definition of a finite element and a mapped finite element is as follows.

Definition 4.1.1 (Finite element)**.** *A finite element is a triple (K, P_K, Σ_K) where:*

(i) K is a compact, connected, non-empty subset of $\mathbb{R}^d$ with a Lipschitz continuous boundary.

(ii) P_K is a finite dimensional vector space of real valued functions, defined over K.

(iii) Σ_K is a set of N linear forms $\{\mathcal{N}_1, \ldots, \mathcal{N}_N\} \subset P_K'$, such that Σ is P_K-unisolvent, i.e. the mapping $P \ni p \mapsto (\mathcal{N}_1(p), \ldots, \mathcal{N}_N(p)) \in \mathbb{R}^N$ is bijective. The linear forms are called nodal functional or local degrees of freedom.

Definition 4.1.2 (Mapped finite element)**.** *Let $(\hat{K}, \hat{P}, \hat{\Sigma})$ be a finite element triple as in Definition 4.1.1, and let $F_K : \hat{K} \to K$ be a bijective mapping, then a mapped finite element (K, P_K, Σ_K) is defined with*

$$P_K := \{\phi \circ F_K^{-1} : \phi \in \hat{P}\}$$

and

$$\Sigma_K := \{\mathcal{N} \in P_K' : \mathcal{N}(\phi \circ F_K^{-1}) = \hat{\mathcal{N}}(\phi), \hat{\mathcal{N}} \in \hat{\Sigma}, \forall \phi \in \hat{P}\} \ .$$

If $\hat{K} \subset \mathbb{R}^{d-n}$, $0 < n < d$ and K is a $(d-n)$-dimensional manifold embedded in $\mathbb{R}^n$, the mapped finite element is also called a parametric finite element.

A mapped finite element is a finite element, provided F_K is a bijective mapping [41]. In a three dimensional space, parametric finite elements could be surface elements or line elements.

Definition 4.1.3 (Mesh)**.** *Let $\Omega \subset \mathbb{R}^d$ be a domain with piecewise smooth boundary. A mesh $\mathcal{T}_h = \{K_j\}_{j=1}^N$ is a set of a finite number of compact, Lipschitz, and non-empty subsets $K_m \subset \Omega$, $j = 1, \ldots, N$ with*

$$\overline{\Omega} = \bigcup_{j=1}^{N} K_j \quad \textit{and} \quad \mathring{K}_i \cap \mathring{K}_j = \emptyset, \ i \neq j.$$

The subsets K_m are called cells. The subscript h refers to the fineness of the mesh, where

$$h_K = \operatorname{diam} K \quad \textit{and} \quad h = \max_{j=1,\ldots,N} h_{K_j} \ ,$$

and h_K is called the local mesh size and h is called the mesh size.

Definition 4.1.4 (Mapped mesh)**.** *Let $\Omega \subset \mathbb{R}^d$ and $\mathcal{T}_h$ be a mesh as in Definition 4.1.3. A mapped mesh is a mesh where each cell is the image of a reference cell $\hat{K}$ of a mapping F_K, i.e.*

$$\forall K \in \mathcal{T}_h : K = F_K(\hat{K}) \ .$$

$F_K : \hat{K} \to \mathbb{R}^d$ is called the reference transformation.

In this work, simplicial meshes are considered, i.e. triangular meshes in two dimensions and tetrahedral meshes in three dimensions. Here, the notation simplicial mesh is somewhat relaxed. The reference cell $\hat{K}$ is required to be a simplex. The mapped cell $K = F_K(\hat{K})$ does not necessarily has to be a simplex. It is allowed to be a curved simplex.

Let the reference element $\hat{K}$ be a $(d-n)$-simplex. If the reference mapping $F_K : \hat{K} \subset \mathbb{R}^{d-n} \to \mathbb{R}^d$, $0 < n < d$ is an affine mapping, then K is a $(d-n)$-simplex embedded in $\mathbb{R}^d$ and F_K can be written as

$$F_K(\hat{\mathbf{x}}) = B_K \hat{\mathbf{x}} + b_K \ , \quad \hat{\mathbf{x}} \in \hat{K} \ ,$$

where $B_K \in \mathbb{R}^{d \times (d-n)}$ and $b_K \in \mathbb{R}^d$.

Let $r = (d-n)$ and a_i, $i = 0, \dots, r$ be the vertices of this r-simplex K, then the affine mapping F_K can also be written as

$$\mathbf{x} = F_K(\hat{\mathbf{x}}) = \sum_{i=0}^{d} a_i \phi_i(\hat{\mathbf{x}}) \ , \quad \hat{\mathbf{x}} \in \hat{K} \ . \tag{4.1.1}$$

The set $\{\phi_i\}_{i=0}^r$ is the Lagrange basis of the space $\mathbb{P}_1(\hat{K})$ of polynomials of order one over $\hat{K}$, respective the points $\hat{a}_i = F_K^{-1}(a_i)$, $i = 0, \dots, r$. The reference simplex $\hat{K}$ is spanned by the vertices $\hat{a}_i$. The $\phi_i(\hat{\mathbf{x}})$ are also called *barycentric coordinates* $\lambda_i = \phi_i(\hat{\mathbf{x}})$ of the simplex K. The matrix B_K and the vector b_K are given by

$$B_K = \begin{pmatrix} a_1 - a_0 \\ \vdots \\ a_r - a_0 \end{pmatrix}^T \ , \quad \text{and} \quad b_K = a_0 \ .$$

The approach (4.1.1) can be generalised to polynomial spaces of higher order. Introducing additional points, respective the order of the polynomial space, the mapped cell is then a cell with curved piecewise polynomial faces. If the polynomial degree of the mapping F_K is equal to the polynomial degree of the finite element approximation space, then the mesh cells are called *isoparametric* cells. Isoparametric cells are used to improve the approximation of the curvature of the interface [74].

Definition 4.1.5 (Parametric polynomial mesh)**.** *Let $\Omega \subset \mathbb{R}^d$ be a domain with piecewise polynomial boundary and let $\mathcal{T}_h$ be a mapped mesh as in Definition 4.1.4. The mesh $\mathcal{T}_h$ is called a parametric polynomial mesh of order s, if for every $K \in \mathcal{T}_h$ it holds*

$$F_K = \sum_{i=0}^{n} a_i \phi_i \ ,$$

where $\{\phi_i\}_{i=0}^n$, with $\mathbb{P}_s(K) = \operatorname{span}\{\phi_i\}_{i=0}^n$, is a Lagrange basis respective the points $F_K^{-1}(a_i)$, $i = 1, \dots, n$.

The points a_i are called nodes or vertices of the mesh.

In the following, the set of all nodes belonging to a cell K is denoted with $\mathcal{N}_K$. The purpose of the following definition is to have a mesh that is aligned to the interface.

Definition 4.1.6 (Fitted mesh)**.** *Let $\Omega \subset \mathbb{R}^d$ with $\Omega = \Omega_1 \cup \Omega_2 \cup \Gamma$ be a domain with an interface Γ and two subdomains Ω_1, Ω_2 with $\Omega_1 \cap \Omega_2 = \emptyset$ and $\Gamma = \overline{\Omega}_1 \cap \overline{\Omega}_2$. Further, let $\mathcal{T}_h$ be a polynomial mesh as in Definition 4.1.5. $\mathcal{T}_h$ is called fitted to Γ, if for each cell $K \in \mathcal{T}_h$ it holds*

$$\mathcal{N}_K \subset \overline{\Omega_1} \quad or \quad \mathcal{N}_K \subset \overline{\Omega_2} \ .$$

A mesh that is fitted to an interface Γ is also denoted with $\mathcal{T}_h^\Gamma$.

Given a fitted mesh for a domain $\Omega = \Omega_1 \cup \Omega_2 \cup \Gamma$, a mesh for the surface Γ is given implicitly. Since, a face of a d-dimensional simplex, is a $(d-1)$-dimensional simplex, selecting all faces F of a mesh $\mathcal{T}_h^\Gamma$ with $\mathcal{N}_F \subset \Gamma$ a parametric polynomial surface mesh is generated.

Definition 4.1.7 (Interface mesh)**.** *Given a fitted mesh $\mathcal{T}_h^\Gamma$ of $\Omega \subset \mathbb{R}^d$ as in Definition 4.1.6 and let $\mathcal{F}(\mathcal{T}_h^\Gamma)$ be the set of all faces of the cells belonging to $\mathcal{T}_h^\Gamma$, then a surface mesh is given by*

$$\mathcal{S}_h^\Gamma := \{F \in \mathcal{F}(\mathcal{T}_h^\Gamma) : \mathcal{N}_F \subset \Gamma\} \ .$$

The domain

$$\Gamma_h := \bigcup_{F \in \mathcal{S}_h^\Gamma} F \ ,$$

is the discrete interface.

Note that Γ_h and Γ are not necessarily the same surface.

A cell F of the surface mesh is then the image of a reference mapping $F_F : \hat{F} \to F$, where $\hat{F} \subset \hat{K}$ is a corresponding reference face. Note, that two faces could be the image of different reference faces of the reference cell.

Having introduced the notion of a finite element and a fitted mesh for a domain with an interface, the finite element space can be introduced. A mapped finite element space on the reference domain $\tilde{\Omega} \subset \mathbb{R}^d$ and on the reference surface $\tilde{\Gamma}$ is introduced in the following.

Definition 4.1.8 (Mapped finite element space)**.** *Let $\Omega \subset \mathbb{R}^d$ be a domain and $\mathcal{T}_h^\Gamma$ a fitted mesh for Ω as in Definition 4.1.6 and $\mathcal{S}_h^\Gamma$ a surface mesh as in Definition 4.1.7.*

A continuous mapped finite element space consisting of piecewise polynomials of order s is defined as

$$\mathcal{P}_s(\Omega) := \{\phi \in H^1(\Omega) : \forall K \in \mathcal{T}_h^\Gamma : \phi|_K = \hat{\phi} \circ F_K^{-1}, \hat{\phi} \in \mathbb{P}_s(\hat{K})\} \ .$$

A phase-wise continuous finite element space consisting of polynomials of order s is defined as

$$\mathcal{D}_s(\Omega) := \{\phi \in H^1(\Omega_1 \cup \Omega_2) : \forall K \in \mathcal{T}_h^\Gamma : \phi|_K = \hat{\phi} \circ F_K^{-1}, \hat{\phi} \in \mathbb{P}_s(\hat{K})\} \ .$$

A continuous parametric surface finite element space is defined as

$$\mathcal{S}_s(\Gamma) := \{\phi \in H^1(\Gamma) : \forall F \in \mathcal{S}_h^\Gamma : \phi|_F = \hat{\phi} \circ F_F^{-1}, \hat{\phi} \in \mathbb{P}_s(\hat{F})\} \ .$$

Having defined a finite element space on the reference domain, a finite element space in the current domain is given as follows.

Definition 4.1.9 (ALE finite element space)**.** *Let $\Omega \subset \mathbb{R}^d$ be a domain and $\tilde{\Omega}$ its reference domain, i.e. $\Omega = \mathcal{A}_t(\tilde{\Omega})$, and let $\mathcal{P}_s(\tilde{\Omega})$, $\mathcal{D}_s(\tilde{\Omega})$, and $\mathcal{S}_s(\tilde{\Gamma})$ be finite element spaces on $\tilde{\Omega}$ as in Definition 4.1.8, then the ALE finite element spaces on Ω are defined as*

$$\begin{aligned}
\mathcal{P}_{\mathcal{A}_t,s}(\Omega) &:= \{\phi \in H^1(\Omega) : \phi = \tilde{\phi} \circ \mathcal{A}_t^{-1}, \tilde{\phi} \in \mathcal{P}_s(\tilde{\Omega})\} \ , \\
\mathcal{D}_{\mathcal{A}_t,s}(\Omega) &:= \{\phi \in H^1(\Omega_1 \cup \Omega_2) : \phi = \tilde{\phi} \circ \mathcal{A}_t^{-1}, \tilde{\phi} \in \mathcal{D}_s(\tilde{\Omega})\} \ , \\
\mathcal{S}_{\mathcal{A}_t,s}(\Gamma) &:= \{\phi \in H^1(\Gamma) : \phi = \tilde{\phi} \circ \mathcal{A}_t^{-1}, \tilde{\phi} \in \mathcal{S}_s(\tilde{\Gamma})\} \ .
\end{aligned}$$

With the finite element spaces for the bulk phases and the surface introduced, the space discretization of problem (3.1.10) can be formulated. For $t \in (t_0, t_b)$, it is set $\mathbb{V}_s(t) = \mathcal{P}_{\mathcal{A}_t,s}(\Omega(t))^d$ as the velocity space, $\mathbb{Q}_s(t) = \mathcal{D}_{\mathcal{A}_t,s}(\Omega(t))$ for the pressure space, $\mathbb{B}_s(t) = \mathcal{D}_{\mathcal{A}_t,s}(\Omega(t))$ for the bulk surfactant space, and $\mathbb{S}_s(t) = \mathcal{P}_{\mathcal{A}_t,s}(\Gamma_h(t))$ for the surface surfactant space.

In order to shorten the notation, the following abbreviations are introduced. The triple form $a_t^{\mathbf{u}} : \mathbb{V}_s(t) \times \mathbb{V}_s(t) \times \mathbb{V}_s(t) \to \mathbb{R}$ with

$$a_t^{\mathbf{u}}(\mathbf{b}; \mathbf{u}, \mathbf{v}) := (\varrho(\mathbf{b} \cdot \nabla)\mathbf{u}, \mathbf{v})_{\Omega(t)} + \left(2\varrho \operatorname{Re}^{-1} \mathbb{D}(\mathbf{u}), \mathbb{D}(\mathbf{v})\right)_{\Omega(t)} \ ,$$

the bilinear form $b_t : \mathbb{V}_s(t) \times \mathbb{Q}_{s-1}(t) \to \mathbb{R}$ with

$$b_t(\mathbf{v}, q) := (p, \nabla \cdot \mathbf{v})_{\Omega(t)} \ ,$$

the triple form $a_t^c : \mathbb{V}_s(t) \times \mathbb{B}_s(t) \times \mathbb{B}_s(t) \to \mathbb{R}$ with

$$a_t^c(\mathbf{b}; c, \phi) := ((\mathbf{b} \cdot \nabla)c, \phi)_{\Omega(t)} + \left(\operatorname{Pe}^{-1} \nabla c, \phi\right)_{\Omega(t)} \ ,$$

the quadruple form $a_t^\Gamma : \mathbb{V}_s(t) \times \mathbb{V}_s(t) \times \mathbb{S}_s(t) \times \mathbb{S}_s(t) \to \mathbb{R}$ with

$$a_t^\Gamma(\mathbf{b}, \mathbf{w}; \gamma, \xi) := \langle \gamma \nabla_\Gamma \cdot \mathbf{w}, \xi \rangle_{\Gamma(t)} + \langle \nabla_\Gamma \cdot (\gamma \mathbf{b}), \xi \rangle_{\Gamma(t)} + \left\langle \operatorname{Pe}_\Gamma^{-1} \nabla_\Gamma \gamma, \nabla_\Gamma \xi \right\rangle_{\Gamma(t)} \ ,$$

the bilinear form $f_t^{\mathbf{u}} : \mathbb{S}_s(t) \times \mathbb{V}_s(t) \to \mathbb{R}$ with

$$f_t^{\mathbf{u}}(\gamma; \mathbf{v}) := \left(\varrho \operatorname{Fr}^{-1} \mathbf{g}, \mathbf{v}\right)_{\Omega(t)} - \left\langle \operatorname{We}^{-1} \sigma(\gamma) \mathbb{P}_\Gamma, \nabla \mathbf{v} \right\rangle_{\Gamma(t)} \ ,$$

the nonlinear form $f_t^c : \mathbb{B}_s(t) \times \mathbb{S}_s(t) \times \mathbb{B}_s(t) \to \mathbb{R}$ with

$$f_t^c(\gamma, c; \phi) := \langle \beta \, \mathcal{Q}_\Gamma(c_1, c_2, \gamma), \phi \rangle_{\Gamma(t)} \ ,$$

and the nonlinear form $f_t^\Gamma : \mathbb{B}_s(t) \times \mathbb{S}_s(t) \times \mathbb{S}_s(t) \to \mathbb{R}$ with

$$f_t^\Gamma(c, \gamma; \xi) := \langle \mathcal{Q}_\Gamma(c_1, c_2, \gamma), \xi \rangle_{\Gamma(t)} \ .$$

Then, the semi-discrete, time continuous problem for the two-phase flow reads:

Problem 4.1.1. *For almost all $t \in (t_0, t_b)$, find*

$$(\mathbf{u}(t), \mathbf{w}(t), p(t), c(t), \gamma(t)) \in \mathbb{V}_s(t) \times \mathbb{V}_s(t) \times \mathbb{Q}_{s-1}(t) \times \mathbb{B}_s(t) \times \mathbb{S}_s(t) \ ,$$

such that with $\mathbf{b}(t) = \mathbf{u}(t) - \mathbf{w}(t)$ it holds

$$(\varrho \partial_t^{\mathbf{w}} \mathbf{u}, \mathbf{v}) + a_t^{\mathbf{u}}(\mathbf{b}; \mathbf{u}, \mathbf{v}) - b_t(\mathbf{v}, p) = f_t^{\mathbf{u}}(\gamma, \mathbf{v}) \ , \tag{4.1.2a}$$

$$b_t(\mathbf{u}, q) = 0 \ , \tag{4.1.2b}$$

$$(\partial_t^{\mathbf{w}} c, \phi) + a_t^c(\mathbf{b}, c, \phi) = f_t^c(c, \gamma, \phi) \ , \tag{4.1.2c}$$

$$\langle \partial_t^{\mathbf{w}} \gamma, \xi \rangle + a_t^\Gamma(\mathbf{b}, \mathbf{w}; \gamma, \xi) = f_t^\Gamma(c, \gamma, \xi) \ , \tag{4.1.2d}$$

for all $(\mathbf{v}, q, \phi, \xi) \in \mathbb{V}_s(t) \times \mathbb{Q}_{s-1}(t) \times \mathbb{B}_s(t) \times \mathbb{S}_s(t)$.

Note, that the equations (4.1.2) have to be augmented by equations for the mesh velocity $\mathbf{w}$. These equations for the mesh velocity $\mathbf{w}$ could be a discrete version of the problems given in Chapter 3. For the harmonic extension (3.2.3) a discrete version could be:

Given $\mathbf{u} \in \mathbb{V}_s(t)$, find $\mathbf{w} \in \mathbb{V}_s(t)$ such that

$$(\nabla \mathbf{w}, \nabla \mathbf{v})_{\Omega(t)} = 0 \ , \tag{4.1.3a}$$

$$\mathbf{w}|_{\Gamma_h} = \mathbf{u}|_{\Gamma_h} \ , \tag{4.1.3b}$$

for all $\mathbf{v} \in \mathbb{V}_s(t)$.

Discrete versions of the surface evolution, will be discussed later in this chapter.

4.2 Inf-Sup Stable Finite Element Space

4.2.1 Spurious Velocities

The finite element pair for the two-phase Navier-Stokes problem has to be chosen carefully. In the finite element discretization of the Navier-Stokes problem, using the Galerkin approach with mixed finite elements for velocity and pressure, the spaces have to fulfil a compatibility condition, the *inf-sup condition*. The inf-sup condition is needed to get a well-posed saddle point problem [11]. Additionally, the discretization of the two-phase Navier-Stokes problem has to consider a discontinuous pressure, see Remark 2.3.1.

The discretization of Navier-Stokes equations lead to a saddle point problem. An abstract saddle point problem, is formulated as follows. Let X and Q be reflexive Banach spaces, and let $a : X \times X \to \mathbb{R}$ and $b : X \times Q \to \mathbb{R}$ be bilinear forms on those spaces. With $f \in X'$ and $g \in Q'$ the saddle point problem reads:

Find $u \in X$ and $p \in Q$, such that

$$a(u, v) + b(v, p) = f(v) \qquad \forall v \in X \ , \tag{4.2.1a}$$

$$b(u, q) = g(q) \qquad \forall q \in Q \ . \tag{4.2.1b}$$

Let X_0 be the kernel of the mapping $v \mapsto b(v, \cdot)$, i.e.

$$X_0 := \{v \in X : b(v, q) = 0, \forall q \in Q\} \ .$$

For the abstract saddle point problem (4.2.1) the following important theorem holds.

Theorem 4.2.1. *Problem* (4.2.1) *has a unique solution if and only if*

(i)

$$\exists \alpha > 0 : \ \inf_{u \in X_0} \sup_{v \in X_0} \frac{a(u, v)}{\|u\|_X \|v\|_X} \geq \alpha \ ,$$
$$\forall v \in X_0 : \ (a(u, v) = 0, \forall u \in X_0) \Rightarrow v = 0 \ .$$

(ii)

$$\exists \beta > 0 : \ \inf_{q \in Q} \sup_{v \in X} \frac{b(v, q)}{\|v\|_X \|q\|_Q} \geq \beta \ .$$

Proof. The proof can be found in [55, p.100]. □

If the bilinear form a is coercive on X_0, the condition *(i)* in Theorem 4.2.1 fulfilled. That is the case for the Stokes equation and the Navier-Stokes equation in the discrete setting. Condition *(i)* from Theorem 4.2.1 is also fulfilled if a is coercive on X. Under the assumption, condition *(i)* in Theorem 4.2.1 is meet, the theorem reduces to the *inf-sup condition* or *Babuška-Brezzi condition* [12, 32].

For the Navier-Stokes or Stokes problem the bilinear form $b : X \times Q \to \mathbb{R}$ reads

$$b(v, q) = (\nabla \cdot v, q) \ , \quad \forall v \in X, \forall q \in Q \ .$$

With this bilinear form, the inf-sup condition, necessary for the well-posedness of the Navier-Stokes equations, is fulfilled if:

There exist a constant $\beta > 0$, such that

$$\inf_{q \in Q} \sup_{v \in X} \frac{(\nabla \cdot v, q)}{\|v\|_X \|q\|_M} \geq \beta \ . \tag{4.2.2}$$

This is a condition at the spaces X and Q, involved in solving the discrete problem. There exist a lot of inf-sup stable finite element pairs. For example, the family of Taylor-Hood elements $\mathbb{P}_{k+1}/\mathbb{P}_k$, $k \geq 1$. The Taylor-Hood elements consist of piecewise polynomials of order $k+1$ for the velocity space X and of polynomials of order k for the pressure space Q.

However, the Taylor-Hood elements have a continuous pressure approximation, which is not suitable for the approximation of a discontinuous pressure across the interface [60]. On the one hand, the order of convergence reduces to $\mathcal{O}(\sqrt{h})$. In Table 4.2 the experimental order of convergence rates, of a two-phase flow problem on a three dimensional tetrahedral grid are shown. It is seen that the order reduces for a continuous pressure space. On the other hand, a discontinuous pressure space is needed to preserve the fluid volume of each phase. This can be seen by using the Reynolds transport theorem

$$\frac{d}{dt}\int_{\Omega_i(t)} 1 \, \mathrm{d}V = \int_{\Omega_i(t)} \nabla \cdot \mathbf{u} \, \mathrm{d}V = \left(\nabla \cdot \mathbf{u}, \mathbf{1}_{\Omega_i(t)}\right) \ ,$$

for $i = 1, 2$, where $\mathbf{1}_{\Omega_i(t)}$ is the characteristic function of domain i. The volume of each phase is preserved if

$$\left(\nabla \cdot \mathbf{u}, \mathbf{1}_{\Omega_i(t)}\right) = 0 \quad \text{for } i = 1, 2 \ . \tag{4.2.3}$$

The divergence constraint in the discrete setting is not strong enough in order to have $\nabla \cdot \mathbf{u} = 0$ point wise. Instead, it is necessary that $\mathbf{1}_{\Omega_i(t)} \in M$, $i = 1, 2$, to fulfil (4.2.3). This is not the case for continuous pressure approximations. A violation of these conditions leads to so called spurious velocities. That are non-physical velocities of the fluids near the interface, which can pollute the solution [19, 60, 64].

A solution to these problems is to use inf-sup stable finite element pairs with a discontinuous pressure space. There exist such pairs, for example the $\mathbb{P}_2^+/\mathbb{P}_1^{\text{disc}}$ space. The continuous $\mathbb{P}_2^+$ space used for the velocity space, denotes the space of piecewise polynomials of order two, enriched with cubic cell bubbles. The discontinuous $\mathbb{P}_1^{\text{disc}}$ space used for the pressure denotes the piecewise polynomials of order one.

Using a pressure space that is discontinuous on a element-wise level, comes with a cost. Enriching the pressure space, requires to enrich the velocity space, in order to fulfil the inf-sup condition. While in two dimensions, it is enough to enrich the velocity space with one cubic bubble function, in three dimensions already five additional bubbles are needed. This implies an increase in the number of degrees of freedom with using a discontinuous pressure approximation on an element level. Especially in three dimensions the increase in number of unknowns is pronounced. Table 4.1 gives an example for the increase in two and three dimensions.

Although, the enriched discontinuous pressure space would increase the quality of the approximation of the divergence constraint, a discontinuous space is not really needed on an element-wise level to prevent spurious velocities. In order to resolve the pressure jump across the interface, the pressure must be discontinuous on a domain-wise level only. A consequence is to use a Taylor-Hood element in each phase, but allow a discontinuous pressure at the interface, i.e. a piecewise Taylor-Hood space ($\mathbb{P}_2/\mathbb{P}_1$-disc). This technique

Table 4.1: Increase with refinement levels of the degrees of freedom for finite elements with continuous and discontinuous pressure, in two dimensions (left) and three dimensions (right)

Level	$\mathbb{P}_2/\mathbb{P}_1$	$\mathbb{P}_2^+/\mathbb{P}_1^{\text{disc}}$
1	347	666
2	1 339	2 626
3	5 267	10 434
4	20 899	41 602

Level	$\mathbb{P}_2/\mathbb{P}_1$	$\mathbb{P}_2^+/\mathbb{P}_1^{\text{disc}}$
1	4 673	16 055
2	32 821	122 365
3	245 254	955 415
4	1 894 568	7 550 827

Table 4.2: Experimental order of convergence rates in three dimensions for discontinuous and continuous pressure spaces

Element	L^2-error	eoc	H_0^1-error	eoc
$\mathbb{P}_2/\mathbb{P}_1$	$1.1141 \cdot 10^{-2}$	1.3757	$4.6523 \cdot 10^{-2}$	0.3110
$\mathbb{P}_2/\mathbb{P}_1$-disc	$6.6595 \cdot 10^{-6}$	3.4789	$9.0207 \cdot 10^{-5}$	2.5422
$\mathbb{P}_2^+/\mathbb{P}_1^{\text{disc}}$	$9.0710 \cdot 10^{-6}$	3.5344	$2.3594 \cdot 10^{-4}$	2.6588

is also called *node doubling*, since it results from not identifying the pressure nodes lying on the interface.

Node doubling increases the number of unknowns by the amount of the pressure nodes lying on the interface. Since the pressure is a scalar quantity and the nodes involved in the interface are usually rare, this is not as much, as compared to enriching the velocity space. Thus, the node doubling technique would bring a good reduction in the number of unknowns, provided it is not necessary to enrich the velocity space, in order to fulfil the inf-sup condition (4.2.2). Fortunately, the velocity space of the Taylor-Hood element is already rich enough, such that the node doubling technique does not violate the inf-sup condition. This is shown in the next section for the two dimensional and three dimensional case.

4.2.2 The Inf-Sup Stability of the Domain-Wise Taylor-Hood Spaces

In the following subsection, the inf-sup stability of the domain-wise Taylor-Hood finite element space is proven. The proof holds for multi-phase domains, i.e. more than two phases are possible. A decomposition of the fluid domain into a fixed but arbitrary number of subdomains is considered. But, these subdomains are required to be polygonal domains.

For the course of this subsection, let $\Omega \subset \mathbb{R}^d$, $d = 2, 3$ be a polygonal multi-phase domain, and let $\{\Omega_i\}_{i=1}^{N_p}$ be a polygonal partition of Ω, such that

$$\overline{\Omega} = \bigcup_{i=1}^{N_p} \overline{\Omega}_i \quad \text{and} \quad \Omega_i \cap \Omega_j = \emptyset, i \neq j \ ,$$

where N_p is the number of phases.

With $\Gamma_{ij} = \overline{\Omega}_i \cap \overline{\Omega}_j$ the interface between Ω_i and Ω_j is indicated. Since Γ_{ij} can be the empty set, or Γ_{ij} can be degenerated to just a point for some i and j, the following set of indices is introduced

$$\mathcal{I}_\Gamma := \{(i,j) : \mathring{\Gamma}_{ij} \neq \emptyset, 1 \leq i < j \leq N_p\} \ .$$

For each $(i,j) \in \mathcal{I}_\Gamma$, Γ_{ij} is a proper interface of the multi-phase domain. Further, let Γ be the union of all proper interfaces

$$\Gamma := \bigcup_{(i,j)\in\mathcal{I}_\Gamma} \Gamma_{ij} \ .$$

Since Ω_i is polygonal, for $i = 1, \ldots, N_p$, each Γ_{ij}, $(i,j) \in \mathcal{I}_\Gamma$, is a piecewise linear hypersurface, that consists of a finite number of segments. Let Γ_{ij}^k be the k-th segment of Γ_{ij}, Then

$$\Gamma_{ij} = \bigcup_{k=1}^{N_{ij}} \Gamma_{ij}^k \ ,$$

where N_{ij} is the number of segments of Γ_{ij}.

Since Γ_{ij} is piecewise smooth only, the normals are not necessarily defined at the boundary points of each of Γ_{ij}^k. But it is possible to define a mean normal, at those points. Let $\mathbf{n}_{ij}^k$ be the normal of the plane segment Γ_{ij}^k. For a point $\mathbf{x} \in \Gamma_{ij}$ that is part of several adjacent segments $\Gamma_{ij}^{k_l}$, $l = 1, \ldots, M$, the sum $\mathbf{s}_{ij}(\mathbf{x})$ of the corresponding normals is

$$\mathbf{s}_{ij}(\mathbf{x}) := \sum_{l\in\mathbb{N}:\mathbf{x}\in\Gamma_{ij}^l} \mathbf{n}_{ij}^l \ .$$

Then, the mean normal $\bar{\mathbf{n}}_{ij}(\mathbf{x})$ at $\mathbf{x} \in \Gamma_{ij}$ is then defined as

$$\bar{\mathbf{n}}_{ij}(\mathbf{x}) := \frac{\mathbf{s}_{ij}(\mathbf{x})}{\|\mathbf{s}_{ij}(\mathbf{x})\|} \ .$$

For convenience in the notation the following set of singular points is introduced

$$\mathcal{X}_{ij}(\Gamma) := \left\{\mathbf{x} \in \Gamma_{ij} : \exists k_1, k_2 \in \mathbb{N} : k_1 \neq k_2 : \mathbf{x} \in \Gamma_{ij}^{k_1} \text{ and } \mathbf{x} \in \Gamma_{ij}^{k_2}\right\} \ .$$

Note, the mean normal $\bar{\mathbf{n}}_{ij}$ is defined for each Γ_{ij}, $(i,j) \in \mathcal{I}_\Gamma$, separately.

The following assumption on the normals and its mean values of Γ_{ij} is needed

Assumption 4.2.1. *There exists a constant $C_\Gamma > 0$, such that for all $(i,j) \in \mathcal{I}_\Gamma$ the following holds. For all $\mathbf{x} \in \mathcal{X}_{ij}$, with $\mathbf{x} \in \Gamma_{ij}^{k_l}$, for $l = 1, \ldots, M$, it must hold*

$$\mathbf{n}_{ij}^{k_l} \cdot \bar{\mathbf{n}}_{ij}(\mathbf{x}) \geq C_\Gamma \ , \ \forall l = 1, \ldots, M \ . \tag{4.2.4}$$

This assumption states that the angles between two adjacent segments are not zero. This assumption is usually fulfilled for polygonal domains. It excludes subdomains with slits, which is not allowed.

The following assumption makes sure that the Taylor-Hood finite element space is inf-sup stable on each subdomain. Let $\{\mathcal{T}_h^\Gamma\}_{h>0}$ be a family meshes of Ω aligned to Γ, the following assumption must hold.

Assumption 4.2.2. *The family of meshes $\left\{\mathcal{T}_h^\Gamma\right\}_{h>0}$ of Ω is shape-regular, i.e. there exists a constant C such that for all h*

$$\frac{h_K}{\rho_K} \leq C \ , \quad \forall K \in \mathcal{T}_h^\Gamma \ ,$$

where ρ_K is the diameter of the largest ball that can be inscribed in K.

Further, each cell of $\mathcal{T}_h^\Gamma$ has at least one vertex which is not part of an interface Γ or the boundary $\partial\Omega$.

The next assumption is a condition on the family of surface meshes $\left\{\mathcal{S}_h^\Gamma\right\}_{h>0}$, that comes with the fitted bulk mesh.

Assumption 4.2.3. *The family of surface meshes $\left\{\mathcal{S}_h^\Gamma\right\}_{h>0}$ is quasi-uniform, i.e. it is shape-regular and there exists a constant C such that for all h*

$$h_F \geq Ch \ , \quad \forall F \in \mathcal{S}_h^\Gamma \ .$$

Further, it is assumed that the surface mesh $\mathcal{S}_h^\Gamma$ is such that $\Gamma_h = \Gamma$, for all h.

Note, since it holds $h_K \geq h_F$ for a cell K and its faces F, the bulk mesh is quasi-uniform regarding all cells $K \in \mathcal{T}_h^\Gamma$, with K has a face belonging to $\mathcal{S}_h^\Gamma$, i.e. the bulk mesh is quasi-uniform in a layer around the interface.

Next, the finite element spaces X_h and Q_h for the Taylor-Hood element with phase-wise continuous pressure are defined. In order to emphasises the discrete setting and the dependency on h, a subscript h is added. The velocity and pressure spaces are as follows

$$\begin{aligned} X_h &:= \{\mathbf{v} \in C(\Omega)^d : \mathbf{v} \in \mathcal{P}_s(\Omega)^d\} \ , \\ Q_h &:= \{q \in L_0^2(\Omega) : q|_{\Omega_i} \in \mathcal{P}_{s-1}(\Omega_i), 1 \leq i \leq N_p\} \ , \end{aligned}$$

for $s \geq 2$. Further, the following spaces are introduced

$$\begin{aligned} X_h(\Omega_i) &:= \{\mathbf{v} \in X_h : \mathbf{v} = 0 \text{ in } \Omega \setminus \Omega_i\} \ , \\ Q_h(\Omega_i) &:= \{q \in L_0^2(\Omega_i) : q \in \mathcal{P}_{s-1}(\Omega_i)\} \ , \\ \bar{Q}_h &:= \{q \in L_0^2(\Omega) : q|_{\Omega_i} = q_i = const., 1 \leq i \leq N_p\} \ . \end{aligned}$$

Further preliminaries to proof the main result about the inf-sup stability of the phase-wise Taylor-Hood finite element space, are laid out in the following. The proof is based on the Boland–Nicolaïdes macro element technique and the Fortin criterion for the inf-sup condition. Therefore, the following theorem by Boland–Nicolaïdes is recalled.

Theorem 4.2.2. *Let the pair of spaces (X_h, Q_h) satisfy the local inf-sup condition*

$$\sup_{\mathbf{v}\in X_h(\Omega_i)} \frac{(q_h, \nabla\cdot\mathbf{v}_h)_{\Omega_i}}{|\mathbf{v}_h|_{1,\Omega_i}} \geq \lambda' \|q_h\|_{0,\Omega_i} \qquad \forall q_h \in Q_h(\Omega_i), \quad 1 \leq i \leq N_p \ , \tag{4.2.5}$$

with $\lambda' > 0$ independent of h and i.

If there exist a subspace $\bar{X}_h$ of X_h such that the pair $(\bar{X}_h, \bar{Q}_h)$ satisfies the inf-sup condition with a constant $\bar{\lambda}$ independent of h, then (X_h, Q_h) also satisfies the inf-sup condition with a constant λ independent of h.

Proof. The theorem and its proof can be found in [26]. □

Further, the Fortin criterion for the inf-sup condition is recalled.

Lemma 4.2.1. *The inf-sup condition* (4.2.2) *for the pair (X_h, Q_h) holds with a constant $\lambda > 0$ independent of h, if and only if there exists an operator $\Pi_h : H_0^1(\Omega)^d \to X_h$ satisfying*

$$(q_h, \nabla\cdot\mathbf{v})_\Omega = (q_h, \nabla\cdot(\Pi_h\mathbf{v}))_\Omega \ , \quad \forall q_h \in Q_h, \quad \forall \mathbf{v} \in H_0^1(\Omega)^d$$

and

$$|\Pi_h\mathbf{v}|_{1,\Omega} \leq C_F\,|\mathbf{v}|_{1,\Omega} \quad \forall \mathbf{v} \in H_0^1(\Omega)^d$$

with a constant $C_F > 0$ independent of h.

Proof. The theorem and its proof can be found in [59] or in [55, p.185]. □

In the case of the phase-wise Taylor-Hood space, the local inf-sup condition is already fulfilled, as stated by the next corollary.

Corollary 4.2.1. *If $\mathcal{T}_h^\Gamma$ fulfils Assumption 4.2.2, then the pair (X_h, Q_h) fulfils the local inf-sup condition* (4.2.5) *with a constant λ' independent of h and i.*

Proof. The restriction $(X_h(\Omega_i), (Q_h(\Omega_i)))$ of (X_h, Q_h) to Ω_i is the standard Taylor–Hood finite element space on Ω_i, for all $1 \leq i \leq N_p$, which is inf-sup stable. □

In the following, a pair of spaces $(\bar{X}_h, \bar{Q}_h)$ is constructed, which is inf-sup stable, as required by the Boland–Nicolaïdes theorem. Let

$$\bar{X}_h := \{\mathbf{v} \in C(\Omega)^d : \mathbf{v}|_K \in \mathbb{P}_2(K)^d, \forall K \in \mathcal{T}_h^\Gamma\} \ ,$$

be the standard $\mathbb{P}_2$ on Ω, then the pair $(\bar{X}_h, \bar{Q}_h)$ is inf-sup stable and meets the requirement of the Boland–Nicolaïdes Theorem 4.2.2. This is shown in the following, by constructing an appropriate Fortin operator Π_h. The construction of Π_h is based on the Scott-Zhang operator. A definition of the Scott-Zhang operator can be found in [105] and is not recalled here.

Before the interpolation operator is constructed and it is shown it has the required properties for the Fortin Lemma 4.2.1, a few properties of the Scott–Zhang operator are recalled.

In the following, the Scott–Zhang operator will be denoted with $\mathcal{Z}_h$. The construction of Scott–Zhang operator requires the following definition of a neighbourhood of a cell K.

Definition 4.2.1. *Let $\mathcal{T}_h^\Gamma$ be a mesh of Ω. The neighbourhood ω_K of $K \in \mathcal{T}_h^\Gamma$ is defined as*

$$\omega_K := \bigcup_{\left\{K' \in \mathcal{T}_h : \overline{K}' \cap \overline{K} \neq \emptyset\right\}} K' \ .$$

Further, the following global and local interpolation properties of the Scott–Zhang operator hold.

Lemma 4.2.2. *Let $\mathcal{Z}_h : H^1(\Omega) \to \bar{X}_h$ be the Scott–Zhang operator, then there exist a constant C independent of h, such that the following holds:*

(a) Stability: For all $0 \leq m \leq \min(1, l)$

$$\|\mathcal{Z}_h \mathbf{v}\|_{m,\Omega} \leq C \|\mathbf{v}\|_{l,\Omega} \ , \quad \forall \mathbf{v} \in H^l(\Omega) \ , \forall h \ . \tag{4.2.6}$$

(b) Approximation: Provided $l < s + 1$, for all $0 \leq m \leq l$

$$\|\mathbf{v} - \mathcal{Z}_h \mathbf{v}\|_{m,K} \leq C h_K^{l-m} |\mathbf{v}|_{l,\omega_k} \ , \quad \forall K \in \mathcal{T}_h^\Gamma \ , \forall h \ . \tag{4.2.7}$$

Proof. The theorem can be found in [55] and its proof in [105]. □

Next, the Fortin operator Π_h is constructed. To do that, a special finite element function is considered. A function that is one in all mesh nodes lying in the interior of an interface Γ_{ij}, and zero at the nodes elsewhere. Considering the nodes (nodal functionals) for the space $\bar{X}_h$ with a standard Lagrange basis. For each interface Γ_{ij}, there are nodes lying on the boundary $\partial\Gamma_{ij}$ and nodes lying in the interior of Γ_{ij}. Let $\mathcal{M}_{ij}$ be the set of all grid nodes, belonging to Γ_{ij}, i.e

$$\mathcal{M}_{ij} := \left\{ a \in \bigcup_{K \in \mathcal{T}_h^\Gamma} \mathcal{N}_K : a \in \Gamma_{ij} \right\} \ .$$

Then, the set of internal nodes of Γ_{ij}, denoted with $\mathring{\mathcal{M}}_{ij}$ is given as

$$\mathring{\mathcal{M}}_{ij} := \{ a \in \mathcal{M}_{ij} : a \notin \partial\Gamma_{ij} \} \ .$$

It is required that $\mathring{\mathcal{M}}_{ij}$ is non-empty.

Assumption 4.2.4. *The mesh $\mathcal{T}_h^\Gamma$ is such that $\mathring{\mathcal{M}}_{ij} \neq \emptyset$ for all h, with $h < h_0$, for a $h_0 > 0$.*

Note that if this is not the case, it is only one regular refinement step required in order to fulfil this assumption.

In the following, the k-th node of $\mathring{\mathcal{M}}_{ij}$ is denoted with a_{ij}^k, such that $\mathring{\mathcal{M}}_{ij} = \left\{a_{ij}^k\right\}_{k=1}^M$, where M is the cardinality of $\mathring{\mathcal{M}}_{ij}$. Further, a normal $\tilde{\mathbf{n}}_{ij}^k$ in a node a_{ij}^k is defined as follows

$$\tilde{\mathbf{n}}_{ij}^k := \begin{cases} \bar{\mathbf{n}}_{ij}(a_{ij}^k) & : \ a_{ij}^k \in \mathcal{X}_{ij} \ , \\ \mathbf{n}_\Gamma & : \ \text{else} \ . \end{cases}$$

Let ϕ_{ij}^k be the Lagrange basis functions of $\bar{X}_h$, belonging to a_{ij}^k, the following vector valued functions $\Phi_{ij} \in \bar{X}_h$ for each interface Γ_{ij} is defined as

$$\Phi_{ij} := \sum_{k=1}^{M} \phi_{ij}^k \tilde{\mathbf{n}}_{ij}^k \qquad \forall (i,j) \in \mathcal{I}_\Gamma \ .$$

Note, Φ_{ij} is the piecewise quadratic interpolation of the normals in the nodes a_{ij}^k.

With this functions, the interpolation operator $\Pi_h : H_0^1(\Omega)^d \to X_h$ is defined as follows

$$\Pi_h \mathbf{v} := \sum_{(i,j)\in\mathcal{I}_\Gamma} \mathcal{N}_{ij}(\mathbf{v}) \Phi_{ij} + \mathcal{Z}_h \mathbf{v} \ , \tag{4.2.8}$$

with

$$\mathcal{N}_{ij}(\mathbf{v}) = \frac{\int_{\Gamma_{ij}} (\mathbf{v} - \mathcal{Z}_h \mathbf{v}) \cdot \mathrm{d}\mathbf{A}}{\int_{\Gamma_{ij}} \Phi_{ij} \cdot \mathrm{d}\mathbf{A}} \quad \forall (i,j) \in \mathcal{I}_\Gamma \ ,$$

and $\mathcal{Z}_{ij}$ is the Scott-Zhang operator as in [105].

Next, it will be shown that the interpolation operator Π_h has the properties as required in Lemma 4.2.1.

Lemma 4.2.3. *For the interpolation operator $\Pi_h : H_0^1(\Omega)^d \to \bar{X}_h(\Omega)$ with the definition (4.2.8) above, it holds*

$$(q_h, \nabla \cdot \mathbf{v}) = (q_h, \nabla \cdot (\Pi_h \mathbf{v})) \qquad \forall q_h \in \bar{Q}_h \ .$$

Proof. Since q_h is constant q_i in each subdomain Ω_i it holds

$$\int_{\Omega_i} q_h \left(\nabla \cdot (\mathbf{v} - \Pi_h \mathbf{v})\right) \mathrm{d}V = q_i \int_{\Omega_i} \nabla \cdot (\mathbf{v} - \Pi_h \mathbf{v}) \ \mathrm{d}V \quad \forall q_h \in \bar{Q}_h \ ,$$

Applying the Gauss theorem gives

$$\int_{\Omega_i} \nabla \cdot (\mathbf{v} - \Pi_h \mathbf{v}) \, \mathrm{d}V = \int_{\partial\Omega_i} (\mathbf{v} - \Pi_h \mathbf{v}) \cdot \mathrm{d}\mathbf{A} \ .$$

Since $\partial\Omega_i$ is the union of some Γ_{ij} for some j with $(i,j) \in \mathcal{I}_\Gamma$, and the supports of the Φ_{ij} are disjoint, it is sufficient to consider the surface integrals over Γ_{ij}. By construction of Π_h it holds

$$\begin{aligned}
\int_{\Gamma_{ij}} (\mathbf{v} - \Pi_h \mathbf{v}) \cdot \mathrm{d}\mathbf{A} &= \int_{\Gamma_{ij}} (\mathbf{v} - \mathcal{Z}_h \mathbf{v}) \cdot \mathrm{d}\mathbf{A} - \int_{\Gamma_{ij}} \mathcal{N}_{ij}(\mathbf{v}) \Phi_h \cdot \mathrm{d}\mathbf{A} \\
&= \int_{\Gamma_{ij}} (\mathbf{v} - \mathcal{Z}_h \mathbf{v}) \cdot \mathrm{d}\mathbf{A} - \int_{\Gamma_{ij}} (\mathbf{v} - \mathcal{Z}_h \mathbf{v}) \cdot \mathrm{d}\mathbf{A} \\
&= 0 \ .
\end{aligned}$$

From this it is concluded that

$$\int_{\Omega_i} \nabla \cdot (\mathbf{v} - \Pi_h \mathbf{v}) \, \mathrm{d}V = 0 \ ,$$

which completes the proof. □

For the stability it holds:

Lemma 4.2.4. *If the assumptions above are fulfilled, then*

$$|\mathbf{v} - \Pi_h \mathbf{v}|_{m,\Omega} \leq C h^{k-m} \, |\mathbf{v}|_{k,\Omega} \qquad \forall \mathbf{v} \in H^k(\Omega) \ ,$$

and in particular

$$|\Pi_h \mathbf{v}|_{1,\Omega} \leq C \, |\mathbf{v}|_{1,\Omega} \qquad \forall \mathbf{v} \in H^1(\Omega) \ .$$

Proof. By construction of the operator Π_h, and using the triangle inequality it holds

$$|\mathbf{v} - \Pi_h \mathbf{v}|_{m,\Omega} \leq |\mathbf{v} - \mathcal{Z}_h \mathbf{v}|_{m,\Omega} + \sum_{(i,j) \in \mathcal{I}_\Gamma} |\mathcal{N}_{ij}(\mathbf{v})| \, |\Phi_{ij}|_{m,\Omega} \ .$$

For the first part, the estimates of the Scott-Zhang operator (4.2.7) deliver the right result, the second part needs a closer look.

By definition of the functional $\mathcal{N}_{ij}$, the following expression has to be estimated

$$\sum_{(i,j) \in \mathcal{I}_\Gamma} |\mathcal{N}_{ij}(\mathbf{v})| \, |\Phi_{ij}|_{m,\Omega} = \sum_{(i,j) \in \mathcal{I}_\Gamma} \frac{\left| \int_{\Gamma_{ij}} (\mathbf{v} - \mathcal{Z}_h \mathbf{v}) \cdot \mathrm{d}\mathbf{A} \right|}{\left| \int_{\Gamma_{ij}} \Phi_{ij} \cdot \mathrm{d}\mathbf{A} \right|} \, |\Phi_{ij}|_{m,\Omega} \ ,$$

which will be done in the following.

The denominator can be estimated from below, as follows. Let $e_K \in \mathcal{S}_h^\Gamma$ be an face of a mesh cell $K \in \mathcal{T}_h^\Gamma$, and $\hat{e}_{\hat{K}}$ be the corresponding face on the reference cell $\hat{K}$. Then it holds

$$\int_{e_K} \Phi_{ij} \cdot \mathrm{d}\mathbf{A} = \sum_{\{k\in\mathbb{N}:\ a_{ij}^k \in e_K\}} \tilde{\mathbf{n}}_{ij}^k \cdot \mathbf{n}_{e_K} \int_{e_K} \phi_{ij}^k \,\mathrm{d}A = \sum_{\{k\in\mathbb{N}:\ a_{ij}^k \in e_K\}} \tilde{\mathbf{n}}_{ij}^k \cdot \mathbf{n}_{e_K} \frac{|e_K|}{|\hat{e}_{\hat{K}}|} \int_{\hat{e}_{\hat{K}}} \hat{\phi}_{ij}^k \,\mathrm{d}A \ ,$$

where $\mathbf{n}_{e_K}$ denotes the normal to the face e_K and $\hat{\phi}_{ij} = \phi_{ij} \circ F_K$ the reference function. Because of assumption (4.2.4) the scalar product $\tilde{\mathbf{n}}_{ij}^k \cdot \mathbf{n}_{e_K}$ is bounded from below, and it follows

$$\int_{e_K} \Phi_{ij} \cdot \mathrm{d}\mathbf{A} \geq C_1 \,|e_K| \ .$$

After summation over all faces belonging to Γ_{ij} it holds

$$\int_{\Gamma_{ij}} \Phi_{ij} \cdot \mathrm{d}\mathbf{A} \geq C_1 \,|\Gamma_{ij}| \ , \tag{4.2.9}$$

independent of h.

Analogue, for a cell $K \in \mathcal{T}_h^\Gamma$, that is part of the support of Φ_h, it holds

$$|\Phi_{ij}|_{m,K} \leq C \sum_{\{k\in\mathbb{N}:\ a_{ij}^k \in K\cap\Gamma_{ij}\}} \left|\mathbf{n}_{ij}^k\right| |\phi_{ij}|_{m,K} \leq C\,|\phi_{ij}|_{m,K} \ .$$

Standard finite element estimates together with Assumption 4.2.3 imply

$$|\Phi_{ij}|_{m,\Omega} \leq Ch^{-m} \ . \tag{4.2.10}$$

It remains to consider the approximation error of the Scott–Zhang operator on the surfaces Γ_{ij}. Using a trace theorem, it follows on a face e_K.

$$\begin{aligned}\left|\int_{e_K} (\mathbf{v} - \mathcal{Z}_h\mathbf{v}) \cdot \mathrm{d}\mathbf{A}\right| &\leq C_3\,|e_K| \int_{\hat{e}_{\hat{K}}} |\widehat{\mathbf{v}} - \widehat{\mathcal{Z}_h\mathbf{v}}| \,\mathrm{d}A \\ &\leq C_3\,|e_K|\,\|\widehat{\mathbf{v}} - \widehat{\mathcal{Z}_h\mathbf{v}}\|_{1,\hat{K}} \ .\end{aligned}$$

Standard finite element estimates and the property (4.2.7) of the Scott-Zhang operator deliver

$$\begin{aligned}\|\widehat{\mathbf{v}} - \widehat{\mathcal{Z}_h\mathbf{v}}\|_{1,\hat{K}} &\leq C_2\,|\det B_K|^{-\frac{1}{2}} \left\{\|\mathbf{v} - \mathcal{Z}_h\mathbf{v}\|_{0,K}^2 + h_K^2\,|\mathbf{v} - \mathcal{Z}_h\mathbf{v}|_{1,K}^2\right\}^{\frac{1}{2}} \\ &\leq C_2\,|\det B_K|^{-\frac{1}{2}}\, h_K^k\,|\mathbf{v}|_{k,\omega_K} \ ,\end{aligned}$$

where ω_K is the neighbourhood of K as in Definition 4.2.1. Since the mesh $\mathcal{T}_h^\Gamma$ is assumed to be shape-regular, ω_K consists of finite many cells independent of h, such that after summation and with (4.2.9), it follows

$$|\mathcal{N}_{ij}(\mathbf{v})| \leq Ch^k\,|\mathbf{v}|_{k,\Omega} \ .$$

Together with (4.2.10), it is deduced that

$$|\mathcal{N}_{ij}(\mathbf{v})|\,|\Phi_{ij}|_{m,\Omega} \leq Ch^{k-m}\,|\mathbf{v}|_{k,\Omega} \ ,$$

and thus

$$|\mathbf{v} - \Pi_h\mathbf{v}|_{m,\Omega} \leq Ch^{k-m}\,|\mathbf{v}|_{k,\Omega} \ ,$$

which completes the proof of the first part of the lemma.

The second part of the lemma is deduced by setting $m = k = 1$ and using

$$|\Pi_h\mathbf{v}|_{1,\Omega} \leq |\mathbf{v} - \Pi_h\mathbf{v}|_{1,\Omega} + |\mathbf{v}|_{1,\Omega} \ ,$$

what finally delivers

$$|\Pi_h\mathbf{v}|_{1,\Omega} \leq (1 + C)\,|\mathbf{v}|_{1,\Omega} \ .$$

That proves the second part of the lemma and completes the proof. □

The following is then a direct consequence of the Fortin lemma and the Boland–Nicolaïdes theorem. For the pair $(\bar{X}_h, \bar{Q}_h)$ the following corollary holds.

Corollary 4.2.2. *Let $\left\{\mathcal{T}_h^\Gamma\right\}_{h>0}$ be a family of regular meshes fulfilling the assumptions above, then the finite element space pair $(\bar{X}_h, \bar{Q}_h)$ is inf-sup stable.*

Proof. This follows directly from the Fortin lemma and Lemma 4.2.3 and Lemma 4.2.4. □

Finally, the main result of this section is stated. For the domain-wise Taylor-Hood finite element space the inf-sup condition holds as follows.

Theorem 4.2.3. *Let $\left\{\mathcal{T}_h^\Gamma\right\}_{h>0}$ be a family of regular meshes fulfilling the assumptions above, then the finite element space pair (X_h, Q_h) is inf-sup stable.*

Proof. This follows from Corollary 4.2.2 and Theorem 4.2.2. □

Remark 4.2.1. *The Corollary 4.2.2 does not prove that the $\mathbb{P}_2/\mathbb{P}_0$ pair is inf-sup stable in three dimensions, which is not the case. Here, it is required that $\mathring{\mathcal{M}}_{ij} \neq \emptyset$. This is not fulfilled in the case of $\mathbb{P}_2$ in three dimensions, where all nodes are edge nodes. Therefore, it is not possible to consider each cell as a separate subdomain, which would be required, in order to prove such a result with the method used above.*

Remark 4.2.2. *The result of this section may be generalised to non Taylor-Hood elements. A finite element pair (X_h, Q_h) could be inf-sup stable on Ω, provided that it is inf-sup stable in each subdomain Ω_i, and the assumptions are fulfilled. This result may be shown by setting $\bar{X}_h = X_h$ and using the construction above.*

4.3 Time Discretization

Let $t_0 < t_1 < \cdots < t_N = t_b$ be a partition of the time interval $[t_0, t_b]$. The following notation is used: For a time dependent function $f = f(\mathbf{x}, t)$, the value at time $t = t_n$ is denoted with $f_n(\cdot) = f(\cdot, t_n)$, for $n = 0, \ldots, N$. A similar notation is used for the time dependent domains, but with an upper script, $\Omega^n = \Omega(t_n)$, $n = 0, \ldots, N$. The finite element function spaces above, also get an upper script, e.g. $\mathbb{V}_s^n = \mathbb{V}_s(t)$. For the forms defined on Ω^n, an integer subscript n for the time slice t_n is used, to indicate the time at which the form is evaluated, e.g. $a_n = a_{t_n}$.

A function $f_n : \Omega^n \to \mathbb{R}$ is defined on the domain Ω^n. However, in the ALE context a function f_n on domain Ω^n can be transformed to a function $g_m : \Omega^m \to \mathbb{R}$ on the domain Ω^m, via

$$\mathbf{x}_n = \mathcal{A}_{t_n}(\mathcal{A}_{t_m}^{-1}(\mathbf{x}_m)) \ ,$$

such that

$$g_m(\mathbf{x}_m) = f_n(\mathcal{A}_{t_n}(\mathcal{A}_{t_m}^{-1}(\mathbf{x}_m)))$$

is a function on the domain Ω^m. In the following, let $\mathcal{A}_m^n$ be an operator transferring the values of a function f_n on the domain Ω^n to a domain Ω^m, via

$$g_m(\mathbf{x}) = (\mathcal{A}_m^n f_n)(\mathbf{x}) := f_n(\mathcal{A}_{t_n}(\mathcal{A}_{t_m}^{-1}(\mathbf{x}))) \ , \quad \mathbf{x} \in \Omega^m \ .$$

In this way, a function defined on a domain Ω^n can be evaluated on a domain Ω^m, and thus, can be used in the forms defined on Ω_m. In order to shorten the notation, the transfer operator is skipped, whenever it is clear on which domain a function is evaluated, e.g. in integrals

$$\int_{\Omega^m} f_n \ \mathrm{d}V := \int_{\Omega^m} \mathcal{A}_m^n f_n \ \mathrm{d}V \ ,$$

or in linear forms

$$a_n(f_n, g_m) := a_n(f_n, \mathcal{A}_n^m g_m) \ .$$

Semi-Implicit Euler Scheme

With $\tau_n = t_{n+1} - t_n$ the time step length of the n-th time step will be denoted. The following time discretizations are introduced. One possibility is to approximate the ALE derivative $\partial_t^{\mathbf{w}} f$ by a semi-implicit Euler type approximation

$$\mathcal{A}_n^{n+1}(\partial_t^{\mathbf{w}} f)_{n+1} \approx \frac{\mathcal{A}_n^{n+1} f_{n+1} - f_n}{\tau_n} \ , \tag{4.3.1}$$

which leads to the following time discretization

$$(\partial_t^{\mathbf{w}} f_{n+1}, g)_n \approx \tau_n^{-1} \left(\mathcal{A}_n^{n+1} f_{n+1} - f_n, g\right)_n = \tau_n^{-1} \left(f_{n+1} - f_n, g\right)_n \ .$$

The integration domain is the old domain at time t_n, whereas the derivative is taken at time t_{n+1}, hence the name semi-implicit.

Another possibility is to use a fully-implicit Euler approximation as follows

$$(\partial_t^{\mathbf{w}} f)_{n+1} \approx \frac{f_{n+1} - \mathcal{A}_{n+1}^n f_n}{\tau_n} \ , \tag{4.3.2}$$

which leads to

$$(f_{n+1}, g)_{n+1} \approx \tau_n^{-1} \left(f_{n+1} - \mathcal{A}_{n+1}^n f_n, g\right)_{n+1} = \tau_n^{-1} \left(f_{n+1} - f_n, g\right)_{n+1} \ .$$

Now, the integration domain is the new domain at time t_{n+1}.

Note that for the fully coupled problem, the new integration domain is a priori unknown at time t_{n+1}. Hence, the fully-implicit choice is impractical and leads to a highly nonlinear problem. For problems where the domain evolution is given, the fully-implicit Euler discretization is applicable.

Applying the semi-implicit Euler time discretization to the fully coupled problem, leads to the following semi-implicit Euler discretization:

Problem 4.3.1. *Given* Ω^n, $\mathbf{u}_n$, c_n *and* γ_n, *find* $(\mathbf{u}_{n+1}, \mathbf{w}_{n+1}, p_{n+1}, c_{n+1}, \gamma_{n+1}) \in \mathbb{V}_s^{n+1} \times \mathbb{V}_s^{n+1} \times \mathbb{Q}_{s-1}^{n+1} \times \mathbb{B}_s^{n+1} \times \mathbb{S}_s^{n+1}$, *such that with* $\mathbf{b}_{n+1} := \mathbf{u}_{n+1} - \mathbf{w}_{n+1}$ *it holds*

$$\left(\varrho\left(\mathbf{u}_{n+1} - \mathbf{u}_n\right), \mathbf{v}\right)_n + \tau_n \left(a_n^{\mathbf{u}}(\mathbf{b}_{n+1}; \mathbf{u}_{n+1}, \mathbf{v}) - b_n(\mathbf{v}, p_{n+1})\right) = \tau_n f_n^{\mathbf{u}}(\gamma_{n+1}, \mathbf{v}) \ , \tag{4.3.3a}$$

$$b_n(\mathbf{u}_{n+1}, q) = 0 \ , \tag{4.3.3b}$$

$$\left(c_{n+1} - c_n, \phi\right)_n + \tau_n a_n^c(\mathbf{b}_{n+1}; c_{n+1}, \phi) = \tau_n f_n^c(c_{n+1}, \gamma_{n+1}, \phi) \ , \tag{4.3.3c}$$

$$\left\langle \gamma_{n+1} - \gamma_n, \xi \right\rangle_n + \tau_n a_n^\Gamma(\mathbf{b}_{n+1}, \mathbf{w}_{n+1}, \gamma_{n+1}, \xi) = \tau_n f_n^\Gamma(c_{n+1}, \gamma_{n+1}, \xi) \ , \tag{4.3.3d}$$

for all $(\mathbf{v}, q, \phi, \xi) \in \mathbb{V}_s^n \times \mathbb{Q}_{s-1}^n \times \mathbb{B}_s^n \times \mathbb{S}_s^n$.

The equations (4.3.3) result in a nonlinear monolithic system. This system can be solved iteratively. Another approach is to decouple parts of the problem, and solve the subproblems separately. Breaking the fully coupled problem into less complex sub problems results in a simpler scheme, in terms of implementation and amount of work needed to solve the algebraic systems.

Decoupling the Navier-Stokes part from the convection–diffusion allows to update the mesh after the Navier-Stokes stage, and use the new mesh in the convection–diffusion stage. It is then possible to use a fully-implicit Euler time discretization for the convection diffusion equations, since the domain is given. Further, the decoupling of the full problem into a flow stage and a surfactant stage, makes it possible to use existing implementations of Navier-Stokes solvers and convection–diffusion solvers, which are quite common.

The Navier-Stokes part can be decoupled from the convection–diffusion part, by taking the right hand side $f_n^{\mathbf{u}}$ in (4.3.3a) explicit regarding the surface surfactant. The decoupled nonlinear Navier-Stokes stage is then solved with a Picard type iteration, as follows.

Problem 4.3.2. *Given* Ω^n, $\mathbf{u}^0_{n+1} := \mathbf{u}_n$, $\mathbf{w}^0_{n+1} := \mathbf{w}_n$, *and* γ_n, *find* $(\mathbf{u}^i_{n+1}, \mathbf{w}^i_{n+1}, p^i_{n+1}) \in \mathbb{V}^{n+1}_s \times \mathbb{V}^{n+1}_s \times \mathbb{Q}^{n+1}_{s-1}$, *such that with* $\mathbf{b}^{i-1}_{n+1} := \mathbf{u}^{i-1}_{n+1} - \mathbf{w}^{i-1}_{n+1}$ *it holds*

$$\begin{aligned}\left(\varrho\left(\mathbf{u}^i_{n+1} - \mathbf{u}_n\right), \mathbf{v}\right)_n + \tau_n a^{\mathbf{u}}_n(\mathbf{b}^{i-1}_{n+1}; \mathbf{u}^i_{n+1}, \mathbf{v}) - \tau_n b_n(\mathbf{v}, p^i_{n+1}) &= \tau_n f^{\mathbf{u}}_n(\gamma_n, \mathbf{v}) \ , \\ b_n(\mathbf{u}^i_{n+1}, q) &= 0 \ ,\end{aligned}$$

for all $(\mathbf{v}, q) \in \mathbb{V}^n_s \times \mathbb{Q}^n_{s-1}$.

The convection–diffusion stage is discretized with the fully-implicit Euler step (4.3.2). The nonlinear system is linearized by a staggered iteration, since the right hand side f^c_n and f^Γ_n are linear in each argument. Taking the bulk surfactant concentration explicit in the surface equation (4.3.3d), while taking the surface surfactant concentration explicit in the bulk equation (4.3.3c), leads to the following nonlinear iteration.

Problem 4.3.3. *Given* Ω^{n+1}, $c^0_{n+1} := c_n$, $\gamma^0_{n+1} := \gamma_n$, $\mathbf{u}_{n+1}$, *and* $\mathbf{w}_{n+1}$, *find* $(\gamma^i_{n+1}, c^i_{n+1}) \in \mathbb{S}^{n+1}_s \times \mathbb{B}^{n+1}_s$, *such that with* $\mathbf{b}_{n+1} := \mathbf{u}_{n+1} - \mathbf{w}_{n+1}$ *it holds*

$$\left\langle \gamma^i_{n+1} - \gamma_n, \xi \right\rangle_{n+1} + \tau_n a^\Gamma_{n+1}(\mathbf{b}_{n+1}, \mathbf{w}_{n+1}; \gamma^i_{n+1}, \xi) = \tau_n f^\Gamma_{n+1}(c^{i-1}_{n+1}, \gamma^i_{n+1}, \xi) \ , \tag{4.3.5a}$$

$$\left(c^i_{n+1} - c_n, \phi\right)_{n+1} + \tau_n a^c_{n+1}(\mathbf{b}_{n+1}; c^i_{n+1}, \phi) = \tau_n f^c_{n+1}(c^i_{n+1}, \gamma^i_{n+1}, \phi) \ , \tag{4.3.5b}$$

for all $(\xi, \phi) \in \mathbb{S}^{n+1}_s \times \mathbb{B}^{n+1}_s$.

Note, that the equations (4.3.3) and (4.3.4) have to be augmented by suitable equations for the domain velocity, like (4.1.3).

Crank-Nicolson and θ-Scheme

The θ-scheme is a convex combination of a forward and a backward Euler step. On a fixed domain it reads,

$$\theta f'_{n+1} + (1-\theta) f'_n \approx \frac{f_{n+1} - f_n}{\tau_n} \ . \tag{4.3.6}$$

for a parameters $\theta \in [0, 1]$. The Crank-Nicolson scheme is obtained for $\theta = \frac{1}{2}$.

As in the implicit Euler scheme with moving domains, the terms can be evaluated either on the new or old domain. The evaluation of equation (4.3.6) on the old domain Ω^n leads to

$$\theta \mathcal{A}^{n+1}_n (\partial^{\mathbf{w}}_t f)_{n+1} + (1-\theta)(\partial^{\mathbf{w}}_t f)_n \approx \frac{\mathcal{A}^{n+1}_n f_{n+1} - f_n}{\tau_n} \ . \tag{4.3.7}$$

The evaluation of equation (4.3.6) using the new domain Ω^{n+1} gives

$$\theta (\partial^{\mathbf{w}}_t f)_{n+1} + (1-\theta) \mathcal{A}^n_{n+1} (\partial^{\mathbf{w}}_t f)_n \approx \frac{f_{n+1} - \mathcal{A}^n_{n+1} f_n}{\tau_n} \ . \tag{4.3.8}$$

A monolithic system could be formulated, using the semi-implicit version (4.3.7). However, the decoupling of the Navier-Stokes equations and the convection–diffusion

equations should also be used in the θ-scheme. By using the same decoupling strategies as in the Euler scheme, the following scheme is obtained.

The Navier-Stokes stage is obtained by using the semi-implicit θ-scheme (4.3.7) and taking the surface surfactant concentration γ_n explicit. The resulting nonlinear Navier-Stokes equation are solved by a Picard type iteration as follows.

Problem 4.3.4. *Given* Ω^n, $\mathbf{u}_{n+1}^0 := \mathbf{u}_n$, $\mathbf{w}_{n+1}^0 := \mathbf{w}_n$ *and* γ_n, *find* $(\mathbf{u}_{n+1}^i, \mathbf{w}_{n+1}^i, p_{n+1}^i) \in \mathbb{V}_s^{n+1} \times \mathbb{V}_s^{n+1} \times \mathbb{Q}_{s-1}^{n+1}$, *such that with* $\mathbf{b}_{n+1}^{i-1} := \mathbf{u}_{n+1}^{i-1} - \mathbf{w}_{n+1}^{i-1}$ *it holds*

$$\begin{aligned}\left(\varrho(\mathbf{u}_{n+1}^i - \mathbf{u}_n), \mathbf{v}\right)_n + \tau_n \left[\theta a_n^{\mathbf{u}}(\mathbf{b}_{n+1}^{i-1}; \mathbf{u}_{n+1}^i, \mathbf{v}) - b_n(\mathbf{v}, p_{n+1})\right] \\ = \tau_n \left[f_n^{\mathbf{u}}(\gamma_n, \mathbf{v}) - (1-\theta) a_n^{\mathbf{u}}(\mathbf{b}_n; \mathbf{u}_n, \mathbf{v})\right] \ ,\end{aligned} \tag{4.3.9a}$$

$$b_n(\mathbf{u}_{n+1}^i, q) = 0 \ , \tag{4.3.9b}$$

for all $(\mathbf{v}, q) \in \mathbb{V}_s^n \times \mathbb{Q}_s^n$.

After the Navier-Stokes stage the mesh is updated. The convection–diffusion stage is then done on the new domain Ω^{n+1}. Again, a staggered iteration is applied to linearize the nonlinear systems, as follows.

Problem 4.3.5. *Given* Ω^{n+1}, $c_{n+1}^0 := c_n$, $\gamma_{n+1}^0 := \gamma_n$, $\mathbf{u}_{n+1}$, *and* $\mathbf{w}_{n+1}$, *find* $(\gamma_{n+1}^i, c_{n+1}^i) \in \mathbb{S}_s^{n+1} \times \mathbb{B}_s^{n+1}$, *such that with* $\mathbf{b}_{n+1} := \mathbf{u}_{n+1} - \mathbf{w}_{n+1}$ *it holds*

$$\begin{aligned}\left\langle \gamma_{n+1}^i - \gamma_n, \xi \right\rangle_{n+1} + \theta\tau_n \left[a_{n+1}^{\Gamma}(\mathbf{b}_{n+1}, \mathbf{w}_{n+1}; \gamma_{n+1}^i, \xi) - f_{n+1}^{\Gamma}(c_{n+1}^{i-1}, \gamma_{n+1}^i, \xi)\right] \\ = (1-\theta)\tau_n \left[f_{n+1}^{\Gamma}(c_n, \gamma_n, \xi) - a_{n+1}^{\Gamma}(\mathbf{b}_{n+1}, \mathbf{w}_{n+1}; \gamma_n, \xi)\right] \ ,\end{aligned} \tag{4.3.10a}$$

$$\begin{aligned}\left(c_{n+1}^i - c_n, \phi\right)_{n+1} + \theta\tau_n \left[a_{n+1}^{c}(\mathbf{b}_{n+1}; c_{n+1}^i, \phi) - f_{n+1}^{c}(c_{n+1}^i, \gamma_{n+1}^i, \phi)\right] \\ = (1-\theta)\tau_n \left[f_{n+1}^{c}(c_n, \gamma_n, \phi) - a_{n+1}^{c}(\mathbf{b}_{n+1}, c_n, \phi)\right] \ ,\end{aligned} \tag{4.3.10b}$$

for all $(\xi, \phi) \in \mathbb{S}_s^n \times \mathbb{B}_s^n$.

Of course, the Navier-Stokes stage has to be completed with equations for the mesh updated, as already stated before.

Fractional Step Θ-Scheme

The fractional step Θ-scheme combines three θ-steps, executed sequentially. A time step is divided into three substeps of different size. In each substep, the θ-scheme is applied, resulting in a A-stable scheme of second order (for fixed domains), provided the parameters for each θ-step are chosen properly.

For the fractional step Θ-scheme, each time interval $[t_n, t_{n+1}]$ is divided into three subintervals $[t_n, t_{n+\Theta}]$, $[t_{n+\Theta}, t_{n+(1-\Theta)}]$, and $[t_{n+(1-\Theta)}, t_{n+1}]$. The subintervals have the length of $\Theta\tau_n$, $(1-2\Theta)\tau_n$, and $\Theta\tau_n$, respectively. In each substep, a θ-scheme is applied, where the parameter θ selected for each substep as follows. For the first substep it is set $\theta = \alpha$, for the second substep it is set $\theta = 1 - \alpha$, and for the third substep it is set $\theta = \alpha$, with an $\alpha \in (0, 1)$.

The fractional step Θ-scheme is of second order if Θ is chosen as $\Theta = 1-\frac{\sqrt{2}}{2}$. Further, the fractional step Θ-scheme is strongly A-stable if $\alpha \in (\frac{1}{2}, 1)$, see [33, 87, 88].

The fractional step Θ-scheme, together with the decoupling techniques above, leads to the following scheme.

Problem 4.3.6. *Let $\Theta = 1-\frac{\sqrt{2}}{2}$, $\Theta' = 1-\Theta$, $\tilde{\Theta} = 1-2\Theta$, $\theta \in (\frac{1}{2}, 1)$ and $\theta' = 1-\theta$. The three substeps of the fractional step Θ-scheme read:*

First substep: Navier-Stokes stage: *Given Ω^n, $\mathbf{u}^0_{n+\Theta} := \mathbf{u}_n$, $\mathbf{w}^0_{n+\Theta} := \mathbf{w}_n$ and γ_n, find $(\mathbf{u}^i_{n+\Theta}, \mathbf{w}^i_{n+\Theta}, p^i_{n+\Theta}) \in \mathbb{V}^{n+\Theta}_s \times \mathbb{V}^{n+\Theta}_s \times \mathbb{Q}^{n+\Theta}_{s-1}$, such that with $\mathbf{b}^{i-1}_{n+\Theta} := \mathbf{u}^{i-1}_{n+\Theta} - \mathbf{w}^{i-1}_{n+\Theta}$ it holds*

$$\begin{aligned}\left(\varrho\left(\mathbf{u}^i_{n+\Theta} - \mathbf{u}_n\right), \mathbf{v}\right)_n &+ \Theta\tau_n\left[\theta a^{\mathbf{u}}_{n+\Theta}(\mathbf{b}^{i-1}_{n+\Theta}; \mathbf{u}^i_{n+\Theta}, \mathbf{v}) - b_n(\mathbf{v}, p_{n+\Theta})\right] \\ &= \Theta\tau_n\left[f^{\mathbf{u}}_n(\gamma_n, \mathbf{v}) - \theta' a^{\mathbf{u}}_n(\mathbf{b}^{i-1}_{n+\Theta}; \mathbf{u}_n, \mathbf{v})\right] \ , \end{aligned} \tag{4.3.11a}$$

$$b_n(\mathbf{u}^i_{n+\Theta}, q) = 0 \ , \tag{4.3.11b}$$

for all $(\mathbf{v}, q) \in \mathbb{V}^n_s \times \mathbb{Q}^n_{s-1}$.

Convection–diffusion stage: *Given $\Omega^{n+\Theta}$, $c^0_{n+\Theta} := c_n$, $\gamma^0_{n+\Theta} := \gamma_n$, $\mathbf{u}_{n+\Theta}$, and $\mathbf{w}_{n+\Theta}$, find $(\gamma^i_{n+\Theta}, c^i_{n+\Theta}) \in \mathbb{S}^{n+\Theta}_s \times \mathbb{B}^{n+\Theta}_s$, such that with $\mathbf{b}_{n+\Theta} := \mathbf{u}_{n+\Theta} - \mathbf{w}_{n+\Theta}$ it holds*

$$\begin{aligned}&\left\langle\gamma^i_{n+\Theta}, \xi\right\rangle_{n+\Theta} + \theta\Theta\tau_n\left[a^{\Gamma}_{n+\Theta}(\mathbf{b}_{n+\Theta}, \mathbf{w}_{n+\Theta}; \gamma^i_{n+\Theta}, \xi) - f^{\Gamma}_{n+\Theta}(c^{i-1}_{n+\Theta}, \gamma^i_{n+\Theta}, \xi)\right] \\ &= \left\langle\gamma_n, \xi\right\rangle_{n+\Theta} + \theta'\Theta\tau_n\left[f^{\Gamma}_{n+\Theta}(c_n, \gamma_n, \xi) - a^{\Gamma}_{n+\Theta}(\mathbf{b}_{n+\Theta}, \mathbf{w}_{n+\Theta}; \gamma_n, \xi)\right] \ , \end{aligned} \tag{4.3.12a}$$

$$\begin{aligned}&\left(c^i_{n+\Theta}, \phi\right)_{n+\Theta} + \theta\Theta\tau_n\left[a^{c}_{n+\Theta}(\mathbf{b}_{n+\Theta}; c^i_{n+\Theta}, \phi) - f^{c}_{n+\Theta}(c^i_{n+\Theta}, \gamma^i_{n+\Theta}, \phi)\right] \\ &= (c_n, \phi)_{n+\Theta} + \theta'\Theta\tau_n\left[f^{c}_{n+\Theta}(c_n, \gamma_n, \phi) - a^{c}_{n+\Theta}(\mathbf{b}_{n+\Theta}, c_n, \phi)\right] \ , \end{aligned} \tag{4.3.12b}$$

for all $(\xi, \phi) \in \mathbb{S}^{n+\Theta}_s \times \mathbb{B}^{n+\Theta}_s$.

Second step: Navier-Stokes stage: *Given $\Omega^{n+\Theta}$, $\mathbf{u}^0_{n+\Theta'} := \mathbf{u}_{n+\Theta}$, $\mathbf{w}^0_{n+\Theta'} := \mathbf{w}_{n+\Theta}$ and $\gamma_{n+\Theta}$, find $(\mathbf{u}^i_{n+\Theta'}, \mathbf{w}^i_{n+\Theta'}, p^i_{n+\Theta'}) \in \mathbb{V}^{n+\Theta'}_s \times \mathbb{V}^{n+\Theta'}_s \times \mathbb{Q}^{n+\Theta'}_{s-1}$, such that with $\mathbf{b}^{i-1}_{n+\Theta'} := \mathbf{u}^{i-1}_{n+\Theta'} - \mathbf{w}^{i-1}_{n+\Theta'}$ it holds*

$$\begin{aligned}\left(\varrho\left(\mathbf{u}^i_{n+\Theta'} - \mathbf{u}_{n+\Theta}\right), \mathbf{v}\right)_{n+\Theta} &+ \tilde{\Theta}\tau_n\left[\theta' a^{\mathbf{u}}_{n+\Theta}(\mathbf{b}^{i-1}_{n+\Theta'}; \mathbf{u}^i_{n+\Theta'}, \mathbf{v}) - b_{n+\Theta}(\mathbf{v}, p_{n+\Theta'})\right] \\ &= \tilde{\Theta}\tau_n\left[f^{\mathbf{u}}_n(\gamma_{n+\Theta}, \mathbf{v}) - \theta a^{\mathbf{u}}_{n+\Theta}(\mathbf{b}^{i-1}_{n+\Theta'}; \mathbf{u}_{n+\Theta}, \mathbf{v})\right] \ , \end{aligned} \tag{4.3.13a}$$

$$b_{n+\Theta}(\mathbf{u}^i_{n+\Theta'}, q) = 0 \ , \tag{4.3.13b}$$

for all $(\mathbf{v}, q) \in \mathbb{V}^{n+\Theta}_s \times \mathbb{Q}^{n+\Theta}_{s-1}$.

Convection–diffusion stage: *Given $\Omega^{n+\Theta'}$, $c^0_{n+\Theta'} := c_{n+\Theta}$, $\gamma^0_{n+\Theta'} := \gamma_{n+\Theta}$, $\mathbf{u}_{n+\Theta'}$, and $\mathbf{w}_{n+\Theta'}$, find $(\gamma^i_{n+\Theta'}, c^i_{n+\Theta'}) \in \mathbb{S}^{n+\Theta'}_s \times \mathbb{B}^{n+\Theta'}_s$, such that with $\mathbf{b}_{n+\Theta'} := \mathbf{u}_{n+\Theta'} - \mathbf{w}_{n+\Theta'}$*

it holds

$$\begin{aligned}&\left\langle \gamma^i_{n+\Theta'},\xi\right\rangle_{n+\Theta'} + \theta'\tilde{\Theta}\tau_n\left[a^{\Gamma}_{n+\Theta'}(\mathbf{b}_{n+\Theta'},\mathbf{w}_{n+\Theta'};\gamma^i_{n+\Theta'},\xi) - f^{\Gamma}_{n+\Theta'}(c^{i-1}_{n+\Theta'},\gamma^i_{n+\Theta'},\xi)\right]\\ &= \left\langle \gamma_{n+\Theta},\xi\right\rangle_{n+\Theta'} + \theta\tilde{\Theta}\tau_n\left[f^{\Gamma}_{n+\Theta'}(c_{n+\Theta},\gamma_{n+\Theta},\xi) - a^{\Gamma}_{n+\Theta'}(\mathbf{b}_{n+\Theta'},\mathbf{w}_{n+\Theta'};\gamma_{n+\Theta},\xi)\right]\ ,\end{aligned} \tag{4.3.14a}$$

$$\begin{aligned}&\left(c^i_{n+\Theta'},\phi\right)_{n+\Theta'} + \theta'\tilde{\Theta}\tau_n\left[a^{c}_{n+\Theta'}(\mathbf{b}_{n+\Theta'};c^i_{n+\Theta'},\phi) - f^{c}_{n+\Theta'}(c^i_{n+\Theta'},\gamma^i_{n+\Theta'},\phi)\right]\\ &= \left(c_{n+\Theta},\phi\right)_{n+\Theta'} + \theta\tilde{\Theta}\tau_n\left[f^{c}_{n+\Theta'}(c_{n+\Theta},\gamma_{n+\Theta},\phi) - a^{c}_{n+\Theta'}(\mathbf{b}_{n+\Theta'},c_{n+\Theta},\phi)\right]\ ,\end{aligned} \tag{4.3.14b}$$

for all $(\xi,\phi)\in\mathbb{S}^{n+\Theta'}_s\times\mathbb{B}^{n+\Theta'}_s$.

Third step: Navier-Stokes stage: *Given* $\Omega^{n+\Theta'}$, $\mathbf{u}^0_{n+1} := \mathbf{u}_{n+\Theta'}$, $\mathbf{w}^0_{n+1} := \mathbf{w}_{n+\Theta'}$ *and* $\gamma_{n+\Theta'}$, *find* $(\mathbf{u}^i_{n+1},\mathbf{w}^i_{n+1},p^i_{n+1})\in\mathbb{V}^{n+1}_s\times\mathbb{V}^{n+1}_s\times\mathbb{Q}^{n+1}_{s-1}$, *such that with* $\mathbf{b}^{i-1}_{n+1} := \mathbf{u}^{i-1}_{n+1} - \mathbf{w}^{i-1}_{n+1}$ *it holds*

$$\begin{aligned}&\left(\varrho\mathbf{u}^i_{n+1} - \mathbf{u}_{n+\Theta'},\mathbf{v}\right)_{n+\Theta'} + \Theta\tau_n\left[\theta a^{\mathbf{u}}_{n+\Theta'}(\mathbf{b}^{i-1}_{n+1};\mathbf{u}^i_{n+1},\mathbf{v}) - b_{n+\Theta'}(\mathbf{v},p_{n+1})\right]\\ &\qquad = \Theta\tau_n\left[f^{\mathbf{u}}_{n+\Theta'}(\gamma_{n+\Theta'},\mathbf{v}) - \theta' a^{\mathbf{u}}_{n+\Theta'}(\mathbf{b}^{i-1}_{n+1};\mathbf{u}_{n+\Theta'}),\mathbf{v})\right]\ ,\end{aligned} \tag{4.3.15a}$$

$$b_{n+\Theta'}(\mathbf{u}^i_{n+1},q) = 0\ , \tag{4.3.15b}$$

for all $(\mathbf{v},q)\in\mathbb{V}^{n+\Theta'}_s\times\mathbb{Q}^{n+\Theta'}_{s-1}$.

Convection–diffusion step: *Given* Ω^{n+1}, $c^0_{n+1} := c_{n+\Theta'}$, $\gamma^0_{n+1} := \gamma_{n+\Theta'}$, $\mathbf{u}_{n+1}$, *and* $\mathbf{w}_{n+1}$, *find* $(\gamma^i_{n+1},c^i_{n+1})\in\mathbb{S}^{n+1}_s\times\mathbb{B}^{n+1}_s$, *such that with* $\mathbf{b}_{n+1} := \mathbf{u}_{n+1} - \mathbf{w}_{n+1}$ *it holds*

$$\begin{aligned}&\left\langle \gamma^i_{n+1},\xi\right\rangle_{n+1} + \theta\Theta\tau_n\left[a^{\Gamma}_{n+1}(\mathbf{b}_{n+1},\mathbf{w}_{n+1};\gamma^i_{n+1},\xi) - f^{\Gamma}_{n+1}(c^{i-1}_{n+1},\gamma^i_{n+1},\xi)\right]\\ &= \left\langle \gamma_{n+\Theta'},\xi\right\rangle_{n+1} + \theta'\Theta\tau_n\left[f^{\Gamma}_{n+1}(c_{n+\Theta'},\gamma_{n+\Theta'},\xi) - a^{\Gamma}_{n+1}(\mathbf{b}_{n+1},\mathbf{w}_{n+1};\gamma_{n+\Theta'},\xi)\right]\ ,\end{aligned} \tag{4.3.16a}$$

$$\begin{aligned}&\left(c^i_{n+1},\phi\right)_{n+1} + \theta\Theta\tau_n\left[a^{c}_{n+1}(\mathbf{b}_{n+1};c^i_{n+1},\phi) - f^{c}_{n+1}(c^i_{n+1},\gamma^i_{n+1},\phi)\right]\\ &= \left(c_{n+\Theta'},\phi\right)_{n+1} + \theta'\Theta\tau_n\left[f^{c}_{n+1}(c_{n+\Theta'},\gamma_{n+\Theta'},\phi) - a^{c}_{n+1}(\mathbf{b}_{n+1},c_{n+\Theta'},\phi)\right]\ ,\end{aligned} \tag{4.3.16b}$$

for all $(\xi,\phi)\in\mathbb{S}^{n+1}_s\times\mathbb{B}^{n+1}_s$.

Also for the fractional step Θ-scheme, the Navier-Stokes stages have to be completed with equations for the mesh updated.

The three different time discretizations, the semi-implicit Euler scheme, the Crank-Nicolson scheme, and the fractional step Θ-scheme, were compared in several numerical tests. The fractional step Θ-scheme allows a significant larger time step size compared to the semi-implicit Euler and Crank-Nicolson scheme. But this is compensated by the higher amount of computational work needed for the fractional step Θ-scheme. The Crank-Nicolson scheme shows less advantage over the semi-implicit Euler scheme. The advantage regarding time step size is less pronounced. The Crank-Nicolson scheme also

needs a little more computational work, than the Euler scheme, since more terms have to be assembled.

The fractional step Θ-scheme and Crank-Nicolson scheme also show less numerical dissipation than the Euler scheme, using the same time step size. However, due to less computational work needed for the Euler scheme, it is always possible to chose a smaller time step size. Overall, it was mostly sufficient to use the semi-implicit Euler scheme compared to the other two. This might be a hint, that not all properties of the Crank-Nicolson and fractional step Θ-scheme transfer from the fixed grid setting to the ALE setting. This could be due to the explicit handling of the domain in the Navier-Stokes stages.

4.4 Discrete Surface Evolution

The evolution and the quality of the surface mesh is of particular importance for numerical methods solving interface and free surface problems. Often, the important physical phenomena happen at the interface, which lead to a higher dynamic in the flow structure near the interface. The quality of the mesh at the interface is crucial for an accurate capturing of those phenomena.

In the classical methods, the nodes of the interface are moved according to the kinematic interface condition $\mathbf{w} \cdot \mathbf{n}_\Gamma = \mathbf{u} \cdot \mathbf{n}_\Gamma$. An Euler stepping scheme is used to update the position of the mesh nodes. In the following, let $\mathbf{x}_{n+1}^l$ and $\mathbf{x}_n^l$ be the position of the l-th node of the interface Γ_h, at time t_{n+1} and t_n, respectively. Further, let $\mathbf{w}_{n+1}^l$ be the velocity of the interface node, and let $\mathbf{u}_{n+1}^l$ be the velocity of the fluid at the l-th node, at time t_{n+1}. Then, the node velocity is approximated by

$$\mathbf{w}_{n+1}^l = \frac{\mathbf{x}_{n+1}^l - \mathbf{x}_n^l}{\tau_n} \ , \tag{4.4.1}$$

and a forward Euler discretization of the dynamic interface condition (2.2.7) leads to

$$\mathbf{x}_{n+1}^l = \mathbf{x}_n^l + \tau_n \mathbf{w}_{n+1}^l \quad \text{or} \quad \mathbf{x}_{n+1}^l = \mathbf{x}_n^l + \tau_n \left(\mathbf{w}_{n+1}^l \cdot \mathbf{n}_n^l \right) \mathbf{n}_n^l \ .$$

Here, $\mathbf{n}_n^l$ is the normal at the mesh node at time t_n. This normal has to be defined, since the discrete surface is not a smooth manifold, and the nodes could be singular points. Typically, the normal is defined in the nodes as the average value of the normals of the adjacent cells of the interface mesh. The average could also be weighted by the cell area. Or, if the discrete interface is an approximation of a given smooth manifold, $\mathbf{n}_n^l$ can be taken from there.

The classical methods are easy and fast to implement. The interface mesh velocity is either given, or the result of Navier-Stokes stage, and the displacement of the nodes is calculated explicit. However, the classical methods suffer from problems arising from the lack of control over the distribution of the nodes. The version with $\mathbf{w}_{n+1}^l = \mathbf{u}(\mathbf{x}_{n+1}^l, t_{n+1})$ describes a Lagrangian interface, hence it suffers from the problems that are typical for full Lagrangian methods. A high dynamic flow structure leads to mesh distortions that

become very fast very large. As a result, the quality of the numerical simulation suffers. In some situations, the version with $\mathbf{w}_{n+1}^l = \left(\mathbf{u}(\mathbf{x}_{n+1}^l, t_{n+1}) \cdot \mathbf{n}_n^l\right) \mathbf{n}_n^l$ can reduce some of the distortions. But mostly, it is a priori not clear which version leads to a better result. In fact, in some situations none of the two versions of the classical method can prevent mesh distortion. For example, in a rising bubble flow, each version will lead to a drifting of nodes in the flow direction. That in turn leads to a coarsening of the mesh at the top, and an accumulation of nodes at the rear of the bubble. This behaviour is introduced through the special vortex type flow profile of such problems (raising bubbles). Such flow profiles result in a constant creation of new surface at the top of the bubble. However, the classical methods are good to use, if the scenario involves only small oscillations, like in case of oscillating bubbles.

4.4.1 Weak Surface Evolution

A discretization of the weak formulation of the surface evolution, i.e. Problem 3.3.1, leads to a numerical scheme with advantageous properties regarding the stability and node distribution. This was shown in [17], where a particular discretization with lumped bilinear forms was studied.

The mesh velocity in (3.3.2) is substituted with the approximation (4.4.1). The Laplace-Beltrami identity is used semi-implicit, i.e. the integration domain is the old interface Γ_h^n, but the position and the curvature are that of the new interface Γ_h^{n+1} and are the unknowns. This leads to the following discrete version of Problem 3.3.1.

Problem 4.4.1. *Given Γ_h^n and $\mathbf{u}$, find $(\mathbf{x}_{n+1}, \mathcal{H}_{n+1}) \in (\mathbb{S}_s^n)^d \times \mathbb{S}_s^n$ such that*

$$\langle \mathbf{x}_{n+1}, \mathbf{n}_\Gamma \psi \rangle_n = \langle \mathbf{x}_n + \tau_n \mathbf{u}, \mathbf{n}_\Gamma \psi \rangle_n \ , \tag{4.4.2a}$$

$$\langle \mathcal{H}_{n+1} \mathbf{n}_\Gamma, \eta \rangle_n - \langle \nabla_\Gamma \mathbf{x}_{n+1}, \nabla_\Gamma \eta \rangle_n = 0 \ , \tag{4.4.2b}$$

for all $(\eta, \psi) \in (\mathbb{S}_s^n)^d \times \mathbb{S}_s^n$.

In this work, the polynomial order s is either one or two, although higher order approximations are possible. But, for the following considerations only isoparametric approximation up to order two are taken into account.

The formulation in Problem 4.4.1 is given in terms of the absolute position $\mathbf{x}_{n+1}$ of the interface. Of course, the problem can be formulated in terms of the mesh velocity $\mathbf{w}_{n+1}$, too. Substituting (4.4.1) and after rearranging the terms, it is obtained:

Problem 4.4.2. *Given Γ_h^n, $\mathbf{x}_n$ and $\mathbf{u}$, find $(\mathbf{x}_{n+1}, \mathcal{H}_{n+1}) \in (\mathbb{S}_s^n)^d \times \mathbb{S}_s^n$ such that*

$$\langle \mathbf{w}_{n+1}, \mathbf{n}_\Gamma \psi \rangle_n = \langle \mathbf{u}, \mathbf{n}_\Gamma \psi \rangle_n \ , \tag{4.4.3a}$$

$$\langle \mathcal{H}_{n+1} \mathbf{n}_\Gamma, \eta \rangle_n - \tau_n \langle \nabla_\Gamma \mathbf{w}_{n+1}, \nabla_\Gamma \eta \rangle_n = - \langle \mathbb{P}_\Gamma, \nabla_\Gamma \eta \rangle_n \ , \tag{4.4.3b}$$

for all $(\eta, \psi) \in (\mathbb{S}_s^n)^d \times \mathbb{S}_s^n$.

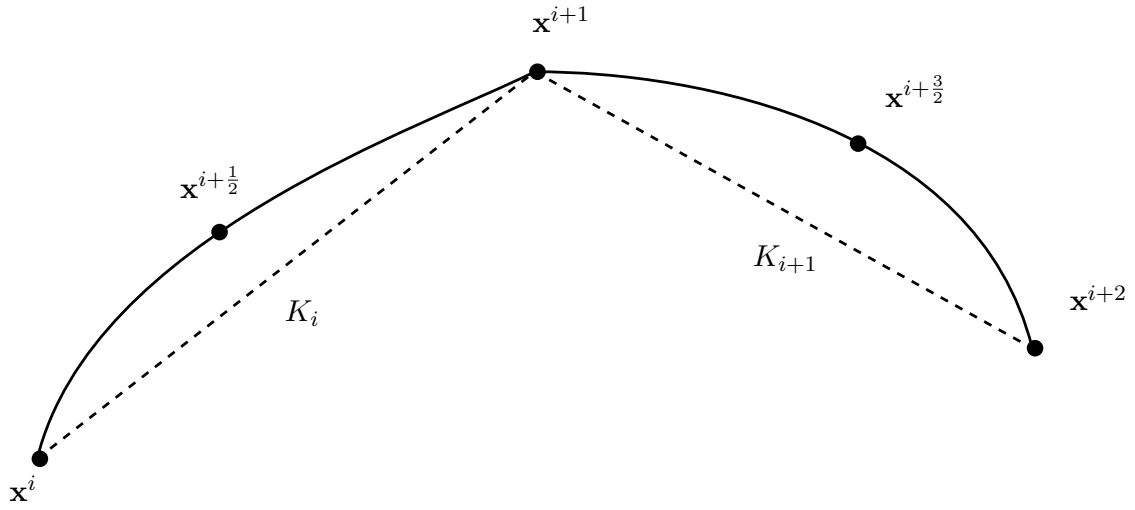

Figure 4.1: Numbering of faces and nodes for the piecewise linear (dashed) and piecewise quadratic (solid) surface mesh.

4.4.2 Weak Surface Evolution: Lumped with $\mathbb{P}_1$ and $\mathbb{P}_2$ Elements

For the following variations of the Problems 4.4.1 and 4.4.2, the dimension d is restricted to $d = 2$, i.e. surface and interface of two dimensional domains. However, the methods as such are applicable for case $d = 3$, too.

Next, a version of (4.4.2) using lumped bilinear forms is introduced, and the lumped bilinear forms $\langle \mathbf{u}, \mathbf{v} \rangle_n^h$ for $s = 1, 2$ are introduced. Let the interface mesh $\mathcal{S}_h^\Gamma$ consist of the faces $F_i \in \mathcal{S}_h^\Gamma$, $i = 1, \ldots, N$. For $s = 1$, the piecewise linear case, each face F_i is the convex combination of the nodes $\mathbf{x}^i$ and $\mathbf{x}^{i+1}$. Compare with Figure 4.1.

For the piecewise linear case, the lumped bilinear form reads

$$\langle \mathbf{u}, \mathbf{v} \rangle_n^{h,1} := \frac{1}{2} \sum_{i=1}^{N} |F_i| \left(\mathbf{u}(\mathbf{x}^i) \cdot \mathbf{v}(\mathbf{x}^i) + \mathbf{u}(\mathbf{x}^{i+1}) \cdot \mathbf{v}(\mathbf{x}^{i+1}) \right). \tag{4.4.4}$$

This is equivalent to applying the trapezoidal integration rule to the standard bilinear form, assuming a piecewise linear interface mesh.

In case of the piecewise quadratic isoparametric interface mesh, the face F_i is the quadratic curve through the nodes $\mathbf{x}_i$, $\mathbf{x}_{i+\frac{1}{2}}$, and $\mathbf{x}_{i+1}$, as shown in Figure 4.1. The lumped bilinear form can be generated by applying the Simpson integration rule. Then, the lumped bilinear form for the quadratic isoparametric case reads

$$\langle \mathbf{u}, \mathbf{v} \rangle_n^{h,2} := \sum_{i=1}^{N} \sum_{k=0}^{2} \omega_k \left\{ \mathbf{u}(\mathbf{x}^{i+\frac{k}{2}}) \cdot \mathbf{v}(\mathbf{x}^{i+\frac{k}{2}}) \left| \det DF_{F_i}(\mathbf{x}^{i+\frac{k}{2}}) \right| \right\} , \tag{4.4.5}$$

where $\omega_k = \frac{1}{6}$, for $k = 0, 2$ and $\omega_k = \frac{4}{6}$ for $k = 1$.

The problem for the weak surface evolution formulated with the lumped bilinear forms is then as follows.

Problem 4.4.3. *For $s = 1, 2$ and given Γ_h^n and $\mathbf{u}$, find $(\mathbf{x}_{n+1}, \mathcal{H}_{n+1}) \in (\mathbb{S}_s^n)^d \times \mathbb{S}_s^n$ such that*

$$\langle \mathbf{x}_{n+1}, \mathbf{n}_\Gamma \psi \rangle_n^{h,s} = \langle \mathbf{x}_n + \tau_n \mathbf{u}, \mathbf{n}_\Gamma \psi \rangle_n^{h,s} \ , \tag{4.4.6a}$$

$$\langle \mathcal{H}_{n+1} \mathbf{n}_\Gamma, \eta \rangle_n^{h,s} - \langle \nabla_\Gamma \mathbf{x}_{n+1}, \nabla_\Gamma \eta \rangle_n = 0 \ , \tag{4.4.6b}$$

for all $(\eta, \psi) \in (\mathbb{S}_s^n)^d \times \mathbb{S}_s^n$.

Besides having diagonal matrices for the lumped bilinear forms, the lumped version for the linear case ($s = 1$) has a remarkable property. As shown in [17], the solution of the semi-discrete (continuous in time) lumped piecewise linear formulation results in a equi-distribution of the mesh points. Hence, all mesh nodes attain the same euclidean distance from each other. For the fully discrete scheme, the equi-distribution is reach after some iterations in time. As shown later in Chapter 5, this property for $s = 1$ seems to be transferred to the quadratic isoparametric case. But unfortunately, the number of iterations needed to reach equi-distribution is much larger compared to the piecewise linear case. In fact, the number of iterations needed is so large that the method becomes unpractical, in terms of the intended equi-distribution of nodes (compare Chapter 5).

For $s = 2$, the method needs to much time to redistribute the nodes in tangential direction, and cannot keep up with the interface movement, if the dynamic of the flow field is large. In this case, the interface mesh loses its quality easily, like in the classical methods. This might be a result of a non-unique interface representation given the nodes in the quadratic isoparametric case. Contrary to the piecewise linear case, two different sets of nodes can represent the same interface, since the isoparametric node can be moved around tangential without changing the shape. This is not the case for piecewise linear interface, assuming the grid cells are not co-planar.

Although, there are no theoretical results, numerical experiments show (Chapter 5) that the non-lumped version has a preferable property, too. The nodes tend to accumulate in regions of high curvature. This is a very useful property, since a high curvature means high details in the surface shape. In order to give an accurate representation of the shape, a higher number of nodes is needed in such regions. As in the lumped case, while the piecewise linear method redistributes the nodes very fast, the piecewise isoparametric quadratic scheme is much slower in redistributing the nodes in tangential direction. That makes it impractical also in the non-lumped case.

In order to transfer the good properties of the piecewise linear scheme to the piecewise quadratic scheme, a trick is used, which is described in the next subsection.

4.4.3 $\mathbb{P}_1$-iso-$\mathbb{P}_2$

In order to use a weak surface evolution scheme, with the properties of the linear case, also for the piecewise quadratic case, the piecewise quadratic interface is substituted by a finer piecewise linear mesh. The finer piecewise linear mesh consists of the same

nodes as the quadratic interface, including the isoparametric points. The polynomials on the piecewise quadratic are substituted by nodal interpolations with piecewise linear functions on the finer mesh.

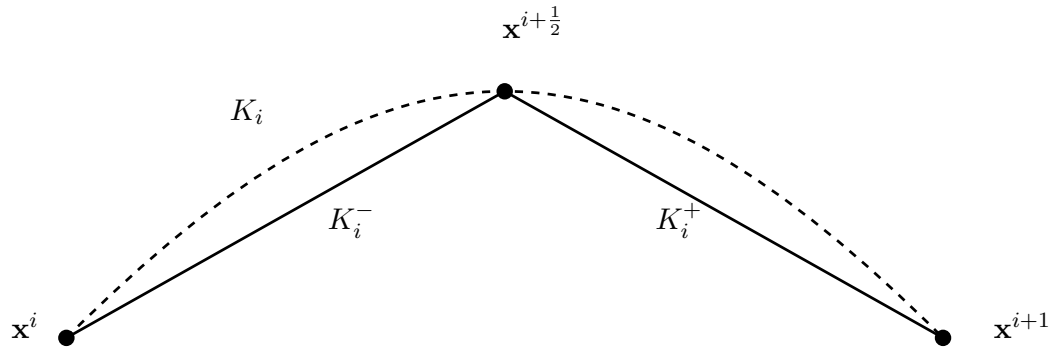

Figure 4.2: Partition of an isoparametric mesh cell.

Each cell $K_i \in \mathcal{S}_h^\Gamma$ is substituted with the two cells K_i^- and K_i^+, which are the straight lines connecting the nodes. K_i^- is the convex combination of $\mathbf{x}^i$ and $\mathbf{x}^{i+\frac{1}{2}}$ as follows

$$K_i^- = \{\mathbf{x} \in \mathbb{R}^2 : \mathbf{x} = s\mathbf{x}^i + (1-s)\mathbf{x}^{i+\frac{1}{2}}, s \in [0,1]\} \ ,$$

while K_i^+ the convex combination of $\mathbf{x}^{i+\frac{1}{2}}$ and $\mathbf{x}^{i+1}$

$$K_i^+ = \{\mathbf{x} \in \mathbb{R}^2 : \mathbf{x} = s\mathbf{x}^{i+\frac{1}{2}} + (1-s)\mathbf{x}^{i+1}, s \in [0,1]\} \ .$$

In application, no additional grid is created, instead the bilinear forms are changed such that the corresponding matrices are generated. Let $\bar{s}_i^- : [0,1] \to K_i^-$ be the parametrization of K_i^- via

$$\mathbf{x}(s) = s\mathbf{x}^i + (1-s)\mathbf{x}^{i+\frac{1}{2}} \ , \quad s \in [0,1] \ ,$$

and $s_i^-(\mathbf{x})$ its inverse. Analogue, let $\bar{s}_i^+ : [0,1] \to K_i^+$ be the parametrization of K_i^+ via

$$\mathbf{x}(s) = s\mathbf{x}^{i+\frac{1}{2}} + (1-s)\mathbf{x}^{i+1} \ , \quad s \in [0,1] \ ,$$

and $s_i^+(\mathbf{x})$ its inverse.

With this definitions, let $\Pi_1^- : \mathbb{S}_2(K_i) \to \mathbb{S}_1(K_i^-)$ be a interpolation operator given as

$$(\Pi_1^- \phi)(\mathbf{x}) = \phi(a_i) s_i^-(\mathbf{x}) + \phi(a_{i+\frac{1}{2}})(1 - s_i^-(\mathbf{x})) \ ,$$

and analogue the interpolation operator $\Pi_1^+ : \mathbb{S}_2(K_i) \to \mathbb{S}_1(K_i^+)$ given as

$$(\Pi_1^+\phi)(\mathbf{x}) = \phi(a_{i+\frac{1}{2}})s_i^+(\mathbf{x}) + \phi(a_{i+1})(1 - s_i^+(\mathbf{x})) \ .$$

The scalar product for the $\mathbb{P}_1$-iso-$\mathbb{P}_2$ non-lumped scheme is given as

$$\langle \phi, \psi \rangle_{K_i}^{\text{iso}} := \left\langle \Pi_i^- \phi, \Pi_i^- \psi \right\rangle_{K_i^-} + \left\langle \Pi_i^+ \phi, \Pi_i^+ \psi \right\rangle_{K_i^+} \ ,$$

and

$$\langle \phi, \psi \rangle_n^{\text{iso}} := \sum_{i=1}^{N} \langle \phi, \psi \rangle_{K_i}^{\text{iso}} \ .$$

Similar the lumped version of the bilinear form is defined as follows,

$$\langle \phi, \psi \rangle_{K_i}^{h,\text{iso}} := \left\langle \Pi_i^- \phi, \Pi_i^- \psi \right\rangle_{K_i^-}^{h,1} + \left\langle \Pi_i^+ \phi, \Pi_i^+ \psi \right\rangle_{K_i^+}^{h,1} \ ,$$

and

$$\langle \phi, \psi \rangle_n^{h,\text{iso}} := \sum_{i=1}^{N} \langle \phi, \psi \rangle_{K_i}^{h,\text{iso}} \ .$$

The problem of the weak surface evolution with the $\mathbb{P}_1$-iso-$\mathbb{P}_2$ bilinear forms is then:

Problem 4.4.4. *Given Γ_h^n and $\mathbf{u}$, find $(\mathbf{x}_{n+1}, \mathcal{H}_{n+1}) \in (\mathbb{S}_s^n)^d \times \mathbb{S}_s^n$ such that*

$$\begin{aligned} \langle \mathbf{x}_{n+1}, \mathbf{n}_\Gamma \psi \rangle_n^{iso} &= \langle \mathbf{x}_n + \tau_n \mathbf{u}, \mathbf{n}_\Gamma \psi \rangle_n^{iso} \ , \\ \langle \mathcal{H}_{n+1} \mathbf{n}_\Gamma, \eta \rangle_n^{iso} - \langle \nabla_\Gamma \mathbf{x}_{n+1}, \nabla_\Gamma \eta \rangle_n &= 0 \ , \end{aligned}$$

for all $(\eta, \psi) \in (\mathbb{S}_s^n)^d \times \mathbb{S}_s^n$.

With the lumped bilinear form it reads as follows:

Problem 4.4.5. *Given Γ_h^n and $\mathbf{u}$, find $(\mathbf{x}_{n+1}, \mathcal{H}_{n+1}) \in (\mathbb{S}_s^n)^d \times \mathbb{S}_s^n$ such that*

$$\begin{aligned} \langle \mathbf{x}_{n+1}, \mathbf{n}_\Gamma \psi \rangle_n^{h,iso} &= \langle \mathbf{x}_n + \tau_n \mathbf{u}, \mathbf{n}_\Gamma \psi \rangle_n^{h,iso} \ , \\ \langle \mathcal{H}_{n+1} \mathbf{n}_\Gamma, \eta \rangle_n^{h,iso} - \langle \nabla_\Gamma \mathbf{x}_{n+1}, \nabla_\Gamma \eta \rangle_n &= 0 \ , \end{aligned}$$

for all $(\eta, \psi) \in (\mathbb{S}_s^n)^d \times \mathbb{S}_s^n$.

4.4.4 Combined Scheme

Having two schemes, one that results in equi-distributed mesh nodes and a second similar scheme resulting in a curvature dependent mesh node distribution, the idea is to combine both schemes in order to get a parameter determining the final node distribution. Taking the convex combination of both schemes, introduces such a parameter.

Then, the parameter can be chosen, such that it is adjustable whether a more uniform node distribution or a more curvature dependent distribution is preferred.

In order to simplify the notation, analogue to the lumped bilinear forms the following notation is allowed. For $s = 1, 2$ it is set

$$\langle \eta, \psi \rangle_n^s := \langle \eta, \psi \rangle_n \ .$$

With this abbreviation the combined scheme for the three versions, $\mathbb{P}_1$, $\mathbb{P}_2$, and $\mathbb{P}_1$-iso-$\mathbb{P}_2$ reads.

Problem 4.4.6. *Given $\lambda \in [0,1]$, Γ_h^n and $\mathbf{u}$, find $(\mathbf{x}_{n+1}, \mathcal{H}_{n+1}) \in (\mathbb{S}_s^n)^d \times \mathbb{S}_s^n$ such that*

$$\begin{aligned}
(1-\lambda)\, \langle \mathbf{x}_{n+1}, \mathbf{n}_\Gamma \psi \rangle_n^{h,\#} + \lambda\, \langle \mathbf{x}_{n+1}, \mathbf{n}_\Gamma \psi \rangle_n^{\#} &= \langle \mathbf{x}_n + \tau_n \mathbf{u}, \mathbf{n}_\Gamma \psi \rangle_n \ , \\
(1-\lambda)\, \langle \mathcal{H}_{n+1} \mathbf{n}_\Gamma, \eta \rangle_n^{h,\#} + \lambda\, \langle \mathcal{H}_{n+1} \mathbf{n}_\Gamma, \eta \rangle_n^{\#} &= \langle \nabla_\Gamma \mathbf{x}_{n+1}, \nabla_\Gamma \eta \rangle_n \ ,
\end{aligned}$$

for all $(\eta, \psi) \in (\mathbb{S}_s^n)^d \times \mathbb{S}_s^n$. Where, with $\# \in \{1, 2, iso\}$, $\langle \cdot, \cdot \rangle_n^{\#}$ and $\langle \cdot, \cdot \rangle_n^{h,\#}$ denotes either the piecewise linear, piecewise quadratic or the $\mathbb{P}_1$-iso-$\mathbb{P}_2$ forms.

Chapter 5

Results

The purpose of Chapter 5 is to validate the ALE finite element scheme for two-phase flows with surfactants, that was developed in the last chapters. Numerical computations for different test scenarios are done.

The first example is a capillary two-phase flow simulating a Taylor bubble train flow. The surfactant is neglected and the pure hydrodynamics of such flows are studied. The numerical computations of the scheme from this work are compared to the results obtained by other numerical schemes. Two dimensional and three dimensional rotational symmetric computations are done.

The second example is a two-phase flow with soluble surfactants, simulating a Taylor bubble under the influence of surfactants. The results are also compared to other numerical schemes. Further, the effect of the surfactant on the Taylor bubble is studied. In this example, the computations are restricted to the two dimensional case.

The third example is an oscillating drop in three dimensions under the influence of a soluble and insoluble surfactant. The computations are compared to analytical approximations of such flows, found in the literature. The frequencies and damping rates, as well as the amplitudes of the oscillating drop is compared with this theoretical results.

The last, and fourth example, considers the schemes for the surface evolution. Different methods are compared, and the properties regarding the node distribution are shown. The behaviour of the lumped and non-lumped schemes, as well as the $\mathbb{P}_1$ and $\mathbb{P}_2$ scheme is demonstrated on a selected example using the mean curvature flow.

All programs (of course, with the exception of those with which the scheme is compared in the first two examples) are written by the author of this work, using the program package MooNMD [77]. MooNMD is a program package written in C++, providing a framework for the development of finite element codes. It was developed on the Otto-von-Guericke Univerity Magdeburg, with the help of the author of this work.

The program codes solving two dimensional problems (and the rotational symmetric ones) are serial codes. Two dimensional computations require fewer amount of computational work, and serial codes can solve such problems in a reasonable time. However, in three dimensional computation the amount of computational work increases significant.

Therefore, for the three dimensional problems, a parallel program code was developed. The parallel program code employs the `MPI` standard [66, 65]. The parallelization was achieved employing the domain decomposition technique. Thus, the parallel code is able to use an (theoretical) arbitrary amount of processors in order to speed up the computations.

5.1 Taylor Flow Comparison without Surfactant

In the following subsection, a numerical simulation of a Taylor bubble train flow is done. The results are compared with the numerical simulations and experimental results of groups within the DFG Priority Program SPP 1506. Also, the results are compared to analytical approximations found in the literature. The content of this subsection was already published in [6].

Taylor bubbles are long bubbles of gas in capillary tube filled with a liquid. Typically, Taylor bubbles have a bullet shape in flow direction, while a thin film of liquid is forming between bubble and tube wall. A Taylor flow is the flow of a series of elongated Taylor bubbles in a narrow channel, where the channel is almost completely filled with bubbles.

Taylor bubbles were originally described by G. Taylor [42]. In his work, he reports on experiments on the rise of bubbles in nitrobenzene. In channels or tubes with a large diameter Taylor bubbles may not appear, whereas in tubes of a small diameter they are very stable [86]. This stability and the distinct shape and flow profile makes the Taylor bubble an excellent tool for validation and benchmarking tests of numerical schemes.

In a theoretical investigation on a two dimensional Taylor bubble flow, a relation between the capillary number and the film width between the bubble and the channel wall was derived in [31]. The Bretherton approximation is valid within an error margin smaller 5% for capillary numbers $\mathrm{Ca} \leq 3 \cdot 10^{-3}$ and reads

$$d_{\mathrm{Film}} = 1.3375 \cdot \mathrm{Ca}\, R \ , \tag{5.1.1}$$

where R is the tube radius. The capillary number is given as

$$\mathrm{Ca} = \frac{\mu_L U}{\sigma_0} \ ,$$

where μ_L is the dynamic viscosity of the liquid phase, U is the characteristic velocity of the Taylor bubble, and σ_0 the surface tension coefficient of the liquid-gas interface. The capillary number is connected to the Weber number We and the Reynolds number Re_L. Let ρ_L be the density of the liquid phase and let

$$\mathrm{Re}_L = \frac{2\rho_L U R}{\mu_L}$$

be the Reynolds number of the liquid, then

$$\mathrm{We} = \mathrm{Re}_L\, \mathrm{Ca} \ .$$

Later, an approximation for the film width was also done for higher capillary numbers. By using a boundary element method and numerical simulations an empiric correlation between film width and capillary number was found [72]. The Halpern approximation is valid for capillary numbers in the range of $0.05 \leq \mathrm{Ca} \leq 100$ and reads

$$d_{\mathrm{Film}} = 0.417 \cdot \left(1 - \exp\left(-1.69 \cdot \mathrm{Ca}^{0.5025}\right)\right) R \ . \tag{5.1.2}$$

In the following, three different scenarios are considered. A two dimensional Taylor bubble flow, where the Bretherton and Halpern approximations are valid, an axis-symmetric Taylor bubble flow, which is closer to a real world example, and a case where an axis-symmetric Taylor bubble flow is compared to data from an experimental setup.

Each scenario is simulated by four different numerical schemes, including the scheme presented in this work. Two schemes employ the ALE technique. Among these are, the scheme of this work, and a quite similar scheme implemented in a program package called *Navier* [15, 14, 23, 79, 80]. The other two schemes employ both a diffuse interface model. One diffuse interface model is implemented in the program package called *AMDiS* [4, 8, 113], the other diffuse interface scheme is implemented in the program package called *EconDrop* [37, 51, 71]. The program package used for the numerical simulations employing the techniques presented in this work, will be called *MooNMD*.

In all simulations, the initial bubble shape is given by a fixed shape. The initial bubble shape is given by two half circles as caps, and straight edges as body connecting the caps (see Figure 5.1). Given the channel width, the radius of the caps is determined by the initial film width. For capillary numbers $\mathrm{Ca} < 0.05$ the initial film width is set according to (5.1.1), for the other capillary numbers equation (5.1.2) is used.

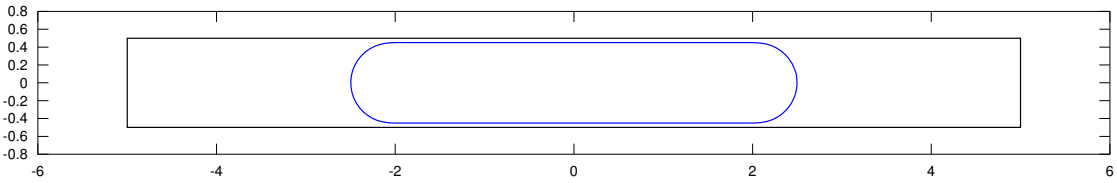

Figure 5.1: Initial bubble shape (rotated by 90 degrees).

5.1.1 Model

The model solved with numerical scheme *MooNMD* is a pressure driven channel flow Problem 3.5.1 and the corresponding rotational symmetric formulation following Chapter 3.5.2. In the two dimensional case, in order to speed up the simulation, the following changes where included. First, the axis symmetry of the problem was exploited. Only one half ($x \geq 0$) was simulated with the appropriate boundary conditions on the symmetry axis. Let $\mathbf{u} = (u_x, u_y)^T$ be the two dimensional velocity field and Γ_S be the symmetry axis, which coincides with the y-axis, the boundary conditions read

$$\begin{aligned} u_x &= 0 \quad \text{on } \Gamma_S \ , \\ \partial_x u_y &= 0 \quad \text{on } \Gamma_S \ . \end{aligned}$$

The x-component of the velocity has a Dirichlet boundary condition, and the y-component has a Neumann boundary condition.

Second, the gas phase, which is the inner of the bubble has been neglected. Such that the problem becomes a free surface problem, and computation of the velocity field in the bubble was skipped.

The Problem 3.5.1 has been discretized according the methods described in the chapters before. Different time discretization were used, but the differences were minimal. Here, the results of the semi-implicit Euler time discretization are presented.

The periodic boundary condition is included in the finite element space. This is done by identifying the mesh nodes on Γ_I with the mesh nodes on Γ_O. Of course, this requires a matched surface mesh for Γ_I and Γ_O.

The prescribed pressure drop δp is adapted in each time step, in order to hold the centre of mass of the Taylor bubble stationary.

5.1.2 Scenario I: Two Dimensional Flow

Scenario I is the two dimensional case. A two dimensional Taylor flow (Bretherton problem) is computed by the different schemes and the results are compared. Although the two dimensional benchmark test is purely numerical, the physical parameters are chosen such that they are close to an experimental realisable situation (a round capillary of approximately 1mm diameter filled with air bubbles in glycerol).

Table 5.1: Physical parameters for the numerical benchmark.

ρ_L	$1{\cdot}10^{3}$	$\frac{kg}{m^3}$	density of liquid phase
ρ_G	$\ll \rho_L$		density of gas phase
μ_L	$1{\cdot}10^{-2}$	$Pa\,s$	dynamic viscosity of liquid phase
μ_G	$\ll \eta_L$		dynamic viscosity of gas phase
σ_0	$5{\cdot}10^{-4}$	$\frac{N}{m}$	surface tension coefficient
U	$1{\cdot}10^{-3}$	$\frac{m}{s}$	characteristic velocity
$2R$	$1{\cdot}10^{-3}$	m	characteristic length, width of computational domain, also called *hydraulic diameter*
L	$1{\cdot}10^{-2}$	m	length of computational domain

In Table 5.1 the physical parameters are given. The corresponding dimensionless numbers are shown in Table 5.2. The capillary number is varied for this benchmark, and the influence of the capillary number on the Taylor flow is studied. The physical parameters given in Table 5.1 corresponds to a capillary number of $\mathrm{Ca} = 2 \cdot 10^{-2}$. Simulations with a capillary number ten times higher, ten times lower and one hundred times lower were additionally done. A varying capillary number can be viewed as varying the bubble speed or as a varying surface tension coefficient. The results are compared with the Bretherton approximation (5.1.1) and the Halpern approximation (5.1.2).

For those schemes that have computed the gas phase, the density ratios of the fluids are not prescribed, since it is not possible to choose them freely in every method. A

typical density ration for an air bubble in glycerol is approximately one to thousand. The density ratio in the simulations are chosen as close as possible.

Table 5.2: Dimensionless quantities for the numerical benchmark.

Re_L	$\frac{\rho_L V d}{\eta_L}$	$1{\cdot}10^{-1}$	Reynolds no. in liquid phase
Re_G	$\frac{\rho_G V d}{\eta_G}$	$\approx Re_L$	Reynolds no. in gas phase
Ca	$\frac{\eta_L V}{\sigma}$	$2{\cdot}10^{\{-4,-3,-2,-1\}}$	capillary no.
We	$Re_L\, Ca$	$1{\cdot}10^{-1} Ca$	Weber no.

In the following a selection of the results are shown.

Film Width

The film width is measured only over a part of the bubble. The minimal distance of the interface to the tube wall is measured from the part, that is one unit length ($2R$) above and below the centre of mass of the bubble. Figure 5.2 shows the film width for the different capillary numbers. The film width is compared between the different codes and the approximation of Bretherton (5.1.1) and Halpern (5.1.2).

An excellent agreement of the results of *MooNMD* to the other schemes and the predictions by Bretherton and Halpern is seen. The agreement is especially good with *Navier* scheme. That is as expected, since the *Navier* scheme is a sharp interface ALE scheme, too. It is also seen how the Bretherton approximation loses accuracy for higher capillary numbers.

Bubble Shape

In Figure 5.3 the shape of the Taylor bubble for the four different schemes are shown. The results are shown for the capillary number $\mathrm{Ca} = 2 \cdot 10^{-2}$. In order to compare the shapes, the centre of gravity of each shape is matched in the figure. A good agreement in the shapes of all schemes is seen, especially in the film. Again the agreement of *MooNMD* is especially good with *Navier*. One code, which employs a diffuse interface model, shows a slight different shape at the front cap and the rear cap, since the bubble is a bit shorter.

Figure 5.4 shows a close up of the front and rear cap. The matching of the shapes in the figure is different from Figure 5.3. The shapes are positioned such that the points at $x = 0$ superimpose. A good agreement in the result of *MooNMD* to the other schemes is seen. A slight deviation in the rear cap of the shape computed by *EconDrop* is observed. Overall, *MooNMD* generates the same Taylor bubble shapes, as the other schemes.

Velocity Profile

The velocities are compared through the comparison of the velocity profiles along a cut parallel to the x-axis. The result is shown in Figure 5.5. The y-position of the cut is

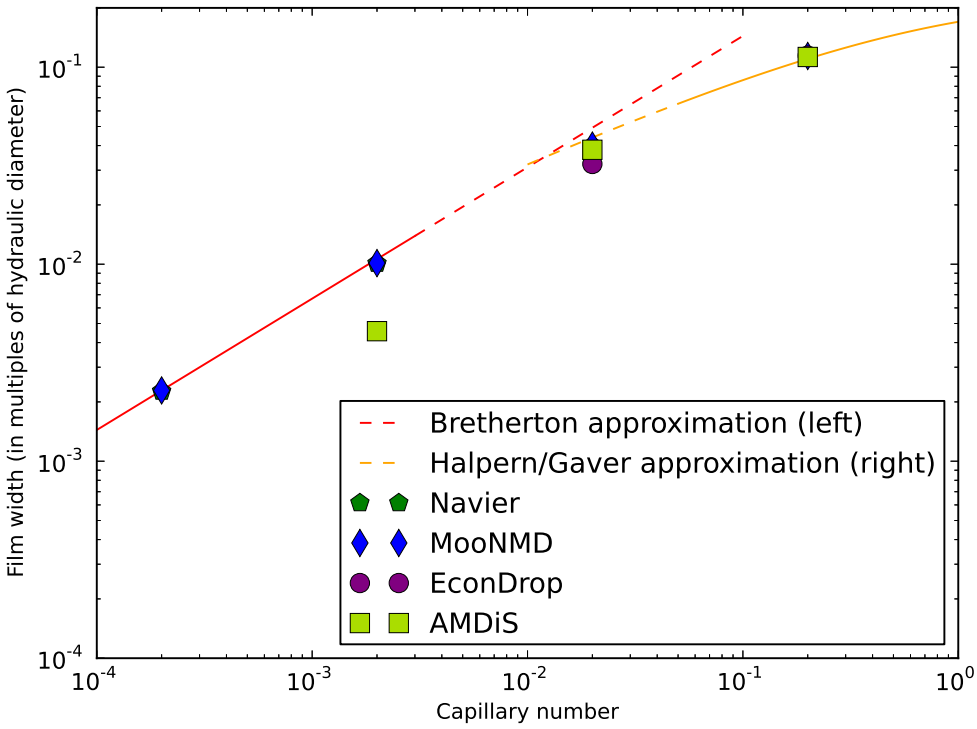

Figure 5.2: Comparison of the film width of a Taylor bubble.

chosen such that the cut is directly at the rear of the bubble. Note, this implies the y-value might be different for each graph.

The left figure of Figure 5.5 shows the x-component of the velocity along the cut. A good agreement of the values produced by *MooNMD* to the other different schemes is seen. Again, a slight deviation is observed for the diffuse interface scheme *EconDrop*. It has to be noticed that, since the bubble is a bit shorter for this scheme, the cut is at a different y value. The right figure in Figure 5.5 shows the y-component of the velocity along the cut. As for the x-component, a good agreement is seen among all four schemes. The deviation to *EconDrop* is even less pronounced.

5.1.3 Scenario II: 3D Axis-Symmetric Flow

Scenario II is a three dimensional scenario under the assumption of rotational symmetry, such that the resulting problem can be computed on a two dimensional mesh. The physical parameters are chosen as in the two dimensional Scenario I. The parameters are given in Table 5.1, and the dimensionless numbers are given in Table 5.2.

Next, a selection of the results for Scenario II are given.

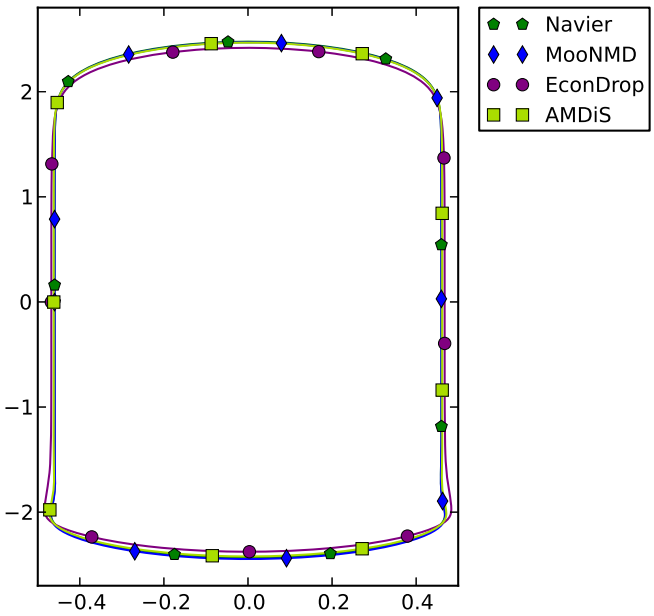

Figure 5.3: Comparison of the bubble shapes for $\mathrm{Ca} = 2 \cdot 10^{-2}$.

Pressure Drop

Figure 5.6 shows the final pressure drop δp needed to hold the bubble flow stationary. The values for the capillary numbers $Ca = 2 \cdot 10^{-4}$ and $Ca = 2 \cdot 10^{-1}$ were not computed by *MooNMD*. For those values computed, a good agreement is seen for the results of *MooNMD*. As before, the match is especially good to the other ALE scheme *Navier*.

Bubble Shape

The shape of the bubbles for the axis-symmetric case is shown in Figure 5.7. The shape presented in the figure is for the capillary number $\mathrm{Ca} = 2 \cdot 10^{-2}$. A good agreement in the shapes from the different schemes is seen. The close up of the cap and rear region of the bubble is shown in Figure 5.8. A good agreement is observed as well. Note, the alignment of the shapes in the figure is chosen as in the two dimensional scenario.

Velocity Profile

Figure 5.9 shows the velocity profile along a cut. The cut is chosen as in the two dimensional scenario. A good agreement is observed for all schemes that have computed the axis-symmetric case for the capillary number $\mathrm{Ca} = 2 \cdot 10^{-2}$. The deviation observed for the scheme *MooNMD*, is due to a coarser grid used by *MooNMD*. The post process,

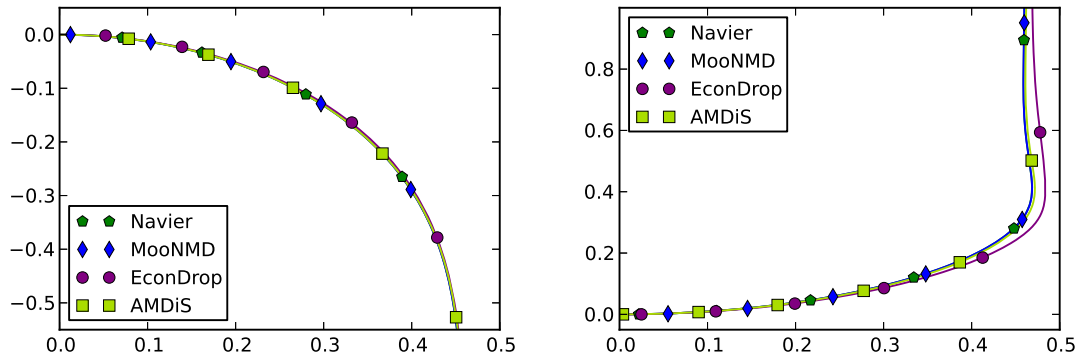

Figure 5.4: Comparison of bubble shapes for $\mathrm{Ca} = 2 \cdot 10^{-2}$: Close up of the front cap (left) and the rear cap (right) of the bubble.

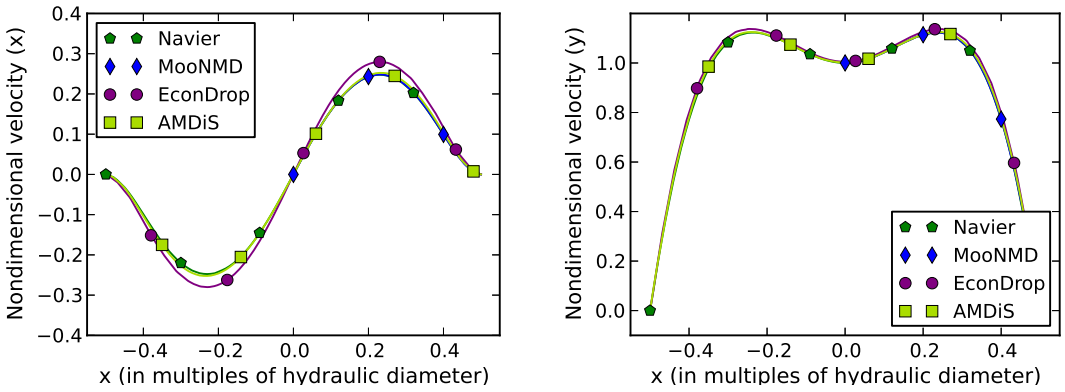

Figure 5.5: Comparison of the velocity profile for $\mathrm{Ca} = 2 \cdot 10^{-2}$.

used to evaluate the velocity profile along the cut ignores the quadratic part of the solution. Although, a coarser grid was used, the agreement is very good.

5.1.4 Scenario III: Experimental Data

Scenario III includes a comparison with a real experimental Taylor flow. For the comparison with experimental data, the bubble shape measured in a radio-graphic projection was available. Other data, like pressure drop and velocity profile was not provided by the experimental setup.

The physical parameters are taken from the experimental setup given in [6]. The parameters are given in Table 5.3. The resulting dimensionless numbers are found in Table 5.4.

The numerical simulation exploits the rotational symmetry of the Taylor bubble. The computation is an axis symmetric computation on a two dimensional mesh.

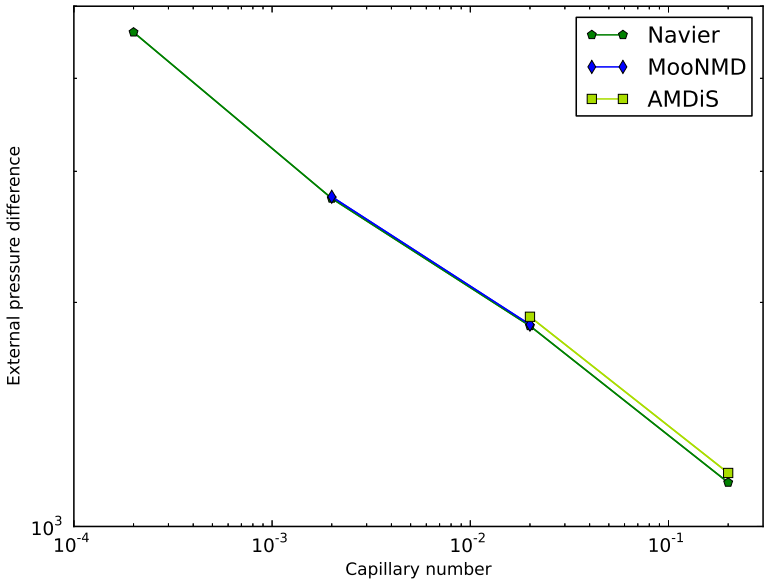

Figure 5.6: Comparison of pressure drops for $\mathrm{Ca} = 2 \cdot 10^{-2}$.

Bubble Shape

Figure 5.10 shows an overview of the shape of the whole bubble, while Figure 5.11 shows the close up at the front and the rear of the bubble. The alignment of the shapes in the figures is as in the scenarios before. While the numerical results are in good accordance, the bullet shape seems to be less pronounced in the experimental data, i.e. the numerical results exhibit too low surface tension effects. It remains unclear whether this is due to some error in the measurement (e.g. by a violation of the assumption of rotational symmetry, wrong physical parameters, etc.) or to some physical effects not considered in the models. However, the bubble shape is reproduced well in the numerical simulations.

Again, the results obtain by *MooNMD* are in good accordance to the other schemes. The agreement is especially good to the scheme *Navier*, which is an ALE scheme, too.

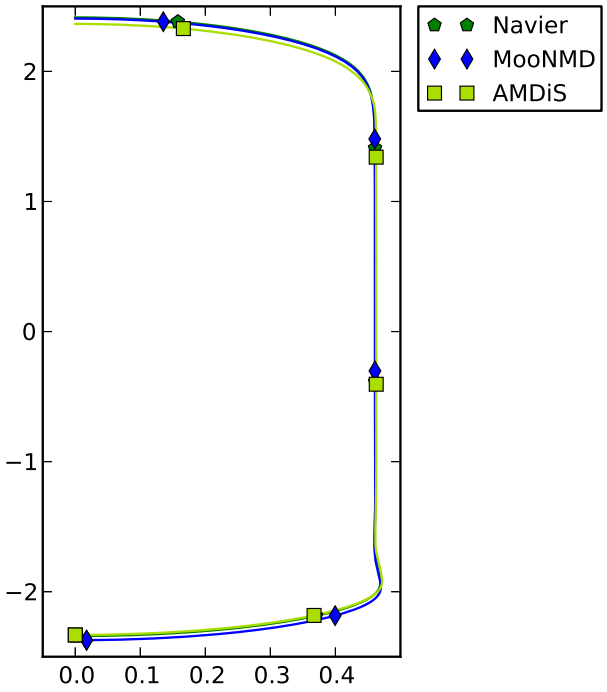

Figure 5.7: Comparison of the bubble shape for $\mathrm{Ca} = 2 \cdot 10^{-2}$.

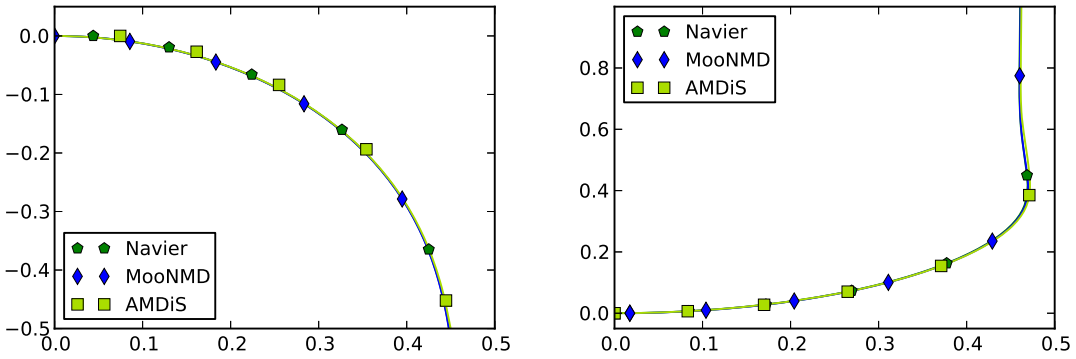

Figure 5.8: Comparison of the bubble shape for $\mathrm{Ca} = 2 \cdot 10^{-2}$: Close up at front cap (left) and rear cap (right) of the bubble.

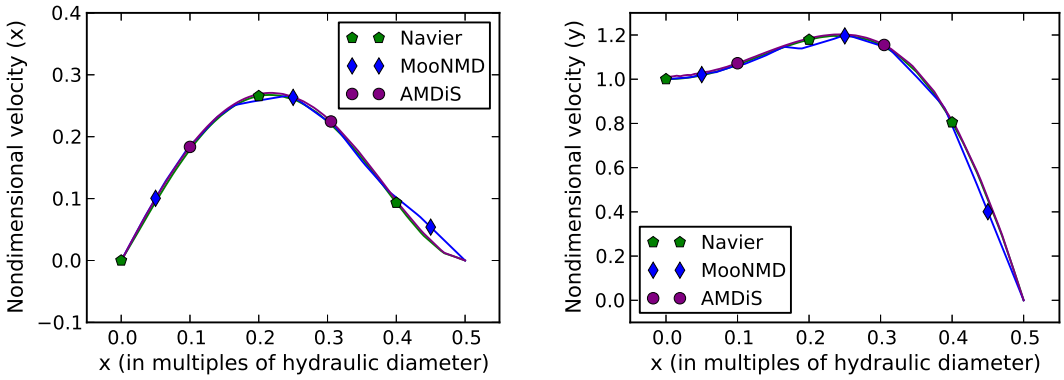

Figure 5.9: Comparison of the velocity profiles.

Table 5.3: Physical parameters for Scenario III.

ρ_L	$1.196{\cdot}10^{3}$	$\frac{kg}{m^3}$	density of liquid phase, literature data fit
ρ_G	$\ll \rho_L$		density of gas phase
μ_L	$29.8{\cdot}10^{-3}$	$Pa\,s$	dynamic viscosity of liquid phase, literature data fit
μ_G	$\ll \eta_L$		dynamic viscosity of gas phase
σ_0	$66.8{\cdot}10^{-3}$	$\frac{N}{m}$	surface tension coefficient, literature data fit
U	$210.2{\cdot}10^{-3}$	$\frac{m}{s}$	bubble velocity, measured in experiment
$2R$	$1.98{\cdot}10^{-3}$	m	hydraulic diameter, measured in radiographic projection
V	$20.68{\cdot}10^{-9}$	m^3	bubble volume, computed from 2D bubble shape measured in radiographic projection
L	$1{\cdot}10^{-2}$	m	length of computational domain

Table 5.4: Dimensionless quantities for Scenario III.

Re_L	$\frac{\rho_L V\, d}{\eta_L}$	$1.67379{\cdot}10^{1}$	Reynolds no. in liquid phase
Re_G	$\frac{\rho_G V\, d}{\eta_G}$	$\approx Re_L$	Reynolds no. in gas phase
Ca	$\frac{\eta_L V}{\sigma}$	$9.39637{\cdot}10^{-2}$	capillary no.
We	$Re_L\, Ca$	$1.57275{\cdot}10^{0}$	Weber no.

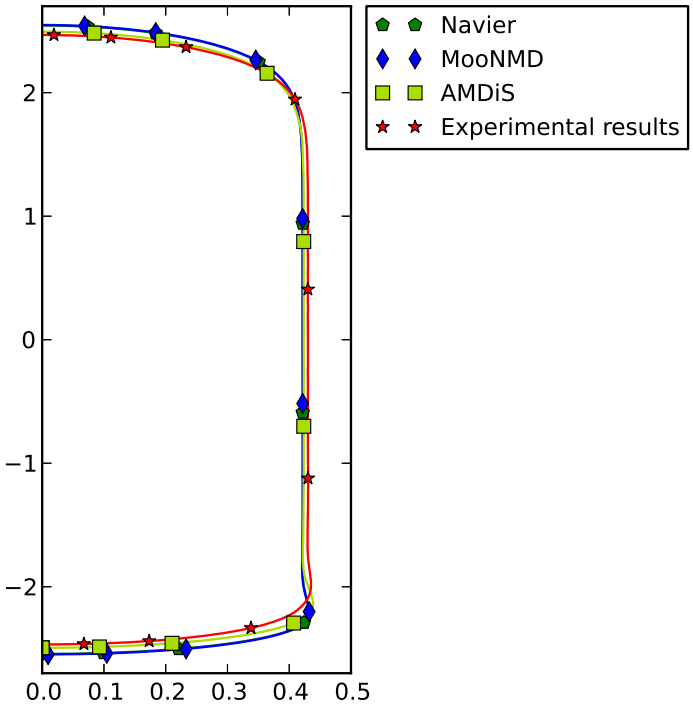

Figure 5.10: Comparison of the bubble shapes: Complete bubble.

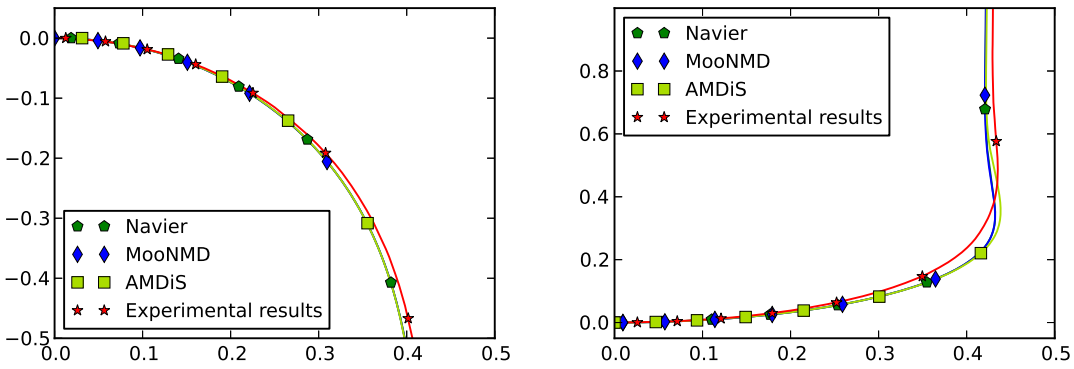

Figure 5.11: Comparison of the bubble shape: Close up at cap (left) and rear (right) of the bubble.

5.2 Taylor Flow Comparison with Surfactants

The Taylor flow comparison of the last subsection is extended to a scenario that includes surfactants. The effect of a surfactant on the Taylor flow is studied. Similar to the Taylor flow comparison without surfactants, the results of the scheme presented in this work are compared to simulation of other groups within the DFG Priority Program SPP 1506. The results shown here were already published in [5].

As in the Taylor flow comparison from the last subsection, two diffuse interface and two sharp interface schemes are involved. But unlike before, the other sharp interface scheme is an Eulerian scheme and does not employ the ALE method. Also, in contrast to the comparison in the last section, a two dimensional scenario is considered this time only.

The setup has been changed, in order to include the surfactant. Instead of simulating a bubble train, a single Taylor bubble in a counter flow scenario is considered now. The surfactant is supposed to be soluble in the liquid phase only. The bubble is rising due to gravity. In order to hold the bubble stationary, the rising bubble is countered by a steady flow. Such that the bubble becomes stationary if both effects cancel each other.

The assumption of periodicity of the flow field is neglected. It is assumed that a laminar pipe flow of a homogeneous surfactant solution enters the computational domain from above through Γ_I, see Figure 3.1. The surfactant solution is allowed to leave the computational domain through Γ_O. Thus, a Dirichlet boundary condition for the fluid and the surfactant is assumed at Γ_I. Let $s : [0,1] \to \Gamma_I$ be a parametrization of Γ_I, a typical parabolic profile is prescribed for the velocity at Γ_I

$$\mathbf{u}_{\Gamma_I} := \mathbf{u}(t, \mathbf{x}(s)) = -4u_{\max}(t)s(1-s)\mathbf{e}_y \quad \text{on } \Gamma_I \ ,$$

where $u_{\max}$ is the maximum inflow velocity. The parameter $u_{\max}$ is used to restrict the vertical movement of the bubble, by changing its value over time according to the bubble velocity. The boundary condition for the surfactant at Γ_I reads

$$c|_{\Gamma_I} = c_0 \quad \text{on } \Gamma_I \ ,$$

where c_0 is the given constant surfactant concentration of the surfactant solution.

On the outflow boundary Γ_O a do-nothing (stress free) condition is assumed for the fluid and for the surfactant as well

$$\mathbb{S}(\mathbf{u}, p)\mathbf{n} = 0 \ , \quad \nabla c \cdot \mathbf{n} = 0 \qquad \text{on } \Gamma_O \ .$$

At the channel wall a no-slip condition is assumed for the fluid, i.e. a homogeneous Dirichlet condition on Γ_W

$$\mathbf{u} = 0 \quad \text{on } \Gamma_W \ .$$

Since no surfactant can enter the channel wall, the flux of surfactant is obstructed. Together with the vanishing velocity of the fluid at the channel wall, this leads to a homogeneous Neumann condition for the surfactant concentration at Γ_W,

$$\nabla c \cdot \mathbf{n} = 0 \quad \text{on } \Gamma_W \ .$$

The parameters chosen for the simulations are similar to that of the last subsection, augmented with the surfactant related parameters. Due to the wide variety of different surfactants with different properties, the surfactant related parameters are chosen freely. The Damköhler and Biot numbers are fixed to $\mathrm{Da} = \mathrm{Bi} = 0.01$. The other surfactant related parameters are varied, in order to see their influence on the Taylor bubble. The surface elasticity is chosen from $\mathrm{E} = \{0.5, 1.0\}$, the surfactant concentration of the surfactant solution is chosen from $c_0 = \{0.02, 0.08\}$. The surface Peclet number Pe_Γ and the bulk Peclet number Pe are assumed to be equal, and are chosen from two different values, $\mathrm{Pe} = \mathrm{Pe}_\Gamma = \{1, 10\}$.

All these values are found empirically in order to have a fast converging and stable simulation for all participating schemes. The remaining dimensionless parameters are as in Table 5.2, namely $\mathrm{Re} = 0.1$, $\mathrm{We} = 2 \cdot 10^{-3}$, and $\mathrm{Fr} = 1 \cdot 10^{-4}$.

The diffuse interface schemes are realised in the program package *AMDiS* and *2PStab*, the sharp interface models are realised in the program packages *BGN* and *MooNMD*, where *MooNMD* employs the methods presented in this work. Further information of the other schemes can be found in [5], and will not be specified here.

The initial domain is chosen as in the last section, given in Figure 5.1. The initial bubble diameter is set to 0.7 units, the initial total bubble length is set to 4.7 units. The initial fluid is in rest, i.e. $\mathbf{u}|_{t=0} = 0$ in $\Omega(0)$. The initial surfactant concentration in the bulk is homogeneous and set to $c|_{t=0} = c_0$. The initial surface surfactant concentration is set to a constant, which is given according to the equilibrium condition

$$\frac{\mathrm{Da}}{\mathrm{Bi}} = \frac{\gamma}{c\,(1-\gamma)} \ .$$

At each time step, the vertical bubble speed u_y^n is measured (velocity in y-direction) through

$$u_y^n := \int_{\Omega_1^n} \mathbf{u}_n \cdot \mathbf{e}_y \ \mathrm{d}V \ ,$$

where $\mathbf{e}_y$ is the unit vector in y-direction. Given the old inflow velocity $u_{\max}^n = u_{\max}(t_n)$ a new inflow velocity $u_{\max}^{n+1}$ found through

$$u_{\max}^{n+1} = u_{\max}^n + u_y^n \ .$$

It has to be noted, that this leads to a quasi stationary bubble, since if $u_y^n = 0$ it follows $u_{\max}^{n+1} = u_{\max}^n$.

In the following, the results of this benchmark are presented.

5.2.1 Results

Different benchmark values are considered. Apart from the direct numerical values c, γ and $u_{\max}$, calculated by the codes, some of them are determined by a post process. Due to the different nature of the methods, the post process can differ.

Here, the film width d_{film} is defined as the minimal distance between bubble and wall. For the sharp-interface schemes, d_{film} is computed directly from the numeric interface representation while the diffuse-interface schemes use the zero level contour line of phase field ϕ.

The bulk surfactant mass m_c and surface surfactant mass m_γ is defined as the total amount of surfactant present in the bulk and on the surface, respectively. In case of the sharp interface schemes the bulk surfactant exist in $\Omega_2(t)$ and the surface surfactant exists on $\Gamma(t)$. The corresponding masses are calculated as

$$m_c(t) = \int_{\Omega_2(t)} c \, \mathrm{d}V, \quad m_\gamma(t) = \int_{\Gamma(t)} \gamma \, \mathrm{d}V \ .$$

In the case of the diffuse-interface schemes, the quantities c and γ are defined in the whole domain $\Omega(t)$ and, thus the masses are calculated as

$$m_c(t) = \frac{1}{2} \int_{\Omega(t)} (1-\phi) c \, \mathrm{d}V, \quad m_c(t) = \int_{\Omega(t)} \delta c \, \mathrm{d}V.$$

Having defined the benchmark values, a closer look at the results is taken in the following.

Inflow Velocity

Figure 5.12 shows the evolution over time of the maximum inflow velocity $u_{\max}$ for the simulation parameters $(c_0, \mathrm{Pe}, \mathrm{Pe}_\Gamma, \mathrm{E}) = (0.02, 1, 1, 1)$, exemplarily. All four schemes show a similar behaviour. After some oscillations, $u_{\max}$ reaches a stationary state already before $t = 1$. The sharp interface results are very close to each other and so are the diffuse interface results. The diffuse interface schemes predict a slightly smaller bubble velocity. Overall, the scheme *MooNMD* reproduces the results of the other schemes very well.

In Table 5.5, the final counter current flow velocity at $t = 10$ (except for 2PStab $t = 1$, unfortunately, due to a very small time step used for *2PStab*, the simulation time was limited for this scheme) is shown for all parameter combinations. A good agreement of the results obtained by *MooNMD* to the other schemes is seen. It has to be noted, that the variation of the flow velocities across the different numerical models, dominates the variation of the velocity across different parameters. The flow velocity seems to be insensitive to the chosen surfactant related parameters.

The missing values in Table 5.5, in particular for $c_0 = 0.08$ and $\mathrm{Pe} = \mathrm{Pe}_\Gamma = 10$, are caused by numerical problems due to high surfactant concentration at the bubble rear and the following low surface tension. The sharp interface schemes seem to have less problems in this situation.

Surfactant Concentration and Surfactant Mass

The development of the surfactant masses over time are shown in Figure 5.13 and Figure 5.14. In Figure 5.13 the course of bulk surfactant mass is shown for the parameter

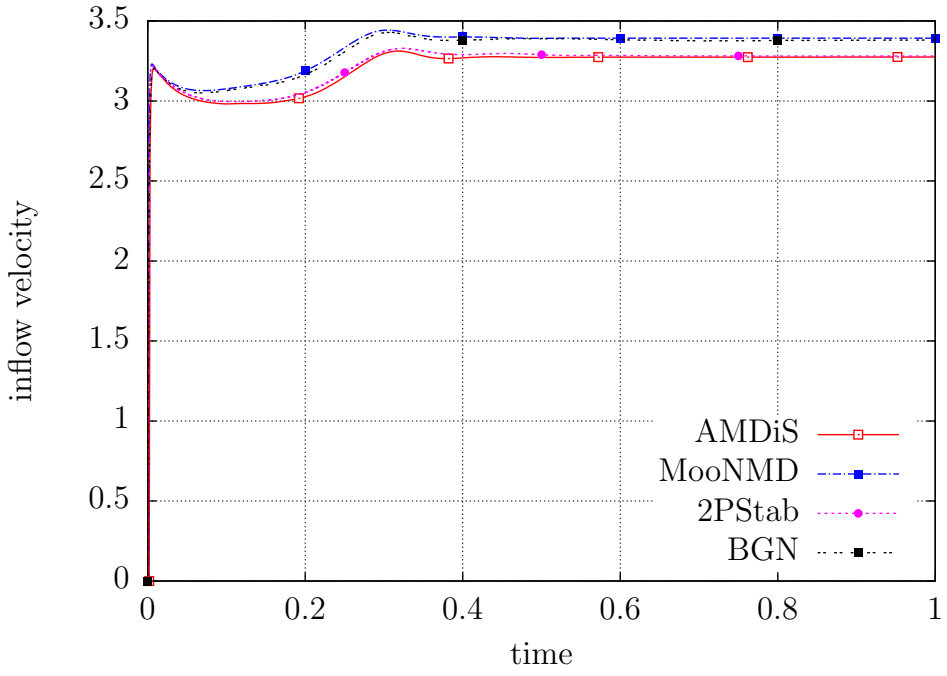

Figure 5.12: Maximum inflow velocity over time for $(c_0, \mathrm{Pe}, \mathrm{Pe}_\Gamma, \mathrm{E}) = (0.02, 1, 1, 1)$.

set $(c_0, \mathrm{Pe}, \mathrm{Pe}_\Gamma, \mathrm{E}) = (0.02, 1, 1, 1)$. The bulk surfactant mass decreases over time and reaches a stationary state. It can be seen that the surfactant mass reaches its equilibrium slower than the inflow velocity and the stationary state is not reached until approximately $t = 5$. Agreement among the schemes is particular high between *MooNMD* and *AMDiS*, despite the conceptual difference between the sharp and diffuse interface models.

Analogue, in Figure 5.14 the temporal evolution of the surface surfactant mass for the parameters $(c_0, \mathrm{Pe}, \mathrm{Pe}_\Gamma, \mathrm{E}) = (0.02, 1, 1, 1)$ are shown. A slow decrease of the surfactant mass over time is observed, indicating that a discrete stationary solution is not yet found at $T = 10$. Although the continuous problem would eventually lead to a stationary state, for which conservation of mass holds trivially, the loss of exact divergence free flow in the discrete setting may lead to a slight, but steady loss of surfactant mass over time. The deviation in the simulation using the *AMDiS* scheme at the beginning of the simulation cannot be explained, but in general the scheme shows the same overall behaviour as the other schemes. *MooNMD* reproduces the results of the other schemes very well.

The stationary local distribution of the surfactant in the bulk phase and on the surface at time $t = 10$ is shown in Figure 5.15, exemplarily for the parameter sets $(c_0, \mathrm{Pe}, \mathrm{Pe}_\Gamma, \mathrm{E}) = (0.02, 1, 1, 1)$ on the right and $(c_0, \mathrm{Pe}, \mathrm{Pe}_\Gamma, \mathrm{E}) = (0.02, 10, 10, 1)$ on the left. The surface, the inner line, is scaled and translated a bit, in order to distinguish it from the bulk. A different distribution due to the different diffusion intensities is noted. For both parameter regimes, the surfactant is adsorbed at the bubble surface, leading to a decrease of the bulk surfactant in the film at the channel wall. Along the bubble

Table 5.5: Maximum counter flow velocity $u_{\max}$ at the stationary state for different simulation parameters.

$c_0 = 0.02$	$Pe = Pe_\Gamma = 1$		$Pe = Pe_\Gamma = 10$	
	$E = 0.5$	$E = 1$	$E = 0.5$	$E = 1$
AMDiS	3.27506	3.27336	3.27539	3.27391
MooNMD	3.39283	3.39284	3.39283	3.39284
2PStab ($t = 1$)	3.28185	3.28102	3.28248	3.28087
BGN	3.37914	3.37773	3.36149	3.35499
$c_0 = 0.08$	$Pe = Pe_\Gamma = 1$		$Pe = Pe_\Gamma = 10$	
	$E = 0.5$	$E = 1$	$E = 0.5$	$E = 1$
AMDiS	3.26413	3.25311	-	-
MooNMD	3.39286	3.38990	3.39198	3.39203
2PStab ($t = 1$)	3.29367	-	-	-
BGN	3.35935	3.33733	3.33063	3.31528

surface, the surfactant is transported with the flow and finally accumulates at the rear cap of the Taylor bubble, where it is continuously desorbed into the bulk. In the case of higher diffusion (left), the local variations in the surfactant concentration are more pronounced.

Figure 5.16 shows the stationary bulk surfactant distribution along the channel wall for the parameter set $(c_0, \mathrm{Pe}, \mathrm{Pe}_\Gamma, \mathrm{E}) = (0.02, 1, 1, 1)$, exemplarily. An excellent agreement among the numerical scheme is found. The characteristic decrease in bulk surfactant concentration in the film can be observed quite well.

Film Thickness

Finally, the effect of the surfactant on the film thickness is investigated. Figure 5.17 shows the film width over time for the parameter set $(c_0, Pe, Pe_\Gamma, E = (0.02, 1, 1, 0.5)$. The behaviour of all four schemes is similar and very close to each other. After some initial oscillations and interface waves, the bubble shape reaches a stationary state after a short time and the film width stays constant.

The stationary film width is given in Table 5.6 for all schemes and all parameters. All values are determined at the final time $t = 10$. Except for the *2PStab* scheme, for which they are taken at time $t = 1$, as before. Fortunately, the solution is already fairly stationary at $t = 1$, such that the comparison seems valid.

In general, the diffuse interface schemes predict a smaller film thickness which might be due to a minimal Cahn–Hilliard dynamics that lead to a slight retraction of the bubble. This explanation is also supported by the slight smaller bubble length of the diffuse interface schemes, seen in Table 5.7.

Figure 5.18 shows a comparison of the film width with varying surface elasticity E (left) and with varying diffusion coefficients Pe and Pe_Γ (right). All codes show that

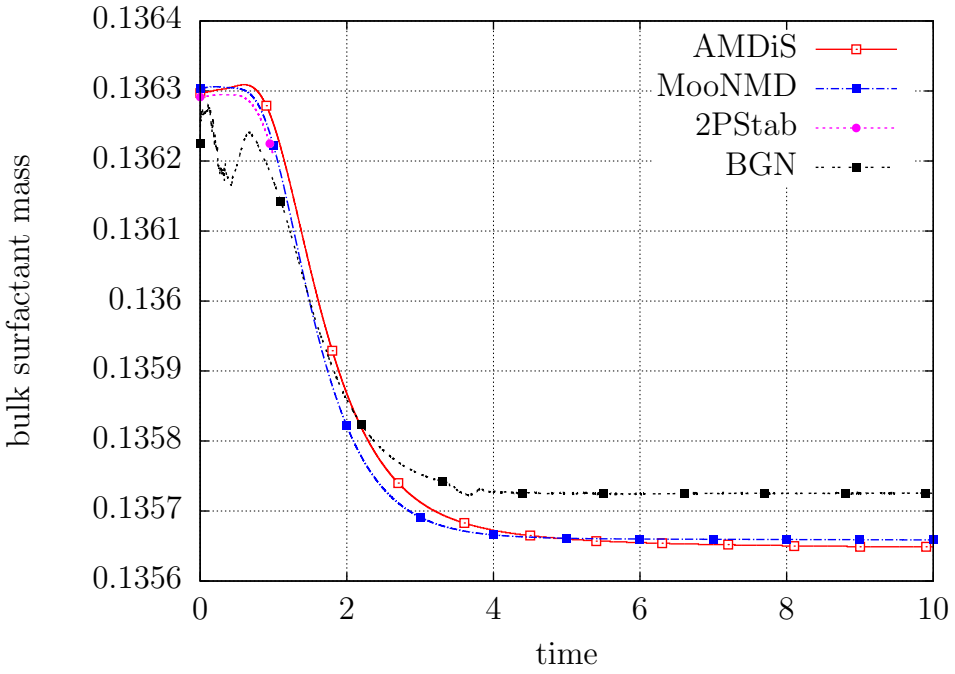

Figure 5.13: Bulk surfactant mass over time, for $(c_0, Pe, Pe_\Gamma, E) = (0.02, 1, 1, 1)$.

an increasing surface elasticity and an increasing surfactant diffusion leads to a larger film thickness. This is consistent with analytic predictions conducted in [100]. Due to the chosen parameters, the change in film width across different parameters is minimal and the differences between the codes may seem large. However, the differences in film thickness between the codes are less than 2% and the equal slope of the lines in Figure 5.18 indicates a good agreement between all four schemes with respect to the dependency of the film thickness on surface elasticity and surfactant diffusion.

From Table 5.5 it can be seen that the bubble velocity is almost independent of the surfactant related parameters, although the film thickness varies. This is in contrast to the results of [31], that predict an increasing bubble velocity with an increasing film width. This might be a unique behaviour due to the presence of the surfactant that was not included in [31].

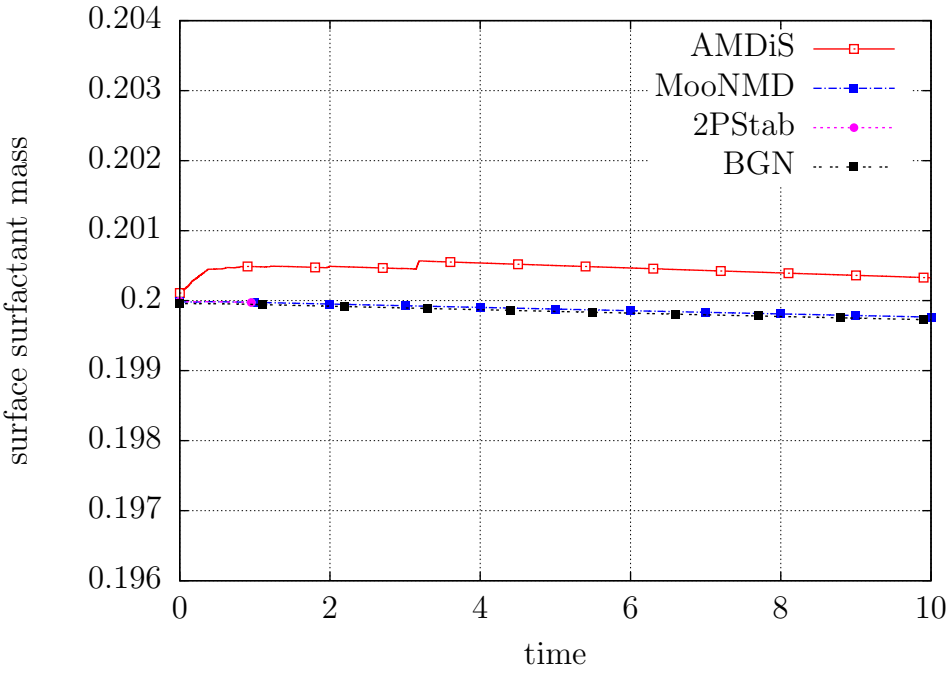

Figure 5.14: Surface surfactant mass over time, for $(c_0, Pe, Pe_\Gamma, E) = (0.02, 1, 1, 1)$.

Table 5.6: Film width for different simulation parameters.

$c_0 = 0.02$	$Pe = Pe_\Gamma = 1$		$Pe = Pe_\Gamma = 10$	
	$E = 0.5$	$E = 1$	$E = 0.5$	$E = 1$
AMDiS	0.14408	0.14802	0.14304	0.14604
MooNMD	0.14724	0.15086	0.14601	0.14853
2PStab ($t = 1$)	0.14627	0.14957	0.14504	0.14739
BGN	0.14674	0.15053	0.14492	0.14789
$c_0 = 0.08$	$Pe = Pe_\Gamma = 1$		$Pe = Pe_\Gamma = 10$	
	$E = 0.5$	$E = 1$	$E = 0.5$	$E = 1$
AMDiS	0.14960	0.14914	-	-
MooNMD	0.15121	0.15113	0.15037	0.15032
2PStab ($t = 1$)	0.14962	-	-	-
BGN	0.15101	0.14932	0.14845	0.15144

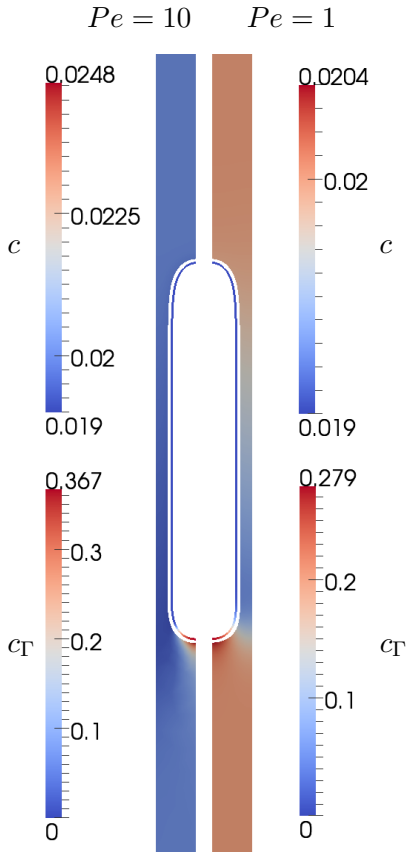

Figure 5.15: Stationary surfactant distribution from MooNMD in the bulk phases and on the surface. For $(c_0, Pe, Pe_\Gamma, E) = (0.02, 1, 1, 1)$ (right), and for $(c_0, Pe, Pe_\Gamma, E) = (0.02, 10, 10, 1)$ (left).

Table 5.7: Bubble length for different simulation parameters.

$c_0 = 0.02$	$Pe = Pe_\Gamma = 1$		$Pe = Pe_\Gamma = 10$	
	$E = 0.5$	$E = 1$	$E = 0.5$	$E = 1$
AMDiS	4.71900	4.72500	4.72000	4.73100
MooNMD	4.76351	4.77366	4.76632	4.77970
2PStab ($t = 1$)	4.73000	4.75000	4.74000	4.76000
BGN	4.75971	4.76951	4.76212	4.77465
$c_0 = 0.08$	$Pe = Pe_\Gamma = 1$		$Pe = Pe_\Gamma = 10$	
	$E = 0.5$	$E = 1$	$E = 0.5$	$E = 1$
AMDiS	4.76200	4.80000	-	-
MooNMD	4.81922	5.05115	4.87267	4.97512
2PStab ($t = 1$)	4.80000	-	-	-
BGN	4.81032	4.82561	4.81045	4.84463

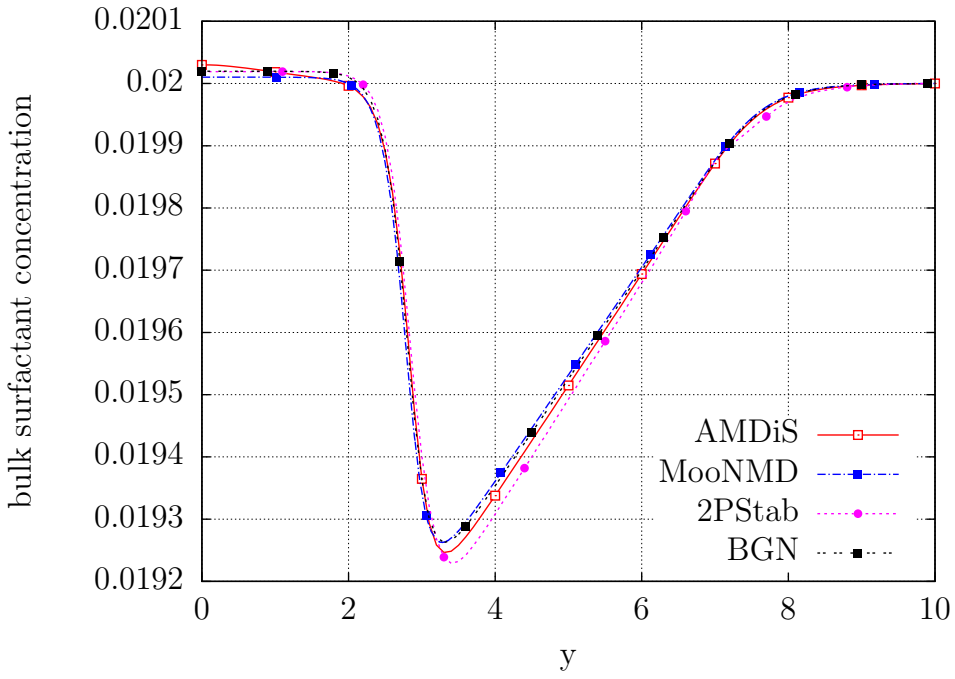

Figure 5.16: Stationary bulk surfactant concentration along the channel wall at time $t = 10$ ($t = 1$ for 2PStab), for $(c_0, Pe, Pe_\Gamma, E) = (0.02, 1, 1, 1)$.

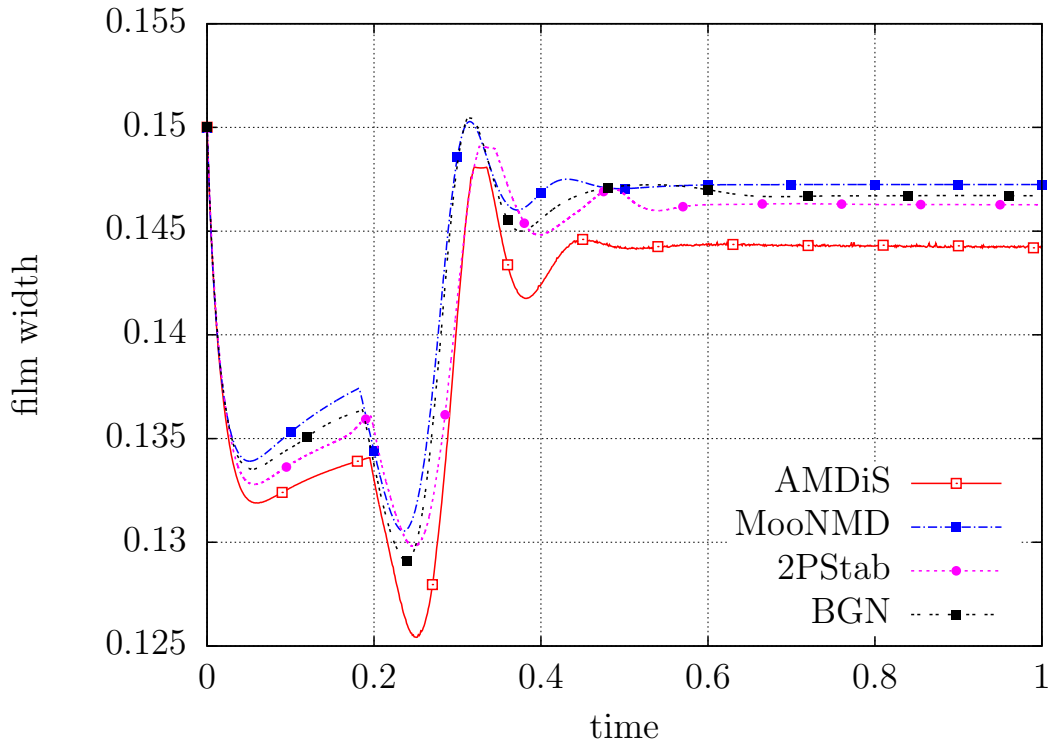

Figure 5.17: Film width over time, for $(c_0, Pe, Pe_\Gamma, E) = (0.02, 1, 1, 0.5)$.

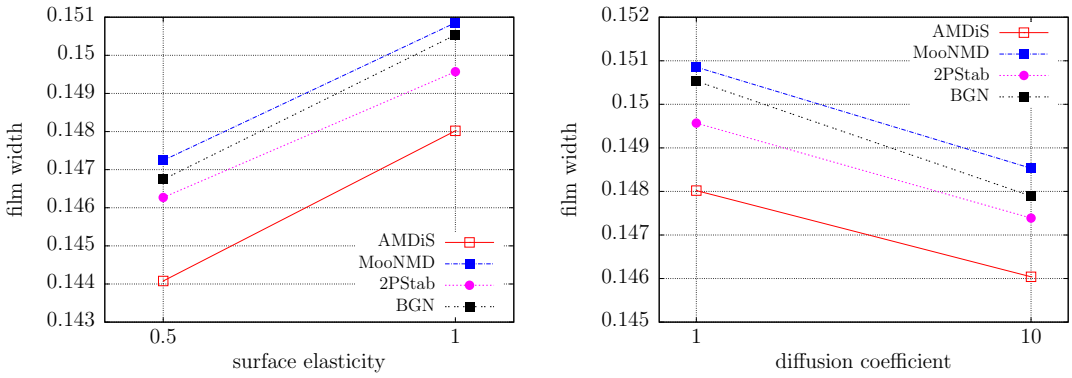

Figure 5.18: Film width with surface elasticity for $(c_0, Pe, Pe_\Gamma) = (0.02, 1, 1)$ (left) and film width with diffusion coefficients for $(c_0, E) = (0.02, 1)$ (right).

5.3 Freely Oscillating Droplet

The goal of this section is to validate the proposed scheme further. The scheme is compared to analytic models of oscillating drops with surfactants. Parts of this subsection are already published in [62].

The understanding of the dynamics of drops and bubbles is of importance in numerous practical applications. The presence of surfactants changes the dynamic features of an interface. Non-uniform surfactant concentrations result in Marangoni forces, and the interface will show additional viscoelastic effects, which alter the dynamic behaviour of the droplet.

There are many theoretical, experimental and numerical investigations into the field of oscillations of drops and bubbles. In fact, the study of small-amplitude oscillations of inviscid fluids has an over one hundred years long history. Initiated with a normal mode analysis for inviscid fluids in [78, 101] at the end of the nineteenth century, the theory was refined further. Later, also weakly viscid fluids are investigated in [38, 82] and in cases where viscous effects cannot be neglected in [89, 98]. Further, large-amplitude oscillations were studied in [24].

Oscillations of drops and bubbles, when surfactants are present were subject to theoretical investigations in [85, 91, 110]. In [91] a weakly viscous fluid with insoluble surfactant is considered. A set of ordinary differential equations for the amplitudes of shape and surfactant concentration oscillation is derived with an analysis of the energy using an averaging method. The velocity field has been approximated by the method of matched asymptotic expansions. In [110] a viscous drop with soluble surfactant is analysed. Analytical approximate solutions for the frequency and the damping rate are derived using a perturbation method. The results from [91, 110] are taken as validation models here.

In this subsection the validation models are compared to the fully three dimensional numerical computations. The numerical scheme solves for a capillary free surface flow with soluble or insoluble surfactant using the ALE-finite element method on moving grids, as presented in Chapter 4.

A short recall on the main theoretical results of oscillating drops as derived in [82, 91, 110] is given. After this the result of the computations are presented.

5.3.1 Basic Oscillating Droplet Dynamics

From the linearized theory of a small-amplitude oscillations of a drop, the angular frequency and the damping rate of the oscillation can be predicted [24, 38, 82, 98]. A spherical drop perturbed by a spherical harmonic, has the surface given by

$$r(\theta, \phi) = r_0 + a_n Y_n(\theta, \phi) \ , \tag{5.3.1}$$

where r_0 is the unperturbed radius and a_n is the perturbation amplitude and

$$Y_n(\theta, \phi) = \sqrt{\frac{2n+1}{4\pi}} P_n(\cos\phi) \tag{5.3.2}$$

is a spherical harmonic with the Legendre polynomial P_n.

The natural angular Lamb frequency $\omega_{0,n}$ for the oscillation of the n-th mode of a drop in vacuum is given by

$$\omega_{0,n}^2 = n(n-1)(n+2)\frac{\sigma}{\varrho r_0^3} \ . \tag{5.3.3}$$

Including weak viscosity, the Lamb damping rate of the oscillation is

$$\delta_n = (n-1)(2n+1)\frac{\eta}{\varrho r_0^2} \ , \tag{5.3.4}$$

and the angular frequency

$$\omega_n = \sqrt{\omega_{0,n}^2 - \delta_n^2} \ . \tag{5.3.5}$$

To obtain a dimensionless form, the physical time is scaled with UL^{-1}. Then the formulas for $\omega_{0,n}$ and δ_n read

$$\omega_{0,n}^2 = n(n-1)(n+2)\mathrm{We}^{-1} \ , \tag{5.3.6}$$

$$\delta_n = (n-1)(2n+1)\mathrm{Re}^{-1} \ , \tag{5.3.7}$$

where the characteristic length L is set to r_0.

For the most important second mode, which is considered here, it is obtained

$$\omega_{0,2}^2 = \frac{8}{\mathrm{We}} \ , \quad \delta_2 = \frac{5}{\mathrm{Re}} \ . \tag{5.3.8}$$

The aperiodic limit is associated with $\omega_{0,2} = \delta_2$, i.e.

$$\frac{\mathrm{We}}{\mathrm{Re}^2} = \frac{\mathrm{Ca}}{\mathrm{Re}} = \frac{8}{25} \ , \tag{5.3.9}$$

where Ca is the capillary number.

Theoretical results for an oscillating droplet with insoluble surfactants are derived in [91]. A set of differential equations for the amplitude a_l of the l-th mode of the shape oscillations and amplitude g_l of the $l-th$ mode of the surface surfactant concentration are given. For the case of a small amount of surfactant and for the second mode the equations read

$$\ddot{a}_2 + \frac{5}{\mathrm{Re}}\dot{a}_2 + \frac{8}{\widehat{\mathrm{We}}}a_2 = -2\frac{\widehat{E}}{\widehat{\mathrm{We}}}g_2 \ , \tag{5.3.10}$$

$$\dot{g}_2 + \frac{6}{\sqrt{\mathrm{Pe}_\Gamma}}g_2 = \dot{a}_2 \ , \tag{5.3.11}$$

with the corrected Weber number $\widehat{\mathrm{We}}$ and surface elasticity $\widehat{E}$

$$\widehat{\mathrm{We}} = \frac{\mathrm{We}}{\sigma(c_\Gamma^{eq})} \ , \quad \widehat{E} = \frac{c_\Gamma^{eq} E}{\sigma(c_\Gamma^{eq})} \ , \tag{5.3.12}$$

where c_Γ^{eq} is the equilibrium surface surfactant concentration.

In order to compare the insoluble theory with the results here, the equations (5.3.10) and (5.3.11) are solved numerically with a Matlab code using the `ode45` routine.

A result for higher viscosities and soluble surfactant is given in [110]. For the dimensionless complex frequency α a first order approximation

$$\alpha = i(1 + \epsilon + \mathcal{O}(\epsilon^2)) \tag{5.3.13}$$

is given. ϵ is given as

$$\epsilon = \frac{1}{2}\frac{(1 + 16(\sqrt{\beta^{-1}i} - 3i)\beta)\hat{P} - 12\beta i}{1 + (\sqrt{\beta^{-1}i} - 3i)(3\hat{P}i + 4\beta)} , \tag{5.3.14}$$

where i is the imaginary unit and $\beta = (\mathrm{Re}\hat{\omega})^{-1}$, with $\hat{\omega} = \sqrt{8/\widehat{\mathrm{We}}}$ and

$$\hat{P} = \frac{E'}{4\hat{G}} + \frac{2i}{\mathrm{Re}\hat{\omega}} , \tag{5.3.15}$$

$$\hat{G} = 1 + \frac{6i}{\mathrm{Pe}_\Gamma\hat{\omega}} - \left(\frac{\mathrm{DaBi}\sqrt{\hat{\omega}}}{\kappa^2\sqrt{\mathrm{Pe}^3 i}} - \frac{\hat{\omega}}{\kappa i}\right)^{-1} , \tag{5.3.16}$$

$$\tag{5.3.17}$$

with $\kappa = c^{eq}\mathrm{Da}+\mathrm{Bi}$ and c^{eq} the equilibrium bulk surfactant concentration. The damping rate is given by the real part, and the frequency by the imaginary part of $\hat{\omega}\alpha$.

5.3.2 Numerical results

The damping rate and the angular frequency is determined from a damped cosine fit to the data, i.e. a non-linear least square fit is done to the function

$$f(t; A_f, \delta_f, \omega_f, \omega_f', \phi_f, C_f) := A_f e^{-\delta_f t}\cos(\omega_f t + \omega_f' t^2 + \phi_f) + C_f , \tag{5.3.18}$$

with the parameters A, δ_f, ω_f, ω_f' ϕ_f and C_f. Note, that a linear time dependent frequency $\omega(t) = \omega_f + \omega_f' t$ is allowed. However, in the following examples the frequency drift was small and is neglected.

The fit is used to determine the parameters from the full three dimensional numerical calculation, where the tip position of the drop is used. The fit is also used to determine the frequency ω_f and damping rate δ_f from the solution of the equation (5.3.10) and (5.3.11) in the insoluble case.

In the numerical computations the initial drop is in rest. The shape is given by (5.3.1) for $n = 2$ with an amplitude of $a_2 = 0.1$. The drop is not in equilibrium and will start to oscillate. The Weber number is fixed to $\mathrm{We} = 0.0081$ in all examples, which will give roughly five oscillations in the time interval $[0, 1]$. The timestep length is $\Delta t = 10^{-4}$, i.e. 10000 steps per computation.

In both cases, the insoluble and the soluble surfactant, the bulk and surface Peclet, the Damkoehler and Biot numbers are $\mathrm{Pe} = 1$, $\mathrm{Pe}_\Gamma = 1$, $\mathrm{Da} = 1$ and $\mathrm{Bi} = 1$, respectively. The equilibrium bulk surfactant concentration c^{eq} and the equilibrium surface surfactant concentration c_Γ^{eq} are

$$c^{eq} = 0.1111 \quad \text{and} \quad c_\Gamma^{eq} = 0.1 \ . \tag{5.3.19}$$

The initial surfactant concentrations are set to c^{eq} and c_Γ^{eq}, respectively.

Two examples are considered, an insoluble case with a Reynolds number of $\mathrm{Re} = 10.684$ and a soluble case with a Reynolds number of $\mathrm{Re} = 1.0684$. The Reynolds numbers are chosen such that the dimensionless viscosity $\sqrt{\mathrm{We}}\mathrm{Re}^{-1} < 0.1$, a bound given in [24, 98], where the viscous effects become negligibly, and the analytic approximations are valid. It has to be noted, this bound excludes the aperiodic limit, which is obtained for $\sqrt{\mathrm{We}}\mathrm{Re}^{-1} = 0.5657$, as given in (5.3.9). For $\mathrm{Re} = 1.0684$ one has $\sqrt{\mathrm{We}}\mathrm{Re}^{-1} = 0.0842$, which is quite close to the bound, and for $\mathrm{Re} = 10.684$ one has $\sqrt{\mathrm{We}}\mathrm{Re}^{-1} = 0.0084$. In Table 5.8 the resulting frequencies and damping rates from the linear Lamb theory are given.

Table 5.8: Lamb frequency, angular frequency and damping rate for different Reynolds numbers.

Re	$\omega_{0,2}$	ω_2	δ_2
1.0684	31.4270	31.0766	4.6799
10.684	31.4270	31.4235	0.4682

In Fig. 5.19 a comparison of the normalized amplitudes of the shape oscillation in the soluble case is shown. Normalized means $a_2(t)$ is scaled with $a_2(0)^{-1}$ such that the graph starts at one. In the figure, (sim) is the shape oscillation by numerical computation and (pred) is the shape oscillation obtain by (5.3.14). The Reynolds number is $\mathrm{Re} = 1.0684$ and the surface elasticity $E = 1.0$. A good agreement is seen, although the prediction runs a little ahead.

In Fig. 5.20 a comparison of the normalized amplitudes of the shape oscillation in the insoluble case is shown. (pred) is the prediction of the shape oscillation obtained by (5.3.10) and (5.3.11). Here the Reynolds number is $\mathrm{Re} = 10.684$, which means lower damping as in the previous example, and the surface elasticity is $E = 1.0$. We see a good agreement, the prediction runs ahead again and shows less damping.

In Fig. 5.21 the damping rates versus different surface elasticities for the numerical simulation (sim) and the prediction after (5.3.14) (pred) is schown. In Fig. 5.22 the same is shown for the frequencies. We see a quite good agreement in the frequencies over the considered range of surface elasticities. The agreement gets better for low surface elasticities. Contrary, an increasing disagreement in the damping rates for lower surface elasticities and a better agreement for higher surface elasticities is seen.

In the case of insoluble surfactant, shown in Fig. 5.23 and Fig. 5.24, a better agreement for the damping rates at lower surface elasticties is seen. The angular frequencies are in good agreement for lower elasticities. Both, the missmatch in damping rate and the frequency increases with higher surface elasticities.

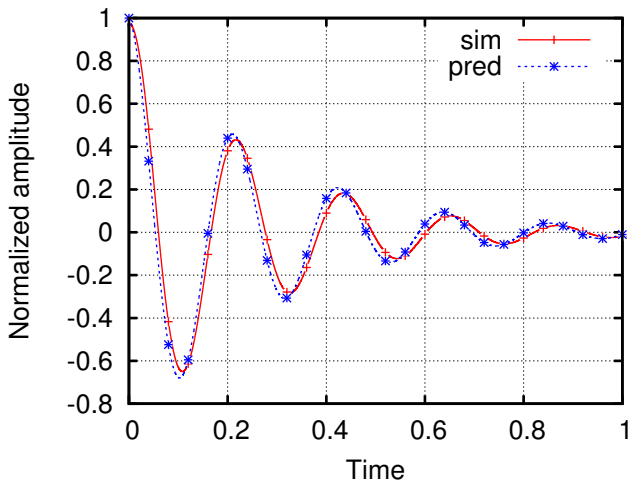

Figure 5.19: Comparison of the course of the second mode of an freely oscillation drop with soluble surfactant between the numerical simulation (sim) and the prediction from (5.3.14) (pred), for $(\mathrm{Re}, E) = (1.0684, 1.0)$.

5.3.3 Conclusion

The numerical method presented in this work was used to solve a capillary free boundary flow with soluble and insoluble surfactants, where the surfactant is allowed to affect the surface tension force and thus changes the dynamical behaviour. The numerical method was validated at the example of a freely oscillating droplet in zero gravity. Thereby, the solution was compared to different simplified models available in the literature.

The presented numerical method confirms, as expected, that the linear theory by Lamb [82] fails to predict damping rates and frequencies for the case of viscous fluid, and fluid with surfactants present.

A quite good agreement give the theories presented in [110] for the soluble surfactant and in [91] for the insoluble surfactant. In both cases an excellent match for the frequencies is observed. Although, the numerical simulation for the soluble and insoluble cases tends to underestimate the frequencies. A different situation is found for the damping rates, here in both cases the numerical simulation overestimates the damping. The disagreement increases with the surface elasticity in the insoluble case, what might be expect, since the theory chosen from [91] is for small surface elasticities. Also, the backward Euler scheme used in the numerical simulation introduces numerical damping. Contrary, in the soluble case the disagreement increases with lower surface elasticities, thus there could be a problem with the numerical damping, and a lower time step size or a time discretization, which introduce less numerical damping, could be necessary in order to get a better agreement.

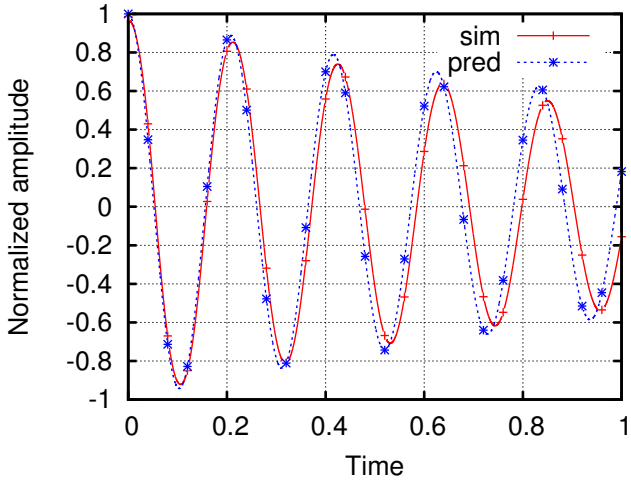

Figure 5.20: Comparison of the course of the second mode of an freely oscillation drop with insoluble surfactant between the numerical simulation (sim) and the prediction from (5.3.10) and (5.3.11) (pred), for $(\mathrm{Re}, E) = (10.684, 1.0)$.

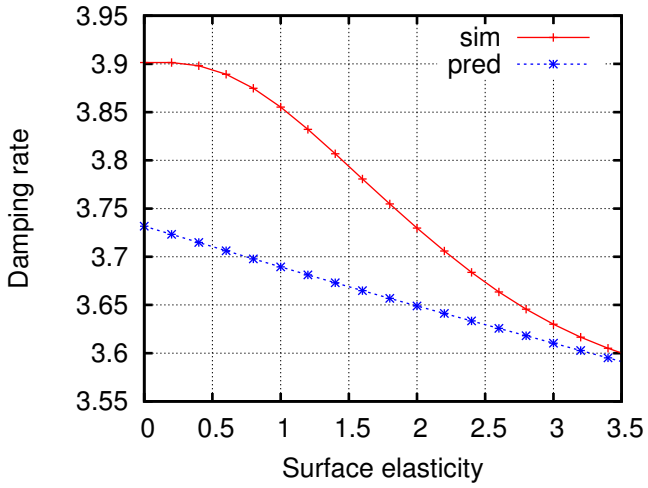

Figure 5.21: Damping rate versus surface elasticity for $\mathrm{Re} = 1.0684$ and soluble surfactant, for the numerical simulation (sim) and the prediction from (5.3.14) (pred).

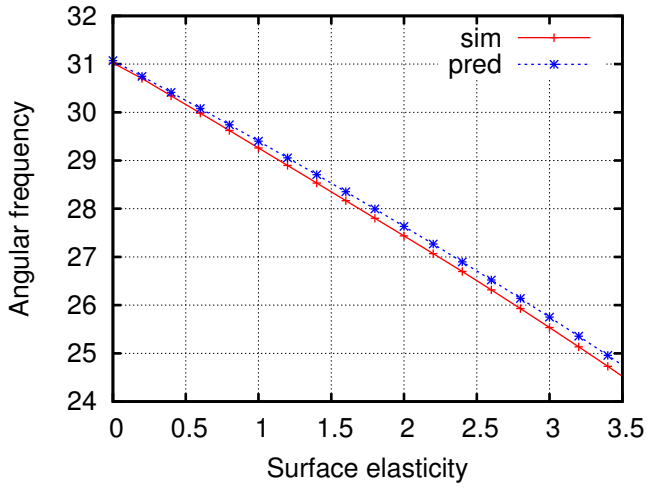

Figure 5.22: Angular frequency versus surface elasticity for Re = 1.0684 and soluble surfactant, for the numerical simulation (sim) and the prediction from (5.3.14) (pred).

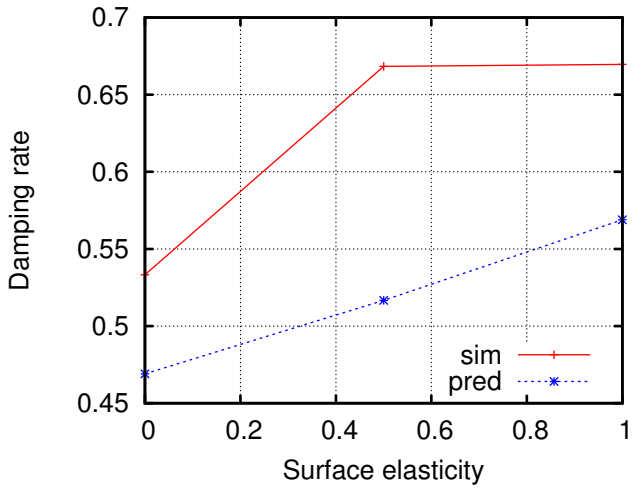

Figure 5.23: Damping rate versus surface elasticity for Re = 10.684 and insoluble surfactant, for the numerical simulation (sim) and the prediction from (5.3.10) and (5.3.11) (pred).

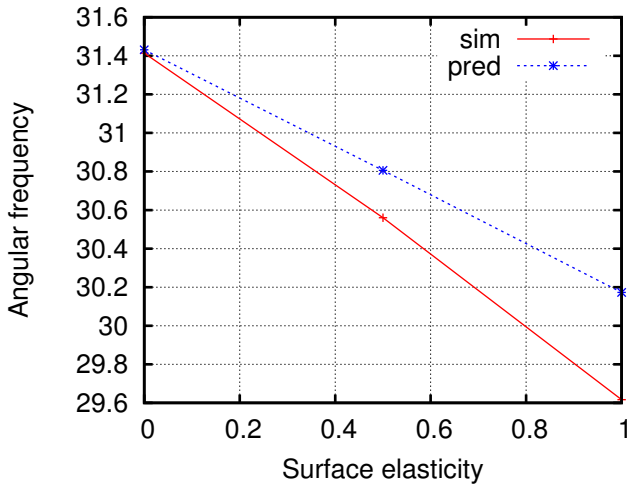

Figure 5.24: Angular frequency versus surface elasticity for Re = 10.684 and insoluble surfactant, for the numerical simulation (sim) and the prediction from (5.3.10) and (5.3.11) (pred).

5.4 Weak Surface Evolution

In this section, numerical tests for the weak surface evolution are performed. The lumped and non-lumped versions, and the piecewise linear and piecewise quadratic schemes are compared.

The interface grid velocity has to be given. Instead of providing a predefined velocity field, the problem of the weak surface evolution is coupled to a mean curvature flow problem, as in [17]. This defines an equilibrium shape and curvature, and the velocity is a consequence of a difference of the current curvature and the curvature in the equilibrium. In the mean curvature flow the velocity of the surface is given as

$$\mathbf{u} \cdot \mathbf{n} = \Delta_\Gamma \mathcal{H} \ .$$

Substituting this in the weak surface evolution formulation in Problem 4.4.2, and applying integration by parts, the following equations arise.

Problem 5.4.1. *Given* Γ_h^n *and* $\mathbf{u}$*, find* $(\mathbf{w}_{n+1}, \mathcal{H}_{n+1}) \in \mathbb{S}_s(\Gamma_h^n)^2 \times \mathbb{S}_s(\Gamma_h^n)$ *such that*

$$\begin{aligned} \langle \mathbf{w}_{n+1}, \mathbf{n}_\Gamma \psi \rangle_n^{h,s} + \langle \nabla_\Gamma \mathcal{H}_{n+1}, \nabla_\Gamma \psi \rangle_n &= 0 \ , \\ \langle \mathcal{H}_{n+1} \mathbf{n}_\Gamma, \eta \rangle_n^{h,s} - \tau_n \langle \nabla_\Gamma \mathbf{w}_{n+1}, \nabla_\Gamma \eta \rangle_n &= \langle \mathbb{P}_\Gamma, \nabla_\Gamma \eta \rangle_n \ , \end{aligned}$$

for all $(\eta, \psi) \in \mathbb{S}_s(\Gamma_h^n)^2 \times \mathbb{S}_s(\Gamma_h^n)$.

The stationary solution of the mean curvature flow is a circle, since $\Delta_\Gamma \mathcal{H} = 0$ implies a constant curvature for closed surfaces. In order to evaluate the weak surface evolution also on shapes with varying curvature a slight modification of Problem 5.4.1 is used. The normal velocity is set to

$$\mathbf{u} \cdot \mathbf{n} = \Delta_\Gamma \left(\mathcal{H} - \mathcal{H}^0 \right) \ ,$$

where $\mathcal{H}^0$ is a given function. For the stationary case $\mathbf{u} \cdot \mathbf{n} = 0$, this results in $\Delta_\Gamma \mathcal{H} = \Delta_\Gamma \mathcal{H}^0$, which means

$$\mathcal{H} = \mathcal{H}^0 + C \ ,$$

where C is a constant. Such that if $\mathcal{H}^0$ is not constant, and describes a shape with a varying curvature instead, the equilibrium shape will also have a varying curvature, which is the desired property.

The resulting problem reads:

Problem 5.4.2. *Given* Γ_h^n*,* $\mathbf{u}$*, and* $\mathcal{H}^0$*, find* $(\mathbf{w}_{n+1}, \mathcal{H}_{n+1}) \in \mathbb{S}_s(\Gamma_h^n)^2 \times \mathbb{S}_s(\Gamma_h^n)$ *such that*

$$\begin{aligned} \langle \mathbf{w}_{n+1}, \mathbf{n}_\Gamma \psi \rangle_n^{h,s} + \langle \nabla_\Gamma \mathcal{H}_{n+1}, \nabla_\Gamma \psi \rangle_n &= \left\langle \nabla_\Gamma \mathcal{H}^0, \nabla_\Gamma \psi \right\rangle_n \ , \\ \langle \mathcal{H}_{n+1} \mathbf{n}_\Gamma, \eta \rangle_n^{h,s} - \tau_n \langle \nabla_\Gamma \mathbf{w}_{n+1}, \nabla_\Gamma \eta \rangle_n &= \langle \mathbb{P}_\Gamma, \nabla_\Gamma \eta \rangle_n \ , \end{aligned}$$

for all $(\eta, \psi) \in \mathbb{S}_s(\Gamma_h^n)^2 \times \mathbb{S}_s(\Gamma_h^n)$.

Next, three test examples are given.

5.4.1 Comparison $\mathbb{P}_1$- and $\mathbb{P}_2$-Scheme

A comparison between the piecewise linear and the piecewise quadratic scheme is given. The mean curvature flow Problem 5.4.1 in the lumped version is solved. The initial shape is an ellipsoid, where the node distribution is highly uneven, see Figure 5.25.

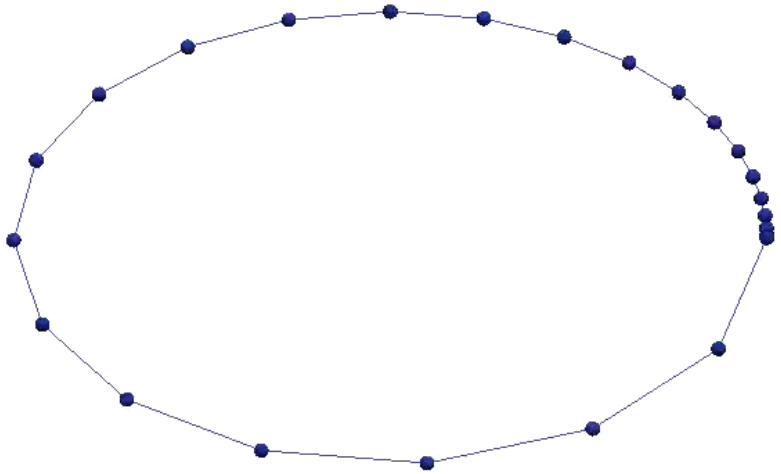

Figure 5.25: Initial shape and node distribution.

Solving Problem 5.4.1, the mean curvature flow will drive the ellipsoid towards a circle over time. Simultaneously, the nodes will redistribute in tangential direction. In Figure 5.26 the result after a few time steps is shown. The shape is not a full circle yet. That can be seen from the colour code of the nodes, which shows the curvature. A red colour decodes a higher curvature, and a blue colour a lower curvature. While the piecewise linear scheme shows a near even node distribution already, the piecewise quadratic scheme shows nearly no difference in tangential node distribution to the initial state.

A few time steps later, both schemes have reached the stationary circular shape, which is shown in Figure 5.27. In the piecewise linear scheme, the nodes are redistributed in tangential direction such that equal distance is achieved. Contrary, in the piecewise quadratic scheme, the node distribution is still near the initial state. The movement of the nodes in tangential direction is far to slow and cannot keep up with the movement in normal direction induced by the dynamic of the mean curvature flow problem.

In Figure 5.28, the result of a continuation of the simulation, after the circular shape is reached, is shown. It shows that even after a time span, more then a hundred times longer than the time span needed to reach the equilibrium circular shape, the piecewise quadratic scheme has not reach equi-distribution of the nodes, yet.

This shows that the piecewise quadratic scheme is not practicable in terms of the desired node distribution.

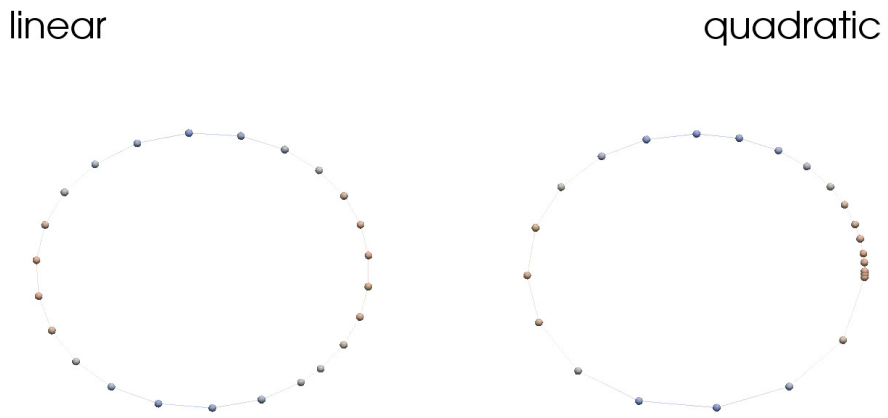

Figure 5.26: Shape and node distribution after a short time.

5.4.2 Lumped vs Non-lumped Scheme

For the comparison of the lumped and the non-lumped scheme a shape with varying curvature is used, since both schemes distinguish in those cases. Thus, Problem 5.4.2 is solved. The right hand side $\mathcal{H}^0$ is chosen as

$$\mathcal{H}^0(x, y) = 16x^2 \ .$$

The choice of $\mathcal{H}^0$ results in a long stretched equilibrium shape, with two top and bottom cap regions of high curvature and a body region of low curvature. For the initial shape, a circle is used shown in Figure 5.29.

Figure 5.30 shows the final shape and node distribution of the lumped (right) and the non-lumped (left) schemes. The difference of the two schemes can be seen clearly. While the lumped scheme attains equi-distribution, the non-lumped scheme carries more nodes the regions of high curvature. In the example used here this results in a better approximation of the shape by the non-lumped scheme. The fixed amount of nodes is used more efficient, to approximate the shape.

5.4.3 Combined Schemes

For the test of the combined scheme, the linear combination of Problem 5.4.2 solved.

Problem 5.4.3. *Given* Γ_h^n, $\mathbf{u}$, $\mathcal{H}^0$, *and* λ, *find* $(\mathbf{w}_{n+1}, \mathcal{H}_{n+1}) \in \mathbb{S}_1(\Gamma_h^n)^2 \times \mathbb{S}_1(\Gamma_h^n)$ *such that*

$$\begin{aligned}
(1-\lambda)\left\langle \mathbf{w}_{n+1}, \mathbf{n}_\Gamma \psi \right\rangle_n^{h,1} + \lambda \left\langle \mathbf{w}_{n+1}, \mathbf{n}_\Gamma \psi \right\rangle_n + \left\langle \nabla_\Gamma \mathcal{H}_{n+1}, \nabla_\Gamma \psi \right\rangle_n &= \left\langle \nabla_\Gamma \mathcal{H}^0, \nabla_\Gamma \psi \right\rangle_n \ , \\
(1-\lambda)\left\langle \mathcal{H}_{n+1}\mathbf{n}_\Gamma, \eta \right\rangle_n^{h,1} + \lambda \left\langle \mathcal{H}_{n+1}\mathbf{n}_\Gamma, \eta \right\rangle_n - \tau_n \left\langle \nabla_\Gamma \mathbf{w}_{n+1}, \nabla_\Gamma \eta \right\rangle_n &= \left\langle \mathbb{P}_\Gamma, \nabla_\Gamma \eta \right\rangle_n \ ,
\end{aligned}$$

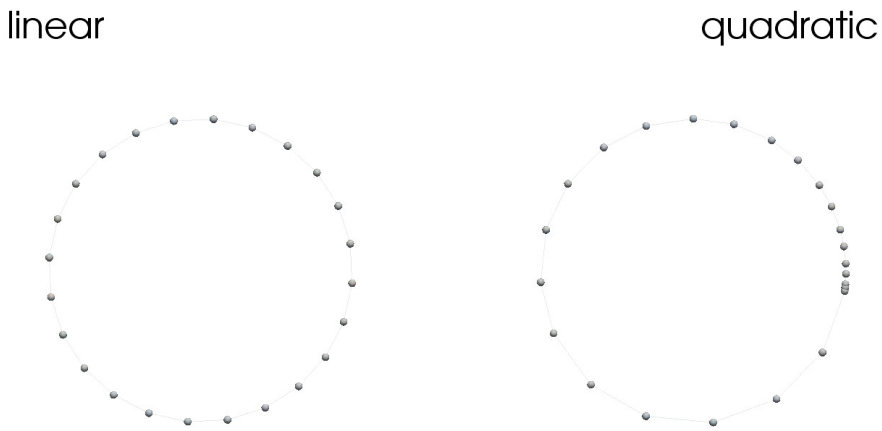

Figure 5.27: Shape and node distribution at the time where the stationary shape is reached.

for all $(\eta, \psi) \in \mathbb{S}_s(\Gamma_h^n)^2 \times \mathbb{S}_s(\Gamma_h^n)$.

Where $\mathcal{H}^0$ is chosen as before

$$\mathcal{H}^0(x, y) = 16x^2 \ .$$

Figure 5.31 the resulting equilibrium shape and node distribution for different values of lambda. It is seen that with lambda it can be gradually chosen between equidistribution and a curvature dependent distribution. The curvature dependent distribution seems to be more suited for the present problem.

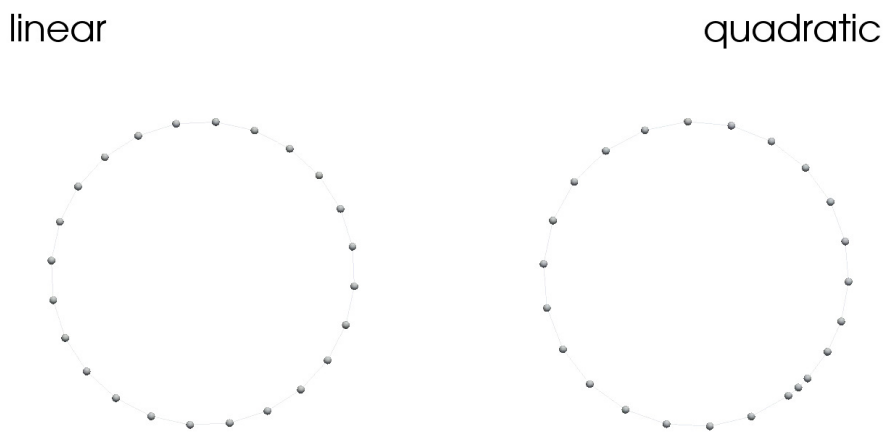

Figure 5.28: Shape and node distribution after a very long time.

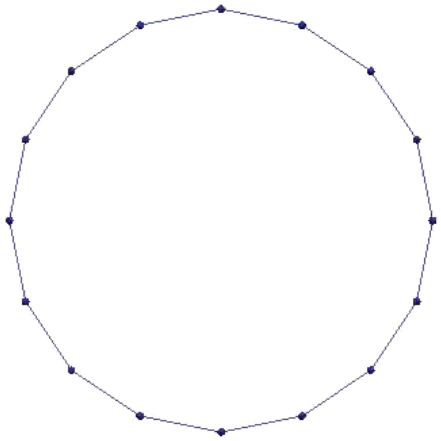

Figure 5.29: Initial shape and node distribution for the lumped vs non-lumped comparison.

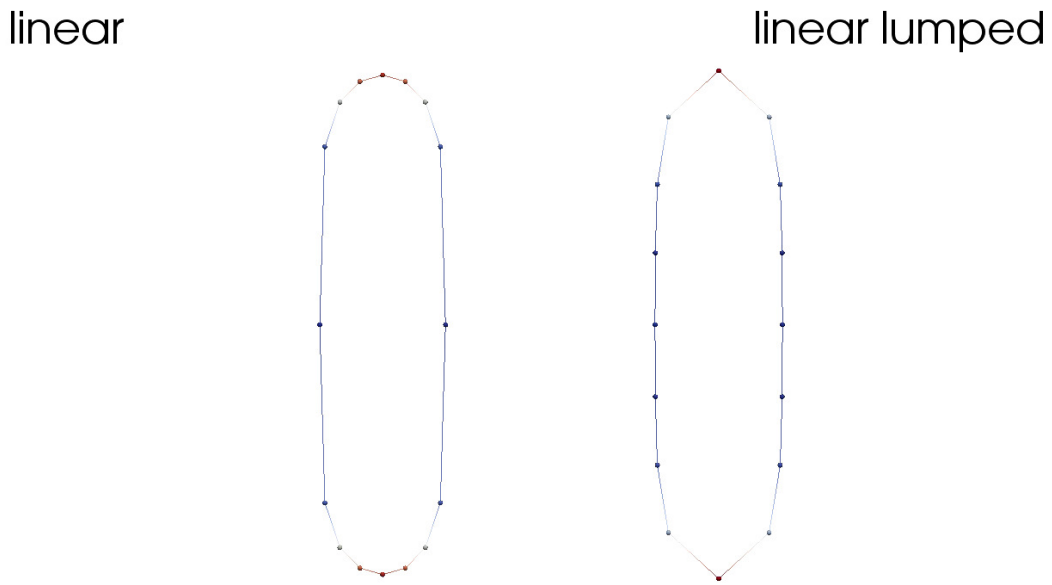

Figure 5.30: Final equilibrium shape and node distribution for the lumped vs non-lumped comparison.

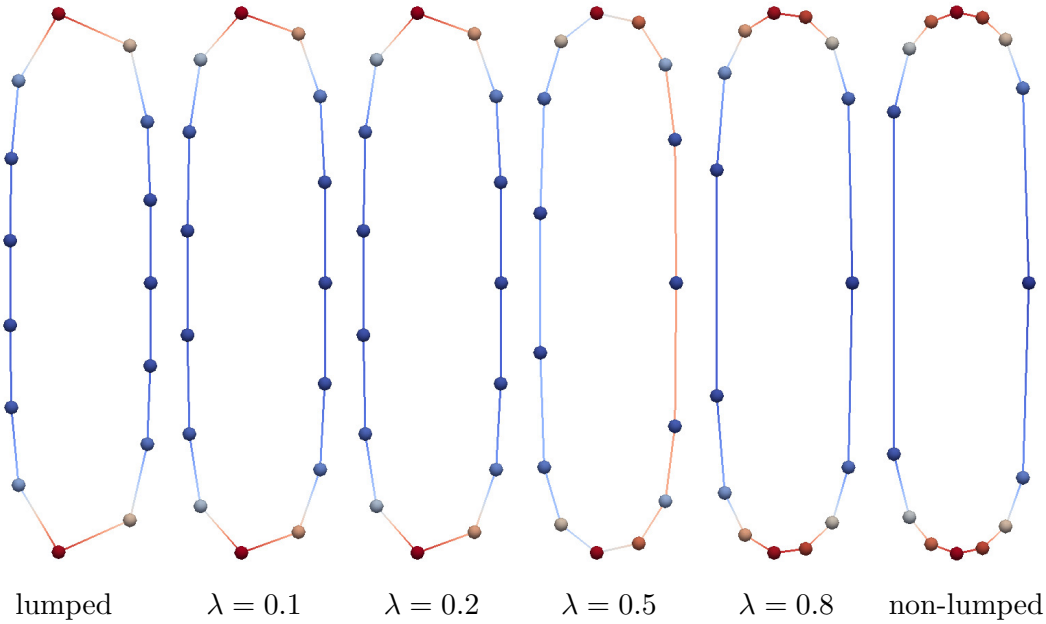

Figure 5.31: Final equilibrium shape and node distribution for different parameters λ. From left to right $\lambda = \{0.0, 0.1, 0.2, 0.5, 0.8, 1.0\}$.

Chapter 6

Summary

The main aim of this work was the development of an accurate and robust numerical scheme for the simulation of two-phase flows with surfactants in two and three dimensions. The developed methods are fitted interface tracking methods employing the Arbitrary Lagrangian Eulerian framework on moving meshes.

First, the governing equations for a two-phase flow with soluble surfactants were derived. A set of Navier-Stokes equations coupled to a set of transport equations in the bulk and on the interface were deduced from physical principles of mass- and momentum conservation. Coupling conditions for the equations governing in each subdomain were obtained by considering the mass- and momentum balances across the interface. The derived equations were transformed into a dimensionless form and a weak formulation was derived.

The coupled flow and transport equation were transformed into a moving frame of reference, the ALE frame. The ALE mapping was introduced, in order to describe the evolution of the time dependent domains the fluid phases occupy. Two different methods to obtain the ALE mapping were considered. A special treatment of the interface evolution, using a weak formulation of the kinematic mass coupling condition, were presented.

Then, the finite element discretization of the ALE formulation of the flow and transport equations were introduced. Simplicial moving meshes were used, i.e. triangles in two dimensions and tetrahedrons in three dimensions. Isoparametric mesh cells were employed, in order to get a higher order approximation of the interface.

The choice for the finite element pair used for the Navier-Stokes equations were discussed. Since, a discontinuous pressure approximation is mandatory for a two-phase flow with a capillary surface, an extended Taylor-Hood element was introduced, that has a discontinuous pressure across the interface. The extended Taylor-Hood finite element prevents spurious velocity, which are observed in the numerical simulation of two-phase flows. Further, it significantly reduces the number of unknowns used, compared to finite element space employing a discontinuous pressure approximation on an element level. The inf-sup stability for this extended Taylor-Hood finite element space was proven.

The known and commonly used time discretization for the one-phase Navier-Stokes

equations, namely the implicit Euler, the θ-scheme, and the fractional Θ-scheme, were adapted to the coupled flow and transport system for two-phase flows with surfactants. Decoupling strategies were introduced to separate the Navier-Stokes equations from the transport problem, such that an iterative solution strategy could be applied to the nonlinear systems.

The weak formulation for the surface evolution were discretized by different methods. The resulting schemes were compared, regarding their surface mesh node distribution and surface mesh quality. A method for piecewise linear surface meshes, that results in equi-distributed nodes, and a scheme resulting in a curvature dependent distribution of nodes, was adopted to piecewise quadratic surface meshes. The obtained scheme for quadratic meshes exhibits the same properties regarding the node distribution.

Finally, the presented methods were validated in several numerical test. The numerical test indicate that the obtained methods are reliable in several different applications.

Of course, this work also lefts open several questions. Future work in this field is in particular the numerical analysis of the proposed scheme or at least some of its subproblems. This could include:

- The study of the inf-sup stability of the extended Taylor-Hood finite element space in case of smooth, non-polygonal interfaces. This would involve, the study of the inf-sup stability of the Taylor-Hood finite element space on a series of non-nested meshes, for which surprisingly no results was found in the literature by the author.
- The transfer of the stability result of the continuous capillary two-phase flow problem (3.4.1) to the discrete case.
- The study of the stability of the proposed time discretization in the context of ALE finite element methods and the discrete GCL condition.
- Theoretical insight regarding the node distribution properties of the weak grid evolution using the non-lumped bilinear forms.
- Numerical analysis of the stationary and non-stationary coupled bulk-surface transport problem in the ALE context.

Acknowledgement

First, I would like to thank all my colleagues at the Institute for Analysis and Numeric at the OvGU in Magdeburg. Most notably, I would like to express sincere thanks to my supervisor Prof. Tobiska, who gave me great advice and support for this PhD thesis. Besides, I would like to give a special thanks my colleagues Sashikumaar Ganesan, who introduced me into the program package MooNMD, and Kristin Simon who always had time for discussions.

I also would like to thank the colleagues at the priority program (SPP) 1506. Especially, my fellow colleagues Sebastian Aland, Christian Kahle, Fabian Klingbeil, Christoph Lehrenfeld, Martin Weissman, and Stephan Weller, who are not only co-authors of two papers, but also helped my work with fruitful discussions.

I gratefully acknowledge the funding of this work by the German Research Foundation (DFG) with the project To143/11.

Finally, I wish to thank all other people, who I have met during my work and were not mentioned here.

Bibliography

[1] H. Abels, D. Depner, and H. Garcke. "Existence of weak solutions for a diffuse interface model for two-phase flows of incompressible fluids with different densities". In: *J. Math. Fluid Mech.* 15.3 (2013), pp. 453–480.

[2] H. Abels, H. Garcke, and G. Grün. "Thermodynamically consistent, frame indifferent diffuse interface models for incompressible two-phase flows with different densities". In: *Math. Models Methods Appl. Sci.* 22.3 (2012), pp. 1150013, 40.

[3] S. Aland and A. Voigt. "Benchmark computations of diffuse interface models for two-dimensional bubble dynamics". In: *Internat. J. Numer. Methods Fluids* 69.3 (2012), pp. 747–761.

[4] S. Aland et al. "Adaptive diffuse domain approach for calculating mechanically induced deformation of trabecular bone". In: *Computer Methods in Biomechanics and Biomedical Engineering* (published online 2012).

[5] S. Aland et al. "Comparative simulations of Taylor-flow with surfactants based on sharp- and diffuse-interface methods". In: *Transport Processes at Fluidic Interfaces*. Ed. by D. Bothe and A. Reusken. Springer International Publishing, 2017. Chap. 22, pp. 639–661.

[6] S. Aland et al. "Quantitative comparison of Taylor flow simulations based on sharp-interface and diffuse-interface models". In: *International Journal for Numerical Methods in Fluids* 73.4 (2013), pp. 344–361.

[7] S. Aland. "Phase field models for two-phase flow with surfactants and biomembranes". In: *Transport Processes at Fluidic Interfaces*. Springer, 2017, pp. 271–290.

[8] S. Aland, J. Lowengrub, and A. Voigt. "A continuum model of colloid-stabilized interfaces". In: *Physics of Fluids* 23.6, 062103 (2011), p. 062103.

[9] D. M. Anderson, G. B. McFadden, and A. A. Wheeler. "DIFFUSE-INTERFACE METHODS IN FLUID MECHANICS". In: *Annual Review of Fluid Mechanics* 30.1 (1998), pp. 139–165.

[10] W. Aniszewski, T. Ménard, and M. Marek. "Erratum to: "Volume of fluid (VOF) type advection methods in two-phase flow: A comparative study". [Comput Fluids 97 (2014) 52–73] [MR3205656]". In: *Comput. & Fluids* 152 (2017), pp. 193–194.

[11] I. Babuška and A Aziz. “Survey Lectures on the Mathematical Foundations of the Finite Element Method”. In: *The Mathematical Foundations of the Finite Element Method with Applications to Partial Differential Equations*. Ed. by A. Aziz. Academic Press, 1972, pp. 1–359.

[12] I. Babuška. “The finite element method with Lagrangian multipliers”. In: *Numer. Math.* 20 (1972/73), pp. 179–192.

[13] S. Badia and R. Codina. “Analysis of a stabilized finite element approximation of the transient convection-diffusion equation using an ALE framework”. In: *SIAM J. Numer. Anal.* 44.5 (2006), pp. 2159–2197.

[14] E. Bänsch. “Finite element discretization of the Navier-Stokes equations with a free capillary surface”. In: *Numer. Math.* 88 (2001), pp. 203–235.

[15] E. Bänsch and B. Höhn. “Numerical simulation of a silicon floating zone with a free capillary surface”. In: *Proceedings of the SCCE II*. Vol. 1. Springer, 1999.

[16] E. Bänsch and S. Weller. “A comparison of several time discretization methods for free surface flows”. In: *Proceedings of the Conference Algoritmy*. 2015, pp. 331–341.

[17] J. W. Barrett, H. Garcke, and R. Nürnberg. “A parametric finite element method for fourth order geometric evolution equations”. In: *J. Comput. Phys.* 222.1 (2007), pp. 441–462.

[18] J. W. Barrett, H. Garcke, and R. Nürnberg. “A stable parametric finite element discretization of two-phase Navier-Stokes flow”. In: *J. Sci. Comput.* 63.1 (2015), pp. 78–117.

[19] J. W. Barrett, H. Garcke, and R. Nürnberg. “Eliminating spurious velocities with a stable approximation of viscous incompressible two-phase Stokes flow”. In: *Comput. Methods Appl. Mech. Engrg.* 267 (2013), pp. 511–530.

[20] J. W. Barrett, H. Garcke, and R. Nürnberg. “Stable finite element approximations of two-phase flow with soluble surfactant”. In: *J. Comput. Phys.* 297 (2015), pp. 530–564.

[21] J. W. Barrett, H. Garcke, and R. Nürnberg. “Stable numerical approximation of two-phase flow with a Boussinesq-Scriven surface fluid”. In: *Commun. Math. Sci.* 13.7 (2015), pp. 1829–1874.

[22] S. Basting and M. Weismann. “A hybrid level set/front tracking approach for finite element simulations of two-phase flows”. In: *J. Comput. Appl. Math.* 270 (2014), pp. 471–483.

[23] K. Bäumler et al. “Drop rise velocities and fluid dynamic behavior in standard test systems for liquid/liquid extractionexperimental and numerical investigations”. In: *Chemical Engineering Science* 66.3 (2011), pp. 426–439.

[24] E. Becker, W. J. Hiller, and T. A. Kowalewski. “Experimental and theoretical investigation of large-amplitude oscillations of liquid droplets”. In: *Journal of Fluid Mechanics* 231 (1991), pp. 189–210.

[25] D. Boffi and L. Gastaldi. "Stability and geometric conservation laws for ALE formulations". In: *Comput. Methods Appl. Mech. Engrg.* 193.42-44 (2004), pp. 4717–4739.

[26] J. M. Boland and R. A. Nicolaides. "Stability of finite elements under divergence constraints". In: *SIAM J. Numer. Anal.* 20.4 (1983), pp. 722–731.

[27] A. Bonito, I. Kyza, and R. H. Nochetto. "Time-discrete higher order ALE formulations: a priori error analysis". In: *Numer. Math.* 125.2 (2013), pp. 225–257.

[28] A. Bonito, I. Kyza, and R. H. Nochetto. "Time-discrete higher-order ALE formulations: stability". In: *SIAM J. Numer. Anal.* 51.1 (2013), pp. 577–604.

[29] D. Bothe and J. Prüss. "On the two-phase Navier-Stokes equations with Boussinesq-Scriven surface fluid". In: *J. Math. Fluid Mech.* 12.1 (2010), pp. 133–150.

[30] D. Bothe et al. "VOF-based simulation of reactive mass transfer across deformable interfaces". In: *Prog. Comput. Fluid Dyn.* 9.6-7 (2009), pp. 325–331.

[31] F. P. Bretherton. "The motion of long bubbles in tubes". In: *J. Fluid Mech.* 10.166 (1961).

[32] F. Brezzi. "On the existence, uniqueness and approximation of saddle-point problems arising from Lagrangian multipliers". In: *Rev. Française Automat. Informat. Recherche Opérationnelle Sér. Rouge* 8.R-2 (1974), pp. 129–151.

[33] M. O. Bristeau, R. Glowinski, and J. Périaux. "Numerical methods for the Navier-Stokes equations. Applications to the simulation of compressible and incompressible viscous flows". In: *Finite elements in physics (Lausanne, 1986)*. North-Holland, Amsterdam, 1987, pp. 73–187.

[34] E. Burman et al. "CutFEM: discretizing geometry and partial differential equations". In: *Internat. J. Numer. Methods Engrg.* 104.7 (2015), pp. 472–501.

[35] E. Burman et al. "Full gradient stabilized cut finite element methods for surface partial differential equations". In: *Comput. Methods Appl. Mech. Engrg.* 310 (2016), pp. 278–296.

[36] J. W. Cahn and J. E. Hilliard. "Free Energy of a Nonuniform System. I. Interfacial Free Energy". In: *The Selected Works of John W. Cahn.* John Wiley & Sons, Inc., 2013, pp. 29–38.

[37] E. Campillo-Funollet, G. Grün, and F. Klingbeil. "On modeling and simulation of electrokinetic phenomena in two-phase flow with general mass densities". In: *SIAM J. Appl. Math.* (2012). in press.

[38] S. Chandrasekhar. *Hydrodynamic and hydromagnetic stability.* The International Series of Monographs on Physics. Clarendon Press, Oxford, 1961, xix+654 pp. (16 plates).

[39] A. J. Chorin and J. E. Marsden. *A mathematical introduction to fluid mechanics.* Springer, 1993.

[40] P. G. Ciarlet. *Mathematical Elasticity. Vol I: Three-Dimensional Elasticity*. North-Holland, 1988.

[41] P. G. Ciarlet and J. L. Lions. *Handbook of Numerical Analysis, Volume II. Finite Element Methods (Part I)*. North-Holland, 1991.

[42] R. M. Davies and G. Taylor. "The Mechanics of Large Bubbles Rising through Extended Liquids and through Liquids in Tubes". In: *Proceedings of the Royal Society of London. Series A, Mathematical and Physical Sciences* 200.1062 (1950), pp. 375–390.

[43] A. Demlow. "Higher-order finite element methods and pointwise error estimates for elliptic problems on surfaces". In: *SIAM J. Numer. Anal.* 47.2 (2009), pp. 805–827.

[44] K. Dieter-Kissling, H. Marschall, and D. Bothe. "Direct numerical simulation of droplet formation processes under the influence of soluble surfactant mixtures". In: *Comput. & Fluids* 113 (2015), pp. 93–105.

[45] K. Dieter-Kissling, H. Marschall, and D. Bothe. "Numerical method for coupled interfacial surfactant transport on dynamic surface meshes of general topology". In: *Comput. & Fluids* 109 (2015), pp. 168–184.

[46] G. Dziuk and C. M. Elliott. "Finite elements on evolving surfaces". In: *IMA J. Numer. Anal.* 27.2 (2007), pp. 262–292.

[47] G. Dziuk and C. M. Elliott. "Surface finite elements for parabolic equations". In: *J. Comput. Math.* 25.4 (2007), pp. 385–407.

[48] G. Dziuk. "Finite elements for the Beltrami operator on arbitrary surfaces". In: *Partial differential equations and calculus of variations*. Vol. 1357. Lecture Notes in Math. Springer, Berlin, 1988, pp. 142–155.

[49] G. Dziuk and C. M. Elliott. "A fully discrete evolving surface finite element method". In: *SIAM J. Numer. Anal.* 50.5 (2012), pp. 2677–2694.

[50] G. Dziuk and C. M. Elliott. "Finite element methods for surface PDEs". In: *Acta Numer.* 22 (2013), pp. 289–396.

[51] C. Eck et al. "On a phase-field model for electrowetting". In: *Interfaces Free Bound.* 11.2 (2009), pp. 259–290.

[52] C. M. Elliott and T. Ranner. "Finite element analysis for a coupled bulk-surface partial differential equation". In: *IMA J. Numer. Anal.* 33.2 (2013), pp. 377–402.

[53] C. M. Elliott and V. Styles. "An ALE ESFEM for solving PDEs on evolving surfaces". In: *Milan J. Math.* 80.2 (2012), pp. 469–501.

[54] H. Emmerich. "Advances of and by phase-field modelling in condensed-matter physics". In: *Advances in Physics* 57.1 (2008), pp. 1–87.

[55] A. Ern and J.-L. Guermond. *Theory and Practice of Finite Elements*. Springer-Verlag New York, LLC, 2004.

[56] S. Étienne, A. Garon, and D. Pelletier. "Perspective on the geometric conservation law and finite element methods for ALE simulations of incompressible flow". In: *J. Comput. Phys.* 228.7 (2009), pp. 2313–2333.

[57] M. Feistauer, J. Felcman, and I. Straskraba. *Mathematical and Computational Methods for Compressible Flow*. Oxford University Press, 2003.

[58] L. Formaggia and F. Nobile. "Stability analysis of second-order time accurate schemes for ALE-FEM". In: *Comput. Methods Appl. Mech. Engrg.* 193.39-41 (2004), pp. 4097–4116.

[59] M. Fortin. "An analysis of the convergence of mixed finite element methods". In: *RAIRO Anal. Numér.* 11.4 (1977), pp. 341–354, iii.

[60] S. Ganesan, G. Matthies, and L. Tobiska. "On spurious velocities in incompressible flow problems with interfaces". In: *Comput. Methods Appl. Mech. Engrg.* 196.7 (2007), pp. 1193–1202.

[61] S. Ganesan and L. Tobiska. "Arbitrary Lagrangian-Eulerian finite-element method for computation of two-phase flows with soluble surfactants". In: *J. Comput. Phys.* 231.9 (2012), pp. 3685–3702.

[62] S. Ganesan et al. "ALE-FEM for Two-Phase and Free Surface Flows with Surfactants". In: *Transport Processes at Fluidic Interfaces*. Ed. by D. Bothe and A. Reusken. Springer International Publishing, 2017. Chap. 1, pp. 5–31.

[63] H. Garcke, K. F. Lam, and B. Stinner. "Diffuse interface modelling of soluble surfactants in two-phase flow". In: *Commun. Math. Sci.* 12.8 (2014), pp. 1475–1522.

[64] J.-F. Gerbeau, C. Le Bris, and M. Bercovier. "Spurious velocities in the steady flow of an incompressible fluid subjected to external forces". In: *Internat. J. Numer. Methods Fluids* 25.6 (1997), pp. 679–695.

[65] W. Gropp, E. Lusk, and A. Skjellum. *Using MPI: Portable Parallel Programming with the Message-Passing Interface*. MIT Press, 1999.

[66] W. Gropp, E. Lusk, and R. Thakur. *Using MPI-2: Advanced Features of the Message-Passing Interface*. MIT Press, 1999.

[67] S. Gross, M. A. Olshanskii, and A. Reusken. "A trace finite element method for a class of coupled bulk-interface transport problems". In: *ESAIM Math. Model. Numer. Anal.* 49.5 (2015), pp. 1303–1330.

[68] S. Groß, V. Reichelt, and A. Reusken. "A finite element based level set method for two-phase incompressible flows". In: *Computing and Visualization in Science* 9.4 (2006), pp. 239–257.

[69] S. Groß and A. Reusken. "An extended pressure finite element space for two-phase incompressible flows with surface tension". In: *J. Comput. Phys.* 224.1 (2007), pp. 40–58.

[70] S. Gross and A. Reusken. *Numerical Methods for Two-phase Incompressible Flows*. Springer, 2011.

[71] G. Grün, K. Mecke, and M. Rauscher. "Thin-film flow influenced by thermal noise". In: *Journal of Statistical Physics* 122.6 (2006), pp. 1261–1291.

[72] D. Halpern and P. Gaver. "Boundary element analysis of the time-dependent motion of a semi-infinite bubble in a channel". In: *J. Comput. Phys.* 115.366 (1994).

[73] A. Hansbo and P. Hansbo. "An unfitted finite element method, based on Nitsche's method, for elliptic interface problems". In: *Comput. Methods Appl. Mech. Engrg.* 191.47-48 (2002), pp. 5537–5552.

[74] C.-J. Heine. "Isoparametric finite element approximation of curvature on hypersurfaces". In: *Preprint Fak. f. Math. Phys. Univ. Freiburg* 26 (2004).

[75] C. Hirt, A. Amsden, and J. Cook. "An arbitrary Lagrangian-Eulerian computing method for all flow speeds". In: *Journal of Computational Physics* 135.2 (1997), pp. 203–216.

[76] C. Hirt and B. Nichols. "Volume of fluid (VOF) method for the dynamics of free boundaries". In: *Journal of Computational Physics* 39.1 (1981), pp. 201 –225.

[77] V. John and G. Matthies. "MooNMD a program package based on mapped finite element methods". In: *Computing and Visualization in Science* 6 (2 2004), pp. 163–170.

[78] L. Kelvin. *Oscillations of a liquid sphere*. Vol. 3. Mathematical and Physical Papers. London: Clay and Sons, 1890.

[79] R. Krahl and J. Gerstmann. "Non-Isothermal Reorientation of a Liquid Surface in an Annular Gap". In: *4^{th} International Berlin Workshop – IBW 4 on Transport Phenomena with Moving Boundaries*. Ed. by F.-P. Schindler. Fortschritt-Berichte VDI, Reihe 3: Verfahrenstechnik 883. Düsseldorf: VDI-Verlag, 2007, pp. 227–241.

[80] R. Krahl et al. "Dependency of the apparent contact angle on nonisothermal conditions". In: *Physics of Fluids* 20.4, 042101 (2008).

[81] P. A. Kralchevsky, K. D. Danov, and N. D. Denkov. *Chemical Physics of Colloid Systems and Interfaces*. CRC Press, 2008.

[82] H. Lamb. *Hydrodynamics*. sixth. Cambridge Mathematical Library. With a foreword by R. A. Caflisch [Russel E. Caflisch]. Cambridge University Press, Cambridge, 1993, pp. xxvi+738.

[83] L. D. Landau and E. M. Lifshitz. *Fluid Mechanics*. Pergamon Press Ltd., 1987.

[84] L. D. Landau, J. M. Lifschitz, and P. Ziesche. *Lehrbuch der theoretischen Physik, Band 1: Mechanik*. Harri Deutsch, 1997.

[85] H.-L. Lu and R. Apfel. "Shape oscillations of drops in the presence of surfactants". In: *Journal of Fluid Mechanics* 222 (1991), pp. 351–368.

[86] X. Lu and A. Prosperetti. "Axial stability of Taylor bubbles". In: *Journal of Fluid Mechanics* 568 (2006), pp. 173–192.

[87] D. Meidner and T. Richter. "A posteriori error estimation for the fractional step theta discretization of the incompressible Navier-Stokes equations". In: *Comput. Methods Appl. Mech. Engrg.* 288 (2015), pp. 45–59.

[88] D. Meidner and T. Richter. "Goal-oriented error estimation for the fractional step theta scheme". In: *Comput. Methods Appl. Math.* 14.2 (2014), pp. 203–230.

[89] C. A. Miller and L. E. Scriven. "The oscillations of a fluid droplet immersed in another fluid". In: *Journal of Fluid Mechanics* 32.3 (1968), pp. 417–435.

[90] M. Muradoglu. "A finite-volume front-tracking method for computations of multiphase flows in complex geometries". In: *Frontiers of computational fluid dynamics 2006*. World Sci. Publ., Hackensack, NJ, 2005, pp. 395–420.

[91] A. Nadim and B. Rush. *Determination of Interfacial Rheological Properties through Microgravity Oscillations of Bubbles and Drops*. Tech. rep. 20000120383. NASA, 2000.

[92] F. Nobile. "Numerical approximation of fluid-structure interaction problems with application to haemodynamics". PhD thesis. École Polytechnique Fédérale de Lausanne, 2001.

[93] F. Nobile and L. Formaggia. "A Stability Analysis for the Arbitrary Lagrangian : Eulerian Formulation with Finite Elements". In: *East-West Journal of Numerical Mathematics* 7.2 (1999), pp. 105–132.

[94] R. H. Nochetto and S. W. Walker. "A hybrid variational front tracking-level set mesh generator for problems exhibiting large deformations and topological changes". In: *J. Comput. Phys.* 229.18 (2010), pp. 6243–6269.

[95] M. A. Olshanskii and A. Reusken. "Error analysis of a space-time finite element method for solving PDEs on evolving surfaces". In: *SIAM J. Numer. Anal.* 52.4 (2014), pp. 2092–2120.

[96] M. A. Olshanskii, A. Reusken, and J. Grande. "A finite element method for elliptic equations on surfaces". In: *SIAM J. Numer. Anal.* 47.5 (2009), pp. 3339–3358.

[97] M. A. Olshanskii, A. Reusken, and X. Xu. "An Eulerian space-time finite element method for diffusion problems on evolving surfaces". In: *SIAM J. Numer. Anal.* 52.3 (2014), pp. 1354–1377.

[98] A. Prosperetti. "Free oscillations of drops and bubbles: the initial-value problem". In: *Journal of Fluid Mechanics* 100.2 (1980), pp. 333–347.

[99] T. Ranner. "Computational surface partial differential equations". PhD thesis. University of Warwick, 2013.

[100] J Ratulowski and H.-C. Chang. "Marangoni effects of trace impurities on the motion of long gas bubbles in capillaries". In: *J. Fluid Mech.* 210 (1990), pp. 303–328.

[101] L. Rayleigh. *The Theory of Sound*. London: Macmillan, 1894.

[102] A. Reusken and Y. Zhang. "Numerical simulation of incompressible two-phase flows with a Boussinesq-Scriven interface stress tensor". In: *Internat. J. Numer. Methods Fluids* 73.12 (2013), pp. 1042–1058.

[103] M. J. Rosen. *Surfactants and Interfacial Phenomena*. Wiley-Interscience, 2004.

[104] J. San Martí n, L. Smaranda, and T. Takahashi. "Convergence of a finite element/ALE method for the Stokes equations in a domain depending on time". In: *J. Comput. Appl. Math.* 230.2 (2009), pp. 521–545.

[105] L. R. Scott and S. Zhang. "Finite element interpolation of nonsmooth functions satisfying boundary conditions". In: *Math. Comp.* 54.190 (1990), pp. 483–493.

[106] J. C. Slattery, L. Sagis, and E.-S. Oh. *Interfacial transport phenomena*. Second. Springer, New York, 2007, pp. xviii+827.

[107] M. Sussman. *A level set approach for computing solutions to incompressible two-phase flow*. Thesis (Ph.D.)–University of California, Los Angeles. ProQuest LLC, Ann Arbor, MI, 1994, p. 115.

[108] R. Taylor and R. Krishna. *Multicomponent Mass Transfer*. Wiley-Interscience, 1993.

[109] K. E. Teigen et al. "A diffuse-interface method for two-phase flows with soluble surfactants". In: *J. Comput. Phys.* 230.2 (2011), pp. 375–393.

[110] Y. Tian, R. G. Holt, and R. E. Apfel. "Investigations of liquid surface rheology of surfactant solutions by droplet shape oscillations: Theory". In: *Phys. Fluids* 7 (1995), p. 2938.

[111] G. Tryggvason et al. "A Front-Tracking Method for the Computations of Multiphase Flow". In: *Journal of Computational Physics* 169.2 (2001), pp. 708 –759.

[112] S. O. Unverdi and G. Tryggvason. "A front-tracking method for viscous, incompressible, multi-fluid flows". In: *Journal of Computational Physics* 100.1 (1992), pp. 25 –37.

[113] S. Vey and A. Voigt. "AMDiS: adaptive multidimensional simulations". In: *Computing and Visualization in Science* 10.1 (2007), pp. 57–67.

[114] J. T. Weber. *Analysis of diffuse interface models for two-phase flows with and without surfactants*. 2016.